

**POLYMORPHISM AND SOLUTION-MEDIATED  
TRANSFORMATION OF DL-METHIONINE**



**Lek Wantha**

**A Thesis Submitted in Partial Fulfillment of the Requirements for the  
Degree of Doctor of Philosophy in Chemical Engineering**

**Suranaree University of Technology**

**Academic Year 2011**

ภาวะพหุสัณฐานและการเปลี่ยนรูปผลึกของดีแอลเมไธโอนีน  
โดยอาศัยสารละลายเป็นสื่อกลาง



นายเล็ก วันทา

วิทยานิพนธ์นี้เป็นส่วนหนึ่งของการศึกษาตามหลักสูตรปริญญาวิศวกรรมศาสตรดุษฎีบัณฑิต  
สาขาวิชาวิศวกรรมเคมี  
มหาวิทยาลัยเทคโนโลยีสุรนารี  
ปีการศึกษา 2554

**POLYMORPHISM AND SOLUTION-MEDIATED  
TRANSFORMATION OF DL-METHIONINE**

Suranaree University of Technology has approved this thesis submitted in partial fulfillment of the requirements for the Degree of Doctor of Philosophy.

Thesis Examining Committee

---

(Dr. Terasut Sookkumnerd)

Chairperson

---

(Assoc. Prof. Dr. Adrian E. Flood)

Member (Thesis Advisor)

---

(Prof. Dr. Chaiyot Tangsathikulchai)

Member

---

(Asst. Prof. Dr. Boris Golman)

Member

---

(Asst. Prof. Dr. Sopark Sonwai)

Member

---

(Prof. Dr. Sukit Limpijumnong)

Vice Rector for Academic Affairs

---

(Assoc. Prof. Flt. Lt. Dr. Kontorn Chamniprasart)

Dean of Institute of Engineering

เล็ก วันทา : ภาวะพหุสัณฐานและการเปลี่ยนรูปผลึกของดีแอลเมไธโอนีนโดยอาศัย  
สารละลายเป็นสื่อกลาง (POLYMORPHISM AND SOLUTION-MEDIATED  
TRANSFORMATION OF DL-METHIONINE) อาจารย์ที่ปรึกษา : รศ. ดร.เอเดรียน พลัด,  
277 หน้า.

พหุสัณฐานของดีแอลเมไธโอนีนมีอยู่สามสัณฐานคือ แอลฟา ( $\alpha$ -DL-met) เบตา ( $\beta$ -DL-met) และแกมมา ( $\gamma$ -DL-met) โดยทั่วไปการเกิดขึ้นของพหุสัณฐานแต่ละสัณฐานจะขึ้นอยู่กับ อุณหพลศาสตร์ จลนศาสตร์ของการตกผลึก จลนศาสตร์ของการละลาย และจลนศาสตร์ของการเปลี่ยนรูปผลึก งานวิจัยนี้มีวัตถุประสงค์เพื่อศึกษา ทำความเข้าใจและวิเคราะห์ถึงลักษณะของ จลนศาสตร์ต่าง ๆ และคุณสมบัติทางอุณหพลศาสตร์ของพหุสัณฐานของดีแอลเมไธโอนีนที่เป็นที่ รู้จักกันโดยทั่วไป คือ แอลฟา และแกมมา นอกจากนี้ยังศึกษาเกี่ยวกับพฤติกรรมการตกผลึกและการ เปลี่ยนรูปผลึกจากสัณฐานแอลฟา ไปเป็น สัณฐานแกมมา โดยอาศัยสารละลายเป็นสื่อกลาง (solution-mediated transformation)

ความสามารถในการละลายในน้ำของสัณฐานแอลฟามีค่าสูงกว่าสัณฐานแกมมา อุณหภูมิ ของการหลอมเหลวและเอนทัลปีของการหลอมเหลวของสัณฐานแกมมามีค่าสูงกว่าสัณฐานแอลฟา พลังงานอิสระกิบส์ (Gibbs free energy) ของสัณฐานแอลฟามีค่าสูงกว่าสัณฐานแกมมา คุณสมบัติ ทางอุณหพลศาสตร์ทั้งสามประการนี้บ่งชี้ว่า ระบบพหุสัณฐานของสัณฐานแอลฟา และสัณฐาน แกมมาเป็นระบบพหุสัณฐานแบบมอโนโทรอปิก (monotropic polymorph) และภายใต้เงื่อนไขของ การตกผลึกในอุตสาหกรรมสัณฐานแกมมาเป็นสัณฐานที่เสถียร ในขณะที่สัณฐานแอลฟาเป็น สัณฐานที่ไม่เสถียร

จลนศาสตร์ของการตกผลึก และจลนศาสตร์ของการละลาย ถูกศึกษาและวัดค่าเพื่อนำไป อธิบายพฤติกรรมการตกผลึกและการเปลี่ยนรูปผลึก โดยอาศัยสารละลายเป็นสื่อกลาง และ นอกจากนั้นยังถูกนำไปใช้ในการจำลองกระบวนการดังกล่าวโดยใช้วิธีการจำลองของสมการสมดุล ประชากร (population balance equation) ของผลึก ผลการทดลองพบว่าอัตราการเกิดนิวคลีโอซัน ของสัณฐานแกมมามีค่าเพิ่มขึ้นตามอุณหภูมิและมีค่าเพิ่มขึ้นแบบเลขชี้กำลังตามค่าความเข้มข้น ยิ่งยวด (supersaturation) จลนศาสตร์ของการเกิดนิวคลีโอซันสามารถอธิบายได้ด้วยทฤษฎีการเกิด นิวคลีโอซันแบบคลาสสิก (classical nucleation theory) และสามารถใช้ในการประมาณค่าพลังงาน พื้นผิว (interfacial energy) ได้โดยการเปรียบเทียบกับผลการทดลอง จุดเริ่มต้นของการเกิด นิวคลีโอซันแบบทุติยภูมิ (secondary nucleation threshold) ถูกวัดก่อนทดลองหาอัตราการเติบโต ของผลึก เพื่อให้แน่ใจว่าไม่มีนิวคลีโอซันเกิดขึ้นในกระบวนการตกผลึก ผลการทดลองพบว่าอัตรา การเติบโตของผลึกของสัณฐานแอลฟาและสัณฐานแกมมามีค่าเพิ่มขึ้นแบบเส้นตรงตามค่าความ

เข้มข้นยิ่งยวด อัตราการละลายของผลึกของสัณฐานแอมมามีค่าเพิ่มขึ้นแบบเส้นตรงตามค่าความเข้มข้นต่ำกว่าสมดุล (undersaturation) ค่าคงที่ของอัตราการเติบโตและการละลายของผลึกของทั้งสองสัณฐานมีค่าเพิ่มขึ้นตามการเพิ่มขึ้นของอุณหภูมิ และเป็นไปตามความสัมพันธ์ของอาร์เรเนียส (Arrhenius relationship)

การเปลี่ยนรูปผลึกจากสัณฐานแอลฟาไปเป็นสัณฐานแอมมาโดยอาศัยสารละลายน้ำเป็นสื่อกลาง ถูกศึกษาโดยการตกผลึกแบบกะโดยใช้ตัวล่อ (seeded batch crystallization) การศึกษาพฤติกรรมของการเปลี่ยนรูปผลึกดังกล่าวสามารถสังเกตได้จากค่าการเปลี่ยนแปลงของความเข้มข้นของตัวถูกละลายและค่าอัตราส่วนโดยมวลของผลึกของสัณฐานแอมมาที่ได้ออกมาที่เวลา ผลการทดลองพบว่ากระบวนการเปลี่ยนรูปผลึกประกอบด้วยสองส่วนที่เกิดขึ้นพร้อม ๆ กัน คือ (ก) การละลายของผลึกของสัณฐานแอลฟา และ (ข) การเกิดนิวเคลียสและการเติบโตของผลึกของสัณฐานแอมมา โดยที่การละลายของผลึกของสัณฐานแอลฟาเป็นขั้นตอนที่ควบคุมกระบวนการเปลี่ยนรูปผลึกจากสัณฐานแอลฟาไปเป็นสัณฐานแอมมา

การจำลองกระบวนการเปลี่ยนรูปผลึก ทำโดยใช้ข้อมูลคุณสมบัติทางอุณหพลศาสตร์และจลนศาสตร์ต่าง ๆ ของทั้งสองสัณฐานที่ได้จากการทดลองมาประกอบเข้ากับสมการสมดุลประชากรของผลึก พร้อมทั้งเปรียบเทียบผลจำลองที่ได้กับผลการทดลอง ผลการจำลองพบว่าเกิดความแตกต่างเป็นอย่างมากระหว่างผลการทดลองกับผลการจำลองหากเอาค่าจลนศาสตร์ต่าง ๆ ที่ได้จากการทดลองโดยตรง (โดยเฉพาะอย่างยิ่ง จลนศาสตร์ของการละลายของผลึกของสัณฐานแอลฟา) มาใช้ แต่อย่างไรก็ตามความแตกต่างระหว่างผลการทดลองกับผลการจำลองมีค่าลดลงหรือค่าทั้งสองมีค่าใกล้เคียงกันมากขึ้น เมื่อมีการปรับเปลี่ยนจลนศาสตร์ของการละลายของผลึกของสัณฐานแอลฟา นั่นคือทำการปรับเปลี่ยนค่าพารามิเตอร์  $K_{D\alpha}$  จนกระทั่งทำให้ผลการทดลองกับผลการจำลองมีค่าใกล้เคียงกันมากที่สุด

LEK WANTHA : POLYMORPHISM AND SOLUTION-MEDIATED  
TRANSFORMATION OF DL-METHIONINE. THESIS ADVISOR :  
ASSOC. PROF. ADRIAN E. FLOOD, Ph.D. 277 PP.

POLYMORPHISM/THERMODYNAMICS/CRYSTALLIZATION KINETICS/  
SOLUTION-MEDIATED TRANSFORMATION/DL-METHIONINE

There are three known polymorphic forms of DL-methionine (DL-met),  $\alpha$ -DL-met,  $\beta$ -DL-met and  $\gamma$ -DL-met. The formation of polymorphs is usually determined by thermodynamics, crystallization and dissolution kinetics, and transformation kinetics. This thesis aims to understand and predict the thermodynamics and kinetics of the two commonly found polymorphs of DL-met ( $\alpha$ -DL-met and  $\gamma$ -DL-met). The behaviors of the crystallization and the solution-mediated transformation (SMT) of  $\alpha$ -DL-met into  $\gamma$ -DL-met in aqueous solutions were also studied.

The solubility of  $\alpha$ -DL-met in water is higher than  $\gamma$ -DL-met. The melting temperature and enthalpy of fusion of  $\gamma$ -DL-met are higher than those of  $\alpha$ -DL-met. The Gibbs free energy of  $\alpha$ -DL-met is higher than  $\gamma$ -DL-met. These properties of the two polymorphs strongly suggest that the system is a monotropic polymorph system where  $\gamma$ -DL-met is the stable polymorph and  $\alpha$ -DL-met is the metastable polymorph under the range of conditions useful for industrial crystallization.

The crystallization and dissolution kinetics were measured and these were used to describe the behavior of the SMT and used in simulations involving the population balance equation (PBE) model. The secondary nucleation threshold (SNT) was determined to ensure that growth was measured under convenient non-nucleating conditions. The nucleation rates of  $\gamma$ -DL-met increase exponentially with respect to the

supersaturation of DL-met and increase with increasing temperature. The measured nucleation kinetics can be described by the classical nucleation theory (CNT) and allow approximate interfacial energies to be estimated by fitting the measured data to CNT. The growth rates of both polymorphs were a linear function of the relative supersaturation and the dissolution rate of  $\gamma$ -DL-met was a linear function of the relative undersaturation. The growth and dissolution rate constants increase with increasing temperature and follow an Arrhenius relationship.

The SMT of  $\alpha$ -DL-met into  $\gamma$ -DL-met in water at 25 °C was studied via a seeded batch crystallization process. The change of the solute concentration and the fraction of  $\gamma$ -DL-met with time during the crystallization process were used to describe the behavior of the SMT. The SMT process consists of the dissolution of  $\alpha$ -DL-met and the crystallization (nucleation and growth) of  $\gamma$ -DL-met; the transformation is a dissolution controlled process. Models of the SMT process were developed based on the PBE models. The results showed the PBE models did not satisfactorily describe the SMT process of DL-met when the measured crystallization and dissolution kinetics were used; there were large mismatches between the simulation and experimental results. Improving the model of the dissolution kinetics of  $\alpha$ -DL-met (which in fact appear different to those of the  $\gamma$ -form) enabled these mismatches to be lowered, and this was done by re-estimating only a single dissolution kinetic parameter,  $K_{D\alpha}$ .

School of Chemical Engineering

Academic Year 2011

Student's Signature \_\_\_\_\_

Advisor's Signature \_\_\_\_\_

## ACKNOWLEDGEMENTS

First and foremost, I would like to express my sincere gratitude to my thesis advisor Assoc. Prof. Dr. Adrian E. Flood for his supporting information and invaluable advice and encouragement that have helped me pass through my difficult times. I appreciate his contributions of time, ideas, and funding in order to make my Ph.D. experience very productive and enormously stimulating. I would like to thank him again very much for everything, especially for all the careful checking, reading, correcting which he has done for this thesis.

I would like to express my appreciation to my thesis examining committee: Dr. Terasut Sookkummerd, Prof. Dr. Chaiyot Tangsathitkulchai, Asst. Prof. Dr. Boris Golman, and Asst. Prof. Dr. Sopark Sonwai for their wonderful questions and guidance.

I would like to thank all of the lecturers at the School of Chemical Engineering, Suranaree University of Technology (SUT) for their good attitude and advice. Especially, I would like to thank Asst. Prof. Dr. Chalongsri Flood, Asst. Prof. Dr. Atichat Wongkoblaph, Asst. Prof. Dr. Panarat Rattanaphanee, and Dr. Supunnee Junpirom. I would also like to thank all of my friends who are graduate students in the School of Chemical Engineering, who shared the experience of graduate student life, and who have made this experience very joyous and memorable. Thanks also are due to Dr. Sukanya and Ms. Natthaya for their invaluable assistance and for their great advice.

The assistance from the technical staff in the Center for Scientific and Technology Equipment, SUT, are appreciated, especially Mrs. Nongnaphat, Mr. Prasit, Mr. Anuchit, Mrs. Sujitra, Mrs. Janjira, and Ms. Utika. Many thanks go to Mrs. Amporn for her skillfull secretarial work and assistance. Many thanks also go to Mr. Saran for his skillfull technical work and assistance.

I gratefully acknowledge the funding sources that made my Ph.D. work possible, especially the Commission on Higher Education, Thailand through the program of Strategic Scholarships for Frontier Research Network for the Ph.D. Program Thai Doctoral degree for sponsoring my study and support for research. Part of the financial support of this work was provided by SUT research fund.

I would like to express my honest gratefulness to everyone in my family, especially my parents for their love and care.

Finally, I gratefully acknowledge the invaluable help of everyone I may have forgotten to mention here.

Lek Wantha

# TABLE OF CONTENTS

	<b>Page</b>
ABSTRACT (THAI).....	I
ABSTRACT (ENGLISH).....	III
ACKNOWLEDGEMENTS .....	V
TABLE OF CONTENTS.....	VII
LIST OF TABLES.....	XIV
LIST OF FIGURES.....	XVII
SYMBOLS AND ABBREVIATIONS.....	XXVIII
<b>CHAPTER</b>	
<b>I INTRODUCTION.....</b>	<b>1</b>
1.1 Background and Significance.....	1
1.2 Research Objectives.....	8
1.3 Scope of Work.....	9
1.4 Research Development.....	10
1.5 Output.....	10
1.6 References.....	11
<b>II POLYMORPHISM AND THERMODYNAMICS</b>	
<b>OF DL-METHIONINE.....</b>	<b>17</b>
2.1 Abstract.....	17
2.2 Introduction.....	18

**TABLE OF CONTENTS (Continued)**

	<b>Page</b>
2.3 Theory .....	23
2.3.1 Definition of Polymorphism.....	23
2.3.2 Solubility and Thermodynamics of Polymorphism.....	26
2.4 Materials and Methods.....	33
2.4.1 Materials.....	33
2.4.2 Apparatus .....	34
2.4.3 Preparation of Na-Met Aqueous Solution.....	34
2.4.4 Preparation of Polymorph .....	35
2.4.5 Polymorph Characterization.....	36
2.4.6 Solubility Measurement .....	36
2.4.7 Characterization of Uncertainty .....	37
2.5 Results and Discussions .....	37
2.5.1 Polymorphism .....	37
2.5.2 Solubility .....	41
2.5.3 Thermodynamics.....	45
2.5.4 The Polymorphic Nature of DL-Met .....	48
2.6 Conclusions.....	49
2.7 References.....	49

## TABLE OF CONTENTS (Continued)

	Page
<b>III SECONDARY NUCLEATION THRESHOLD AND NUCLEATION KINETICS OF <math>\gamma</math>-DL-METHIONINE.....</b>	<b>58</b>
3.1 Abstract.....	58
3.2 Introduction.....	58
3.3 Theory.....	65
3.3.1 Supersaturation.....	66
3.3.2 Metastable Zone and Secondary Nucleation Threshold.....	68
3.3.3 Nucleation Kinetics.....	70
3.4 Materials and Methods.....	75
3.4.1 Materials.....	75
3.4.2 Apparatus.....	75
3.4.3 Secondary Nucleation Threshold Measurement.....	75
3.4.4 Nucleation Rate Measurement.....	76
3.4.5 Characterization of Uncertainty.....	80
3.5 Results and Discussions.....	80
3.5.1 Secondary Nucleation Threshold.....	80
3.5.2 Nucleation Kinetics of $\gamma$ -DL-Met.....	85

## TABLE OF CONTENTS (Continued)

	Page
3.6 Conclusions.....	92
3.7 References.....	93
<b>IV GROWTH AND DISSOLUTION KINETICS OF</b>	
<b><math>\alpha</math> AND <math>\gamma</math> POLYMORPHS OF DL-METHIONINE .....</b>	<b>100</b>
4.1 Abstract.....	100
4.2 Introduction.....	101
4.3 Theory.....	105
4.3.1 Supersaturation and Undersaturation.....	105
4.3.2 Crystal Growth.....	105
4.3.3 Crystal Dissolution .....	111
4.4 Materials and Methods.....	113
4.4.1 Materials.....	113
4.4.2 Apparatus .....	113
4.4.3 Preparation of the Polymorphic Forms of DL-Met.....	114
4.4.4 Crystal Growth Rate Measurement.....	114
4.4.5 Crystal Dissolution Rate Measurement .....	117
4.5 Results and Discussions.....	118
4.5.1 Crystal Growth Kinetics of $\alpha$ -DL-Met and $\gamma$ -DL-Met.....	118

## TABLE OF CONTENTS (Continued)

	<b>Page</b>
4.5.2 Crystal Dissolution Kinetics.....	133
4.5.3 Discussion .....	141
4.6 Conclusions.....	142
4.7 References.....	143
<b>V POLYMORPHIC TRANSFORMATION OF</b>	
<b>DL-METHIONINE IN AQUEOUS SOLUTION:</b>	
<b>EXPERIMENTATION.....</b>	<b>148</b>
5.1 Abstract.....	148
5.2 Introduction .....	149
5.3 Theory.....	153
5.4 Experimental Methods.....	156
5.4.1 Materials.....	156
5.4.2 Apparatus .....	156
5.4.3 Preparation of Polymorph.....	157
5.4.4 Analysis of the Polymorphic Fraction.....	157
5.4.5 Polymorphic Transformation Experiments.....	161
5.4.6 Characterization of Uncertainty.....	163
5.5 Results and Discussions.....	163
5.5.1 Analysis of the Polymorphic Fraction .....	163
5.5.2 Polymorphic Transformation.....	166

## TABLE OF CONTENTS (Continued)

	<b>Page</b>
5.5.3 Discussion .....	176
5.6 Conclusions .....	177
5.7 References .....	178
<b>VI POLYMORPHIC TRANSFORMATION OF DL-METHIONINE IN AQUEOUS SOLUTION: MODELING .....</b>	<b>183</b>
6.1 Abstract .....	183
6.2 Introduction .....	184
6.3 Theory .....	189
6.3.1 Population Balance .....	189
6.3.2 Mass Balance .....	191
6.3.3 Method of Moments .....	192
6.3.4 Numerical Solution of the Ordinary Differential Equations .....	195
6.4 Modeling Methods .....	197
6.4.1 Mathematical Development .....	197
6.4.2 Crystallization and Dissolution Kinetics .....	201
6.4.3 Material Properties for the Mathematical Model .....	203
6.4.4 Initial Conditions .....	203

## TABLE OF CONTENTS (Continued)

	<b>Page</b>
6.4.5 Numerical Solution Procedures .....	204
6.4.6 Parameter Estimation .....	207
6.5 Results and Discussions .....	208
6.6 Conclusions .....	218
6.7 References .....	219
<b>VII CONCLUSIONS AND RECOMMENDATIONS.....</b>	<b>223</b>
7.1 Conclusions .....	223
7.2 Recommendations .....	227
 <b>APPENDICES</b>	
APPENDIX A. CONFIDENCE INTERVAL FOR MEAN VALUES.....	229
APPENDIX B. CONFIRMATION OF THE LOG-NORMAL DISTRIBUTION.....	233
APPENDIX C. SIMULATION RESULTS.....	238
APPENDIX D. EXAMPLE OF THE SOLUTION-MEDIATED TRANSFORMATION CODE.....	248
APPENDIX E. LIST OF PUBLICATIONS AND CONFERENCE PROCEEDINGS.....	258
<b>BIOGRAPHY.....</b>	<b>277</b>

## LIST OF TABLES

<b>Table</b>		<b>Page</b>
2.1	Crystallographic data of each polymorph of DL-met.....	22
2.2	Thermodynamic parameters of $\alpha$ -DL-met and $\gamma$ -DL-met.....	38
2.3	Solubility of $\alpha$ -DL-met and $\gamma$ -DL-met in water.....	42
2.4	Mole fraction solubility ( $x$ ) of $\alpha$ -DL-met and $\gamma$ -DL-met in water.....	46
3.1	Experimental conditions for nucleation measurements.....	79
3.2	Secondary nucleation experimental results at 10 °C, replicate number 1.....	81
3.3	The predicted constants $a$ and $b$ in equation (3.18), and calculated nucleation rate ( $J$ ) from equation (3.21).....	90
3.4	The predicted interfacial energy and pre-exponential factor.....	92
4.1	Experimental conditions for the growth experiments.  The seed size of $\alpha$ -DL-met is 64 - 125 $\mu\text{m}$ and that of $\gamma$ -DL-met is 180 - 250 $\mu\text{m}$ .....	116
4.2	Experimental conditions for the dissolution experiments.  The seed is only $\gamma$ -DL-met.....	117
4.3	Example for calculation of crystal growth rates as a function of relative supersaturation for experimental results of a batch run of $\gamma$ -DL-met at 25 °C and initial supersaturation of 0.114.....	124

## LIST OF TABLES (Continued)

Table	Page
4.4	Example for calculation of crystal dissolution rates as a function of relative undersaturation for experimental results of a batch run of $\gamma$ -DL-met at 25 °C and initial undersaturation of 0.082 .....135
4.5	Dissolution and growth kinetic parameters of the polymorphs of DL-met.....139
5.1	Compositions of the synthetic mixtures for the multi-component system. Note that the weight percent of $\gamma$ -DL-met is based on the binary mixture of $\alpha$ -DL-met and $\gamma$ -DL-met.....160
5.2	Experimental conditions of the polymorphic transformation experiments where the seed is $\alpha$ -DL-met. SNT indicates the SNT for $\gamma$ -DL-met.....162
6.1	Crystallization and dissolution kinetic parameters .....202
6.2	The physical properties of the polymorphs used in the models.....203
6.3	Initial conditions for the model at 25 °C with initial solute concentration of 40.5 kg/m <sup>3</sup> and the induction time in the period of 0 - 30 min .....204
6.4	Initial conditions for the model at 25 °C with initial solute concentration of 37.0 kg/m <sup>3</sup> and the induction time is in the period of 2 - 3 days .....204

**LIST OF TABLES (Continued)**

<b>Table</b>	<b>Page</b>
A.1 Percentage points $t_{\alpha,\nu}$ of the t-distribution.....	231
B.1 Particle size distribution of product crystals obtained at 45 min for the growth experiment of $\gamma$ -DL-met at 25 °C and $\sigma_{G0} = 0.114$ .....	235



## LIST OF FIGURES

Figure	Page
2.1	Chemical structure of methionine .....20
2.2	Predicted morphologies of the polymorphs of DL-methionine by the BFDH method. $\alpha$ -DL-met (a), $\beta$ -DL-met (b) and $\gamma$ -DL-met (c).....22
2.3	Polymorphs of L-glutamic acid. (a) crystal of the metastable alpha phase, and (b) crystal of the stable beta phase.....24
2.4	Polymorphs of barium fluoride. (a) crystal of metastable phase II, and (b) crystal of stable phase I .....24
2.5	Fundamental <i>E/T</i> diagram of a dimorphic enantiotropic system.....30
2.6	Fundamental <i>E/T</i> diagram of a dimorphic monotropic system.....31
2.7	Solubility curves for two polymorphic forms of L-glutamic acid .....32
2.8	Solubility curves of L-phenylalanine polymorph .....33
2.9	The 0.5 L batch crystallizer.....34
2.10	DSC curves of $\alpha$ -DL-met and $\gamma$ -DL-met crystals. The sample weight was 2.10 mg and the heating rate was 10 °C/min. A nitrogen purge was used.....38
2.11	PXRD patterns of $\alpha$ -DL-met and $\gamma$ -DL-met crystals .....40
2.12	Photomicrographs of $\alpha$ -DL-met (a) and $\gamma$ -DL-met (b) crystals .....40
2.13	Dissolution profiles for $\alpha$ -DL-met and $\gamma$ -DL-met in water.....42
2.14	Solubility of $\alpha$ -DL-met and $\gamma$ -DL-met in water .....43

## LIST OF FIGURES (Continued)

Figure	Page
2.15	Plot of van't Hoff solubility data of real and ideal solubility of $\alpha$ -DL-met and $\gamma$ -DL-met in water .....47
2.16	Plot of Gibbs free energy of $\alpha$ -DL-met and $\gamma$ -DL-met. The solid lines are given to guide the eye .....48
3.1	Instantaneous metastable zone widths for different nucleation mechanisms. The variables $t_{SNT}$ , $t_{ind,HEN}$ , and $t_{ind,HON}$ , are the induction time for secondary nucleation, heterogeneous, and homogeneous nucleation, respectively.....69
3.2	A diagrammatic representation of the secondary nucleation thresholds of solution crystallization.....70
3.3	Position in the phase diagram and temperature profile during a nucleation experiment .....77
3.4	Schematic of the experiment setup. The nucleation cell is made from acrylic, and flat-bottom wells are used .....78
3.5	The time dependence of the secondary nucleation zone width based on DL-met concentrations at temperatures of 10, 25, 40, and 61 °C. The dashed line represents the model for data at 10 and 25 °C. The solid line represents the model for 40 and 61 °C .....82

## LIST OF FIGURES (Continued)

Figure	Page
3.6	Secondary nucleation thresholds for $\gamma$ -DL-met at operating times of 0.1, 0.5, 1.0, and 2.0 h.....84
3.7	Micrographs of crystals nucleated in a droplet at various nucleation times; measurement at 18 °C and $S = 1.36$ : 10 s (a), 15 s (b), 40 s (c), 60 s (d).....85
3.8	Mean number of crystals as a function of nucleation time ( $\Delta t_1$ ) and supersaturation at 18 °C .....88
3.9	Mean number of crystals as a function of nucleation time ( $\Delta t_1$ ) and supersaturation at 25 °C .....88
3.10	Mean number of crystals as a function of nucleation time ( $\Delta t_1$ ) and supersaturation at 35 °C .....89
3.11	Nucleation rate as a function of supersaturation.....91
4.1	The model representation of the concentration driving force (a), and the two-step crystal growth process (b).....106
4.2	Development of a crystal growth spiral starting from a screw dislocation .....110
4.3	Crystal growth arising from a surface nucleation (birth and spread) mechanism.....110
4.4	Particle size distributions of seed and product crystals for the growth experiment of $\alpha$ -DL-met at 25 °C and $\sigma_{G0} = 0.043$ .....120

## LIST OF FIGURES (Continued)

Figure	Page
4.5	Particle size distributions of seed and product crystals for the growth experiment of $\gamma$ -DL-met at 25 °C and $\sigma_{G0} = 0.114$ .....120
4.6	Photomicrographs of seed crystals and product crystals from the growth experiment of $\alpha$ -DL-met at 25 °C and $\sigma_{G0} = 0.043$ .....121
4.7	Photomicrographs of seed crystals and product crystals from the growth experiment of $\gamma$ -DL-met at 25 °C and $\sigma_{G0} = 0.114$ .....122
4.8	Desupersaturation curves and time dependence of crystal sizes from a batch run of $\gamma$ -DL-met at 25 °C with different initial supersaturation.....125
4.9	Desupersaturation curves and time dependence of crystal sizes from a batch run of $\gamma$ -DL-met at 25 °C with different seed masses. The solid lines are given to guide the eye.....126
4.10	Desupersaturation curves from a batch run of $\gamma$ -DL-met at different temperatures. The solid lines are given to guide the eye.....127
4.11	Mean crystal growth rates for $\alpha$ -DL-met as a function of relative supersaturation at 25 °C with different initial supersaturation.....129
4.12	Mean crystal growth rates for $\gamma$ -DL-met as a function of relative supersaturation at 25 °C with different initial supersaturation .....129
4.13	Mean crystal growth rates for $\gamma$ -DL-met as a function of relative supersaturation at 25 °C with different seed masses.....130

## LIST OF FIGURES (Continued)

Figure	Page
4.14 Mean crystal growth rates of $\alpha$ -DL-met as a function of relative supersaturation and temperature .....	132
4.15 Mean crystal growth rates of $\gamma$ -DL-met as a function of relative supersaturation and temperature .....	132
4.16 Particle size distributions of seed and crystals in suspension vs time from a dissolution experiment of $\gamma$ -DL-met at 25 °C and $\sigma_{D0} = 0.082$ .....	133
4.17 Photomicrographs of seed and final crystals from dissolution experiment of $\gamma$ -DL-met at 25 °C and $\sigma_{D0} = 0.082$ .....	134
4.18 Time dependence of undersaturation and crystal sizes from a batch run of $\gamma$ -DL-met at 25 °C with different initial undersaturations.....	136
4.19 Mean dissolution rates for $\gamma$ -DL-met as a function of relative undersaturation at 25 °C with different initial undersaturation.....	137
4.20 Mean dissolution rates of $\gamma$ -DL-met as a function of relative undersaturation and temperature.....	139
4.21 An Arrhenius plot of the growth rate and dissolution rate constants for DL-met for determination of the activation energy of crystal growth and dissolution .....	140
4.22 Mean dissolution rates of $\gamma$ -DL-met as a function of relative undersaturation at 25 °C with different seed sizes.....	141

## LIST OF FIGURES (Continued)

Figure	Page
5.1 Thermodynamic and kinetic features of the SMT: (a) typical solubility curves of a monotropically related stable polymorph (polymorph I) and metastable polymorph (polymorph II), (b) general features of the time dependence of supersaturation ratios in a SMT.....	154
5.2 Concentration as a function of time during SMT: curve (1) growth-controlled transformation, curve (2) dissolution-controlled transformation.....	156
5.3 XRPD patterns for $\alpha$ -DL-met, $\gamma$ -DL-met, and NaCl.....	158
5.4 XRPD patterns ( $5 - 50^\circ 2\theta$ ) of various compositions of $\alpha$ -DL-met, $\gamma$ -DL-met, and NaCl.....	164
5.5 The calibration curve for analysis of the fraction of $\gamma$ -DL-met based on the peak intensities. XRPD measurements (circle) and the fit (solid line).....	165
5.6 The calibration curve for analysis of the fraction of $\gamma$ -DL-met based on the area of the peaks. XRPD measurements (circle) and the fit (solid line).....	166
5.7 XRPD patterns of the solid mixture taken at various times during the polymorphic transformation of $\alpha$ -DL-met into $\gamma$ -DL-met at $25^\circ\text{C}$ and $C_0 = 40.5 \text{ g DL-met/kg water}$ .....	168

## LIST OF FIGURES (Continued)

Figure	Page
5.8 Solute concentration and fraction of $\gamma$ -DL-met in the crystal phase during the polymorphic transformation of $\alpha$ -DL-met into $\gamma$ -DL-met at 25 °C and $C_0 = 40.5$ g DL-met/kg water. The solid lines are given to guide the eye.....	169
5.9 The magnification of the solute concentration in Figure 5.8 in the range of 0 - 60 min. The solid line is given to guide the eye.....	170
5.10 XRPD patterns of the solid mixture taken at various times during the polymorphic transformation of $\alpha$ -DL-met into $\gamma$ -DL-met at 25 °C and $C_0 = 37.0$ g DL-met/kg water.....	173
5.11 Solute concentration and fraction of $\gamma$ -DL-met in the crystal phase during the polymorphic transformation of $\alpha$ -DL-met into $\gamma$ -DL-met at 25 °C and $C_0 = 37.0$ g DL-met/kg water. The solid lines are given to guide the eye.....	174
5.12 The magnification of the solute concentration in Figure 5.11 in the range of 0 - 70 min. The solid line is given to guide the eye.....	175
6.1 Euler's method .....	196
6.2 Seeded batch crystallization system.....	197
6.3 The simulated solute concentration profiles during the first 60 min for the simulation at 25 °C with initial solute concentration of 40.5 kg/m <sup>3</sup> .....	206

## LIST OF FIGURES (Continued)

Figure	Page
6.4 Comparison between simulated and experimental solute concentration and fraction of $\gamma$ -DL-met in the crystal phase during the polymorphic transformation of $\alpha$ -DL-met into $\gamma$ -DL-met at 25 °C and $C_0 = 40.5 \text{ kg/m}^3$ . The dissolution kinetics obtained from Chapter IV were applied to the simulation.....	209
6.5 The magnification of the comparison between simulated and experimental solute concentration in Figure 6.4 on the range of 0 - 60 min.....	210
6.6 Comparison between simulated and experimental solute concentration and fraction of $\gamma$ -DL-met in the crystal phase during the polymorphic transformation of $\alpha$ -DL-met into $\gamma$ -DL-met at 25 °C and $C_0 = 37.0 \text{ kg/m}^3$ . The dissolution kinetics obtained from Chapter IV were applied to the simulation.....	211
6.7 The magnification of the comparison between simulated and experimental solute concentration in Figure 6.6 in the range of 0 - 70 min.....	212

## LIST OF FIGURES (Continued)

Figure	Page
6.8 Comparison between simulated and experimental solute concentration and fraction of $\gamma$ -DL-met in the crystal phase during the polymorphic transformation of $\alpha$ -DL-met into $\gamma$ -DL-met at 25 °C and $C_0 = 40.5 \text{ kg/m}^3$ . The dissolution kinetics were estimated from the combination of the modeling method with the SMT experimental data.....	214
6.9 The magnification of the comparison between simulated and experimental solute concentration in Figure 6.8 on the range of 0 - 60 min.....	215
6.10 Comparison between simulated and experimental solute concentration and fraction of $\gamma$ -DL-met in the crystal phase during the polymorphic transformation of $\alpha$ -DL-met into $\gamma$ -DL-met at 25 °C and $C_0 = 37.0 \text{ kg/m}^3$ . The dissolution kinetics were estimated from the combination of the modeling method with the SMT experimental data.....	216
6.11 The magnification of the comparison between simulated and experimental solute concentration in Figure 6.10 on the range of 0 - 70 min.....	217
B.1 Particle size distribution of product crystals obtained at 45 min for the growth experiment of $\gamma$ -DL-met at 25 °C and $\sigma_{G0} = 0.114$ .....	236

## LIST OF FIGURES (Continued)

Figure	Page
B.2	Plot of the PSD of product crystals obtained at 45 min for the growth experiment of $\gamma$ -DL-met at 25 °C and $\sigma_{G0} = 0.114$ on log-normal probability paper.....237
C.1	The change of $\mu_{\alpha,0}$ with time during the SMT of $\alpha$ -DL-met into $\gamma$ -DL-met at 25 °C, $C_0 = 40.5 \text{ kg/m}^3$ and $K_{D\alpha} = 7.4766 \times 10^{-9} \text{ m/s}$ .....240
C.2	The change of $\mu_{\alpha,1}$ with time during the SMT of $\alpha$ -DL-met into $\gamma$ -DL-met at 25 °C, $C_0 = 40.5 \text{ kg/m}^3$ and $K_{D\alpha} = 7.4766 \times 10^{-9} \text{ m/s}$ .....240
C.3	The change of $\mu_{\alpha,2}$ with time during the SMT of $\alpha$ -DL-met into $\gamma$ -DL-met at 25 °C, $C_0 = 40.5 \text{ kg/m}^3$ and $K_{D\alpha} = 7.4766 \times 10^{-9} \text{ m/s}$ .....241
C.4	The change of $\mu_{\alpha,3}$ with time during the SMT of $\alpha$ -DL-met into $\gamma$ -DL-met at 25 °C, $C_0 = 40.5 \text{ kg/m}^3$ and $K_{D\alpha} = 7.4766 \times 10^{-9} \text{ m/s}$ .....241
C.5	The change of $\mu_{\gamma,0}$ with time during the SMT of $\alpha$ -DL-met into $\gamma$ -DL-met at 25 °C, $C_0 = 40.5 \text{ kg/m}^3$ and $K_{D\alpha} = 7.4766 \times 10^{-9} \text{ m/s}$ .....242
C.6	The change of $\mu_{\gamma,1}$ with time during the SMT of $\alpha$ -DL-met into $\gamma$ -DL-met at 25 °C, $C_0 = 40.5 \text{ kg/m}^3$ and $K_{D\alpha} = 7.4766 \times 10^{-9} \text{ m/s}$ .....242
C.7	The change of $\mu_{\gamma,2}$ with time during the SMT of $\alpha$ -DL-met into $\gamma$ -DL-met at 25 °C, $C_0 = 40.5 \text{ kg/m}^3$ and $K_{D\alpha} = 7.4766 \times 10^{-9} \text{ m/s}$ .....243
C.8	The change of $\mu_{\gamma,3}$ with time during the SMT of $\alpha$ -DL-met into $\gamma$ -DL-met at 25 °C, $C_0 = 40.5 \text{ kg/m}^3$ and $K_{D\alpha} = 7.4766 \times 10^{-9} \text{ m/s}$ .....243
C.9	The change of $\mu_{\alpha,0}$ with time during the SMT of $\alpha$ -DL-met into $\gamma$ -DL-met at 25 °C, $C_0 = 37.0 \text{ kg/m}^3$ and $K_{D\alpha} = 7.4766 \times 10^{-9} \text{ m/s}$ .....244

## LIST OF FIGURES (Continued)

Figure	Page
C.10	The change of $\mu_{\alpha,1}$ with time during the SMT of $\alpha$ -DL-met into $\gamma$ -DL-met at 25 °C, $C_0 = 37.0 \text{ kg/m}^3$ and $K_{D\alpha} = 7.4766 \times 10^{-9} \text{ m/s}$ .....244
C.11	The change of $\mu_{\alpha,2}$ with time during the SMT of $\alpha$ -DL-met into $\gamma$ -DL-met at 25 °C, $C_0 = 37.0 \text{ kg/m}^3$ and $K_{D\alpha} = 7.4766 \times 10^{-9} \text{ m/s}$ .....245
C.12	The change of $\mu_{\alpha,3}$ with time during the SMT of $\alpha$ -DL-met into $\gamma$ -DL-met at 25 °C, $C_0 = 37.0 \text{ kg/m}^3$ and $K_{D\alpha} = 7.4766 \times 10^{-9} \text{ m/s}$ .....245
C.13	The change of $\mu_{\gamma,0}$ with time during the SMT of $\alpha$ -DL-met into $\gamma$ -DL-met at 25 °C, $C_0 = 37.0 \text{ kg/m}^3$ and $K_{D\alpha} = 7.4766 \times 10^{-9} \text{ m/s}$ .....246
C.14	The change of $\mu_{\gamma,1}$ with time during the SMT of $\alpha$ -DL-met into $\gamma$ -DL-met at 25 °C, $C_0 = 37.0 \text{ kg/m}^3$ and $K_{D\alpha} = 7.4766 \times 10^{-9} \text{ m/s}$ .....246
C.15	The change of $\mu_{\gamma,2}$ with time during the SMT of $\alpha$ -DL-met into $\gamma$ -DL-met at 25 °C, $C_0 = 37.0 \text{ kg/m}^3$ and $K_{D\alpha} = 7.4766 \times 10^{-9} \text{ m/s}$ .....247
C.16	The change of $\mu_{\gamma,3}$ with time during the SMT of $\alpha$ -DL-met into $\gamma$ -DL-met at 25 °C, $C_0 = 37.0 \text{ kg/m}^3$ and $K_{D\alpha} = 7.4766 \times 10^{-9} \text{ m/s}$ .....247

## SYMBOLS AND ABBREVIATIONS

### Symbols

$A$	=	Area under peak, - Pre-exponential kinetic parameter in nucleation model, $\text{m}^{-3} \text{s}^{-1}$ Surface area of crystal, $\text{m}^2$
$A_{BCF}$	=	Constant in Burton-Caberra-Frank growth model, $\text{m/s}$
$A_{B+S}$	=	Constant in birth and spread growth model, $\text{m/s}$
$a$	=	Characteristic length, $\text{\AA}$
$a$	=	Activity, - Exponent in secondary nucleation rate model, -
$B$	=	Birth term in population balance equation, $\#/\text{m}^3 \cdot \text{m} \cdot \text{s}$ Thermodynamic parameter in nucleation model, -
$B^0$	=	Nucleation rate, $\#/\text{m}^3 \cdot \text{s}$
$B_{BCF}$	=	Constant in Burton-Caberra-Frank growth model, -
$B_{B+S}$	=	Constant in birth and spread growth model, -
$b$	=	Characteristic length, $\text{\AA}$
$b$	=	Exponent in secondary nucleation rate model, -
$C$	=	Solute concentration, $\text{g solute/kg solvent}$ or $\text{kg solute}/\text{m}^3$ solution
$C^*$	=	Solubility, $\text{g solute/kg solvent}$ or $\text{kg solute}/\text{m}^3$ solution
$C_s$	=	Solid concentration, $\text{kg crystal}/\text{m}^3$ solution

## SYMBOLS AND ABBREVIATIONS (Continued)

$c$	=	Characteristic length, Å
$c$	=	Exponent in secondary nucleation rate model, -
$D$	=	Death term in population balance equation, $\#/m^3 \cdot m \cdot s$ Dissolution rate, m/s or $\mu m/min$
$\bar{D}$	=	Mean dissolution rate, m/s or $\mu m/min$
$d$	=	Exponent in secondary nucleation rate model, -
$E_D$	=	Activation energy of dissolution, kJ/mol
$E_G$	=	Activation energy of growth, kJ/mol
$G$	=	Gibbs free energy, J/mol Growth rate, m/s or $\mu m/min$
$\bar{G}$	=	Mean growth rate, m/s or $\mu m/min$
$H$	=	Enthalpy, J/mol
$\Delta H_{diss}$	=	Enthalpy of dissolution, J/mol
$\Delta H_{fus}$	=	Enthalpy of fusion, J/mol
$\Delta H_{t,III}$	=	Heat of transition, J/mol
$h$	=	Step size, s
$I$	=	Peak intensity, cps
$J$	=	Nucleation rate, $\#/m^3 \cdot s$
$K_D$	=	Dissolution rate constant, m/s or $\mu m/min$
$K_G$	=	Growth rate constant, m/s or $\mu m/min$
$k$	=	Boltzmann constant, $1.38 \times 10^{-23}$ J/K
$k_a$	=	Area shape factor, -

## SYMBOLS AND ABBREVIATIONS (Continued)

$k_D^0$	=	Pre-exponential constant in dissolution model, m/s or $\mu\text{m}/\text{min}$
$k_d$	=	Mass transfer coefficient, m/s
$k_G^0$	=	Pre-exponential constant in growth model, m/s or $\mu\text{m}/\text{min}$
$k_g$	=	Growth rate constant, m/s
$k_N$	=	Crystal nucleation rate constant, depends on model
$k_r$	=	Integration rate constant, m/s
$k_v$	=	Volume shape factor, -
$L$	=	Crystal size, m or $\mu\text{m}$
		Characteristic dimension, m or $\mu\text{m}$
$\bar{L}$	=	Number mean crystal size, $\mu\text{m}$
$L'$	=	Geometric median of the distribution, m or $\mu\text{m}$
$M$	=	Molecular mass, g/mol
$M_c$	=	Mass of the dried solid crystal, g
$M_{sol}$	=	Mass of the solution sample, g
$M_T$	=	Suspension density, g crystal/g suspension
$m$	=	Mass of crystal, kg
		Dissolution rate order, -
mp	=	Melting point, K
$N$	=	Cumulative number distribution, $\#/m^3$
		Number of crystal, #
		Number of experimental point, #
$N_A$	=	Avogadro number, $6.02 \times 10^{23} \text{ mol}^{-1}$

## SYMBOLS AND ABBREVIATIONS (Continued)

$N_{d,i}$	=	Number of the data points per experiment, #
$N_e$	=	Number of experiment, #
$n$	=	Growth rate order, -
		Number density distribution, $\#/m^3 \cdot m$
		Number of nuclei, #
$n^*$	=	Nucleus size, -
$p$	=	Exponent in birth and spread growth model, -
$Q$	=	Flow rate, $m^3/s$
$R$	=	Ideal gas constant, $8.314 \text{ J/mol} \cdot \text{K}$
$R_G$	=	Mass deposition flux, $\text{kg}/m^2 \cdot \text{s}$
rmsd	=	Root mean square deviation, -
$S$	=	Entropy, $\text{J}/\text{mol} \cdot \text{K}$
		Supersaturation ratio, -
$S_D$	=	Undersaturation ratio, -
$S_G$	=	Supersaturation ratio, -
$\Delta S_{diss}$	=	Entropy of dissolution, $\text{J}/\text{mol} \cdot \text{K}$
$\Delta S_{fus}$	=	Entropy of fusion, $\text{J}/\text{mol} \cdot \text{K}$
$s$	=	Standard deviation, depends on the measured variable
$T$	=	Temperature, K or $^{\circ}\text{C}$
$t$	=	Time, s or min or hr or day
$tp$	=	Transition point, K

## SYMBOLS AND ABBREVIATIONS (Continued)

$V$	=	Crystallizer volume, $m^3$
		Volume of the solution droplet, $\mu L$
$v_0$	=	Molecular volume, $m^3$
$W^*$	=	Nucleation work, J
$w$	=	Mass fraction, wt. %
$x$	=	Mole fraction of solute in the solution, -
		Solubility (as mole fractions), -
		Variable $x$ , depends on model
$x_{mV}$	=	Median of the volume distribution, $\mu m$
$x_{NL}$	=	Number mean crystal size, $\mu m$
$Y$	=	Calculation factor, -
$Y_A$	=	Calculation factor (based on area of the peaks), -
$Y_I$	=	Calculation factor (based on peak intensities), -
$y$	=	Variable $y$ , depends on model
$Z$	=	Number of molecule, molecule

### Greek Symbols

$\beta$	=	Characteristic angle, $^\circ$
$\Delta$	=	Change in a variable
$\gamma$	=	Activity coefficient, -
		Interfacial energy, $J/m^2$
$\gamma_{eff}$	=	Effective interfacial energy, $J/m^2$

## SYMBOLS AND ABBREVIATIONS (Continued)

$\rho$	=	Density, kg/m <sup>3</sup>
$\mu$	=	Chemical potential, J/mol
		$j^{\text{th}}$ moment about the origin, #·m <sup>j</sup> /m <sup>3</sup>
$\Delta\mu$	=	Supersaturation, J/mol
$\omega$	=	Agitation speed, s <sup>-1</sup>
$\sigma$	=	Relative supersaturation, -
$\sigma_D$	=	Relative undersaturation, -
$\sigma_G$	=	Relative supersaturation, -
$\sigma_g$	=	Geometric standard deviation of the volume distribution, $\mu\text{m}$

### Superscripts

*	=	Equilibrium
<i>exp</i>	=	Experimental value
<i>sim</i>	=	Simulated value

### Subscripts

<i>A</i>	=	Area under peak
<i>a</i>	=	Activity
$\alpha$	=	$\alpha$ -DL-methionine
<i>c</i>	=	Calculated value
		Crystal
<i>D</i>	=	Dissolution

## SYMBOLS AND ABBREVIATIONS (Continued)

<i>exp</i>	=	Experimental value
<i>fus</i>	=	Fusion
<i>G</i>	=	Growth
$\gamma$	=	$\gamma$ -DL-methionine
<i>HEN</i>	=	Heterogeneous nucleation
<i>HON</i>	=	Homogeneous nucleation
<i>I</i>	=	Peak intensity
		Polymorph I
<i>II</i>	=	Polymorph II
<i>i</i>	=	$i^{\text{th}}$ experimental point
		$i^{\text{th}}$ polymorph
		$i^{\text{th}}$ stream
		Bulk solution
		Interface
<i>in</i>	=	Inlet stream
<i>ind</i>	=	Induction
<i>j</i>	=	$j^{\text{th}}$ moment
<i>l</i>	=	Liquid
<i>liq</i>	=	Liquid
<i>N</i>	=	NaCl
<i>out</i>	=	Outlet stream
<i>SNT</i>	=	Secondary nucleation threshold

## SYMBOLS AND ABBREVIATIONS (Continued)

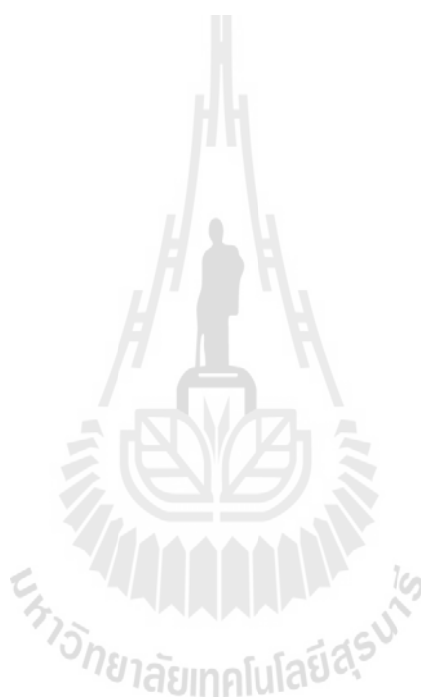
<i>s</i>	=	Seed crystal
		Solid
<i>sat</i>	=	Saturation
<i>sol</i>	=	Solution
<i>t</i>	=	Time
		Transition
0	=	Initial

### Abbreviations

$\alpha$ -DL-met	=	$\alpha$ -DL-methionine
BCF	=	Burton-Caberra-Frank growth model
CNT	=	Classical nucleation theory
DSC	=	Differential scanning calorimetry
$\gamma$ -DL-met	=	$\gamma$ -DL-methionine
HEN	=	Heterogeneous nucleation
HON	=	Homogeneous nucleation
Met	=	Methionine
Na-Met	=	Sodium methioninate
PBE	=	Population balance equation
PSD	=	Particle size distribution
SMT	=	Solution-mediated transformation
SNT	=	Secondary nucleation threshold

**SYMBOLS AND ABBREVIATIONS (Continued)**

SSE	=	Sum of square errors
SST	=	Solid-state transformation
XRPD	=	X-ray powder diffractometry



# CHAPTER I

## INTRODUCTION

### 1.1 Background and Significance

Amino acids are significant industrial chemicals, because they are important for human and animal nutrition (they are the basic building blocks of proteins, and many of common amino acids are essential for survival), but also because there are many which are important reagents in the production of other chemicals, including food additives (monosodium glutamate produced from glutamic acid for example, and aspartame from aspartic acid and phenylalanine), cosmetics and toiletries ('AMIHOPE LL', which is an amino acid based functional powder, and is produced from L-lysine), surfactants ('AMISOFT', which is produced from L-glutamic acid), and pharmaceuticals (L-DOPA: 3,4-dihydroxy-L-phenylalanine for management of Parkinson's disease, sleep aid, and appetite suppressant), among many other applications as reagents or intermediates, feed (animal nutrition) and other materials (optical material, biomaterial, etc.). (Ajinomoto Co., Inc. 2011; Flood, 2008)

Many amino acids occur as several crystal polymorphs (the same chemical in a different crystal structure) and/or pseudopolymorphs and solvates (the same chemical, but with a water or solvent molecule in the crystal structure) (Bernstein, 2002; Jiang, 2009; Mangin, Puel, and Veessler, 2009). Polymorphs and solvates can have different mechanical, thermal, physical, and chemical properties, such as compressibility, melting point, crystal habit, color, density, dissolution rate, and

solubility. These can have a great influence on the bioavailability, meaning the dissolution rate and solubility of the active pharmaceutical ingredient (the substance in a drug that is pharmaceutically active), hygroscopicity (the ability of a substance to attract water molecules from the surrounding environment through either absorption or adsorption), and stability (Mangin et al., 2009; Schmidt, 2005; Yu, Reutzel, and Stephenson, 1998). Also, polymorphs influence the downstream processing, such as filtration (Ferrari and Davey, 2004), drying (Matsunaga, Nambu, and Nagai, 1976), and grinding and tableting (Kaneniwa and Otsuka, 1985). Polymorphism is of great interest to many industries, such as the pharmaceutical, chemical, food, dye and pigment, and photographic industries (Bernstein, 2002).

In experimental and industrial crystallizations, if the crystallization kinetics of the metastable polymorph are faster than that of the stable polymorph, it is commonly observed that the metastable polymorph appears instead of the stable polymorph, and then the metastable polymorph may transform into the more stable one. This has been stated as a rule known as Ostwald's rule of stages (Threlfall, 2003). According to Ostwald's rule, in crystallization from the melt or from solution, the metastable polymorph forms first, followed by transformation to the more stable polymorph via the solution-mediated transformation (SMT) mechanism. It is generally known that this rule is not a physical law and that more stable polymorphs can crystallize directly as well (Roelands et al., 2006). In many cases, if both polymorphs crystallize at approximately similar rates, the two polymorphs may crystallize simultaneously from the solution, also called concomitant polymorphism (Bernstein, Davey, and Henck, 1999), even with the unstable polymorph predominating, and this is sometimes not acceptable from the point of view of obtaining polymorphically pure compounds

suitable for sale, particular in the food and other material products. On the other hand, in the field of pharmaceuticals, metastable polymorphs may be more desirable than stable one (Yamanobe, Takiyama, and Matsuoka, 2002).

Because of the different properties of polymorphs, it is advantageous to choose the proper polymorph for the desired application. Therefore, in the crystallization processes involving polymorphs, the formation of the desired polymorph has to be controlled and such a process should be robust and reproducible. In the polymorphic crystallization, relative nucleation rates, relative growth rates, and the transformation of crystallizing polymorphs should be controlled individually. The thermodynamic stability and the transformation behavior are influenced by temperature, because the dependence of the solubility of each polymorph on temperature is different between these crystals (Tóth, Kardos-Fodor, and Halász-Péterfi, 2005). The other influential factors are supersaturation (Kitamura, 2002), stirring rate (Cashell, Corcoran, and Hodnett, 2004), mixing rate of reactant solutions (in the case of reactive crystallization) (Kitamura, Konno, Yasui, and Masuoka, 2002), seeding (Kitamura, 1993; Maruyama and Ooshima, 2000), addition rate (Kim et al., 2003), solvents (Kitamura, Furukawa, and Asaeda, 1994; Kitamura and Nakamura, 2002), and additives (Mohan, Koo, Strege, and Myerson, 2001).

Therefore, the determination of the crystallization (nucleation and growth) and dissolution kinetics, and thermodynamics are important for characterization of the crystallization behavior and transformation of the polymorphs. Thermodynamics determines the polymorphic forms (stable or metastable) and their properties such as solubility (Anuar, Wan Daud, Roberts, Kamarudin, and Tasirin, 2009; Svärd, Nordström, Jasnobulka, and Rasmuson, 2010). The nucleation, growth and dissolution

kinetics determine the kinetics of the crystallization and SMT of the polymorphs. Usually, the crystallization kinetics of the metastable polymorphs should be faster than the stable polymorphs when the metastable polymorphs appear first and then transforms to more stable polymorphs (Bernstein et al., 1999; Rodríguez-Spong, Price, Jayasankar, Matzger, and Rodríguez-Hornedo, 2004). This has been found in various crystalline substances, for example, L-glutamic acid (Ono, ter Horst, and Jansens, 2004), L-histidine (Roelands et al., 2006), and *o*-aminobenzoic acid (Jiang, ter Horst, and Jansens, 2008). In the behavior of the SMT, the transformation process is usually controlled by the growth of the stable polymorph, for example, L-histidine (Kitamura, 1993), taltireline (Maruyama, Ooshima, and Kato, 1999), L-glutamic acid (Dharmayat et al., 2008; Ono, Kramer, ter Horst, and Jansens, 2004), and carbamazepine (Qu, Louhi-Kultanen, Rantanen, and Kallas, 2006). On the other hand, the dissolution rate of the metastable  $\beta$  polymorph is the rate-determining step in the glycine system (Ferrari, Davey, Cross, Gillon, and Towler, 2003).

The SMT can be studied by either monitoring the SMT during the crystallization or modeling the SMT. Monitoring the SMT is a method where the solute concentration, transformation time, polymorphic fraction, etc. are measured during crystallization from solution. There are many analytical techniques for measuring the polymorphic fraction (Bernstein, 2002), for example, infrared spectroscopy (IR), Raman spectroscopy,  $^{13}\text{C}$  solid-state nuclear magnetic resonance (SSNMR) spectroscopy, X-ray powder diffractometry (XRPD), differential scanning calorimetry (DSC), and Fourier transform infrared spectroscopy (FT-IR). These techniques can be used both off-line (Ferrari et al., 2003; Maruyama et al., 1999) and for in situ measurements (Dharmayat et al., 2008; Jiang, Jansens, and ter Horst, 2010).

Modeling the SMT can be carried in at least three ways: pseudoglobal processes using molecular modeling, estimating the kinetic rate expression of each mechanism from a combination of the population balance equation (PBE) and the results from a SMT experiment, and separately distinguishing each mechanism combined with the population balance equation (PBE). The first method makes it quite easy to determine the effects of several process parameters such as temperature or supersaturation level (Davey, Blagden, Righini, Alison, and Ferrari, 2002). The second method requires estimation of the rates of crystallization and dissolution of each polymorph using a combination of polymorphic fraction measurements and the supersaturation profile (which are obtained from the SMT experiment), and the PBE (Cornel, Kidambi, and Mazzotti, 2010; Ono, Kramer et al., 2004). The third method is a two step method (Scully, 2010; Févotte, Alexandre, and Nida, 2007). First, the rates of crystallization and dissolution of each polymorph are obtained through specific experiments. Second, the rates of crystallization and dissolution of each polymorph are then combined in the PBE in order to estimate the time of the transformation, polymorphic fraction profile, concentration profile, etc., which can then be compared with the results from a SMT experiment.

The kinetic parameter estimation from the simulation technique is not yet proven to agree with experiments performed on a single polymorphic form. The main disadvantage of this technique is that the results can be skewed by incorrect parameter estimation of other parameters, such as the crystal growth rate kinetics, which may lead to non-realistic estimates of nucleation rates. Due to the disadvantage of this technique, in this work the crystallization (nucleation and growth) and dissolution kinetics of each polymorph were experimentally determined and were then applied in

a PBE model of the SMT in order to estimate the time of the transformation, polymorphic fraction profile, concentration profile, etc., which were then compared with the results from SMT experiments.

Since amino acids occur as several crystal polymorphs, and each polymorph has different properties, the characterizations and the thermodynamic properties of each polymorph of DL-methionine (DL-met) were studied in this research. Moreover, the influences of the crystallization parameters on the polymorphic transformation and crystallization of DL-met crystals were also studied.

DL-met was chosen as the model substance because it is one of the essential amino acids that are required by both humans and animals, and only a very limited proportion of the literature on the problematic issue of polymorphism and crystallization concerns it. “DL-met ( $C_5H_{11}NO_2S$ ) is the sulfur containing amino acid. Being a principal supplier of sulfur, it prevents disorders of the hair, skin and nails. It helps to lower cholesterol levels by increasing the liver's production of lecithin, thus reduces liver fat and protects the kidneys. It serves as a natural chelating agent for heavy metals and regulates the formation of ammonia and creates ammonia-free urine, which reduces bladder irritation. Further, it also influences hair follicles and promotes hair growth. In-vivo studies in rat urolithiasis proved that methionine feeding leads to protection from stone formation.” (Ramachandran and Natarajan, 2006)

DL-met is used as dietary component in the poultry and animal feed. It is also used as component in human nutrition because it is not synthesized by the human body. Moreover, it is used as medicines or active pharmaceutical ingredients, and also as a precursor to other amino acids.

A fermentation method to produce methionine has not been developed, though many methods have been tried, unlike many of the other amino acids. Instead, supplemental methionine is produced in a complex chemical synthetic process. Numerous companies located (Ajinomoto Co., Inc., Japan; Shijiazhuang Haitian Fine Chemicals Co., Ltd., China; etc.) around the world produce DL-met commercially. All industrial producers of DL-met start with the same raw materials, acrolein (a 3-carbon aldehyde) derived from propylene, methyl mercaptan (methanethiol) derived from methanol and various sulfur sources, hydrogen cyanide, and ammonia or ammonium carbonate. Methyl mercaptan is reacted with acrolein to produce beta-methylmercaptopropionaldehyde, known as MMP. The MMP is then reacted with hydrogen cyanide to produce alpha-hydroxy-gamma-methylthiobutyronitrile, which on treatment with ammonia followed by hydrolysis yields DL-met (Aldrich, 2007).

DL-met has been known to have two polymorphs,  $\alpha$ -DL-met and  $\beta$ -DL-met, with almost equal stability (Mathieson, 1952) and the crystal structures of each polymorph are known (Taniguchi, Takaki, and Sakurai, 1980). Single crystals of both forms were grown from an ethanol-water solution by slow evaporation and occur as soft plates (Mathieson, 1952; Taniguchi et al., 1980). The crystal growth of  $\beta$ -DL-met was discovered rather accidentally while attempting to grow crystals of greater plate thickness from several crystallization batches. Moreover,  $\alpha$ -DL-met crystals were obtained by the reaction crystallization of sodium methioninate (Na-Met) aqueous solutions with liquid acids such as hydrochloric, acetic, nitric, sulphoric or formic acids (Matsuoka, Yamanobe, Tezuka, Takiyama, and Ishii, 1999). Also, Matsuoka et al. (1999) reported the third polymorph, the  $\gamma$ -DL-met, as well as its preparation

method and crystal structure. The  $\gamma$ -DL-met crystals were obtained by the reaction crystallization of Na-Met aqueous solutions with a solid benzoic acid or by cooling crystallization of aqueous solutions of DL-met.

## 1.2 Research Objectives

The overall objective of this thesis is to study and characterize the crystallization and SMT processes of the polymorphs of DL-met in aqueous solution. This includes measurement and analysis of the solid properties of each polymorph, measurement and analysis of the crystallization and dissolution kinetics of each polymorph, studying the effect of the process conditions on these kinetics, and studying the SMT kinetics. The specific objectives of this research are as follow.

1. To study the polymorphism and solid-state properties of  $\alpha$ -DL-met and  $\gamma$ -DL-met using analytical equipment and measurement of the solubility in water. The thermodynamic parameters for each polymorph are to be estimated.

2. To determine the nucleation, growth and dissolution kinetics of  $\alpha$ -DL-met and  $\gamma$ -DL-met in aqueous solution. The effects of temperature and supersaturation (or undersaturation for dissolution) on these kinetics are studied. The secondary nucleation threshold (SNT) of this system is determined to ensure that the growth measurement is operated under convenient non-nucleating conditions.

3. To study the SMT of  $\alpha$ -DL-met into  $\gamma$ -DL-met in aqueous solution via seeded batch transformation experiments, where  $\alpha$ -DL-met was used as seed crystals. The kinetics of the transformation are described.

4. To study the SMT of  $\alpha$ -DL-met to  $\gamma$ -DL-met in aqueous solution via a combination of the population and mass balance modeling. The kinetic parameter for the dissolution rate of  $\alpha$ -DL-met is estimated.

### 1.3 Scope of Work

This study includes characterizations of the polymorphs and measurements of the solubility and the related thermodynamic properties for each polymorph of DL-met, and also measurements of kinetic rates of nucleation, crystal growth and dissolution and polymorphic transformation of the polymorphs of DL-met as a function of temperature, initial concentration, supersaturation (or undersaturation), and other key variables. The studies also analyze the crystalline products from SMT experiments to determine the polymorphic purity of the mixture, and the composition of each polymorph in the product. Simulation studies of the polymorphic transformation are also performed for comparison with experimental results.

The research is performed in batch crystallizer and small nucleation cell with cooling and reaction crystallization operations. Pure polymorph crystals are characterized using X-ray powder diffractometry (XRPD), differential scanning calorimetry (DSC), and microscopic observation using an Olympus system. Crystallization is analyzed using standard techniques, including particle size analysis using Malvern Mastersizer/S and microscopic observation, and total solids concentration determinations using the dry substance technique. Product crystals are analyzed by XRPD to determine the polymorphic composition of products containing various polymorphs. The polymorphic transformation process is simulated using a combination of the population and mass balance modeling.

## 1.4 Research Development

This thesis is divided into 7 chapters. The introduction in **Chapter I** describes the background, significance, objectives, and scope of the research. The solid state properties of  $\alpha$ -DL-met and  $\gamma$ -DL-met, such as the melting point, enthalpy of fusion, and solubility in water are studied in **Chapter II**. The temperature dependence of the solubility and polymorphic natures of DL-met are also described. Measurements of the nucleation rates and secondary nucleation threshold of  $\gamma$ -DL-met are described in **Chapter III**. These include investigations of the effects of temperature and supersaturation on the induction time and nucleation rate. The nucleation kinetics is described by the classical nucleation theory (CNT). In **Chapter IV**, measurements of the growth and dissolution kinetics of  $\alpha$ -DL-met and  $\gamma$ -DL-met are presented. These include investigations of the effects of temperature and supersaturation (or undersaturation) on the growth and dissolution rates. The growth and dissolution kinetics are described for each set of conditions by the power-law model. The experiments to study the polymorphic transformation of the polymorphs of DL-met are presented in **Chapter V**. The mechanisms of this phenomenon are also described. **Chapter VI** presents the simulation of the polymorphic transformation of the polymorphs of DL-met and a comparison between the results from the experiment and the simulation methods. Finally, **Chapter VII** concludes the results from this thesis and gives some recommendations for future study.

## 1.5 Output

The understanding of the polymorphism and crystallization kinetics of the polymorphs of DL-met will provide useful data for the development and design of

crystallization processes to control the polymorph formation. An understanding of the behavior of polymorphic transformation of DL-met, and using crystallization of a means of achieving polymorphically pure amino acid (in this research DL-met is an example of an amino acid) products through crystallization will be achieved. This will benefit industry, because the knowledge is necessary to reliably produce these very important products. The study will help industry produce an important industrial commodity suitable for sale and specified application.

## 1.6 References

- Ajinomoto Co., Inc. (2011). **Encyclopedia of amino acids**. [On-line]. Available: <http://www.ajinomoto.com/amino/>.
- Aldrich, G. (2007). **DL-Methionine: Several vital functions**. [On-line]. Available: <http://www.petfoodindustry.com/>.
- Anuar, N., Wan Daud, W.R., Roberts, K.J., Kamarudin, S.K., and Tasirin, S.M. (2009). An examination of the solution chemistry, nucleation kinetics, crystal morphology, and polymorphic behavior of aqueous phase batch crystallized L-isoleucine at 250 mL scale size. **Cryst. Growth Des.** 9(6): 2853-2862.
- Bernstein, J. (2002). **Polymorphism in molecular crystals**. Oxford: Oxford University Press.
- Bernstein, J., Davey, R.J., and Henck, J.O. (1999). Concomitant polymorphs. **Angew. Chem. Int. Ed.** 38(23): 3440-3461.
- Cashell, C., Corcoran, D., and Hodnett, B.K. (2004). Control of polymorphism and crystal size of L-glutamic acid in the absence of additives. **J. Cryst. Growth** 273(1-2): 258-265.

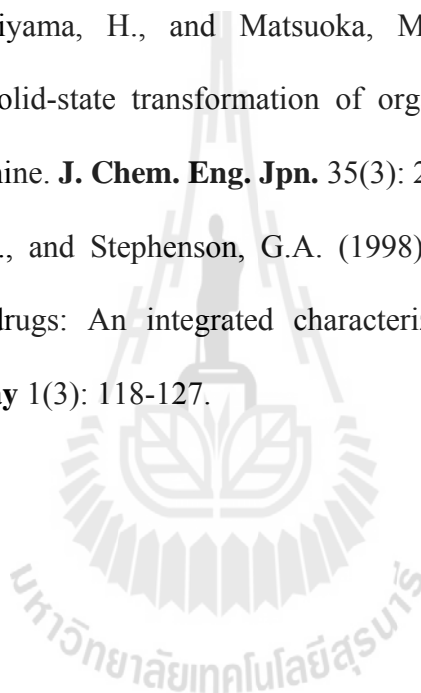
- Cornel, J., Kidambi, P., and Mazzotti, M. (2010). Precipitation and transformation of the three polymorphs of D-mannitol. **Ind. Eng. Chem. Res.** 49(12): 5854-5862.
- Davey, R.J., Blagden, N., Righini, S., Alison, H., and Ferrari, E.S. (2002). Nucleation control in solution mediated polymorphic phase transformations: The case of 2,6-dihydroxybenzoic acid. **J. Phys. Chem. B** 106(8): 1954-1959.
- Dharmayat, S., Hammond, R.B., Lai, X., Ma, C., Purba, E., Roberts, K.J., Chen, Z-P., Martin, E., Morris, J., and Bytheway, R. (2008). An examination of the kinetics of the solution-mediated polymorphic phase transformation between  $\alpha$ - and  $\beta$ -forms of L-glutamic acid as determined using online powder X-ray diffraction. **Cryst. Growth Des.** 8(7): 2205-2216.
- Ferrari, E.S., and Davey, R.J. (2004). Solution-mediated transformation of  $\alpha$  and  $\beta$  L-glutamic acid: Rate enhancement due to secondary nucleation. **Cryst. Growth Des.** 4(5): 1061-1068.
- Ferrari, E.S., Davey, R.J., Cross, W.I., Gillon, A.L., and Towler, C.S. (2003). Crystallization in polymorphic systems: The solution-mediated transformation of  $\beta$  to  $\alpha$  glycine. **Cryst. Growth Des.** 3(1): 53-60.
- Févoite, G., Alexandre, C., and Nida, S.O. (2007). A population balance model of the solution-mediated phase transition of citric acid. **AIChE J.** 53(10): 2578-2589.
- Flood, A.E. (2008). Recent patents on the optical resolution of amino acid enantiomers by crystallization from solution. **Rec. Patents Mat. Sci.** 1(2): 98-115.
- Jiang, S. (2009). **Crystallization kinetics in polymorphic organic compounds.** Ph.D. Thesis, Delft University of Technology, The Netherlands.

- Jiang, S., Jansens, P.J., and ter Horst, J.H. (2010). Control over polymorph formation of o-aminobenzoic acid. **Cryst. Growth Des.** 10(6): 2541-2547.
- Jiang, S., ter Horst, J.H., and Jansens, P.J. (2008). Concomitant polymorphism of o-aminobenzoic acid in antisolvent crystallization. **Cryst. Growth Des.** 8(1): 37-43.
- Kaneniwa, N., and Otsuka, M. (1985). Effect of grinding on the transformations of polymorphs of chloramphenicol palmitate. **Chem. Pharm. Bull.** 33(4): 1660-1668.
- Kim, Y., Haam, S., Shul, Y.G., Kim, W-S., Jung, J.K., Eun, H-C., and Koo, K-K. (2003). Pseudopolymorphic crystallization of L-ornithine-L-aspartate by drowning out. **Ind. End. Chem. Res.** 42(4): 883-889.
- Kitamura, M. (1993). Crystallization behavior and transformation kinetics of L-histidine polymorphs. **J. Chem. Eng. Jpn.** 26(3): 303-307.
- Kitamura, M. (2002). Controlling factor of polymorphism in crystallization process. **J. Cryst. Growth.** 237-239: 2205-2214.
- Kitamura, M., Furukawa, H., and Asaeda, M. (1994). Solvent effect of ethanol on crystallization and growth process of L-histidine polymorphs. **J. Cryst. Growth** 141(1-2): 193-199.
- Kitamura, M., Konno, H., Yasui, A., and Masuoka, H. (2002). Controlling factors and mechanism of reactive crystallization of calcium carbonate polymorphs from calcium hydroxide suspensions. **J. Cryst. Growth** 236(1-3): 323-332.
- Kitamura, M., and Nakamura, K. (2002). Effects of solvent composition and temperature on polymorphism and crystallization behavior of thiazole-derivative. **J. Cryst. Growth** 236(4): 676-686.

- Mangin, D., Puel, F., and Veessler, S. (2009). Polymorphism in processes of crystallization in solution: A practical review. **Org. Process Res. Dev.** 13(6): 1241-1253.
- Maruyama, S., and Ooshima, H. (2000). Crystallization behavior of taltirelin polymorphs in a mixture of water and methanol. **J. Cryst. Growth** 212(1-2): 239-245.
- Maruyama, S., Ooshima, H., and Kato, J. (1999). Crystal structures and solvent-mediated transformation of taltireline polymorphs. **Chem. Eng. J.** 75(3): 193-200.
- Mathieson, A.M. (1952). The crystal structures of the dimorphs of DL-methionine. **Acta Cryst.** 5: 332-341.
- Matsunaga, J., Nambu, N., and Nagai, T. (1976). Polymorphism of phenylbutazone. **Chem. Pharm. Bull.** 24(6): 1169-1172.
- Matsuoka, M., Yamanobe, M., Tezuka, N., Takiyama, H., and Ishii, H. (1999). Polymorphism, morphologies and bulk densities of DL-methionine agglomerate crystals. **J. Cryst. Growth** 198-199: 1299-1306.
- Mohan, R., Koo, K-K., Strege, C., and Myerson, A.S. (2001). Effect of additives on the transformation behavior of L-phenylalanine in aqueous solution. **Ind. Eng. Chem. Res.** 40(26): 6111-6117.
- Ono, T., Kramer, H.J.M., ter Horst, J.H., and Jansens, P.J. (2004). Process modeling of the polymorphic transformation of L-glutamic acid. **Cryst. Growth Des.** 4(6): 1161-1167.

- Ono, T., ter Horst, J.H., and Jansens, P.J. (2004). Quantitative measurement of the polymorphic transformation of L-glutamic acid using in-situ Raman spectroscopy. **Cryst. Growth Des.** 4 (3): 465-469.
- Qu, H., Louhi-Kultanen, M., Rantanen, J., and Kallas, J. (2006). Solvent-mediated phase transformation kinetics of an anhydrate/hydrate system. **Cryst. Growth Des.** 6(9): 2053-2060.
- Ramachandran, E., and Natarajan, S. (2006). Gel growth and characterization of  $\beta$ -DL-methionine. **Cryst. Res. Technol.** 41(4): 411-415.
- Rodríguez-Spong, B., Price, C.P., Jayasankar, A., Matzger, A.J., and Rodríguez-Hornedo, N. (2004). General principles of pharmaceutical solid polymorphism: A supramolecular perspective. **Adv. Drug Deliv. Rev.** 56(3): 241-274.
- Roelands, C.P.M., Jiang, S., Kitamura, M., ter Horst, J.H., Kramer, H.J.M., and Jansens, P.J. (2006). Antisolvent crystallization of the polymorphs of L-histidine as a function of supersaturation ratio and of solvent composition. **Cryst. Growth Des.** 6(4): 955-963.
- Schmidt, A.C. (2005). Solid-state characterization of chlorprocaine hydrochloride: part VI. Crystal polymorphism of local anaesthetic drugs. **J. Therm. Anal. Cal.** 81(2): 291-297.
- Scully, J. (2010). **Numerical simulation of the L-glutamic acid polymorphic system.** Ph.D. thesis, University of Limerick, Ireland.
- Svärd, M., Nordström, F.L., Jasnobulka, T., and Rasmuson, Å.C. (2010). Thermodynamics and kinetics of *m*-aminobenzoic acid polymorphs. **Cryst. Growth Des.** 10(1): 195-204.

- Taniguchi, T., Takaki, Y., and Sakurai, K. (1980). The crystal structures of the  $\alpha$  and  $\beta$  forms of DL-methionine. **Bull. Chem. Soc. Jpn.** 53(3): 803-804.
- Threlfall, T. (2003). Structural and thermodynamic explanations of Ostwald's rule. **Org. Process Res. Dev.** 7(6): 1017-1027.
- Tóth, J., Kardos-Fodor, A., and Halász-Péterfi, S. (2005). The formation of fine particles by salting-out precipitation. **Chem. Eng. Proc.** 44(2): 193-200.
- Yamanobe, M., Takiyama, H., and Matsuoka, M. (2002). Kinetic study on polymorphic solid-state transformation of organic compound: Bisphenol A and DL-methionine. **J. Chem. Eng. Jpn.** 35(3): 247-254.
- Yu, L., Reutzel, S.M., and Stephenson, G.A. (1998). Physical characterization of polymorphic drugs: An integrated characterization strategy. **Pharm. Sci. Technol. Today** 1(3): 118-127.



# CHAPTER II

## POLYMORPHISM AND THERMODYNAMICS OF DL-METHIONINE

### 2.1 Abstract

Pure of the polymorphs  $\alpha$ -DL-methionine ( $\alpha$ -DL-met) and  $\gamma$ -DL-methionine ( $\gamma$ -DL-met) were prepared by reaction crystallization of sodium methioninate (Na-Met) aqueous solutions with HCl, and cooling crystallization of aqueous solutions of DL-met, respectively. The polymorphism and thermodynamics of DL-met were studied by a range of techniques including X-ray powder diffractometry (XRPD), determination of the temperatures and enthalpies of fusion by differential scanning calorimetry (DSC), photo microscopy, and solubility measurements. The solubility of each polymorph was determined between 5 and 70 °C in water. The van't Hoff equation was used to describe the temperature dependence of the solubility. The results showed that XRPD, DSC, photo microscopy, and solubility can be used to describe the differences between the polymorphs. XRPD is the best method for a clear and fast identification and quantification of the polymorphs or polymorphic fraction during crystallization. The solubility of both  $\alpha$ -DL-met and  $\gamma$ -DL-met in water increases with increasing temperature, and the solubility values of  $\alpha$ -DL-met are approximately 5.76% higher than  $\gamma$ -DL-met. DSC measurements show that the melting temperatures of  $\alpha$ -DL-met and  $\gamma$ -DL-met are  $278.17 \pm 0.40$  and  $281.74 \pm 0.71$  °C, respectively, whereas the enthalpies of fusion of  $\alpha$ -DL-met and  $\gamma$ -DL-met are  $88.81 \pm 4.93$  and  $98.76 \pm 8.28$

kJ/mol, respectively. The Gibbs free energy values of  $\alpha$ -DL-met are approximately 1.10% higher than  $\gamma$ -DL-met. The solubility data, DSC thermograms and Gibbs free energies of the two polymorphs strongly suggest that the system is a monotropic polymorph system with  $\gamma$ -DL-met being the stable polymorph for all temperature below the melting points of the compounds.

## 2.2 Introduction

Polymorphism is the ability of a solid compound to exist in more than one crystalline form (Grant, 1999). These crystalline forms, although containing the same molecules, result from a different ordered arrangement of molecules within the crystalline lattice. Polymorphs can have different mechanical, thermal, physical, and chemical properties, such as compressibility, melting point, crystal habit, color, density, dissolution rate, and solubility. These can have a great influence on the bioavailability (Miyazaki, Arita, Hori, and Ito, 1974; Takayama, Nambu, and Nagai, 1980), hygroscopicity (Dong et al., 2002; Schmidt, 2005), and stability (Kitamura, 1993; Yu, Reutzel, and Stephenson, 1998). Also, polymorphs influence the downstream processing, such as filtration (Ferrari and Davey, 2004; Maruyama, and Ooshima, 2000), drying (Matsunaga, Nambu, and Nagai, 1976; Umeda et al., 1984), and grinding and tableting (Kaneniwa and Otsuka, 1985).

In experimental and industrial crystallizations, it is commonly observed that the metastable polymorph appears first instead of the stable polymorph, and this observation is stated as a rule known as Ostwald's rule of stages (Threlfall, 2003). According to Ostwald's rule of stages, in crystallization from the melt or from solution, the metastable polymorph (the least stable of the metastable polymorphs if

there is more than two polymorphs) forms first, followed by transformation to the more stable polymorph. It is generally known that this rule is not a physical law and that more stable polymorphs can first crystallize directly as well (Roelands et al., 2006). The unstable polymorph is sometimes not acceptable from the point of view of obtaining polymorphically pure compounds suitable for sale, particular in the food and other material products. On the other hand, in the field of pharmaceuticals, metastable polymorphs may be more desirable than the stable one (Yamanobe, Takiyama, and Matsuoka, 2002a).

The melting point, enthalpy of fusion, and solubility are important properties which may be used to model the thermodynamics of the system. It is known that the solubility of the stable polymorph is always lower than that of the metastable polymorph. If a polymorph is stable relative to all others at all temperatures below the melting point, then the system only ever has one stable polymorph; such a system is known as a monotropic polymorphic system. Where the stable polymorphic form depends on the temperature and pressure of the system, there is reversible transition point below the melting points of the polymorphs where the relative thermodynamics stabilities change; such a system is known as an enantiotropic system.

Currently, there are several techniques that have been used to characterize crystalline solids, and identify the polymorphic forms. Examples of such techniques are microscopy (Cashell, Sutton, Corcoran, and Hodnett, 2003; Ferrari and Davey, 2004; Jiang, Jansens, and ter Horst, 2010), FTIR spectroscopy (Lu, Wang, Yang, and Ching, 2007; Yamanobe, Takiyama, and Matsuoka, 2002b), Raman spectroscopy (Cornel, Kidambi, and Mazzotti, 2010; Jiang et al., 2010; Ono, ter Horst, and Jansens, 2004), DSC (Picciochi, Diogo, and Minas da Piedade, 2011; Urakami, Shono,

Higashi, Umemoto, and Godo, 2002), XRPD (Dharmayat, Hammond, et al., 2008; Grooff, Liebenberg, and De Villiers, 2011; Liu, Wei, and Black, 2009),  $^{13}\text{C}$  solid-state nuclear magnetic resonance (SSNMR) spectroscopy (Hughes and Harris, 2008; Dong et al., 2002; Shaibat, Casabianca, Siberio-Pérez, Matzger, and Ishii, 2010), and solubility measurement (Anuar, Wan Daud, Roberts, Kamarudin, and Tasirin, 2009; Nordström and Rasmuson, 2006; Urakami et al., 2002). In the present study, a number of these techniques were applied to investigate the polymorphic behavior of DL-methionine (DL-met).

In this work DL-met (Figure 2.1) has been chosen as the model substance. This is due to DL-met is one of the essential amino acids that are required by both humans and animals, and only a very limited proportion of the literature on the problematic issue of polymorphism and thermodynamics concerns it. DL-met is used as dietary component in poultry and animal feeds. It is used as component in human nutrition because it is not synthesized by the human body. Moreover, it is used in medicines and active pharmaceutical ingredients, and also as a precursor to other amino acids.

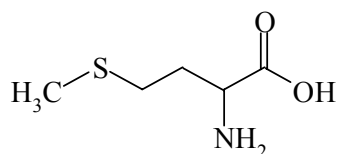


**Figure 2.1** Chemical structure of methionine.

DL-met is reported to have three polymorphs;  $\alpha$ -DL-met,  $\beta$ -DL-met, and  $\gamma$ -DL-met (Mathieson, 1952; Matsuoka, Yamanobe, Tezuka, Takiyama, and Ishii, 1999). The crystal structures of  $\alpha$ -DL-met and  $\beta$ -DL-met are shown by Taniguchi,

Takaki, and Sakurai (1980), and that of  $\gamma$ -DL-met is shown by Matsuoka et al. (1999). Single crystals of  $\alpha$ -DL-met and  $\beta$ -DL-met were grown from an ethanol-water solution by slow evaporation and occur as soft plates (Mathieson, 1952; Taniguchi et al., 1980). Both these forms have almost equal stability. Ramachandran and Natarajan (2006) showed that  $\beta$ -DL-met crystal can be obtained by crystallization in sodium metasilicate gel for the first time by the reduction of solubility method. Matsuoka et al. (1999) showed that  $\alpha$ -DL-met crystals were obtained by the reaction crystallization of sodium methioninate (Na-Met) aqueous solutions with liquid acids such as hydrochloric, acetic, nitric, sulfuric or formic acids. Also, Matsuoka et al. (1999) reported that  $\gamma$ -DL-met crystals were obtained by the reaction crystallization of Na-Met aqueous solutions with solid benzoic acid, or by cooling crystallization of aqueous solutions of DL-met. The crystallographic data and morphology of each polymorph are shown in Table 2.1 and Figure 2.2, respectively. In this study,  $\alpha$ -DL-met and  $\gamma$ -DL-met were studied because  $\gamma$ -DL-met is found in the cooling crystallization of aqueous solution of DL-met and  $\alpha$ -DL-met can transform to  $\gamma$ -DL-met in aqueous solution of DL-met (Yamanobe, Takiyama, and Matsuoka, 2002c).



diffraction (XRPD), crystal morphology, and the solubility in water. Moreover, the thermodynamic parameters for each polymorph were measured and estimated, and the polymorphic nature of DL-met is described.

## 2.3 Theory

### 2.3.1 Definition of Polymorphism

Polymorphism occurs when a compound can exist in more than one crystalline form. These crystalline forms contain the same molecules but have a different arrangement of molecules within the crystalline lattice. Polymorphs are found among many molecular and ionic compounds. For example, the two polymorphs of the amino acid L-glutamic acid are shown in Figure 2.3. Two polymorphs are also known for the ionic compound barium fluoride and these are shown in Figure 2.4.

Polymorphs possess different product properties because of their difference in crystal structures. Examples of properties that can be structure-dependent are solubility and dissolution rate, density, stability, melting point, color and morphology (Roelands, 2005). These properties are usually related to the performance of the compound in its application. For examples, the color shade of pigments, bioavailability of pharmaceutical compounds and stability of explosives are applications where using the correct polymorph is vital. Only one of the polymorphic structures is thermodynamically stable but the formation of a metastable structure may be kinetically favored, eventually followed by transformation to the stable structure.

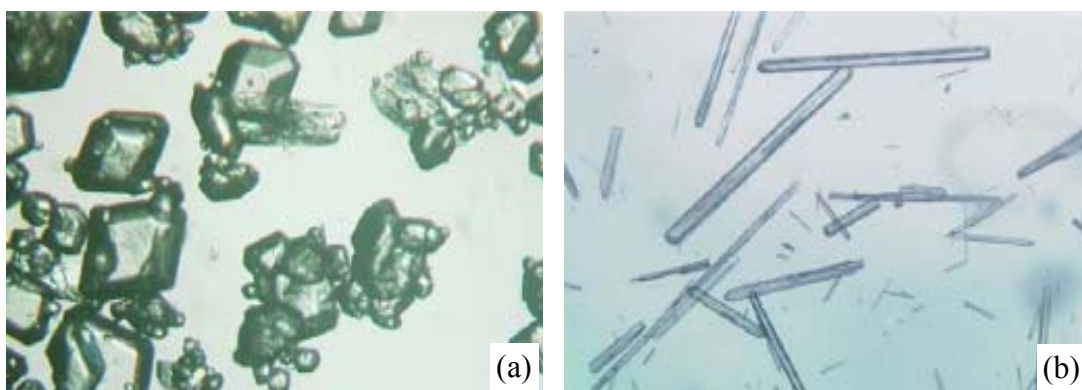


**Figure 2.3** Polymorphs of L-glutamic acid. (a) crystal of the metastable alpha phase, and (b) crystal of the stable beta phase. (Dharmayat, Anda, et al., 2006)

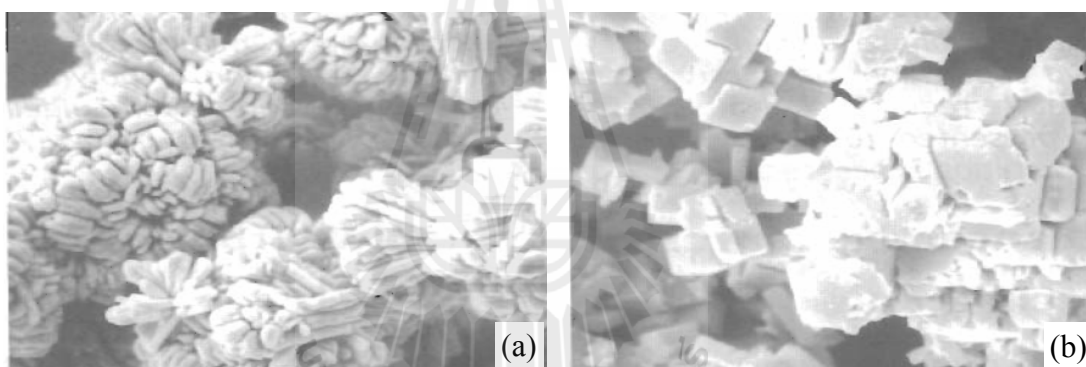


**Figure 2.4** Polymorphs of barium fluoride. (a) crystal of metastable phase II, and (b) crystal of stable phase I. (Kolar, Binsma, and Subotić, 1986, quoted in Roelands (2005))

The protease inhibitor ritonavir in a formulation containing the compound in ethanol/water based solution had been on the market in 1996. A more stable form was found in 1998. The solubility of the more stable form in the hydroalcoholic formation was lower than the less stable form. Since the compound is

not bioavailable in the solid state, this phenomenon forced the company to withdraw their product from the market (Bauer et al., 2001). The metastable polymorph was obtained again in manufacturing by use of a seeding procedure (Chemburkar et al., 2000). The differences in melting point and solubility of ritonavir polymorphs were also investigated by Chemburkar.

Solvates, which are often referred to as pseudopolymorphs, are crystalline solid adducts containing a solvent molecule (or molecules) within the crystal structure (Vippagunta, Brittain, and Grant, 2001). If water is the solvent which is incorporated into the crystal structure the solvate is termed a hydrate. Calcium carbonate is an example of compound that is able to form multiple polymorphs (vaterite, calcite and aragonite) and hydrates ( $.6\text{H}_2\text{O}$  and  $\text{.H}_2\text{O}$ ) (Brečević and Nielsen, 1993; Kitamura, 2001; Kitamura, Konno, Yasui, and Masuoka, 2002). Magnesium sulphate is able to form hydrates including a metastable polymorph form of a hydrate:  $\text{.H}_2\text{O}$ ,  $\text{.7H}_2\text{O(I)}$ ,  $\text{.7H}_2\text{O(II)}$  and  $\text{.12H}_2\text{O}$  are all hydrates of magnesium sulfate (Himawan, 2005).

Many previous studies concern polymorphism from a pharmaceutical perspective because both polymorphism and formation of solvates are especially widespread among pharmaceutical compounds.

The differences of the properties of each polymorph often are related to the performance of the compound in its application. Therefore, control over polymorphism is important in a variety of industrial applications. In many chemical, pharmaceutical and food processing industries polymorphism is encountered in crystallization processes. There are many parameters influencing the formation of polymorphs, such as temperature, pressure, supersaturation, solvent, seeding, and

additives. Moreover, understanding of the crystallization mechanism is required with special attention to the process of nucleation, dissolution, growth and transformation.

### 2.3.2 Solubility and Thermodynamics of Polymorphism

Variations in solubility, dissolution rate and hence bio-availability of pharmaceuticals may have a serious impact in industrial crystallization processes. Solubility data are of importance in the study of crystal nucleation and growth kinetics. Solubility, melting temperature, and enthalpy of melting parameters are experimental quantities from which thermodynamics parameters for each polymorph can be calculated.

The solubility is a physical property referring to the ability for the solute to dissolve in a solvent by measuring the maximum amount of solute dissolved in a solvent at equilibrium. The resulting solution is called a saturated solution. The main factors that have an effect on solubility are the nature of the solute and solvent, temperature and pressure. In most case it is not necessary to determine the full phase diagram (determining the solubility as a function of these parameters) because determining the solubility as a function of temperature suffices (Beckmann, 2000).

The solubility (on a mole fraction basis) of real solutions can be expressed as (Flood, 2009)

$$\ln(x\gamma) = \frac{\Delta H_{fus}}{R} \left[ \frac{1}{T_{fus}} - \frac{1}{T} \right] + \frac{1}{RT} \int_T^{T_{fus}} \Delta C_P dT - \frac{1}{R} \int_T^{T_{fus}} \frac{\Delta C_P}{T} dT \quad (2.1)$$

where  $x$  is the mole fraction of solute in the solution,  $\gamma$  is the activity coefficient of the solute,  $T$  is the saturated solution temperature (K),  $T_{fus}$  is the fusion temperature (melting point) of the solute (K),  $\Delta H_{fus}$  is the enthalpy of fusion (J/mol),  $\Delta C_P$  is the

difference in the heat capacities of the pure solid and pure liquid phases between the temperature of interest and the melting point ( $J/mol\cdot K$ ), and  $R$  is the ideal gas constant and is equal to  $8.314 J/mol\cdot K$ . The problem in using this equation is the  $\Delta C_P$  term. It is difficult to measure these two heat capacities (usually requiring experiments for each phase to be performed on an extremely carefully calibrated DSC), and the fact that the pure liquid at these temperatures is an unstable phase makes the problem even more difficult. This difficulty can be treated by assuming either that the  $\Delta C_P$  is small enough to be assumed to be zero over the entire of the integral, or else that the last two terms in the right hand side of equation (2.1) cancel each other. Under either of these assumptions, equation (2.1) becomes

$$\ln(x\gamma) = \frac{\Delta H_{fus}}{R} \left[ \frac{1}{T_{fus}} - \frac{1}{T} \right] \quad (2.2)$$

For ideal solutions, the activity coefficient of the solute is equal to 1 and equation (2.2) reduces to the van't Hoff equation (Mullin, 2001)

$$\ln(x) = \frac{\Delta H_{fus}}{R} \left[ \frac{1}{T_{fus}} - \frac{1}{T} \right] = -\frac{\Delta H_{fus}}{RT} + \frac{\Delta S_{fus}}{R} \quad (2.3)$$

where  $\Delta S_{fus} = \Delta H_{fus}/T_{fus}$  is the entropy of fusion ( $J/mol\cdot K$ ). In reality, the solubility is solvent dependent, which means that the enthalpy and entropy of mixing must be taken into account by replacing  $\Delta H_{fus}$  with  $\Delta H_{diss}$  and  $\Delta S_{fus}$  with  $\Delta S_{diss}$  (Mullin, 2001), i.e., using

$$\ln(x) = -\frac{\Delta H_{diss}}{RT} + \frac{\Delta S_{diss}}{R} \quad (2.4)$$

where  $\Delta H_{diss}$  and  $\Delta S_{diss}$  are the enthalpy and entropy of dissolution, respectively. Therefore, a plot of  $\ln(x)$  versus  $1/T$  gives a straight line. The slope of the line is equal to  $-\Delta H_{diss}/R$ , and the intercept is equal to  $\Delta S_{diss}/R$ .

The information of the fusion temperature and enthalpy of fusion can be used along with equation (2.2) to estimate activity coefficients in the system. If the activity coefficient is less than one, then the actual solubility is higher than the ideal solubility, and the system shows negative deviations from ideality. On the other hand, if the activity coefficient is more than one, then the actual solubility is less than the ideal solubility, and the system shows positive deviation from ideality (Flood, 2009).

The Gibbs free energy ( $G$ ) of a compound is another important thermodynamic parameter. The exact value of the Gibbs free energy cannot be found experimentally, however, the relative Gibbs free energy of solids can be determined from solubility data and expressed by the following equation (Grunenberg, Henck, and Siesler, 1996)

$$\Delta G_{I(s)-(l)} = G_{I(s)} - G_{(l)} = RT \ln x_I \quad (2.5)$$

$$\Delta G_{II(s)-(l)} = G_{II(s)} - G_{(l)} = RT \ln x_{II} \quad (2.6)$$

$$\Delta G_{I(s)-II(s)} = G_{I(s)} - G_{II(s)} = RT \ln \frac{x_I}{x_{II}} \quad (2.7)$$

where  $G_{I(l)}$  and  $G_{II(l)}$  are the Gibbs free energy of the polymorphs I and II in solution (J/mol),  $G_{I(s)}$  and  $G_{II(s)}$  are the Gibbs free energy of the solid of the polymorphs I and II (J/mol), and  $x_I$  and  $x_{II}$  are the solubility (as mole fractions) of the polymorphs I and II in solution.

The compounds of polymorphic systems can be crystallized in a number of structures that have different lattice free energy. At a given pressure and temperature the stable polymorph is the structure that has the lowest free energy, while all other structures that have higher free energies are metastable polymorphs. Grunenberg et al. (1996) depicted an energy versus temperature- $(E/T)$  diagram, which describes the change of the Gibbs free energy  $G = H - TS$  as a function of temperature  $T$ , with the change of the enthalpy ( $H$ ) and the entropy ( $S$ ) of the system. At absolute zero (at 0 K) the entropy term disappears and the Gibbs free energy becomes equal to the enthalpy term. The most stable polymorph has the lowest enthalpy at this point.

Example  $E/T$ -diagrams of dimorphic systems are shown in Figures 2.5 and 2.6. In Figure 2.5 the melting points  $mp_I$  and  $mp_{II}$  are the point that the Gibbs free energy lines of the two polymorphs cross the Gibbs free energy lines of the liquid state. Form I is the high melting polymorph. The point where the lines of Gibbs free energy of the two polymorphs cross each other is the transition point  $tp_{I/II}$ . This indicates that the system is an enantiotropic system because the Gibbs free energy of the two polymorphs crosses each other below the melting point. In this system polymorph II is the stable polymorph below the transition point and polymorph I is the stable polymorph above the transition point. If a sample of polymorph II is heated,

for example in a DSC, it may transform starting from the transition point into polymorph I.

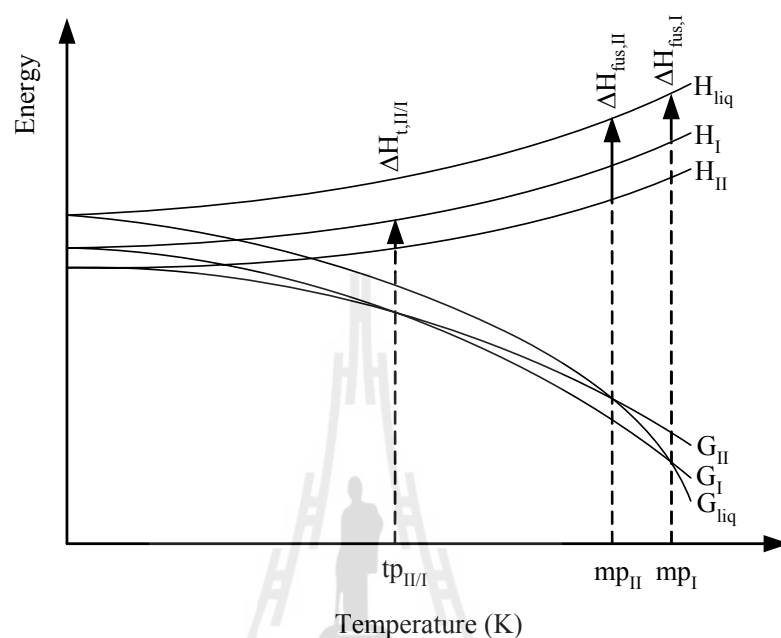


**Figure 2.5** Fundamental  $E/T$  diagram of a dimorphic enantiotropic system.

(Grunenberg et al., 1996)

The  $E/T$  diagram of a monotropic system is shown in Figure 2.6. The lines for the Gibbs free energies of two polymorphs do not cross below their melting points. Form I is the stable polymorph over the whole temperature range from absolute zero until its melting point.

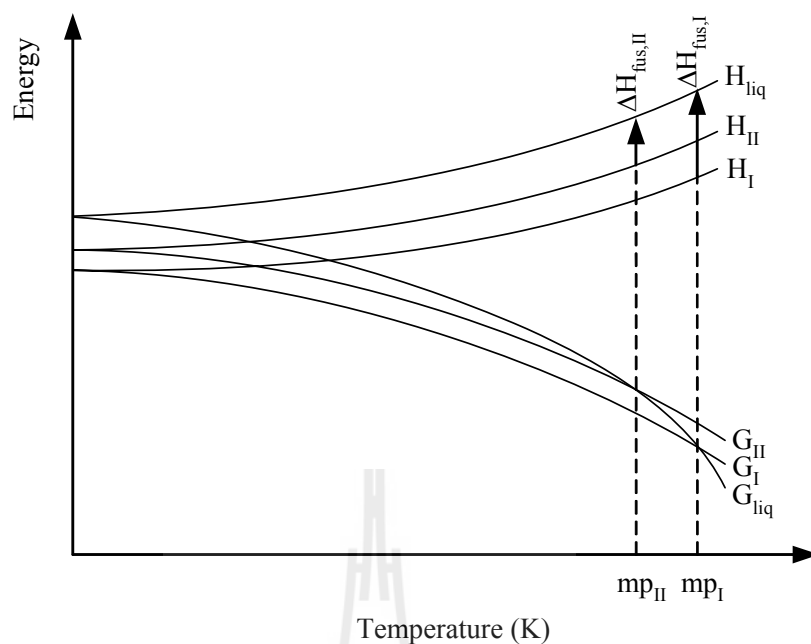


**Figure 2.6** Fundamental  $E/T$  diagram of a dimorphic monotropic system.

(Grunenberg et al., 1996)

A number of rules; the heat of transition rule, the heat of fusion rule, and the density rule have been derived by Burger and Ramberger (1979a, 1979b, quoted in Grunenberg et al., 1996) and are also helpful for checking whether a polymorphic system is monotropic or enantiotropic.

Polymorphic forms differ in solubility because this property is directly proportional to the Gibbs free energy. The fundamental solubility curves of the polymorphic forms of each system are shown in Figures 2.7 and 2.8. The solubility of the stable polymorph (polymorph I) is always lower than that of the metastable polymorph (polymorph II). This is since the stable polymorph has the lowest Gibbs free energy

$$G_{I(s)} < G_{II(s)} \quad (2.8)$$

Substituting equations (2.5) and (2.6) into equation (2.8) results in the equation

$$x_I < x_{II} \quad (2.9)$$

This result shows that the more stable polymorph always has the lower solubility than the metastable polymorph, whatever the solvent that is in contact with the solid (Mangin, Puel, Veessler, 2009).

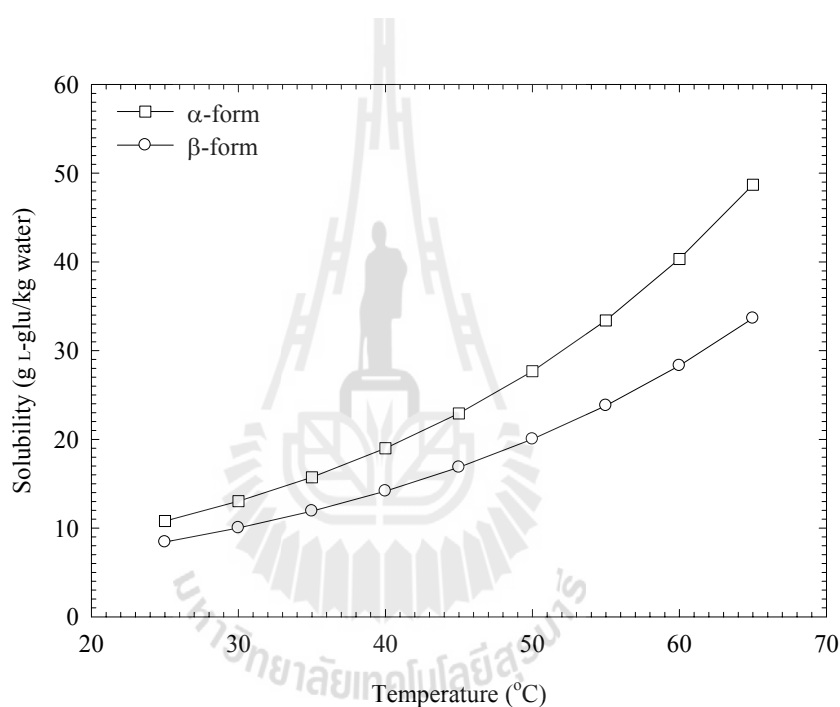


**Figure 2.7** Solubility curves for two polymorphic forms of L-glutamic acid.

(Kee, Tan, and Braatz, 2009)

L-glutamic acid is one example of a monotropic system; its solubility is shown in Figure 2.7. The  $\beta$ -form is stable relative to the others at all temperatures below the melting point; the polymorphs are not interconvertible, and the solubility is always lower than that of the metastable  $\alpha$ -form.

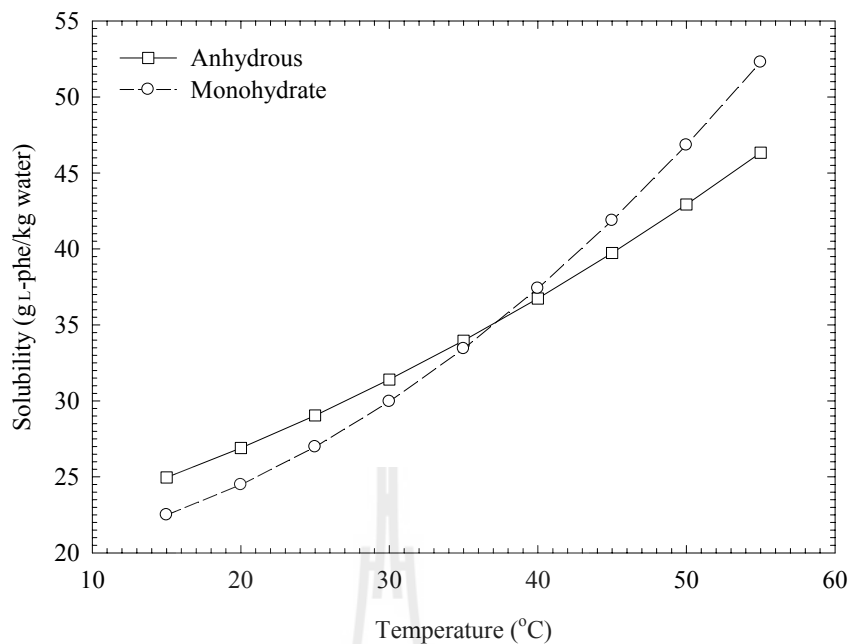


**Figure 2.8** Solubility curves of L-phenylalanine polymorph.

(Mohan, Koo, Strege, and Myerson, 2001)

L-phenylalanine is one example of an enantiotropic system; its solubility is shown in Figure 2.8. The stable polymorphic form depends on the temperature and pressure of the system, there is a reversible transition point below the melting points of the polymorphs where the relative thermodynamic stabilities change. Moreover, the metastable form may exist for a long time and the presence of the stable form results in mediated phase transformation.

## 2.4 Materials and Methods

### 2.4.1 Materials

DL-met was purchased from Acros Organics, purity >99%. NaOH (purity >97%), Na<sub>2</sub>CO<sub>3</sub> (purity >99.5%), and HCl (37%) were purchased from Carlo Erba. All chemicals and deionized water were used without further purification.

### 2.4.2 Apparatus

A 0.5 L batch crystallizer with a sealed glass lid to reduce solvent evaporation (Figure 2.9) was used to prepare  $\gamma$ -DL-met, and to measure the solubility of  $\alpha$ -DL-met and  $\gamma$ -DL-met. The slurry is continuously agitated by a centrally located four-blade impeller driven by an overhead mixer. The crystallizer was placed inside a constant temperature water bath, where the temperature was controlled within  $\pm 0.5$  °C.

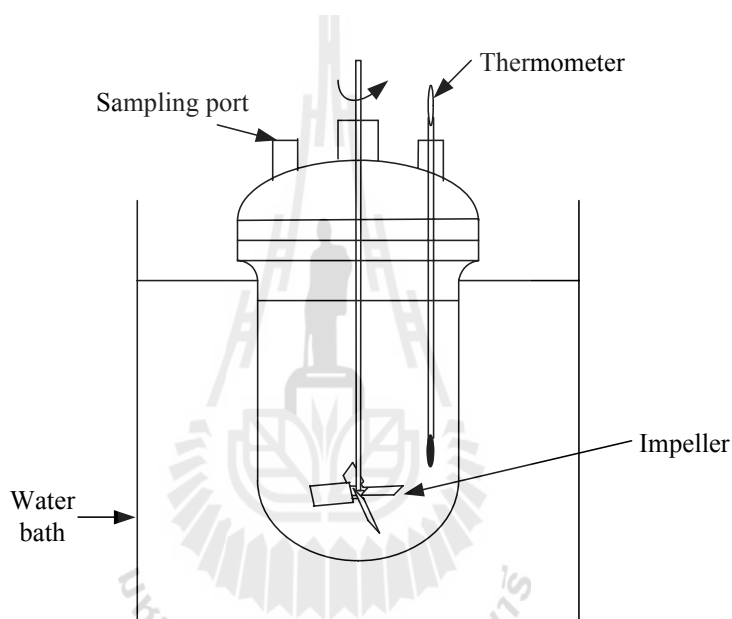


**Figure 2.9** The 0.5 L batch crystallizer.

250 mL and 500 mL glass beakers were used as batch crystallizers to prepare  $\alpha$ -DL-met and sodium methioninate (Na-Met) aqueous solution, respectively. The temperature control and the agitation systems were the same as used in the 0.5 L batch crystallizer.

### 2.4.3 Preparation of Na-Met Aqueous Solution

Aqueous solutions of Na-Met were prepared by a method previously described (Huthmacher et al., 2000). 50 g of DL-met and 13.5 g of NaOH were

dissolved in 166.5 mL of water in a 500 mL glass beaker at room temperature, with the addition of 20 g of  $\text{Na}_2\text{CO}_3$ . After mixing, solutions were stirred with a magnetic stirrer for 6 h, and about 150 mL of water was removed from the solution by distillation; the precipitate formed was separated by filtration over a hot ( $> 100\text{ }^\circ\text{C}$ )  $8\text{ }\mu\text{m}$  filter by a vacuum pump. The filtrate contained 71% sodium methioninate.

#### 2.4.4 Preparation of Polymorph

$\alpha$ -DL-met was prepared using reaction crystallization of Na-Met aqueous solutions as follows: 32 mL of concentrated HCl (37%) was fed at the rate of 2 mL/min into diluted Na-Met aqueous solutions (80 mL of 71% Na-Met aqueous solution diluted by 40 mL of water) in a 250 mL glass beaker at  $35\text{ }^\circ\text{C}$ . The mixed solutions were continuously agitated by a centrally located four-blade impeller driven by an overhead stirrer at 300 rpm. The pH of the solutions reached the isoelectric point of DL-met (pH = 5.7 - 5.9) after the full amount of HCl was added. The resulting crystals were collected by filtration over a  $2\text{ }\mu\text{m}$  filter by a vacuum pump and dried over silica gel.  $\gamma$ -DL-met was prepared by cooling crystallization of aqueous solutions of DL-met as follows. DL-met (21 g) was dissolved in 350 mL of water in a 0.5 L batch crystallizer maintained above  $60\text{ }^\circ\text{C}$ . This solution was continuously agitated by a centrally located four-blade impeller driven by an overhead stirrer at 300 rpm, and the solution was cooled and maintained at  $25\text{ }^\circ\text{C}$ , after which the crystals were removed and filtered. Since these crystals were too large for use as seed crystals a further crystallization was performed. The solution at  $25\text{ }^\circ\text{C}$  was heated to  $30\text{ }^\circ\text{C}$ , then cooled to  $5\text{ }^\circ\text{C}$  and held at this temperature for 24 h. After 24 h, the suspension was filtered over a  $2\text{ }\mu\text{m}$  filter by a vacuum pump and dried over silica gel.

#### 2.4.5 Polymorph Characterization

The crystals of the pure polymorph of each form obtained from section 2.4.4 were characterized by X-ray powder diffractometry (XRPD) (Bruker axs, D5005), differential scanning calorimetry (DSC) (PerkinElmer, DSC7), and microscopic observation (Olympus, CH30).

#### 2.4.6 Solubility Measurement

The solubility of each polymorph was determined in water as a function of temperature (5 - 70 °C), and was measured by a gravimetric method. 200 mL of water was added into a 0.5 L batch crystallizer (Figure 2.9) and stabilized at the desired (measurement) temperature. Excess amounts of each polymorph crystal were then added into water and the system was agitated. To ensure the equilibrium state, the solutions were stirred (300 rpm) for about 24 h at a constant temperature with an uncertainty  $\pm 0.5$  °C. The concentration was periodically recorded by the dry substance method (Garside, Mersmann, and Nyvlt, 2002): the suspensions were withdrawn from the crystallizer using a 10 mL plastic syringe together with a 0.45  $\mu\text{m}$  filter, the clear liquid solutions were evaporated at 100 - 105 °C, and the weight of the dry DL-met was used to calculate the concentration of DL-met (the weight was repeatedly recorded throughout the drying process with complete dryness determined when the mass of DL-met remained constant over time). After water was completely evaporated, the concentration ( $C$ ) was determined by the following equation

$$C = \frac{M_c}{M_{sol} - M_c} \quad (2.10)$$

where  $M_{sol}$  is the mass of the solution sample (g) and  $M_c$  is the mass of the dried solid crystals (g). The solubility was estimated by averaging the concentration at equilibrium. At equilibrium, the residual solids were analyzed by XRPD to consider the solution-mediated transformation (SMT) between the two forms. Note that at the temperature higher than 25 °C the syringe and filters must be pre-heated to exceed the solution temperature. This was performed to stop nucleation occurring inside the syringe and filters during sampling.

#### 2.4.7 Characterization of Uncertainty

Wherever uncertainty is indicated in this chapter the uncertainty is represented by 90% confidence interval (see Appendix A).

## 2.5 Results and Discussions

### 2.5.1 Polymorphism

The polymorphic form was corroborated through analyses by XRPD, DSC, and photo microscopy.

DSC thermograms of the two polymorphs are shown in Figure 2.10. There is no evidence of significant phase transformation between the polymorphs upon heating.  $\alpha$ -DL-met melts at  $274.02 \pm 0.37$  °C. For  $\gamma$ -DL-met there is a small endothermic transition near 52 °C, and this polymorph melts at  $277.18 \pm 0.78$  °C. The measured peak fusion temperatures and enthalpies, and estimated entropies of the two polymorphs are shown in Table 2.2. From these observations, it appears most likely that there is a conformational difference between  $\alpha$ -DL-met and  $\gamma$ -DL-met.

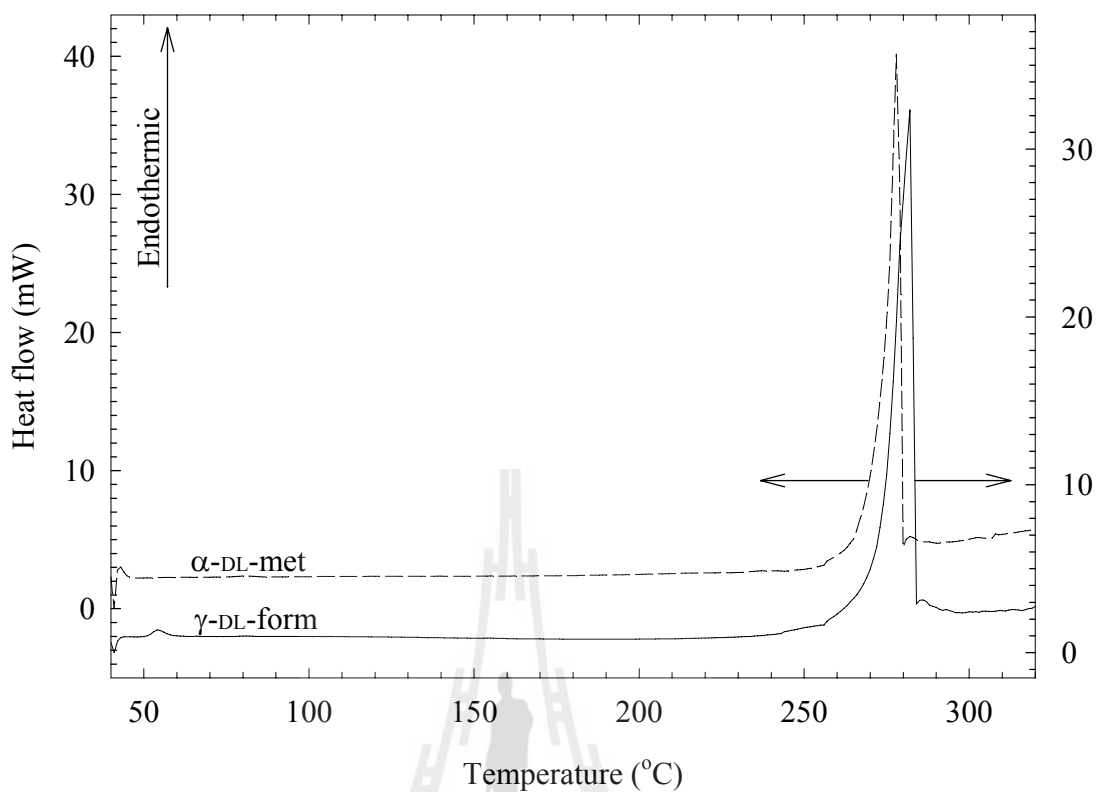


**Figure 2.10** DSC curves of  $\alpha$ -DL-met and  $\gamma$ -DL-met crystals. The sample weight was 2.10 mg and the heating rate was 10 °C/min. A nitrogen purge was used.

**Table 2.2** Thermodynamic parameters of  $\alpha$ -DL-met and  $\gamma$ -DL-met.

Form	$\alpha$	$\gamma$
Peak fusion temperature, $T_{fus}$ (°C)	278.17±0.40	281.74±0.71
Melting enthalpy, $\Delta H_{fus}$ (kJ/mol)	88.81±4.93	98.76±8.28
Melting entropy, $\Delta S_{fus}$ (kJ/mol/K)	0.1610±0.009	0.1780±0.015
Dissolution enthalpy, $\Delta H_{diss}$ (kJ/mol)	17.87	18.23
Dissolution entropy, $\Delta S_{diss}$ (J/mol/K)	14.83	15.52

XRPD patterns for  $\alpha$ -DL-met and  $\gamma$ -DL-met are given in Figure 2.11. The XRPD patterns are identical to patterns given by Matsuoka et al. (1999). The XRPD patterns show clearly that the polymorphs possess different crystal structures. The characteristic peaks of  $\alpha$ -DL-met are observed at  $25.3^\circ/2\theta$  and  $32.84^\circ/2\theta$ , while the characteristic peaks of  $\gamma$ -DL-met are observed at  $28.06^\circ/2\theta$  and  $33.82^\circ/2\theta$ . Therefore the XRPD method is a good method for clear and fast identification and quantification of the polymorphs or polymorphic fraction during crystallization. The composition of  $\gamma$ -DL-met could be estimated using a calibration curve obtained from the relationship between the mass fraction of  $\gamma$ -DL-met and the intensity of characteristic peaks, which is described in Chapter V.

The crystal morphology of the two polymorphs differ (Figure 2.12). The crystals of  $\alpha$ -DL-met are agglomerated and have laminate structures; the constituent elementary particles are primarily plate-like, whereas the shape of  $\gamma$ -DL-met crystals is a prism-like hexagon. Therefore, the transformation from  $\alpha$ -DL-met to  $\gamma$ -DL-met during crystallization could also be followed using a microscope. The morphologies of the two polymorphs obtained are identical to the results given by Matsuoka et al. (1999) and Yamanobe-Hada, Ito, and Shindo (2005).

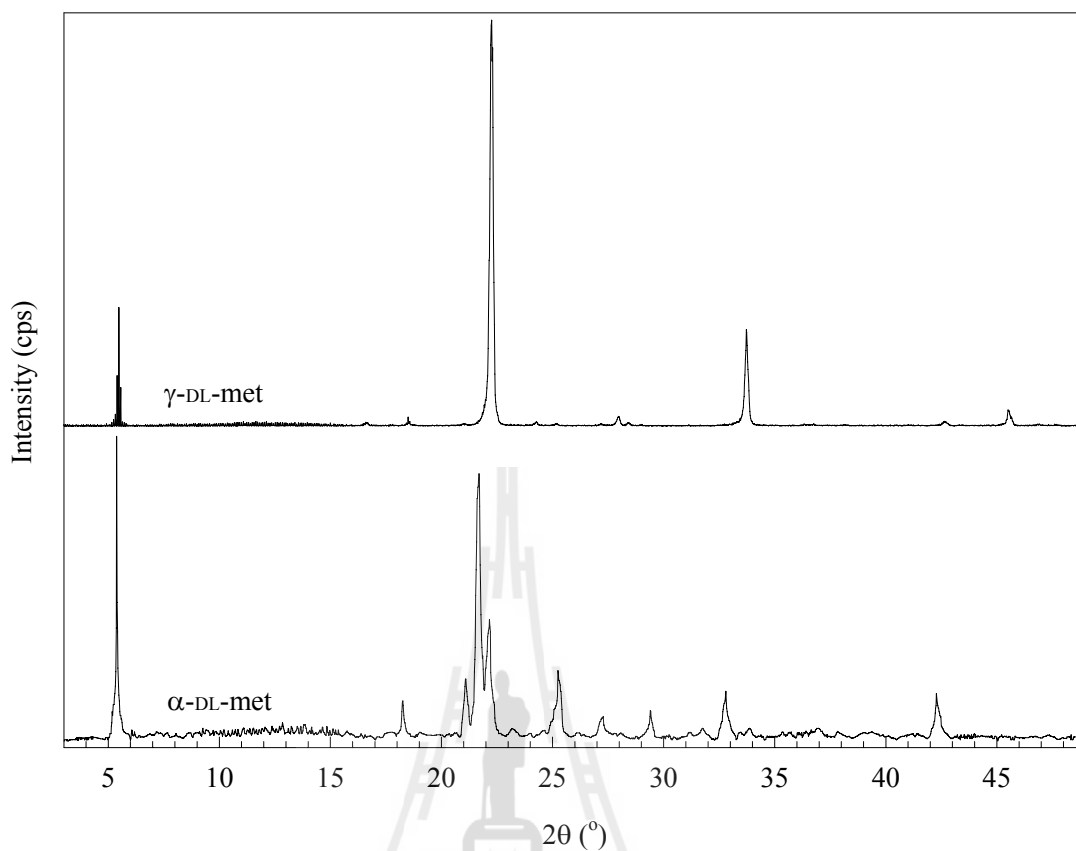


**Figure 2.11** PXRD patterns of  $\alpha$ -DL-met and  $\gamma$ -DL-met crystals.

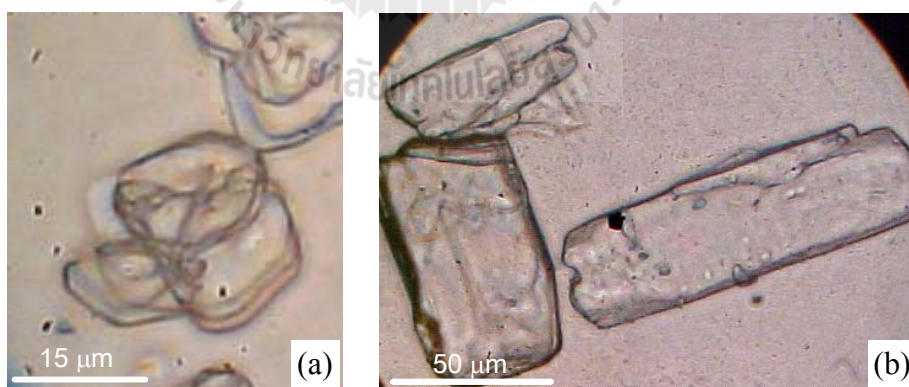


**Figure 2.12** Photomicrographs of  $\alpha$ -DL-met (a) and  $\gamma$ -DL-met (b) crystals.

The purity of the crystallized polymorphs was found based on the difference between the two polymorphs, as observed via the different methods of analysis. XRPD contributed particularly important information as the two polymorphs showed very different patterns. DSC also provided some knowledge, as analysis of the polymorphic forms showed differences in the melting properties. Additionally investigation by photo microscopy facilitated elucidating the purity since the two polymorphs differed in crystal morphology.

### 2.5.2 Solubility

The dissolution profiles of  $\alpha$ -DL-met and  $\gamma$ -DL-met in water are shown in Figure 2.13. The plot in Figure 2.13 shows the concentrations attained in water for each polymorphic pair as a function of time in the presence of an excess of the solid phase. The solubilities were estimated by averaging the concentrations at equilibrium (the constant concentration with time in Figure 2.13). The solubilities of the two polymorphs are listed in Table 2.3 and shown in Figure 2.14. A sample of the solid phase was examined by XRPD analysis both before and after each solubility measurement.

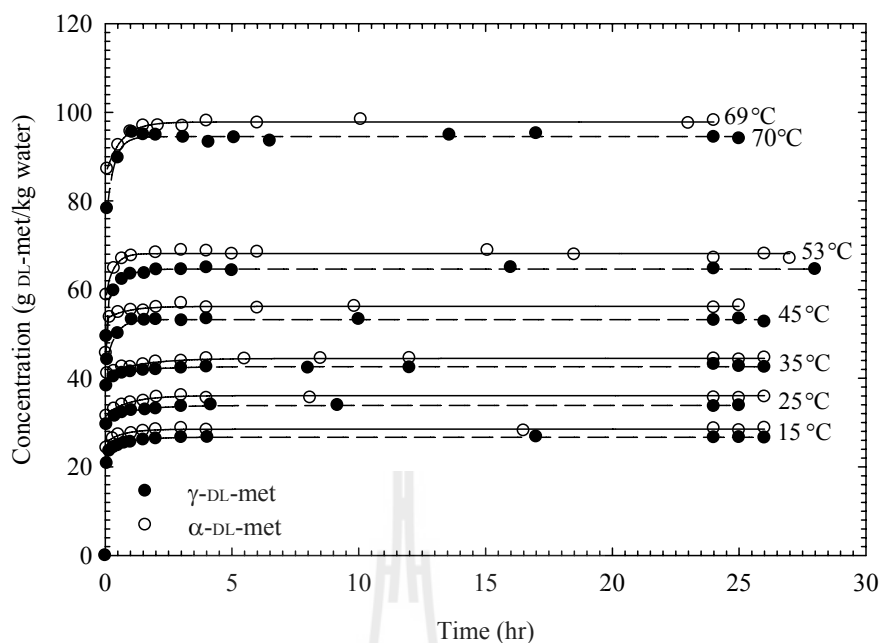


**Figure 2.13** Dissolution profiles for  $\alpha$ -DL-met and  $\gamma$ -DL-met in water.

**Table 2.3** Solubility of  $\alpha$ -DL-met and  $\gamma$ -DL-met in water.

Temperature (°C)	Solubility (standard deviation, s) (g DL-met/kg water)	
	$\alpha$ -DL-met	$\gamma$ -DL-met
5	22.67 (0.27)	20.80 (0.33)
15	28.55 (0.23)	26.69 (0.11)
25	35.62 (0.10)	33.70 (0.20)
35	44.44 (0.13)	42.70 (0.41)
45	56.23 (0.40)	53.03 (0.38)
53	67.91 (0.72)	64.78 (0.32)
69	97.97 (0.38)	-
70	-	94.34 (0.64)

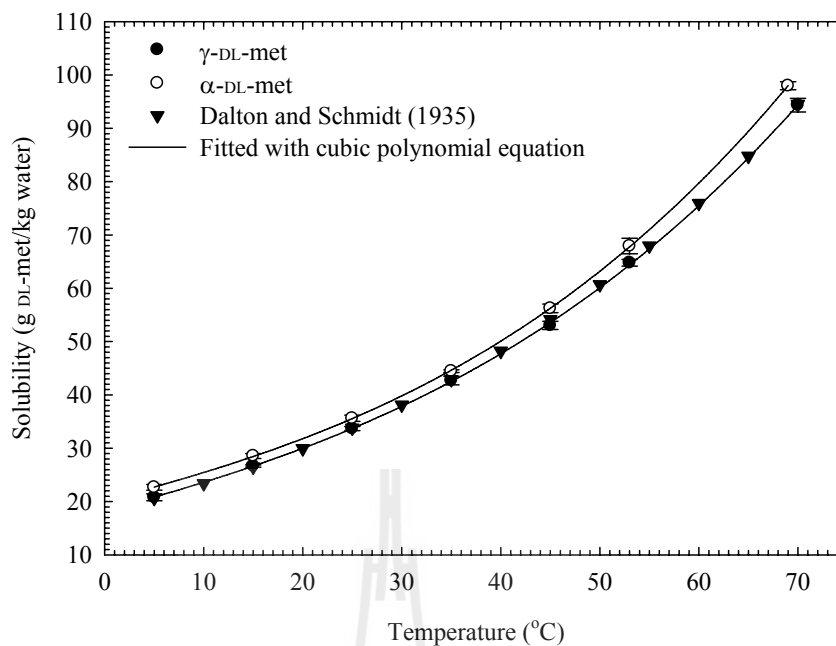


**Figure 2.14** Solubility of  $\alpha$ -DL-met and  $\gamma$ -DL-met in water.

No conversion of  $\gamma$ -DL-met was observed even after the solubility measurement of  $\gamma$ -DL-met. Some conversion from  $\alpha$ -DL-met to  $\gamma$ -DL-met was observed, but the transformation was not close to complete in the time interval of this measurement. From the experimental and simulation results of Yamanobe et al. (2002c) it was seen that during transformation from  $\alpha$ -DL-met to  $\gamma$ -DL-met the concentration of the solution was saturated with  $\alpha$ -DL-met (at the solubility of  $\alpha$ -DL-met) and after all of  $\alpha$ -DL-met transformed to  $\gamma$ -DL-met the concentration started to decrease to the solubility of  $\gamma$ -DL-met. Therefore, the saturation concentrations during the transformation of  $\alpha$ -DL-met in this experiment are expected to be the solubility of  $\alpha$ -DL-met. These indicate that  $\gamma$ -DL-met is the stable polymorph and  $\alpha$ -DL-met is the metastable polymorph.

The solubility curves showed the solubility of both  $\alpha$ -DL-met and  $\gamma$ -DL-met increased with increasing temperature, and the solubility of  $\alpha$ -DL-met is higher than that of  $\gamma$ -DL-met over the entire studied temperature range of 5 - 70 °C. This also indicates that  $\gamma$ -DL-met is the stable polymorph and  $\alpha$ -DL-met is the metastable polymorph between 5 and 70 °C: the solubility of the stable polymorph is always lower than that of the metastable form (Threfall, 2003). Scarce reference data for the solubility data of DL-met is available. The solubility of  $\gamma$ -DL-met in water is in agreement with the solubility of the industrial DL-met (a mixture of  $\alpha$ -DL-met and  $\gamma$ -DL-met) given by Dalton and Schmidt (1935). This indicates that the solubility of DL-met was determined after all of  $\alpha$ -DL-met transformed to  $\gamma$ -DL-met.

The solubility data in the temperature range of 5 - 70 °C was fitted using a cubic polynomial equation, with the results shown in equations (2.11) (for  $\alpha$ -DL-met) and (2.12) (for  $\gamma$ -DL-met), where  $C^*$  is the solubility in g of DL-met/kg of water and  $T$  is the experimental temperature in °C.

For  $\alpha$ -DL-met:

$$C^* = 20.02 + 4.897 \times 10^{-1}T + 2.566 \times 10^{-3}T^2 + 9.680 \times 10^{-5}T^3 \quad (2.11)$$

For  $\gamma$ -DL-met:

$$C^* = 18.23 + 5.053 \times 10^{-1}T + 2.436 \times 10^{-3}T^2 + 8.410 \times 10^{-5}T^3 \quad (2.12)$$

The root mean square deviation (rmsd) is defined as

$$\text{rmsd} = \left[ \frac{1}{N} \sum_{i=1}^N \left( \frac{C_c^* - C_{\text{exp}}^*}{C_{\text{exp}}^*} \right)^2 \right]^{1/2} \quad (2.13)$$

where  $C_c^*$  stands for values calculated by equation (2.10) or (2.11),  $C_{\text{exp}}^*$  stands for experimental values, and  $N$  stands for number of experimental points. The rmsd values for the fitting equation of  $\alpha$ -DL-met and  $\gamma$ -DL-met are 0.0021 and 0.0018, and R-squared values are 1.0 and 1.0, respectively. These values indicate that the solubility of  $\alpha$ -DL-met and  $\gamma$ -DL-met in water can be fitted with cubic polynomial equation well.

### 2.5.3 Thermodynamics

Fitting the mole fraction solubility data (Table 2.4) of  $\alpha$ -DL-met and  $\gamma$ -DL-met in water to equation (2.4) ( $\ln(x)$  against  $1/T$ ) will result in a straight line approximation, as shown in Figure 2.15. The  $\Delta H_{\text{diss}}$  and  $\Delta S_{\text{diss}}$  can be obtained from the slope of the solubility curve and the intercept with the  $y$  axis, respectively. As shown in Figure 2.15, the experimental solubility data fits well for both  $\alpha$ -DL-met and  $\gamma$ -DL-met. The estimated value of the  $\Delta H_{\text{diss}}$  and  $\Delta S_{\text{diss}}$  of the both polymorphs are listed in Table 2.2. The fitting equations of the two polymorphs are shown in equations (2.14) and (2.15), where  $T$  is in K.

For  $\alpha$ -DL-met:

$$\ln x = -\frac{2.1491 \times 10^3}{T} + 1.7837 \quad (2.14)$$

For  $\gamma$ -DL-met:

$$\ln x = -\frac{2.1927 \times 10^3}{T} + 1.8673 \quad (2.15)$$

**Table 2.4** Mole fraction solubility ( $x$ ) of  $\alpha$ -DL-met and  $\gamma$ -DL-met in water.

Temperature (K)	100x (100s) (mole fraction, [-])	
	$\alpha$ -DL-met	$\gamma$ -DL-met
278	0.2727 (0.0032)	0.2503 (0.0039)
288	0.3433 (0.0028)	0.3209 (0.0013)
298	0.4279 (0.0053)	0.4049 (0.0023)
308	0.5333 (0.0015)	0.5125 (0.0049)
318	0.6737 (0.0048)	0.6356 (0.0045)
326	0.8126 (0.0086)	0.7754 (0.0038)
342	1.1681 (0.0044)	-
343	-	1.1253 (0.0075)

The van't Hoff plots of real and ideal systems calculated using equations (2.2) and (2.3) respectively are shown in Figure 2.15. The solubility values in the van't Hoff plots were calculated using the values of  $T_{fus}$  and  $\Delta H_{fus}$  (equation (2.3)). The estimated activity coefficients are in the range of  $10^{-7}$  -  $10^{-4}$  which are very low values. This indicates that the system shows negative deviations from ideality where the real solubility is higher than the ideal solubility. The real solubility is higher than ideal solubility because of the strong interactions between DL-met and water molecules (Davey, Mullin, and Whiting, 1982). This means that

there are strong interactions between the hydrophilic head of DL-met molecules (consisting of  $-\text{NH}_3^+$  and  $-\text{COO}^-$ ) and the surrounding water molecules. The positive value of  $\Delta H_{diss}$  is due to the endothermic reaction of breaking the hydrogen bonds to create a cavity for the solutes within the aqueous solution (Anuar et al., 2009). The positive value of  $\Delta S_{diss}$  leads to the dissolution process will occur spontaneously at any temperatures below the melting point.

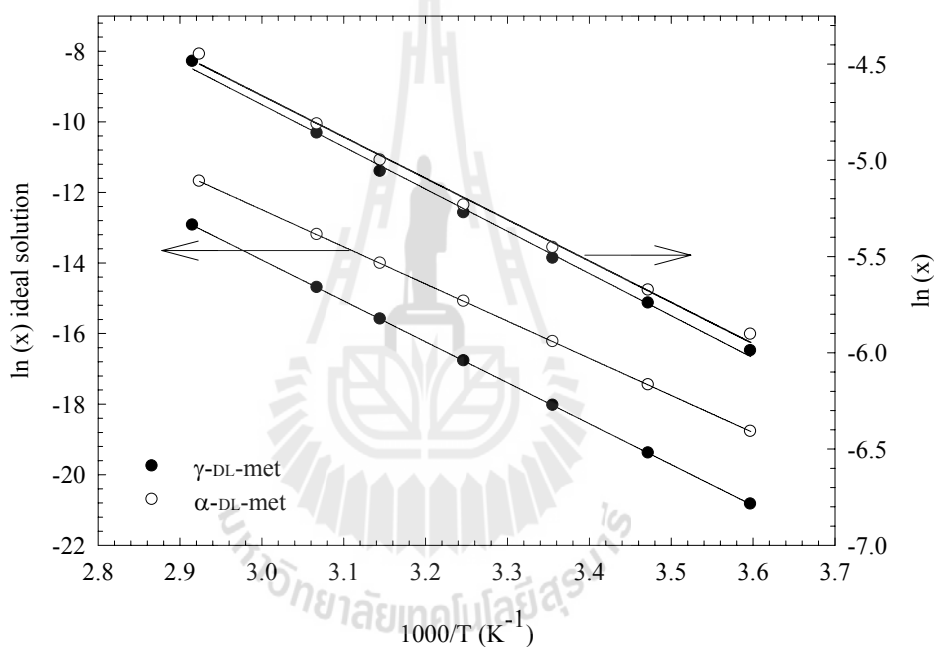


**Figure 2.15** Plot of van't Hoff solubility data of real and ideal solubility of  $\alpha$ -DL-met and  $\gamma$ -DL-met in water.

The plots of the change of the Gibbs free energy of the two polymorphs using equations (2.5) and (2.6) are shown in Figure 2.16. The Gibbs free energy of both polymorphs also confirms that  $\gamma$ -DL-met (which has a lower Gibbs free

energy) is the stable polymorph and  $\alpha$ -DL-met (which has a higher Gibbs free energy) is the metastable polymorph.

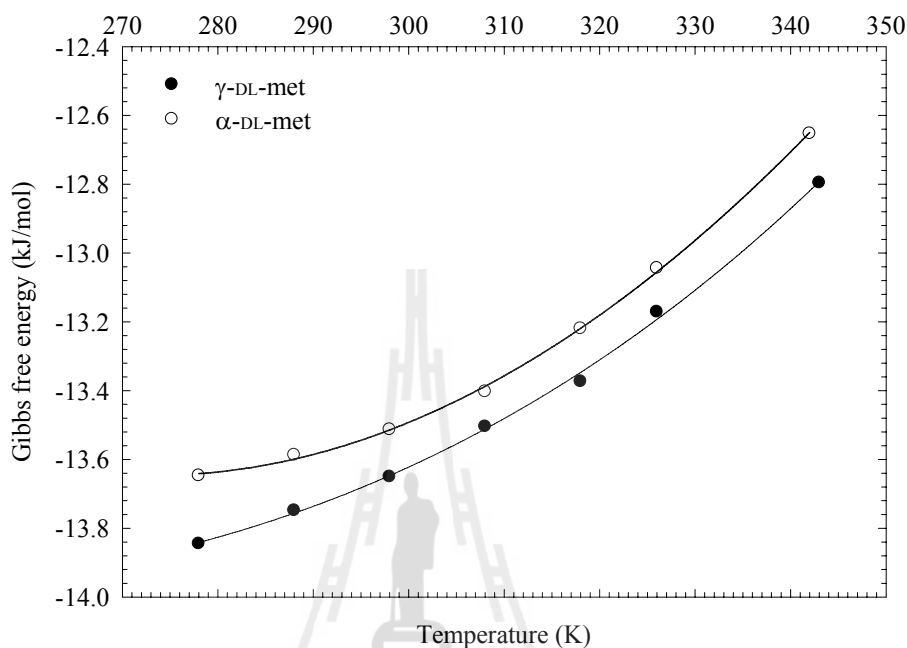


**Figure 2.16** Plot of Gibbs free energy of  $\alpha$ -DL-met and  $\gamma$ -DL-met. The solid lines are given to guide the eye.

#### 2.5.4 The Polymorphic Nature of DL-Met

In the DSC thermogram of the two polymorphs, the melting temperature of  $\gamma$ -DL-met is higher than that of  $\alpha$ -DL-met and the melting enthalpy of  $\gamma$ -DL-met is also higher than that of  $\alpha$ -DL-met. According to the Burger and Ramberger polymorphic rules (Grunenberg et al., 1996), this suggests monotropic polymorphism. Also the solubility curve of van't Hoff plot, and the plot of the Gibbs free energy strongly suggest that the two polymorphs are monotropic, since  $\gamma$ -DL-met is stable relative to  $\alpha$ -DL-met at all temperatures below the melting point, the polymorphs are not interconvertible, and the solubility of  $\gamma$ -DL-met is always lower than  $\alpha$ -DL-met.

## 2.6 Conclusions

The physical and chemical properties of the two main polymorphs of DL-met have been characterized. The polymorphic behavior was confirmed through analyses by XRPD, DSC, photo microscopy, as well as through solubility. It was shown that XRPD is the best method for a clear and fast identification and quantification of the polymorphs or polymorphic fraction during crystallization. DSC measurements show that the melting temperature and enthalpy of fusion of  $\gamma$ -DL-met are higher than those of  $\alpha$ -DL-met.  $\gamma$ -DL-met is shown to be the stable phase and  $\alpha$ -DL-met to be the metastable phase between 5 and 70 °C. The solubility of the metastable polymorph is higher than that of the stable polymorph. The solubility data of the two polymorphs are well fitted with the van't Hoff equation. The enthalpy of dissolution of the two polymorphs can be calculated from the slope of the van't Hoff plot, with the enthalpy of dissolution of  $\gamma$ -DL-met being higher than that of  $\alpha$ -DL-met. Based on the solubility data, DSC measurements, and Gibbs free energy the polymorphic nature of DL-met is a monotropic system.

## 2.7 References

- Anuar, N., Wan Daud, W.R., Roberts, K.J., Kamarudin, S.K., and Tasirin, S.M. (2009). An examination of the solution chemistry, nucleation kinetics, crystal morphology, and polymorphic behavior of aqueous phase batch crystallized L-isoleucine at 250 mL scale size. **Cryst. Growth Des.** 9(6): 2853-2862.
- Bauer, J., Spanton, S., Henry, R., Quick, J., Dziki, W., Porter, W., and Morris, J. (2001). Ritonavir: An extraordinary example of conformational polymorphism. **Pharm. Res.** 18(6):859-866.

- Beckmann, W. (2000). Seeding the desired polymorph: background, possibilities, limitations, and case studies. **Org. Process Res. Dev.** 4(5): 372-383.
- Brečević, L., and Nielsen, A.E. (1993). Solubility of calcium carbonate hexahydrate. **Acta Chem. Scand.** 47: 668-673.
- Burger, A., and Ramberger, R. (1979a). On the polymorphism of pharmaceuticals and other molecular crystals. I Theory of thermodynamic rules. **Microchim. Acta.** 72: 259-271. Quoted in Grunenberg, A., Henck, J-O., and Siesler, H.W. (1996). Theoretical derivation and practical application of energy/temperature diagrams as an instrument in preformulation studies of polymorphic drug substances. **Inter. J. Pharm.** 129(1-2): 147-158.
- Burger, A., and Ramberger, R. (1979b). On the polymorphism of pharmaceuticals and other molecular crystals. II Applicability of thermodynamic rules. **Microchim. Acta.** 72: 273-316. Quoted in Grunenberg, A., Henck, J-O., and Siesler, H.W. (1996). Theoretical derivation and practical application of energy/temperature diagrams as an instrument in preformulation studies of polymorphic drug substances. **Inter. J. Pharm.** 129(1-2): 147-158.
- Cashell, C., Sutton, D., Corcoran, D., and Hodnett, B.K. (2003). Inclusion of the stable form of a polymorph within crystals of its metastable form. **Cryst. Growth Des.** 3(6): 869-872.
- Chemburkar, S.R., Bauer, J., Deming, K., Spiwek, H., Patel, K., Morris, J., Henry, R., Spanton, S., Dziki, W., Porter, W., Quick, J., Bauer, P., Donaubaue, J., Narayanan, B.A., Soldani, M., Riley, D., and McFarland, K. (2000). Dealing with the impact of ritonavir polymorphs on the late stages of bulk drug process development. **Org. Process Res. Dev.** 4(5): 413-417.

- Cornel, J., Kidambi, P., and Mazzotti, M. (2010). Precipitation and transformation of the three polymorphs of D-mannitol. **Ind. Eng. Chem. Res.** 49(12): 5854-5862.
- Dalton, J., and Schmidt, C.L.A. (1935). The solubilities of certain amino acids and related compounds in water, the densities of their solutions at twenty-five degrees, and the calculated heats of solution and partial molal volumes. II. **J. Biol. Chem.** 109(1): 241-248.
- Davey, R.J., Mullin, J.W., and Whiting, M.J.L. (1982). Habit modification of succinic acid crystals grown from different solvents. **J. Cryst. Growth** 58(2): 304-312.
- Dharmayat, S., Anda, J.C.D., Hammond, R.M., Lai, X., Roberts, K.J., and Wang, X.Z. (2006). Polymorphic transformation of L-glutamic acid monitored using combined on-line video microscopy and X-ray diffraction. **J. Cryst. Growth** 294(1): 35-40.
- Dharmayat, S., Hammond, R.B., Lai, X., Ma, C., Purba, E., Roberts, K.J., Chen, Z-P., Martin, E., Morris, J., and Bytheway, R. (2008). An examination of the kinetics of the solution-mediated polymorphic phase transformation between  $\alpha$ - and  $\beta$ -forms of L-glutamic acid as determined using online powder X-ray diffraction. **Cryst. Growth Des.** 8(7): 2205-2216.
- Dong, Z., Padden, B.E., Salsbury, J.S., Munson, E.J., Schroeder, S.A., Prakash, I., and Grant, D.J.W. (2002). Neotame anhydrate polymorphs I: Preparation and characterization. **Pharm. Res.** 19(3): 330-336.
- Ferrari, E.S., and Davey, R.J. (2004). Solution-mediated transformation of  $\alpha$  and  $\beta$  L-glutamic acid: Rate enhancement due to secondary nucleation. **Cryst. Growth Des.** 4(5): 1061-1068.

- Flood, A.E. (2009). **Industrial crystallization from solution: A primer**. Thailand: Suranaree University of Technology.
- Garside, J., Mersmann, A., and Nyvlt, J. (2002). **Measurement of crystal growth and nucleation rates** (2<sup>nd</sup>). UK: Institute of Chemical Engineering.
- Grant, D.J.W. (1999). Theory and origin of polymorphism. In: H.G. Brittain (ed.). **Polymorphism in pharmaceutical solids, drugs and the pharmaceutical sciences Vol. 95** (pp 1-34). New York: Marcel Dekker.
- Grooff, D., Liebenberg, W., and De Villiers, M.M. (2011). Preparation and transformation of true nifedipine polymorphs: Investigated with differential scanning calorimetry and X-ray diffraction pattern fitting methods. **J. Pharm. Sci.** 100(5): 1944-1957.
- Grunenberg, A., Henck, J-O., and Siesler, H.W. (1996). Theoretical derivation and practical application of energy/temperature diagrams as an instrument in preformulation studies of polymorphic drug substances. **Inter. J. Pharm.** 129(1-2): 147-158.
- Himawan, C. (2005). **Characterization and population balance modeling of eutectic freeze crystallization**. Ph.D. Thesis, Delft University of Technology, The Netherlands.
- Hughes, C.E., and Harris, K.D.M. (2008). A Technique for in situ monitoring of crystallization from solution by solid-state <sup>13</sup>C CPMAS NMR spectroscopy. **J. Phys. Chem. A** 112(30): 6808-6810.

- Huthmacher, K; Binder, W; Hasselbach, H.J; Korfer, M; Rohland, L; Alt, H.C; Kniesel, H. Process for the preparation of aqueous sodium methioninate solutions and use of those solutions in the production of a granulate. U.S. 6,126,972, October 3, 2000.
- Jiang, S., Jansens, P.J., and ter Horst, J.H. (2010). Mechanism and kinetics of the polymorphic transformation of o-aminobenzoic acid. **Cryst. Growth Des.** 10(5): 2123-2128.
- Kaneniwa, N., and Otsuka, M. (1985). Effect of grinding on the transformations of polymorphs of chloramphenicol palmitate. **Chem. Pharm. Bull.** 33(4): 1660-1668.
- Kee, N.C.S., Tan, R.B.H., and Braatz, R.D. (2009). Selective crystallization of the metastable  $\alpha$ -form of L-glutamic acid using concentration feedback control. **Cryst. Growth Des.** 9(7): 3044-3051.
- Kitamura, M. (1993). Crystallization behavior and transformation kinetics of L-histidine polymorphs. **J. Chem. Eng. Jpn.** 26(3): 303-307.
- Kitamura, M. (2001). Crystallization and transformation mechanism of calcium carbonate polymorphs and the effect of magnesium ion. **J. Colloid Interface Sci.** 236(2): 318-327.
- Kitamura, M., Konno, H., Yasui, A., and Masuoka, H. (2002). Controlling factors and mechanism of reactive crystallization of calcium carbonate polymorphs from calcium hydroxide suspensions. **J. Cryst. Growth** 236(1-3): 323-332.

- Kolar, Z., Binsma, J.J.M., and Subotić, B. (1986). The formation of orthorhombic BaF<sub>2</sub> by precipitation from aqueous solutions and its transformation into cubic BaF<sub>2</sub>. **J. Cryst. Growth**. 76(2): 408-412. Quoted in C.P.M. Roelands. (2005). **Polymorphism in precipitation process**. Ph.D. thesis, Delft University of Technology, The Netherlands.
- Liu, W., Wei, H., and Black, S. (2009). An investigation of the transformation of carbamazepine from anhydrate to hydrate using in situ FBRM and PVM. **Org. Process Res. Dev.** 13(3): 494-500.
- Lu, J., Wang, X-J., Yang, X., and Ching, C-B. (2007). Polymorphism and crystallization of famotidine. **Cryst. Growth Des.** 7(9): 1590-1598.
- Mangin, D., Puel, F., and Veessler, S. (2009). Polymorphism in processes of crystallization in solution: A practical review. **Org. Process Res. Dev.** 13(6): 1241-1253.
- Maruyama, S., and Ooshima, H. (2000). Crystallization behavior of taltirelin polymorphs in a mixture of water and methanol. **J. Cryst. Growth** 212(1-2): 239-245.
- Mathieson, A.M. (1952). The crystal structures of the dimorphs of DL-methionine. **Acta Cryst.** 5: 332-341.
- Matsunaga, J., Nambu, N., and Nagai, T. (1976). Polymorphism of phenylbutazone. **Chem. Pharm. Bull.** 24(6): 1169-1172.
- Matsuoka, M., Yamanobe, M., Tezuka, N., Takiyama, H., and Ishii, H. (1999). Polymorphism, morphologies and bulk densities of DL-methionine agglomerate crystals. **J. Cryst. Growth** 198-199: 1299-1306.

- Miyazaki, S., Arita, T, Hori, R., and Ito, K. (1974). Effect of polymorphism on the dissolution behavior and gastrointestinal absorption of chlortetracycline hydrochloride. **Chem. Pharm. Bull.** 22(3): 638-642.
- Mohan, R., Koo, K-K., Strege, C., and Myerson, A.S. (2001). Effect of additives on the transformation behavior of L-phenylalanine in aqueous solution. **Ind. Eng. Chem. Res.** 40(26): 6111-6117.
- Mullin, J.W. (2001). **Crystallization** (4<sup>th</sup> ed.). Oxford: Butterworth-Heinemann.
- Nordström, F.L., and Rasmuson, Å.C. (2006). Polymorphism and thermodynamics of m-hydroxybenzoic acid. **Eur. J. Pharm. Sci.** 28(5):377-384.
- Ono, T., ter Horst, J.H., and Jansens, P.J. (2004). Quantitative measurement of the polymorphic transformation of L-glutamic acid using in-situ Raman spectroscopy. **Cryst. Growth Des.** 4(3): 465-469.
- Picciochi, R., Diogo, H.P., and Minas da Piedade, M.E. (2011). Thermodynamic characterization of three polymorphic forms of piracetam. **J. Pharm. Sci.** 100(2): 594-603.
- Ramachandran, E., and Natarajan, S. (2006). Gel growth and characterization of  $\beta$ -DL-methionine. **Cryst. Res. Technol.** 41(4): 411-415.
- Roelands, C.P.M. (2005). **Polymorphism in precipitation process**. Ph.D. thesis, Delft University of Technology, The Netherlands.
- Roelands, C.P.M., Jiang, S., Kitamura, M., ter Horst, J.H., Kramer, H.J.M., and Jansens, P.J. (2006). Antisolvent crystallization of the polymorphs of L-histidine as a function of supersaturation ratio and of solvent composition. **Cryst. Growth Des.** 6(4): 955-963.

- Schmidt, A.C. (2005). Solid-state characterization of chlorprocaine hydrochloride: part VI. Crystal polymorphism of local anaesthetic drugs. **J. Therm. Anal. Cal.** 81(2): 291-297.
- Shaibat, M.A., Casabianca, L.B., Siberio-Pérez, D.Y., Matzger, A.J., and Ishii, Y. (2010). Distinguishing polymorphs of the semiconducting pigment copper phthalocyanine by solid-state NMR and Raman spectroscopy. **J. Phys. Chem. B** 114(13): 4400-4406.
- Takayama, K., Nambu, N., and Nagai, T. (1980). Dissolution kinetics for coprecipitates of indomethacin with polyvinylpyrrolidone. **Chem. Pharm. Bull.** 28(11): 3304-3309.
- Taniguchi, T., Takaki, Y., and Sakurai, K. (1980). The crystal structures of the  $\alpha$  and  $\beta$  forms of DL-methionine. **Bull. Chem. Soc. Jpn.** 53(3): 803-804.
- Threlfall, T. (2003). Structural and thermodynamic explanations of Ostwald's rule. **Org. Process Res. Dev.** 7(6): 1017-1027.
- Umeda, T., Ohnishi, N., Yokoyama, T., Kuroda, K., Kuroda, T., Tatsumi, E., and Matsuda, Y. (1984). Kinetics of the thermal transition of carbamazepine polymorphic forms in the solid state. **Yakugaku Zasshi** 104(7): 786-792.
- Urakami, K., Shono, Y., Higashi, A., Umemoto, K., and Godo, M. (2002). A novel method for estimation of transition temperature for polymorphic pairs in pharmaceuticals using heat of solution and solubility data. **Chem. Pharm. Bull.** 50(2): 263-267.
- Vippagunta, S.R., Brittain, H.G., and Grant, D.J.W. (2001). Crystalline solids. **Adv. Drug Del. Rev.** 48(1): 3-26.

- Yamanobe, M., Takiyama, H., and Matsuoka, M. (2002a). Kinetic study on polymorphic solid-state transformation of organic compound: Bisphenol A and DL-methionine. **J. Chem. Eng. Jpn.** 35(3): 247-254.
- Yamanobe, M., Takiyama, H., and Matsuoka, M. (2002b). FT-IR study on the effect of solvents on polymorphic crystallization of organic compounds. **J. Chem. Eng. Jpn.** 35(6): 569-573.
- Yamanobe, M., Takiyama, H., and Matsuoka, M. (2002c). Polymorphic transformation of DL-methionine crystals in aqueous solutions. **J. Cryst. Growth** 237-239: 2221-2226.
- Yamanobe-Hada, M., Ito, A., and Shindo, H. (2005). Study of spontaneous cleavage and change in surface structure of DL-methionine crystals. **J. Cryst. Growth** 275(1-2): e1739-e1743.
- Yu, L., Reutzel, S.M., and Stephenson, G.A. (1998). Physical characterization of polymorphic drugs: An integrated characterization strategy. **Pharm. Sci. Technol. Today** 1(3): 118-127.

# CHAPTER III

## SECONDARY NUCLEATION THRESHOLD AND NUCLEATION KINETIS OF $\gamma$ -DL-METHIONINE

### 3.1 Abstract

The secondary nucleation threshold (SNT) of  $\gamma$ -DL-methionine ( $\gamma$ -DL-met) in aqueous solution was measured in an agitated batch system for the temperature range 10 - 61 °C. The width of the SNT is weakly temperature dependent with slightly smaller induction times at higher temperatures. Nucleation kinetics of  $\gamma$ -DL-met were measured in aqueous solution at 18, 25, and 35 °C using direct determination of the rate of nucleation based on measurements of particle (crystal) counts as a function of time. The number of crystals appearing in a microdroplet was counted by observation under a microscope. The nucleation rates increase with increasing temperature, and were found to exponentially increase with respect to the supersaturation of DL-met. The measured nucleation kinetics follows the trends expected from classical nucleation theory (CNT) allowing approximate interfacial energies to be estimated by fitting the measured data to CNT.

### 3.2 Introduction

In the crystallization from solution of a polymorphic compound when a driving force is imposed, the system tends to minimize its free energy. This leads to the crystallization of the most stable polymorph. However, the system may crystallize

into the less stable polymorph first if its crystallization kinetics are faster, and then the less stable polymorph may transform into the more stable one (Roelands, 2005). This phenomenon of formation of the kinetically controlled polymorph over the thermodynamically favored form is known as Ostwald's rule of stages (Threlfall, 2003). Moreover, if both polymorphs crystallize at similar rates, a mixture of the two polymorphs is initially obtained; this is called concomitant polymorphism (Bernstein, Davey, and Henck, 1999).

In the case of Ostwald's rule, there are three different steps that can be identified as fundamental mechanisms that govern the transformation process (Schöll, Bonalumi, Vicum, and Mazzotti, 2006; Jiang, Jansens, and ter Horst, 2010). The first step is the nucleation and growth of the metastable polymorph. During this step, the solute concentration drops from the initial value to the solubility of the metastable polymorph. The second step is the solution-mediated transformation (SMT), which consists of the nucleation and crystal growth of the stable polymorph and the dissolution of the metastable polymorph. The solute concentration remains constant at the solubility of the metastable polymorph during this step. During the third step, the solute concentration starts to decrease and the whole transformation process is complete when the solute concentration reaches the solubility of the stable polymorph.

For crystallization with seeding, which is commonly found in industrial crystallization, and if the metastable polymorph is seeded (if this polymorph is the required product), the metastable polymorph will transform to the stable polymorph via SMT (Davey, Cardew, McEwan, and Sadler, 1986; Kitamura, 2009). Therefore, crystallization processes involving polymorphs consist of the competitive nucleation

and crystal growth of the polymorphs, and the transformation from the metastable to the stable polymorph. To control polymorph formation, the mechanism of each elementary step in the crystallization process needs to be understood. Accurate kinetic information allows process modeling and enables process design, optimization, and control.

The determination of crystallization (nucleation and growth) and dissolution kinetics are important for characterization of the crystallization behavior and transformation of the polymorphs. Usually, the crystallization kinetics of the metastable polymorphs should be faster than the stable polymorphs when the metastable polymorphs appear first and then transform to more stable polymorphs (Bernstein et al., 1999; Rodríguez-Spong, Price, Jayasankar, Matzger, and Rodríguez-Hornedo, 2004). This has been found in various crystalline substances, for example, L-glutamic acid (Ono, Kramer, ter Horst, and Jansens, 2004), L-histidine (Roelands et al., 2006), and *o*-aminobenzoic acid (Jiang, ter Horst, and Jansens, 2008). In analysis of the mechanism and kinetics of SMT there are numerous publications describing the transformation process being controlled by the growth of the stable polymorph, for example, L-histidine (Kitamura, 1993), taltireline (Maruyama, Ooshima, and Kato, 1999), L-glutamic acid (Dharmayat et al., 2008; Ono et al., 2004; Schöll, Bonalumi et al., 2006), and carbamazepine (Qu, Louhi-Kultanen, Rantanen, and Kallas, 2006). On the other hand, the dissolution rate of the metastable  $\beta$  polymorph is the rate-determining step in the glycine system (Ferrari, Davey, Cross, Gillon, and Towler, 2003).

In this chapter the nucleation kinetics of  $\gamma$ -DL-met are described. The growth kinetics of  $\alpha$ -DL-met and  $\gamma$ -DL-met and dissolution kinetics of  $\alpha$ -DL-met are described

in Chapter IV. Only the nucleation kinetics of  $\gamma$ -DL-met are studied because  $\alpha$ -DL-met is seeded in the SMT experiment (as described in Chapter V) but  $\gamma$ -DL-met is not seeded. The supersaturation used in the SMT experiments is lower than the secondary nucleation threshold (SNT) of  $\alpha$ -DL-met and thus it does not nucleate. This leads to only the nucleation kinetics of  $\gamma$ -DL-met being required to describe the transformation process in aqueous solution, together with the growth and dissolution kinetics. Therefore, the nucleation kinetics of  $\gamma$ -DL-met are enough for considering the polymorphic transformation of DL-met for the applications we are considering in this thesis. Moreover, in this chapter, the SNT of this system is determined to ensure that the system for determining the growth and dissolution kinetics are operated under convenient non-nucleating conditions.

Determination of the nucleation rate is of key importance for the development of process models that can be used for process design and optimization. This is a difficult step in crystallization process design and development. Measurement and analysis of crystallization kinetics has proven to be challenging and currently there is not an established standard measurement procedure suitable in general (Schöll, Vicum, Müller, and Mazzotti, 2006). Numerous techniques for determination of the nucleation rate for crystallization process have been proposed in the literature, for example, methods using combined particle (crystal) counting and process time measurements (Lindenberg and Mazzotti, 2011; Galkin and Vekilov, 1999; Tsekova, Dimitrova, and Nanev, 1999), mixed-suspension mixed-product removal (MSMPR) experiments in combination with particle size distribution (PSD) measurements (Garside, Mersmann, and Nyvlt, 2002; Mersmann, 2001), induction time measurements (Lindenberg and Mazzotti, 2009; Teychené and Biscans, 2008) and

metastable zone experiments (Nagy, Fujiwara, Woo, and Braatz, 2008; Mitchell and Frawley, 2010). An overview of these techniques can be found elsewhere (Garside et al., 2002). The following examples are the different techniques to determine nucleation rate of the polymorphs that have been reported in the literature. The nucleation rate of metastable  $\alpha$  polymorph on the surface of the metastable  $\delta$  polymorph of D-mannitol was determined using direct counting of the number of  $\alpha$  polymorph crystals appearing on the surface of the  $\delta$  polymorph using observation under a microscope (Tao and Yu, 2006). The nucleation rates of the metastable  $\alpha$  polymorph of L-glutamic acid during reactive precipitation were determined from the induction time measurements, where the metastable  $\alpha$  polymorph precipitated from the reactive precipitation system (Schöll, Vicum et al., 2006; Lindenberg and Mazzotti, 2009). The nucleation rates of the A and B polymorphs of eflucimibe during the isothermal crystallization from ethanol and *n*-heptane solution at 35 °C were determined by induction time measurements; the nucleation rate of the B polymorph was determined at high supersaturation, while the nucleation rate of the A polymorph was determined at low supersaturation (Teychené and Biscans, 2008).

In the literature, the kinetics of nucleation together with the kinetics of growth and dissolution of each polymorph can also be estimated from the combination of the data from the polymorph transformation experiments and population balance modeling and parameter estimation. For example, this technique was applied to L-glutamic acid using both seeded and unseeded polymorph transformation (Cornel, Lindenberg, and Mazzotti, 2009; Ono et al., 2004; Schöll, Bonalumi et al., 2006), and continuous precipitation of polymorphs of calcium carbonate (Chakraborty and Bhatia, 1996a, 1996b).

Methods using combined particle (crystal) counting and process time measurements and MSMPR experiments in combination with PSD measurements are accurate enough for determining the nucleation kinetics of the polymorphs. The accuracy depends on the reliability and robustness of the experimental assumptions, experimental techniques, characterization techniques, data analysis, etc. Methods of induction time and metastable zone measurements are poor techniques to estimate the nucleation rates. This is since they are indirect methods to estimate the nucleation rates, and there are a lot of assumptions applied to these techniques; it hard to know whether the assumptions are correct or not, which may lead to non-realistic estimates of nucleation rates. The simulation technique is not yet proven to agree with experiments performed on a single polymorphic form. The drawback of this method is that the results can be skewed by incorrect parameter estimation of other parameters such as the crystal growth rate kinetics, which may lead to non-realistic estimates of nucleation rates. Therefore, in this work the nucleation rate was measured using methods of combined particle (crystal) counting and process time measurements.

The metastable zone width (MZW) is the width of the region between the supersolubility and the solubility curve. The secondary nucleation threshold (SNT) is the metastable limit for secondary nucleation, which is the upper limit of the metastable zone with regard to secondary nucleation (Srisa-nga, Flood, and White, 2006). MZW and SNT are not very much different. Both try to measure how much supersaturation can be generated before the system starts to nucleate, although these also depend on time. SNT is usually measured at constant temperature and concentration. The solutions are created and held at constant temperature, and the induction time is measured as the time at which the initial nucleation occurs

(Srisa-nga et al., 2006). MZW is a measurement which starts at the equilibrium i.e. ( $T^*$ ,  $C^*$ ) and then cools the solution at a constant rate ( $dT/dt$ ), and the time and temperature difference ( $\Delta T$ ) when the solution nucleates are measured (Zhang and Li, 2011; Lu, Wang, Yang, and Ching, 2007). This needs to be done at several cooling rates in order to estimate the MZW. Both measure times and supersaturation when the solutions nucleate, and both can be done for primary nucleation and for secondary nucleation.

In polymorphic systems the metastable limits can be measured as with the other systems (Zhang and Li, 2011; Lu et al., 2007). Usually for MZW measurement, after the crystals are nucleated the crystals are analyzed immediately to identify the polymorph. The identified crystal polymorph suggests the MZW of that polymorph. If the nucleated crystals are the stable polymorph (when the crystallization kinetics of the stable polymorph are faster than the metastable polymorph) the measured MZW is the MZW for the stable polymorph. However, if the nucleated crystals are the metastable polymorph (when the crystallization kinetics of the metastable polymorph are faster than the stable polymorph) the measured MZW is the MZW for the metastable polymorph. Examples of studies of such systems are the MZW of the metastable polymorph B of abecarnil in isopropyl acetate (Beckmann, Nickisch, and Budde, 1998), MZWs of stable polymorph A of famotidine in methanol and in acetonitrile (Lu et al., 2007), and MZW of concomitant polymorphs of eflucimibe in ethanol and *n*-heptane mixture (Teychené, Autret, and Biscans, 2004). Lu et al. (2007) also found that the MZW of metastable polymorph B in water was at 70 - 90°C, stable polymorph A was at 0 - 65°C, and concomitant polymorphs occurred at 65 - 70°C.

The aim of this work is to determine the SNT and nucleation rates of the stable  $\gamma$ -DL-met in aqueous solution. The SNT was determined to ensure that the growth is operated under convenient non-nucleating conditions and using an isothermal method similar to that of Srisa-nga et al. (2006). The nucleation rate was measured using methods of combined particle (crystal) counting and process time measurements. This was developed from the methods that were proposed by Galkin and Vekilov (1999) and Tsekova et al. (1999). The effects of supersaturation and temperature on nucleation rates and SNT were investigated.

### 3.3 Theory

Crystallization is a phase change in which a crystalline product is obtained from solution. A solution is a homogeneous single phase that is formed by the mixing of two or more species. Solutions are normally liquid, however, solutions may include solids and even gases. Typically, for the current work, the term solution means a liquid solution consisting of a solvent, which is a liquid as a pure species at the conditions,  $(T, P)$ , of the solution, and a solute, which is a solid as a pure species at the conditions of interest. The term melt means a material that is solid at ambient conditions and is heated until it becomes a molten liquid. Melts may be pure material or they may be mixtures of materials.

It has been said that “crystallization from solution is usually the result of two processes; crystal nucleation and crystal growth. These two processes can proceed either consecutively (in series) or simultaneously (in parallel) throughout the whole, or during only part, of the crystallization period depending on supersaturation levels” (Mullin, 2001).

Through this section the primary focus is on the theory of supersaturation, SNT, and nucleation. Other important terms of crystallization from solution, such as growth and dissolution, are described in Chapter IV.

### 3.3.1 Supersaturation

Crystallization from solution occurs when supersaturation is created because this acts as the driving force for crystallization. Supersaturation occurs when the solute concentration in a solvent exceeds its solubility (Randolph and Larson, 1988). The state of supersaturation is an essential requirement for all crystallization operations.

From a thermodynamic point of view this driving force is the difference in the Gibbs free energy between the actual condition of the system and its equilibrium condition. For a single-component crystal in a liquid solution under isothermal and isobaric conditions the supersaturation  $\Delta\mu$  is defined as

$$\Delta\mu = \mu_{sol} - \mu_c \quad (3.1)$$

where  $\mu_{sol}$  and  $\mu_c$  are the chemical potential of the molecule in solution and in the bulk of the crystal phase, respectively. When  $\Delta\mu > 0$ , the system is supersaturated and nucleation and growth of the crystals is possible. The driving force can be rewritten as (Mullin, 2001)

$$\Delta\mu = RT \ln S_a \quad (3.2)$$

with  $R$  is the ideal gas constant and is equal to 8.314 J/mol/K.  $S_a$  is the activity-based supersaturation ratio is defined as (Schwartz and Myerson, 2002)

$$S_a = \frac{a}{a^*} = \frac{\gamma C}{\gamma^* C^*} \quad (3.3)$$

where  $a$  is the actual activity,  $a^*$  is the equilibrium activity,  $\gamma$  is the actual activity coefficient,  $\gamma^*$  is the equilibrium activity coefficient,  $C$  is the actual concentration, and  $C^*$  is the equilibrium concentration. It is common practice to use the concentration  $C$  instead of  $x$  (mole fraction). Substituting equation (3.3) into equation (3.2) results in the equation

$$\frac{\Delta\mu}{RT} = \ln \frac{a}{a^*} = \ln \frac{\gamma C}{\gamma^* C^*} \quad (3.4)$$

Usually, the activity coefficients are not known and the dimensionless chemical potential difference is approximated by a dimensionless of concentration difference

$$\sigma = \frac{C - C^*}{C^*} = \frac{C}{C^*} - 1 = S - 1 \quad (3.5)$$

where  $\sigma$  is known as the concentration-based relative supersaturation and  $S$  is known as the concentration-based supersaturation ratio. This substitution is only accurate when  $\gamma/\gamma^* = 1$  and  $\sigma \ll 1$  (the system is dilute), so that equation (3.4) becomes

$$\frac{\Delta\mu}{RT} = \ln \frac{a}{a^*} \approx \ln(\sigma + 1) \approx \sigma \quad (3.6)$$

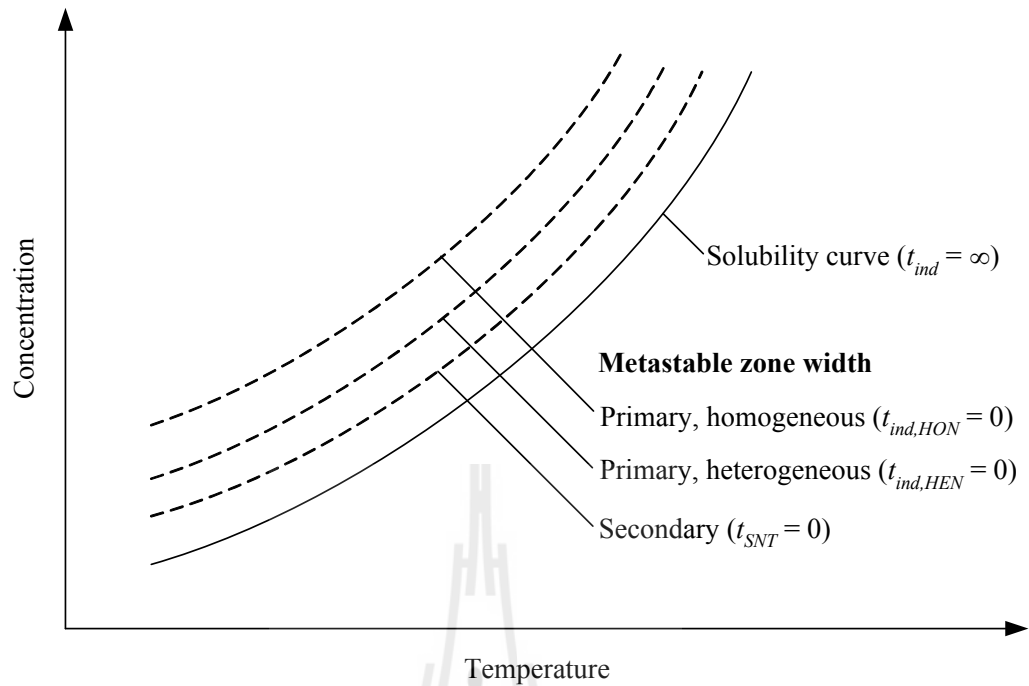
The supersaturation can also be expressed as concentration difference

$$\Delta C = C - C^* \quad (3.7)$$

### 3.3.2 Metastable Zone and Secondary Nucleation Threshold

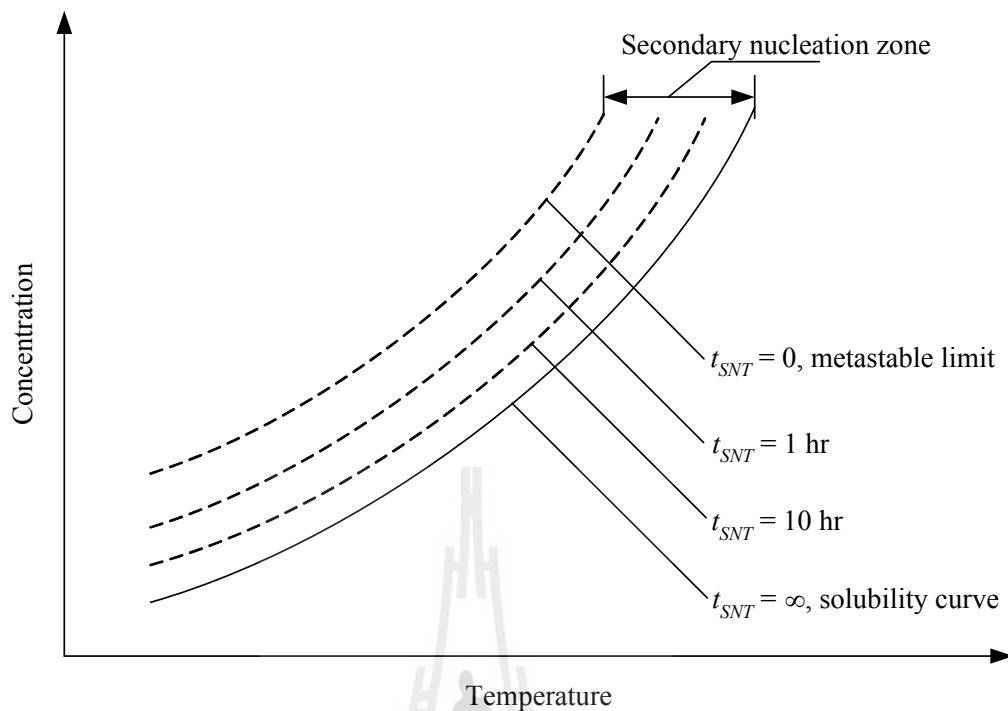
Crystals can grow without significant birth of new crystals (nuclei) in a metastable zone which is often exhibited by supersaturated solutions. When the supersaturation is sufficiently high, secondary nucleation in the presence of prior crystals occurs; the limit of this regime is referred to as the metastable limit for secondary nucleation (Srisa-nga et al. 2006) or the secondary nucleation threshold (SNT), depending on the method of measurement. The SNT is the upper limit of the metastable zone with regard to secondary nucleation. Nucleation is typically avoided or minimized in crystallization processes because it is difficult to control and gives a bad product size distribution. In batch processes the operation is usually undertaken in the metastable zone, and crystallization is initiated through the addition of seed crystals, thus avoiding large amounts of nucleation.

Figure 3.1 shows a metastable zone exhibited by supersaturated solutions together with the solubility curve (lowest solid line), where the widths of the zone for different nucleation mechanisms are drawn. At the solubility curve, the induction time,  $t_{ind}$ , is defined as the time where the nuclei appear (both primary and secondary) is approaching infinity. The increasing of the supersaturation above the solubility will cause the solution to reach a value where secondary nucleation, heterogeneous primary nucleation, and homogeneous primary nucleation, occur progressively. The limits of these regimes are referred to as the metastable limit or nucleation threshold for the particular mechanism. The zone boundaries are all time dependent, i.e. they depend on the induction time.



**Figure 3.1** Instantaneous metastable zone widths for different nucleation mechanisms (adapted from Mersmann, 2001). The variables  $t_{SNT}$ ,  $t_{ind,HEN}$ , and  $t_{ind,HON}$ , are the induction time for secondary nucleation, heterogeneous, and homogeneous nucleation, respectively.

The secondary nucleation zone in Figure 3.1 is expanded in Figure 3.2. The instantaneous secondary nucleation threshold (metastable limit,  $t_{SNT} = 0$ ) is represented by the upper dashed line. The time dependent secondary nucleation zone is the zone between this line and the solubility curve. The time dependent secondary nucleation thresholds are also drawn in this zone. The time necessary to induce secondary nuclei varies from zero (at the metastable limit for secondary nucleation) to infinity (at the solubility curve). This is since the smaller the supersaturation the greater the time required to induce nucleation to occur in the presence of the solute crystals in the system.



**Figure 3.2** A diagrammatic representation of the secondary nucleation thresholds of solution crystallization.

### 3.3.3 Nucleation Kinetics

Nucleation involves a process of fluctuation of the size of nanoscopically small molecular clusters potentially creating nuclei of the new crystalline phase. This leads to the formation of new crystals in the liquid solution. The number  $n$  of molecules constituting the cluster is used to identify the size of a cluster. The clusters of size  $n = n^*$ , which stay in unstable equilibrium with the ambient solution, are called nuclei (or critical nuclei), and the smaller ( $n < n^*$ ) or the larger ( $n > n^*$ ) clusters are the subnuclei or the supernuclei, respectively. Only the supernuclei can grow spontaneously to macroscopic sizes. Therefore, the nucleation rate  $J$  is defined as the number of supernuclei generated in the system per unit time

and per unit volume (or area for surface nucleation) is an important kinetic characteristic of the nucleation process (Kashchiev and van Rosmalen, 2003).

Nucleation is classified into primary and secondary nucleation (Figure 3.1). Primary nucleation is the birth of new crystals from a liquid or solution that contains no crystalline material of the nucleating solute, and is divided into homogeneous primary nucleation and heterogeneous primary nucleation. In homogeneous primary nucleation there are no external nucleation sites available (as could be caused by the walls of the vessel, dust particles, crystals or solids of other solutes, etc.), and the nuclei are formed by statistical fluctuations of solute entities that cluster together (Kramer and van Rosmalen, 2009). Heterogeneous primary nucleation occurs when the presence of such foreign surfaces assists in obtaining primary nuclei. Secondary nucleation is the formation of new nuclei which occurs due to the presence of crystals of the crystallizing material that are already present in the solution. Secondary nucleation is far more significant than primary nucleation in most industrial crystallization units because the vessel is run continuously having solute crystals inside.

### **Primary nucleation**

The classical nucleation (CNT) theory has been described as follows by Kashchiev (2000). The rate of nucleation,  $J$  ( $\#/m^3 \cdot s$ ), can be described according to the following equation

$$J = AS \exp\left(\frac{-W^*}{kT}\right) \quad (3.8)$$

where  $A$  is the pre-exponential kinetic parameter ( $\text{m}^{-3} \text{s}^{-1}$ ),  $W^*$  is the nucleation work (J),  $k$  is the Boltzmann constant and is equal to  $1.38 \times 10^{-23}$  J/K and  $T$  is the temperature (K).

For homogeneous nucleation (HON)  $A_{HON}$  is inversely proportional to the molecular volume  $v_0$  ( $\text{m}^3$ )

$$v_0 = \frac{M}{\rho_c N_A} \quad (3.9)$$

where  $M$  is the molecular mass (g/mol),  $\rho_c$  is the crystal density ( $\text{kg}/\text{m}^3$ ), and  $N_A$  is the Avogadro number ( $\text{mol}^{-1}$ ) and is equal to  $6.02 \times 10^{23}$   $\text{mol}^{-1}$ . Assuming spherical nuclei, the nucleation work in the exponent in equation (3.8) is defined as

$$W^* = \frac{16\pi v_0^2 \gamma^3}{3(kT)^2 \ln^2 S} = \frac{1}{2} n^* kT \ln S \quad (3.10)$$

where  $\gamma$  is the interfacial energy ( $\text{J}/\text{m}^2$ ). The nucleus size  $n^*$  (-) is defined according to the Gibbs-Thomson equation

$$n^* = \frac{32\pi v_0^2 \gamma^3}{3(kT)^3 \ln^3 S} \quad (3.11)$$

Nucleus size and nucleation work depend on two main parameters: the externally controlled supersaturation ratio and the material surface/solution composition-dependent interfacial energy. Substitution of equations (3.10) and (3.11) into equation (3.8) gives

$$J = AS \exp\left(-\frac{B}{\ln^2 S}\right) \quad (3.12)$$

where  $B$  is a thermodynamic parameter and is defined as

$$B = \frac{16\pi v_0^2 \gamma^3}{3(kT)^3} \quad (3.13)$$

In practice, most primary nucleation is likely to occur by the heterogeneous mechanism which is induced by the surfaces of foreign particles. Therefore, it requires significantly lower supersaturations than homogeneous nucleation. The rate equation appears to be of similar form to that of homogeneous nucleation but the supersaturation required is lower (Dirksen and Ring, 1991).

For 3D heterogeneous nucleation (HEN), the effective interfacial energy,  $\gamma_{eff}$  will be reduced by an activity factor,  $0 < \varphi < 1$ , compared to the interfacial energy  $\gamma$  for HON. The work of formation for HEN is substantially reduced compared to that for HON because  $\gamma_{eff} < \gamma$  since part of the surface is created by growth onto imperfections in the solid substrate. Furthermore, for HEN the  $A_{HEN}$  becomes inversely proportional to the concentration of heterogeneous particles,  $C_a$  ( $m^{-3}$ ), which is much smaller than the molecular volume,  $v_0$ . Typically  $A_{HEN} \approx 10^{15} - 10^{25} \ll A_{HON} \approx 10^{35}$  (Roelands et. al., 2006).

### **Secondary nucleation**

Secondary nucleation is far more significant than primary nucleation in most industrial crystallization units because the vessel is run continuously having solute crystals inside. There are five principle mechanisms of secondary nucleation, as shown below (Randolph and Larson, 1988)

1. Contact nuclei are formed from crystal-crystal, crystal-vessel wall, and crystal-impeller contacts that result in the removal of an adsorbed layer from a growing crystal. If the amount of adsorbed layer removed is above the size of the critical nucleus, it forms a nucleus.
2. Shear nucleation is a similar mechanism where the adsorbed layer is removed by fluid shear.
3. Fracture nucleation is caused by breakage of crystals due to collisions similar to those in (1).
4. Attrition nuclei are attrition fragments of larger crystals caused by contacts similar to those in (1).
5. Needle breeding results from the removal of dendritic fragments from a larger crystal.

For design and analysis purposes, nucleation is most often modeled with empirical models of the form (Flood, 2009)

$$B^0 = k_N \sigma^a T^b \omega^c M_T^d \quad (3.14)$$

where  $B^0$  is the nucleation rate,  $\sigma$  is the supersaturation,  $T$  is the temperature,  $\omega$  is the agitation speed, and  $M_T$  is the 'suspension density' (g crystal/g suspension).  $k_N$ ,  $a$ ,  $b$ ,  $c$ , and  $d$  are empirical constants obtained from experimental measurements.

## 3.4 Materials and Methods

### 3.4.1 Materials

DL-met (>99%) was purchased from Acros Organics and inert liquid paraffin was purchased from Vidhyasom (Thailand). The deionized water used was treated by reverse osmosis.

### 3.4.2 Apparatus

A 0.5 L batch crystallizer with a sealed glass lid to reduce solvent evaporation (Figure 2.9 in Chapter II) was used to measure the SNT. The slurry is continuously agitated at the set speed by a centrally located four-blade impeller driven by an overhead stirrer. The crystallizer was placed inside a constant temperature water bath, where the temperature was controlled within  $\pm 0.5^\circ\text{C}$ .

### 3.4.3 Secondary Nucleation Threshold Measurement

SNT experiments were performed at 10, 25, 40, and 61 °C in a 0.5 L batch crystallizer (Figure 2.9 in Chapter II) for a range of supersaturated solutions containing  $\gamma$ -DL-met seed crystals using a method similar to that of Srisa-nga et al. (2006). A series of supersaturated solution were prepared and heated to 20 °C above the experimental temperature (this is also at least 5 °C above saturation temperature) for 30 to 40 min to ensure that no ghost nuclei remained in the solution. Approximately 3 mg of sieved  $\gamma$ -DL-met crystals, 75 - 105  $\mu\text{m}$  in size, was added to each solution to induce secondary nucleation. Nucleation was observed by the naked eye at particular time intervals, with nucleation being indicated by precipitation or clouding due to the very fine nuclei particles. The clouding occurring in the experiments was clearly visible and the distinction between solutions that had precipitated at a particular measurement time and those that had not was clear. The

highest concentration solution that had not nucleated at a particular time and the lowest concentration that had nucleated were both recorded. All experiments were duplicated to check reproducibility.

#### 3.4.4 Nucleation Rate Measurement

Crystals obtained from cooling crystallization from aqueous solutions of DL-met have previously been found to be  $\gamma$ -DL-met (Matsuoka, Yamanobe, Tezuka, Takiyama, and Ishii, 1999), and this work obtains the same polymorph using identification by XRPD (see Chapter II: Preparation of Polymorph).

The direct determinations of the rate of nucleation are described as follows. The principle of this technique is illustrated in Figure 3.3 and the experiment setup is illustrated in Figure 3.4. A saturated solution at the temperature under consideration was prepared at a temperature  $T_0$  (see Figure 3.3), chosen to prevent nucleation of crystals. To prepare this solution, a known amount of DL-met was dissolved in 300 mL of water in a 0.5 L batch crystallizer agitated at 350 rpm by an overhead stirrer maintained at a constant temperature,  $T_0$ . Note that  $T_0$  is at least 5 °C above  $T_{sat}$  and at least 20 °C above  $T_1$ .

A solution droplet with a volume of 0.2  $\mu$ L (prepared using a micropipette) at  $T_0$  was placed in the nucleation cell which was maintained at the selected  $T_1$ . This temperature was such that the nucleation process was initiated at the desired supersaturation level. After a specific time interval ( $\Delta t_1$ ) for nucleation, the temperature  $T_1$  was raised to a temperature  $T_2$  at which the supersaturation was at a sufficiently low level to prevent further nucleation, but allowed existing crystals to grow to a visible size. During this stage the numbers of crystals that appeared in the solution droplet was counted using observation under a microscope. After plotting the

total number of crystals detected in the droplet as a function of  $\Delta t_1$ , the nucleation rate was determined from the slope of this plot as  $\Delta t_1$  approaches zero divided by the volume of the solution droplet. Note that the times required to change the temperature from  $T_0$  to  $T_1$  and  $T_1$  to  $T_2$  depend on the thermal property of the material of the nucleation cell and the size of droplet. In this case the times were about 5 - 10 sec because of the very small size of droplet. At a high nucleation temperature, 35 °C for this work, inert liquid paraffin was used to cover the solution droplet to reduce the effect of the liquid evaporation due to very small size of the droplet.

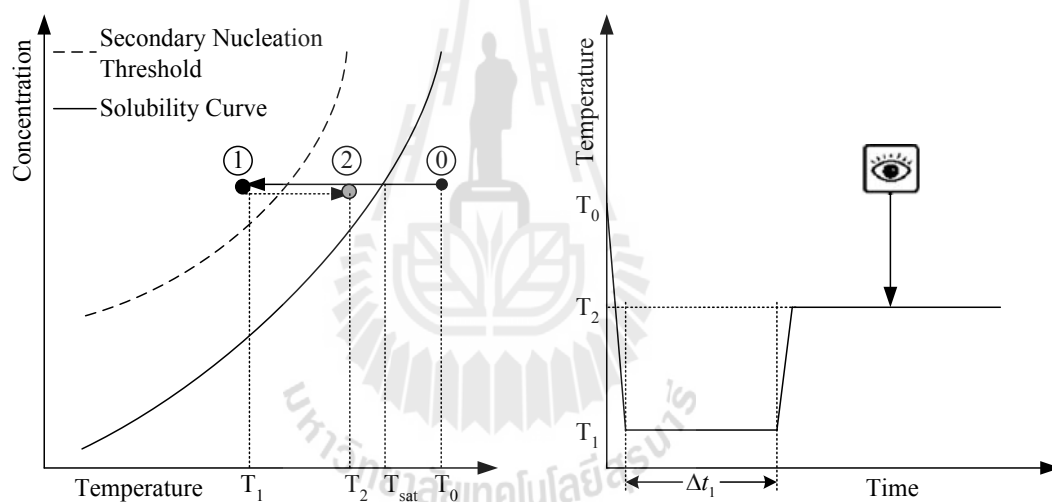


**Figure 3.3** Position in the phase diagram and temperature profile during a nucleation experiment.

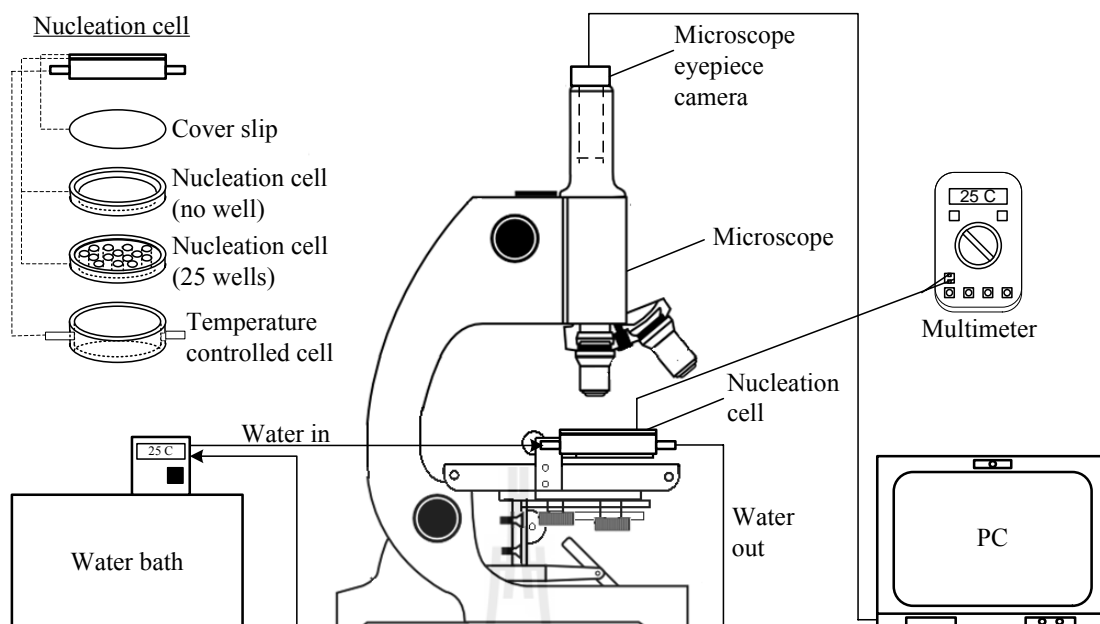


**Figure 3.4** Schematic of the experiment setup. The nucleation cell is made from acrylic, and flat-bottom wells are used.

The experimental conditions for nucleation measurements are shown in Table 3.1. The nucleation rates of  $\gamma$ -DL-met in aqueous solution were determined for three different temperatures ( $T_1$ ): 18, 25 and 35 °C, and at each temperature the nucleation rate was determined at various values of supersaturation ( $\sigma_1$ ). For each value of the initial supersaturation the number of crystals that appeared in the solution droplet was counted at 4 - 6 values of the nucleation time  $\Delta t_1$ , and for each value of  $\Delta t_1$  the measurements were performed with 3 - 6 replicates. For each value of  $\Delta t_1$  the number of crystals was counted at particular times during the growth stage, and stopped when the number of crystals did not change with time. The number of crystals detected at the end of this period is the number of crystals nucleated during  $\Delta t_1$ ; the experiment must be performed in this way since newly nucleated crystals are too small to be detected until growth to a visible size has occurred. The growth occurs

at a supersaturation ( $\sigma_2$ ) within the SNT width (for the time period of the measurement) and hence no new nuclei are formed during the growth period.

**Table 3.1** Experimental conditions for nucleation measurements.

Exp. no. (no. of runs <sup>*</sup> )	$T_{sat}$ (°C)	$T_1$ (°C)	$\sigma_1 = S_1-1$ (-)	$T_2$ (°C)	$\sigma_2 = S_2-1$ (-)
1(18)	25.00	18	0.17	22.00	0.067
2(22)	27.75	18	0.26	24.00	0.092
3(21)	29.00	18	0.29	26.00	0.072
4(21)	29.50	18	0.31	27.00	0.061
5(18)	31.50	18	0.36	28.00	0.079
6(20)	31.50	25	0.17	29.00	0.060
7(19)	33.25	25	0.21	31.00	0.053
8(20)	34.00	25	0.24	32.00	0.050
9(16)	35.00	25	0.26	32.50	0.057
10(15)	35.50	25	0.28	33.00	0.060
11(20)	41.00	35	0.15	38.00	0.072
12(20)	41.75	35	0.17	39.00	0.065
13(20)	42.50	35	0.19	40.00	0.058
14(19)	44.00	35	0.23	42.00	0.052

Note: <sup>\*</sup> The number of runs consists of all runs for the condition. A typical condition is measured for 5 nucleation times with 4 replicate experiments at each nucleation time.

### 3.4.5 Characterization of Uncertainty

Wherever uncertainty is indicated in this chapter the uncertainty is represented by 90% confidence interval (see Appendix A).

## 3.5 Results and Discussions

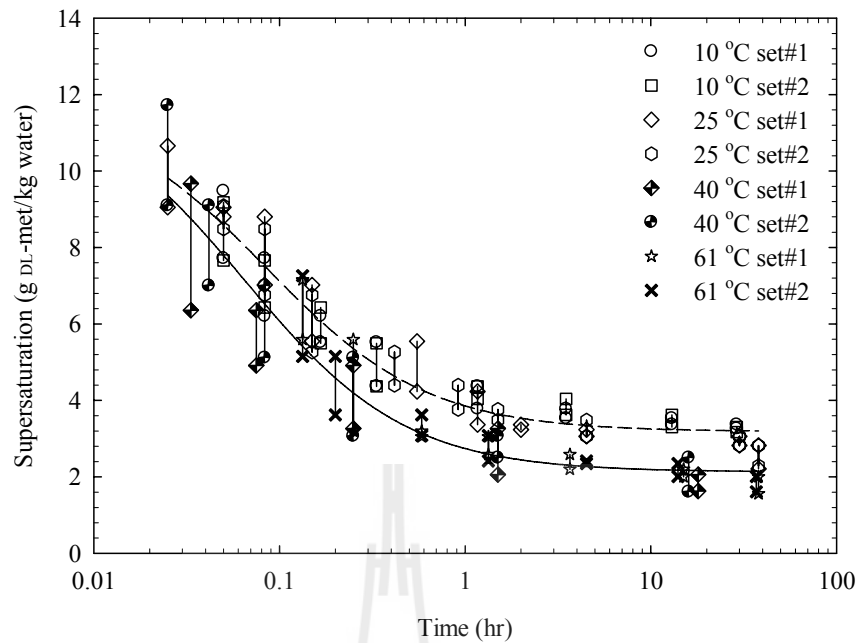
### 3.5.1 Secondary Nucleation Threshold

Table 3.2 shows an example of the observation time on the measured secondary nucleation for the first replicate experiment at 10 °C. The effect of induction time on the measured SNT at different temperatures is shown in Figure 3.5. In this figure, the upper point on each vertical line represents the lowest absolute supersaturation that had nucleated, and the lower point represents the highest absolute supersaturation that had not nucleated. This means that the true value of the SNT must lie between these two points. The mean value of these two points is an approximation for the true SNT at this experimental time. This figure shows the time dependence of the SNT, with the SNT decreasing as the induction time increases. In terms of absolute supersaturation, the initial time SNT is about 11.8 g of DL-met/kg of water for 10 and 25 °C, and 12.1 g of DL-met/kg of water for 40 and 61 °C. At large induction times, greater than 50 h, the SNT is about 3.2 g of DL-met/kg of water for 10 and 25 °C, and 2.2 g of DL-met/kg of water for 40 and 61 °C. After 2 days there were still some solutions of low supersaturation which had not nucleated.

**Table 3.2** Secondary nucleation experimental results at 10 °C, replicate number 1.

Inspection time (hr)	Concentration (g DL-met/kg water)								
	26.66	26.77	26.93	27.18	27.77	28.92	29.60	31.12	32.88
0.03	X	X	X	X	X	X	X	X	X
0.05	X	X	X	X	X	X	X	X	√
0.08	X	X	X	X	X	X	X	√	√
0.17	X	X	X	X	X	X	√	√	√
0.33	X	X	X	X	X	√	√	√	√
1.00	X	X	X	X	?	√	√	√	√
1.17	X	X	X	X	√	√	√	√	√
2.50	X	X	X	X	√	√	√	√	√
3.00	X	X	X	?	√	√	√	√	√
3.50	X	X	X	√	√	√	√	√	√
8.00	X	X	X	√	√	√	√	√	√
11.0	X	X	?	√	√	√	√	√	√
12.0	X	X	?	√	√	√	√	√	√
13.0	X	X	√	√	√	√	√	√	√
24.0	X	X	√	√	√	√	√	√	√
28.0	X	?	√	√	√	√	√	√	√
29.0	X	√	√	√	√	√	√	√	√
46.0	X	√	√	√	√	√	√	√	√

Note: The tick symbol indicates that secondary nuclei were observed, the cross symbol indicates that secondary nuclei were not observed, and the question mark represents cases where the result could not be clearly determined.



**Figure 3.5** The time dependence of the secondary nucleation zone width based on DL-met concentrations at temperatures of 10, 25, 40, and 61 °C. The dashed line represents the model for data at 10 and 25 °C. The solid line represents the model for data at 40 and 61 °C.

Since the SNTs at temperatures of 10 and 25, and 40 and 61 °C do not overlap when plotted in terms of the absolute value of supersaturation, the induction time dependence of the SNT is plotted separately. This indicates that temperature has an effect on the SNT over the range of temperatures that DL-met is likely to be crystallized.

The data in Figure 3.5 were fitted with a hyperbolic decay with three parameters. Equations (3.15) and (3.16) show the fitted equations, where  $C$  represents the total DL-met concentration (g of DL-met/kg of water) for the SNT,  $C^*$  is the solubility, and  $t_{ind}$  is the observation time in hours.

$$C - C^* = 3.1828 + \frac{0.7266}{0.0845 + t_{ind}} \quad \text{for } 5^\circ\text{C} < T < 40^\circ\text{C} \quad (3.15)$$

$$C - C^* = 2.1287 + \frac{0.6519}{0.0651 + t_{ind}} \quad \text{for } 40^\circ\text{C} < T < 70^\circ\text{C} \quad (3.16)$$

The solubility data of  $\alpha$ -DL-met and  $\gamma$ -DL-met in the temperature range of 5 - 70 °C are described in Chapter II and is plotted as a function of temperature in Figure 3.6. The solubility of  $\gamma$ -DL-met (g of DL-met/kg of water) was fitted using a cubic polynomial with the result shown in equation (3.17), where  $T$  represents the experimental temperature in °C.

$$C^* = 18.23 + 5.053 \times 10^{-1}T + 2.436 \times 10^{-3}T^2 + 8.410 \times 10^{-5}T^3 \quad (3.17)$$

Substitution of equation (3.17) into equation (3.15) gives the SNT concentration as a function of time between 5 and 40 °C, and substitution of equation (3.17) into equation (3.16) gives the SNT concentration as a function of time between 40 and 70 °C.

The induction time dependence of the SNT of  $\gamma$ -DL-met in aqueous solution is shown in Figure 3.6. SNT determines limitations on either the operating concentration or the batch time to ensure that nuclei are not formed, so it is very important for control of seeded batch crystallizations. For example, when the crystallization is performed at 25 °C and the operating time is within 1 h, the initial concentration that can operate without a significant birth of new crystals is up to 37 g of DL-met/kg of water. This example is reasonable when the seeding rate is very low (or the growth rate is very low) and then the concentration is constant. If the seeding

rate is higher, and the growth rate is not low, then the concentration drops quickly during the batch, and the batch may stay within the SNT for all  $t = 0$  to  $t = \infty$ .

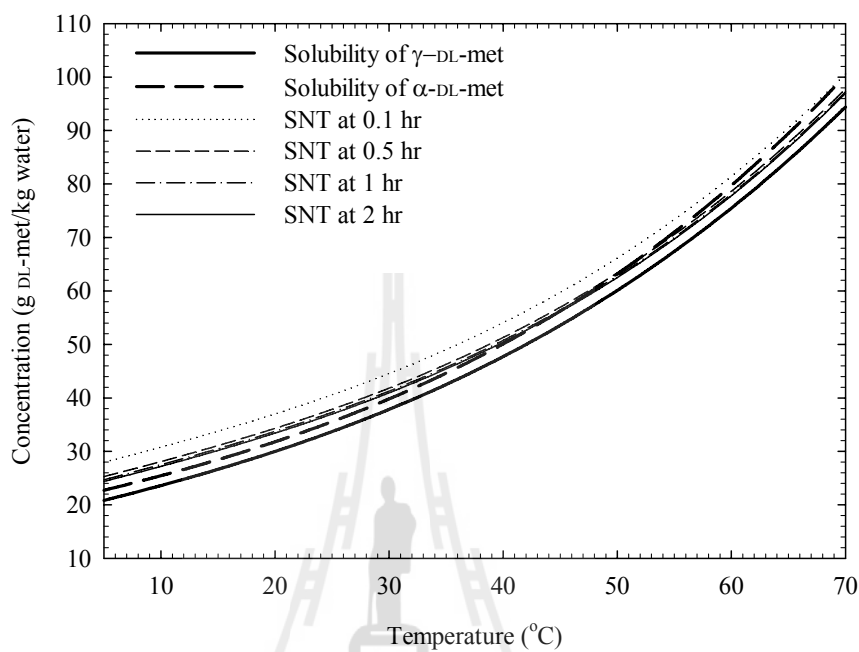


**Figure 3.6** Secondary nucleation thresholds for  $\gamma$ -DL-met at operating times of 0.1, 0.5, 1.0, and 2.0 hr.

The SNT of  $\alpha$ -DL-met was not measured in this work since experiments were performed in regions where only  $\gamma$ -DL-met will nucleate. The SNT technique used by Lu et al. (2009) is appropriate for the metastable form. However, growth experiments for  $\alpha$ -DL-met can only be performed within the area between the SNT of  $\gamma$ -DL-met and the solubility of  $\alpha$ -DL-met. This is reasonable for the temperature range 5 - 35 °C.

### 3.5.2 Nucleation Kinetics of $\gamma$ -DL-Met

Figure 3.7 illustrates photomicrographs of crystals nucleated in a droplet from a measurement at 18 °C and  $S = 1.36$ . The number of crystals nucleated during  $\Delta t_1$  are 47, 84, 114, and 124 crystals respectively for nucleation times of 10, 15, 40, and 60 seconds. During the measurement the shape and size of droplet did not change, which indicates that evaporation from the solution droplet did not occur during nucleation measurement.

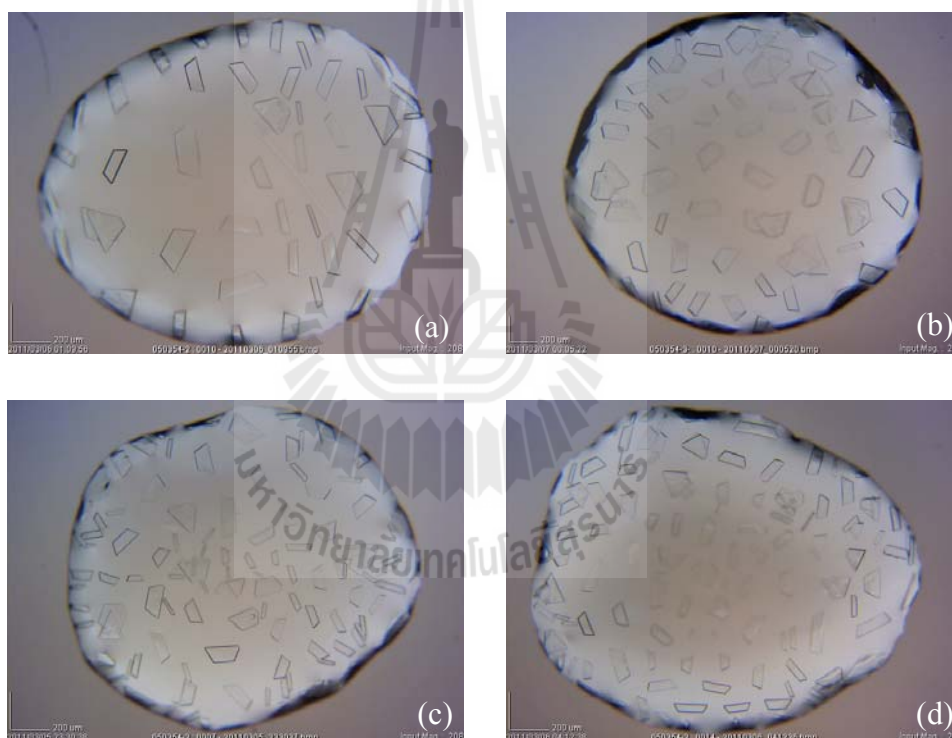


**Figure 3.7** Micrographs of crystals nucleated in a droplet at various nucleation times; measurement at 18 °C and  $S = 1.36$ :  
10 s (a), 15 s (b), 40 s (c), 60 s (d).

Figures 3.8, 3.9, and 3.10 show that the mean number of nucleated crystals ( $N$ ) increases with increasing nucleation time and supersaturation for the nucleation rate measurements at 18, 25, and 35 °C, respectively. The plots start from zero crystals (no nucleation) at  $\Delta t_1 = 0$  because the measurement starts with a clear solution. At higher nucleation times the mean number of nucleated crystals approaches a constant value because the solution concentration approaches the metastable limit due to the crystal growth during the experiment. Usually, for each  $\Delta t_1$  measurement the crystals that appeared in the solution droplet consist of the new crystals formed and crystals that grow to larger size. To cancel the effect of the change in supersaturation due to growth, the nucleation rate should be determined for the earlier stages (at small values of  $\Delta t_1$ ) of the measurement. This also indicates that the nucleation rate is measured at constant concentration because at very small  $\Delta t_1$  the concentration is nearly constant because the number of nuclei produced is small. The nucleation rate is determined from the slope of these plots as  $\Delta t_1$  approaches zero divided by the volume of the solution droplet ( $V$ ):

$$J = \left. \frac{dN}{dt} \right|_{\Delta t_1=0} \cdot \frac{1}{V} \quad (3.18)$$

To reduce the difficulty of the determination the plots were fitted with an exponential rise to a maximum (solid lines in Figures 3.8, 3.9, and 3.10):

$$N = a(1 - e^{-bt}) \quad (3.19)$$

which fits the available data very well. In equation (3.19)  $a$  and  $b$  are equation constants obtained from fitting the equation with experimental data. This equation gives

$$\frac{dN}{dt} = abe^{-bt} \quad (3.20)$$

and therefore

$$\left. \frac{dN}{dt} \right|_{\Delta t_1=0} = ab \quad (3.21)$$

This leads to the nucleation rate

$$J = \frac{ab}{V} \quad (3.22)$$

where  $J$  is the nucleation rate in  $\#/m^3 \cdot s$ ,  $ab$  is the initial slope in  $\#/s$ , and  $V$  is the volume of the droplet in  $m^3$  and is equal to  $0.2 \mu L$  ( $2 \times 10^{-10} m^3$ ). The predicted constants  $a$  and  $b$  in equation (3.19), and calculated nucleation rate ( $J$ ) from equation (3.22) are shown in Table 3.3.

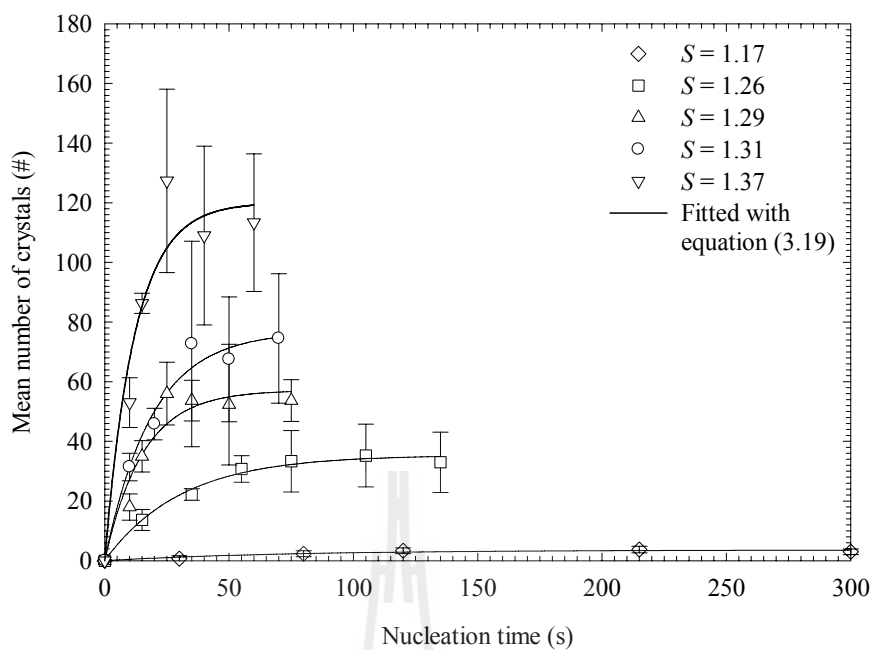


**Figure 3.8** Mean number of crystals as a function of nucleation time ( $\Delta t_I$ ) and supersaturation at 18 °C.

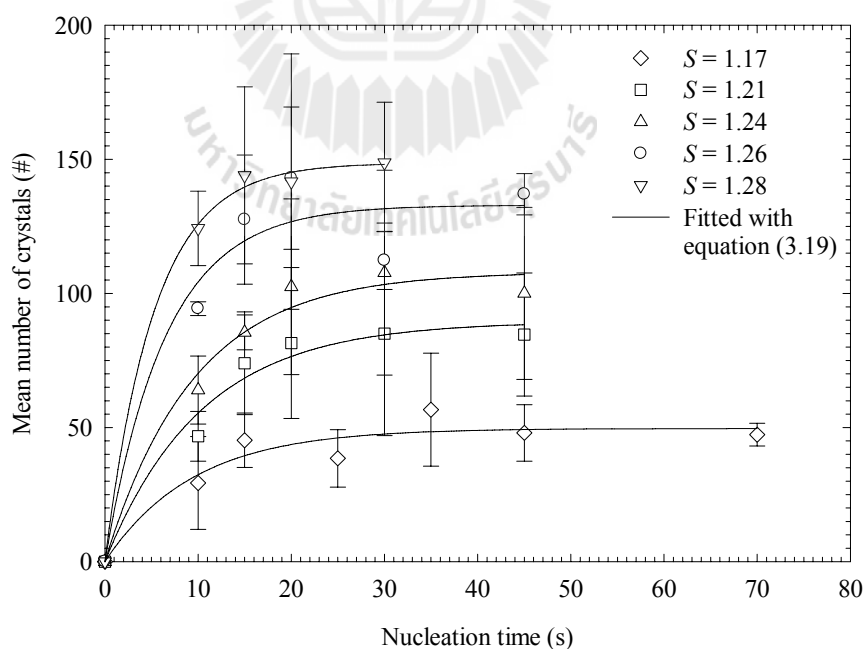


**Figure 3.9** Mean number of crystals as a function of nucleation time ( $\Delta t_I$ ) and supersaturation at 25 °C.

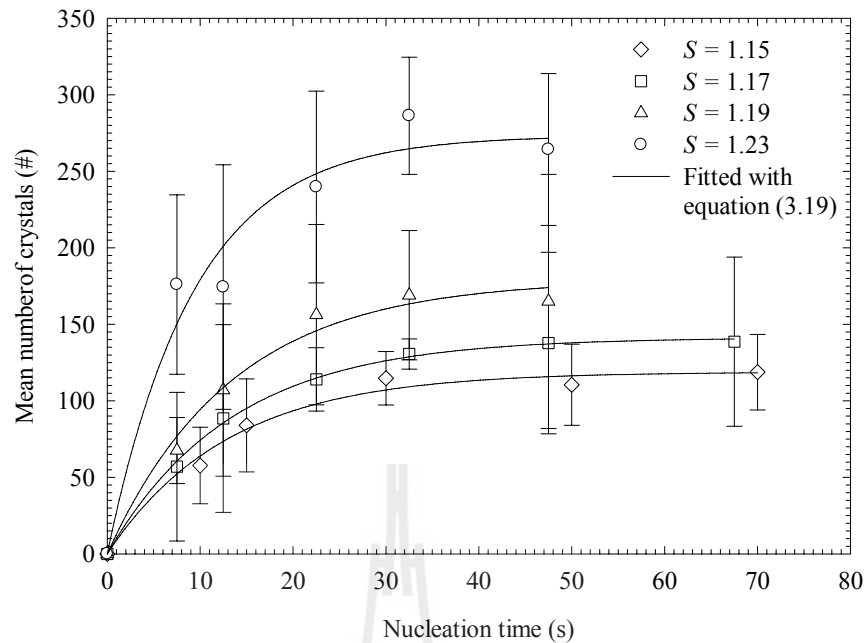


**Figure 3.10** Mean number of crystals as a function of nucleation time ( $\Delta t_l$ ) and supersaturation at 35 °C.

The dependence of the nucleation rates on the supersaturation and temperature are shown in Figure 3.11. It can be seen that at constant temperature the nucleation rates increase exponentially with increasing supersaturation. This is since the higher supersaturation ( $S = C/C^* = \text{actual concentration/solubility}$ ) leads to a higher driving force ( $\Delta C = C - C^*$ ) for nucleation. Also, at constant supersaturation the nucleation rates increase with increasing temperature. This is due to the change in the pre-exponential constant with temperature and is typical with kinetic processes.

**Table 3.3** The predicted constants  $a$  and  $b$  in equation (3.18), and calculated nucleation rate ( $J$ ) from equation (3.21).

Exp. no.	$T_1$ (°C)	$S_1$ (-)	$a$ (#)	$b$ (s <sup>-1</sup> )	$J$ (#/m <sup>3</sup> /s)
1	18	1.17	3.5646	0.0138	$2.46 \times 10^8$
2	18	1.26	35.3713	0.0324	$5.73 \times 10^9$
3	18	1.29	57.1358	0.0650	$1.86 \times 10^{10}$
4	18	1.31	76.8439	0.0526	$2.02 \times 10^{10}$
5	18	1.36	120.0404	0.0826	$4.96 \times 10^{10}$
6	25	1.17	49.6610	0.1060	$2.63 \times 10^{10}$
7	25	1.21	89.5260	0.0960	$4.30 \times 10^{10}$
8	25	1.24	107.9700	0.1050	$5.67 \times 10^{10}$
9	25	1.26	132.9110	0.1530	$1.02 \times 10^{11}$
10	25	1.28	148.6730	0.1870	$1.39 \times 10^{11}$
11	35	1.15	118.8588	0.0771	$4.58 \times 10^{10}$
12	35	1.17	141.2891	0.0745	$5.26 \times 10^{10}$
13	35	1.19	179.1238	0.0747	$6.69 \times 10^{10}$
14	35	1.23	273.2949	0.1064	$1.45 \times 10^{11}$

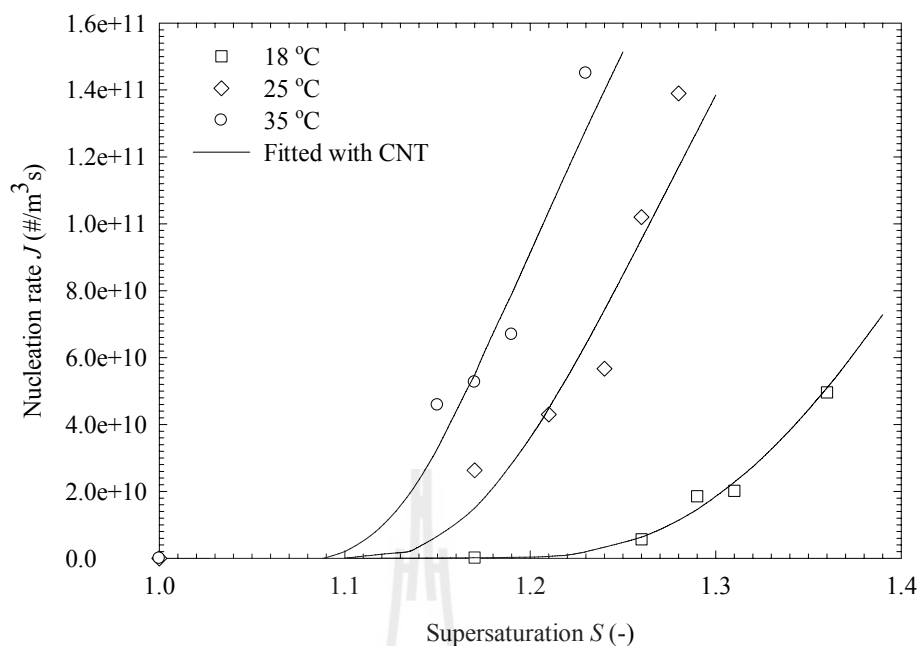


**Figure 3.11** Nucleation rate as a function of supersaturation.

The nucleation rate ( $J$ ) can be predicted as a function of supersaturation based on the CNT according to equations (3.12) and (3.13). Where  $v_0$  is molecular volume and is calculated from equation (3.9), where the molecular mass is equal to 149.21 g/mol and the crystal density is equal to 1,340 kg/m<sup>3</sup> for DL-met. Therefore,  $v_0$  is equal to  $18.50 \times 10^{-29}$  m<sup>3</sup>. The experimental data were fitted equation (3.12), with the results shown in Figure 3.11. The model fits the data well, with root mean square deviations (rmsd) of 0.030, 0.059, and 0.040, and R-squared values of 1.0, 0.7741, and 0.8083, respectively for 18, 25, and 35 °C. The results show that the measured nucleation kinetics follow the trends expected from the CNT. The best-fit values of  $A$  and  $B$  are shown Table 3.4. Approximate interfacial energy ( $\gamma$ ) values for all temperatures can be predicted from the parameter  $B$ , and these are also tabulated in Table 3.4. It is important to note that these may only be approximations to true surface energies. The  $\gamma$  values are temperature dependent

which correspond to other systems such as L-glutamic acid (Lindenberg and Mazzotti, 2009) and potassium alum (Mullin, 2001). A large value of  $\gamma$  indicates a large time required to initiate nucleation of the crystal (a lower nucleation rate). This means that the nucleation rates of  $\gamma$ -DL-met increase with increasing temperature (Figure 3.11) due to the decrease of interfacial energy with increasing temperature (Table 3.4). The  $\gamma$  values obtained are comparable to those reported for other poorly water soluble organic molecules, for example L-histidine (Jiang and ter Horst, 2011) (5.1 mJ/m<sup>2</sup>) and paracetamol (Granberg, Ducreux, Gracin, and Rasmuson, 2001) (1.4 - 2.8 mJ/m<sup>2</sup>). The values obtained for  $A$  are relatively low but are comparable to values for lysozyme (Galkin and Vekilov, 2001) ( $10^7 - 10^9 \text{ m}^{-3}\text{s}^{-1}$ ) and L-asparagine (Mahajan and Kirwan, 1994) ( $10^{11} \text{ m}^{-3}\text{s}^{-1}$ ).

**Table 3.4** The predicted interfacial energy and pre-exponential factor.

Temperature (°C)	Pre-exp. Factor, $A$ (m <sup>3</sup> /s)	Parameter, $B$ (-)	Interfacial Energy, $\gamma$ (mJ/m <sup>2</sup> )
18	$5.10 \times 10^{11}$	0.2468	3.03
25	$3.47 \times 10^{11}$	0.0813	2.14
35	$3.08 \times 10^{11}$	0.0464	1.84

### 3.6 Conclusions

The SNT of  $\gamma$ -DL-met in aqueous solutions was determined in an agitated batch system prior the crystal growth experiment to ensure no nucleation would take place in the crystallizer. The SNT decreases with increasing induction time. The SNT in these measurement units is weakly temperature dependent. Direct determinations of

the rate of nucleation of  $\gamma$ -DL-met in aqueous solution were performed using a method which is based on direct particle (crystal) counts as a function of time. The nucleation rate was determined from the limiting slope of the plot between the total number of crystals and the nucleation time as the nucleation time approached zero, divided by the volume of the solution droplet. The results show that the number of nucleated crystals increases with increasing nucleation time and supersaturation, and approaches a constant value at higher nucleation time, because at higher nucleation times there is sufficient growth to deplete the solution. The determined nucleation rates follow the trends expected from the CNT. The nucleation rates increase with increasing temperature and exponentially increase with increasing supersaturation. Based on the CNT, the kinetic parameter  $A$  and thermodynamic parameter  $B$  were estimated by fitting the determined nucleation rates with CNT. The interfacial energy was estimated from the parameter  $B$  and the values are in the range 1.8 - 3.1 mJ/m<sup>2</sup>. The interfacial energy value tends to decrease with increasing solubility.

### 3.7 References

- Beckmann, W., Nickisch, N., and Budde, U. (1998). Development of a seeding technique for the crystallization of the metastable A modification of abecarnil. **Org. Process Res. Dev.** 2(5): 298-304.
- Bernstein, J., Davey, R.J., and Henck, J.O. (1999). Concomitant polymorphs. **Angew. Chem. Int. Ed.** 38(23): 3440-3461.
- Chakraborty, D., and Bhatia, S.K. (1996a). Formation and aggregation of polymorphs in continuous precipitation. 1. Mathematical modeling. **Ind. Eng. Chem. Res.** 35(6): 1985-1994.

- Chakraborty, D., and Bhatia, S.K. (1996b). Formation and aggregation of polymorphs in continuous precipitation. 2. Kinetics of CaCO<sub>3</sub> precipitation. **Ind. Eng. Chem. Res.** 35(6): 1995-2006.
- Cornel, J., Lindenberg, C., and Mazzotti, M. (2009). Experimental characterization and population balance modeling of the polymorph transformation of L-glutamic acid. **Cryst. Growth Des.** 9(1): 243-252.
- Davey, R.J., Cardew, P.T., McEwan, D., and Sadler, D.E. (1986). Rate controlling processes in solvent-mediated phase transformations. **J. Cryst. Growth** 79(1-3): 648-653.
- Dharmayat, S., Hammond, R.B., Lai, X., Ma, C., Purba, E., Roberts, K.J., Chen, Z-P., Martin, E., Morris, J., and Bytheway, R. (2008). An examination of the kinetics of the solution-mediated polymorphic phase transformation between  $\alpha$ - and  $\beta$ -forms of L-glutamic acid as determined using online powder X-ray diffraction. **Cryst. Growth Des.** 8(7): 2205-2216.
- Dirksen, J.A., and Ring, T.A. (1991). Fundamentals of crystallization: Kinetic effects on particle size distributions and morphology. **Chem. Eng. Sci.** 46(10): 2389-2472.
- Ferrari, E.S., Davey, R.J., Cross, W.I., Gillon, A.L., and Towler, C.S. (2003). Crystallization in polymorphic systems: The solution-mediated transformation of  $\beta$  to  $\alpha$  glycine. **Cryst. Growth Des.** 3(1): 53-60.
- Flood, A.E. (2009). **Industrial crystallization from solution: A primer.** Thailand: Suranaree University of Technology.
- Galkin, O., and Vekilov, P.G. (1999). Direct determination of the nucleation rates of protein crystals. **J. Phys. Chem. B** 103(49): 10965-10971.

- Galkin, O., and Vekilov, P.G. (2001). Nucleation of protein crystals: Critical nuclei, phase behavior, and control pathways. **J. Cryst. Growth** 232(1-4): 63-76.
- Garside, J., Mersmann, A., and Nyvlt, J. (2002). **Measurement of crystal growth and nucleation rates** (2<sup>nd</sup> ed.). UK: Institute of Chemical Engineering.
- Granberg, R.A., Ducreux, C., Gracin, S., and Rasmuson, Å.C. (2001). Primary nucleation of paracetamol in acetone-water mixtures. **Chem. Eng. Sci.** 56(7): 2305-2313.
- Jiang, S., Jansens, P.J., and ter Horst, J.H. (2010). Control over polymorph formation of *o*-aminobenzoic acid. **Cryst. Growth Des.** 10(6): 2541-2547.
- Jiang, S., and ter Horst, J.H. (2011). Crystal nucleation rates from probability distributions of induction times. **Cryst. Growth Des.** 11(1): 256-261.
- Jiang, S., ter Horst, J.H., and Jansens, P.J. (2008). Concomitant polymorphism of *o*-aminobenzoic acid in antisolvent crystallization. **Cryst. Growth Des.** 8(1): 37-43.
- Kashchiev, D. (2000). **Nucleation: basic theory with applications**. Oxford: Butterworth-Heinemann.
- Kashchiev, D., and van Rosmalen, G.M. (2003). Review: Nucleation in solutions revisited. **Cryst. Res. Technol.** 38(7-8): 555-574.
- Kitamura, M. (1993). Crystallization behavior and transformation kinetics of L-histidine polymorphs. **J. Chem. Eng. Jpn.** 26(3): 303-307.
- Kitamura, M. (2009). Strategy for control of crystallization of polymorphs, **CrystEngComm.** 11(6): 949-964.

- Kramer, H.J.M., and van Rosmalen, G.M. (2009). Crystallization. In: I.D., Wilson and C.F., Poole (ed.). **Handbook of methods and instrumentation in separation science volume 2** (pp 1-20). London: Academic Press.
- Lindenberg, C., and Mazzotti, M. (2009). Effect of temperature on the nucleation kinetics of  $\alpha$ -L-glutamic acid. **J. Cryst. Growth** 311(4): 1178-1184.
- Lindenberg, C., and Mazzotti, M. (2011). Continuous precipitation of L-asparagine monohydrate in a micromixer: Estimation of nucleation and growth kinetics. **AIChE J.** 57(4): 942-950.
- Lu, J., Wang, X-J., Yang, X., and Ching, C-B. (2007). Polymorphism and crystallization of famotidine. **Cryst. Growth Des.** 7(9): 1590-1598.
- Mahajan, A.J., and Kirwan, D.J. (1994). Nucleation and growth kinetics of biochemicals measured at high supersaturations. **J. Cryst. Growth** 144(3-4): 281-290.
- Maruyama, S., Ooshima, H., and Kato, J. (1999). Crystal structures and solvent-mediated transformation of taltireline polymorphs. **Chem. Eng. J.** 75(3): 193-200.
- Matsuoka, M., Yamanobe, M., Tezuka, N., Takiyama, H., and Ishii, H. (1999). Polymorphism, morphologies and bulk densities of DL-methionine agglomerate crystals. **J. Cryst. Growth** 198-199: 1299–1306.
- Mersmann, A. (2001). **Crystallization technology handbook** (2<sup>nd</sup> ed.). New York: Marcel Dekker Inc.
- Mitchell, N.A., and Frawley, P.J. (2010). Nucleation kinetics of paracetamol-ethanol solutions from metastable zone widths. **J. Cryst. Growth** 312(19): 2740-2746.

- Mullin, J.W. (2001). **Crystallization** (4<sup>th</sup> ed.). Oxford: Butterworth-Heinemann.
- Nagy, Z.K., Fujiwara, M., Woo, X.Y., and Braatz, R.D. (2008). Determination of the kinetic parameters for the crystallization of paracetamol from water using metastable zone width experiments. **Ind. Eng. Chem. Res.** 47(4): 1245-1252.
- Ono, T., Kramer, H.J.M., ter Horst, J.H., and Jansens, P.J. (2004). Process modeling of the polymorphic transformation of L-glutamic acid. **Cryst. Growth Des.** 4(6): 1161-1167.
- Qu, H., Louhi-Kultanen, M., Rantanen, J., and Kallas, J. (2006). Solvent-mediated phase transformation kinetics of an anhydrate/hydrate system. **Cryst. Growth Des.** 6(9): 2053-2060.
- Randolph, A.D., and Larson, M.A. (1988). **Theory of particulate processes: Analysis and techniques of continuous crystallization** (2<sup>nd</sup> ed.). California: Academic Press.
- Rodríguez-Spong, B., Price, C.P., Jayasankar, A., Matzger, A.J., and Rodríguez-Hornedo, N. (2004). General principles of pharmaceutical solid polymorphism: A supramolecular perspective. **Adv. Drug Deliv. Rev.** 56(3): 241-274.
- Roelands, C.P.M. (2005). **Polymorphism in precipitation process**. Ph.D. thesis, Delft University of Technology, The Netherlands.
- Roelands, C.P.M., Jiang, S., Kitamura, M., ter Horst, J.H., Kramer, H.J.M., and Jansens, P.J. (2006). Antisolvent crystallization of the polymorphs of L-histidine as a function of supersaturation ratio and of solvent composition. **Cryst. Growth Des.** 6(4): 955-963.

- Schöll, J., Bonalumi, D., Vicum, L., and Mazzotti, M. (2006). In situ monitoring and modeling of the solvent-mediated polymorphic transformation of L-glutamic acid. **Cryst. Growth Des.** 6(4): 881-891.
- Schöll, J., Vicum, L., Müller, M., and Mazzotti, M. (2006). Precipitation of L-glutamic acid: Determination of nucleation kinetics. **Chem. Eng. Technol.** 29(2): 257-264.
- Schwartz, A.M., and Myerson, A.S. (2002). Solutions and solution properties. In: A.S. Myerson (ed.). **Handbook of industrial crystallization** (2<sup>nd</sup> ed., pp 1-31). USA: Butterworth-Heinemann.
- Srisa-nga, S., Flood, A.E., and White, E.T. (2006). The secondary nucleation threshold and crystal growth of  $\alpha$ -glucose monohydrate in aqueous solution. **Cryst. Growth Des.** 6(3): 795-801.
- Tao, J., and Yu, L. (2006). Kinetics of cross-nucleation between polymorphs. **J. Phys. Chem. B** 110(14): 7098-7101
- Teychené, S. Autret, J.M., and Biscans, B. (2004). Crystallization of eflocimibe drug in a solvent mixture: Effects of process conditions on polymorphism. **Cryst. Growth Des.** 4(5): 971-977.
- Teychené, S., and Biscans, B. (2008). Nucleation kinetics of polymorphs: Induction period and interfacial energy measurements. **Cryst. Growth Des.** 8(4): 1133-1139.
- Threlfall, T. (2003). Structural and thermodynamic explanations of Ostwald's rule. **Org. Process Res. Dev.** 7(6): 1017-1027.
- Tsekova, D., Dimitrova, S., and Nanev, C.N. (1999). Heterogeneous nucleation (and adhesion) of lysozyme crystals. **J. Cryst. Growth** 196(2-4): 226-233.

Zhang, Y., and Li, Z. (2011). Effects of cooling rate, saturation temperature, and solvent on the metastable zone width of triethanolamine hydrochloride.

**Ind. Eng. Chem. Res.** 50(10): 6375-6381.



# CHAPTER IV

## GROWTH AND DISSOLUTION KINETICS OF $\alpha$ AND $\gamma$ POLYMORPHS OF DL-METHIONINE

### 4.1 Abstract

Growth and dissolution kinetics of the two common polymorphs of DL-methionine (DL-met),  $\alpha$ -DL-met and  $\gamma$ -DL-met, were studied in aqueous solution. The growth experiments were performed isothermally in an agitated batch crystallizer at 5, 15, and 25 °C for  $\alpha$ -DL-met, and 10, 25, and 40 °C for  $\gamma$ -DL-met. The dissolution experiments of  $\gamma$ -DL-met were performed isothermally at 10, 25, and 40 °C in an agitated batch crystallizer. The effect of the initial supersaturation and seed mass on crystal growth were also studied at 25 °C. The initial growth rate (during the first 20 min of the batch) is significantly higher than subsequent crystal growth, a phenomenon previously seen with other species. The measured growth rates are independent of seed mass, as expected, for the usable portion of the growth rate data. The growth rates of  $\alpha$ -DL-met and  $\gamma$ -DL-met were found to be linearly dependent on the relative supersaturation of DL-met in the system. The dissolution rate of  $\gamma$ -DL-met was found to linearly depend on the relative undersaturation of DL-met in the system. Both the growth and dissolution rate constants are temperature dependent and follow an Arrhenius relationship. To consider the polymorphic transformation kinetics, the same dissolution rates for both polymorphs are assumed due to the dissolution being considered as a single step (diffusion controlled) process. At all temperatures studied,

both the growth of  $\alpha$ -DL-met and dissolution rate of  $\gamma$ -DL-met are faster than the growth rate of  $\gamma$ -DL-met.

## 4.2 Introduction

Crystallization processes which include transformation between polymorphs consist of the competitive nucleation and crystal growth of the polymorphs and the transformation from the metastable polymorph to the stable polymorph, usually via a solution-mediated mechanism (SMT). SMT consists of the nucleation and crystal growth of the stable polymorph and the dissolution of the metastable polymorph. The mechanism of each elementary step in the crystallization process needs to be understood to predict and control polymorph formation. Accurate kinetic information allows process modeling and enables process design, optimization, and control.

As described in Chapter III (Section 3.2: Introduction), the determination of nucleation, growth, and dissolution kinetics are important for characterization of the crystallization behavior and transformation of the polymorphs. The nucleation kinetic was studied in Chapter III. In this chapter the growth and dissolution kinetics were studied.

Experimental determination of the crystal growth rate is easier than determination of the nucleation rate. There are two main groups of techniques used to measure crystal growth rate (Myerson and Ginde, 2002). The first group is the single crystal methods, where the growth mechanism and kinetics of different crystal faces are usually determined by optical or atomic force microscopy (AFM) (Kitamura and Ishizu, 1998; Pantaraks and Flood, 2005; Gougazeh, Omar, and Ulrich, 2009). The second group is the methods involving the growth of a suspension of seed crystals

(multiparticle system) (Flood, Johns, and White, 2000; Srisa-nga, Flood, and White, 2006; Tanrikulu, Eroğlu, Bulutcu, and Özkar, 1998). Discussion of experimental methods can be found in a number of references (Garside, Mersmann, and Nyvlt, 2002; Mullin, 2001; Randolph and Larson, 1988). These techniques usually involve measurement of the change in mass or size of a crystal (or crystals) at a fixed temperature and supersaturation. The desupersaturation experiment is another technique which is based on the measurement of the change of the PSDs and solute concentrations with time in a seeded isothermal batch experiment (Garside et al., 2002; Glade, Ilyaskarov, and Ulrich, 2004; Schöll, Lindenberg, Vicum, Brozio, and Mazzotti, 2007). This method has the advantage that the growth data can be obtained from one experiment. The following examples give different techniques to determine crystal growth rate of the polymorphs that have been reported in the literature. The growth of suspensions of both the metastable B and stable A polymorphs of L-histidine in aqueous and aqueous-ethanol solutions were measured in a seeded isothermal batch crystallizer, where the growth rates were estimated from the change of the crystal weights and no transformation took place during the measurement of the growth rate of B crystals (Kitamura, Furukawa, and Asaeda, 1994). The single crystal growth of both metastable  $\alpha$  and stable  $\beta$  polymorphs of L-glutamic acid were measured in flowing aqueous solutions, where the growth mechanism and kinetics of different crystal faces were determined by microscopy (Kitamura and Ishizu, 2000). The growth rates of the metastable  $\alpha$  polymorph of L-glutamic acid in reactive precipitation were also measured in a suspension system using a desupersaturation experiment in a seeded isothermal batch crystallizer, where the growth rates were

determined using the desupersaturation data and population balance modeling combined with a non-linear least squares optimization algorithm (Schöll et al., 2007).

The dissolution rate can be measured by the same method as the growth rate, where the size of a seed crystal (or crystals) increases with time during the growth experiment, while the size of a seed crystal (or crystals) decreases with time during the dissolution experiment. Determining dissolution rates using single crystal dissolution methods can be found in a number of papers (Gougazeh et al., 2009; Prasad, Ristic, Sheen, and Sherwood, 2002). Determining the dissolution rate using multiparticle dissolution methods can be also found in a number of papers (Hurley, Jones, and Drummond, 1997; Tanrikulu et al., 1998). There are limited numbers of papers that report the determination of the dissolution rate of polymorphs. For example, the dissolution rates of the calcite and aragonite polymorphs of calcium carbonate in water were measured by a multiparticle dissolution method (Gutjahr, Dabringhaus, and Lacmann, 1996a, 1996b).

In the literature, the kinetics of nucleation, growth and dissolution of each polymorph can be also estimated from the combination of the data from the polymorph transformation experiments with population balance modeling and parameter estimation. For example, this technique was applied to L-glutamic acid using both seeded and unseeded polymorph transformation (Cornel, Lindenberg, and Mazzotti, 2009; Ono, Kramer, ter Horst, and Jansens, 2004; Schöll, Bonalumi, Vicum, and Mazzotti, 2006), and continuous precipitation of the polymorphs of calcium carbonate (Chakraborty and Bhatia, 1996a, 1996b).

The last technique is where the growth kinetics of the stable polymorph and the dissolution kinetics of the metastable polymorph can be estimated respectively

from the rate of increase of the mass of the stable polymorph and the rate of the decrease of the mass of the metastable polymorph from seeded polymorph transformations experiments (Kitamura, 1993, 2009).

The first three techniques (the experimental techniques which performed on a single polymorphic form) are accurate enough for determining the growth and dissolution kinetics of the polymorphs. The accuracy depends on the reliability and robustness of the experimental assumptions, experimental techniques, characterization techniques, data analysis, etc. The last two techniques (the simulation techniques) are not yet proven to agree with experiments performed on a single polymorphic form. Therefore, in this work the growth and dissolution kinetics of each form are experimentally determined. These experimental results are applied to the simulation method in Chapter VI and the validation is explained.

The aims of this work are to determine the growth and dissolution rates of the stable  $\gamma$ -DL-met, and the growth rates of the metastable  $\alpha$ -DL-met in aqueous solution. The dissolution rates of  $\alpha$ -DL-met were determined based on the measurement of  $\gamma$ -DL-met by assuming that they have the same dependence on the undersaturation of the relevant polymorph. The growth and dissolution rates were measured using the method of the growth (or dissolution) of a suspension of seed crystals with desupersaturation (or deundersaturation) experiments in an isothermal batch crystallizer. The effects of supersaturation (or undersaturation) and temperature on the growth and dissolution rates were investigated.

### 4.3 Theory

In this section the primary focus is on the theory of supersaturation, undersaturation, crystal growth, and crystal dissolution. Other important phenomena relating to crystallization from solution, such as the secondary nucleation threshold and nucleation are described in Chapter III.

#### 4.3.1 Supersaturation and Undersaturation

Dissolution of solid in solution occurs when undersaturation is created which acts as the driving force for dissolution. This means that the solute concentration in the solution is less than its solubility ( $\Delta\mu < 0$ ). The expression of undersaturation is equivalent to that of supersaturation (see Chapter III) but the concentration of solution is below that of the equilibrium concentration. For practical use in this work the supersaturation for the growth experiment is represented by  $\Delta C_G = \Delta C$  or  $S_G = S$  or  $\sigma_G = \sigma$ , while the undersaturation for the dissolution experiment is represented by  $\Delta C_D = -\Delta C$  or  $S_D = -S$  or  $\sigma_D = -\sigma$ .

#### 4.3.2 Crystal growth

Crystal growth is the growth of crystals to larger sizes. In the theory of crystal growth there are two successive mechanisms; a diffusion step and a surface integration step (Randolph and Larson, 1988). The first step (diffusion) is where the transfer of molecules from the bulk solution to the crystal surface occurs, and the second step concerns the insertion of molecules into the surface (a reaction step), as shown in Figure 4.1.

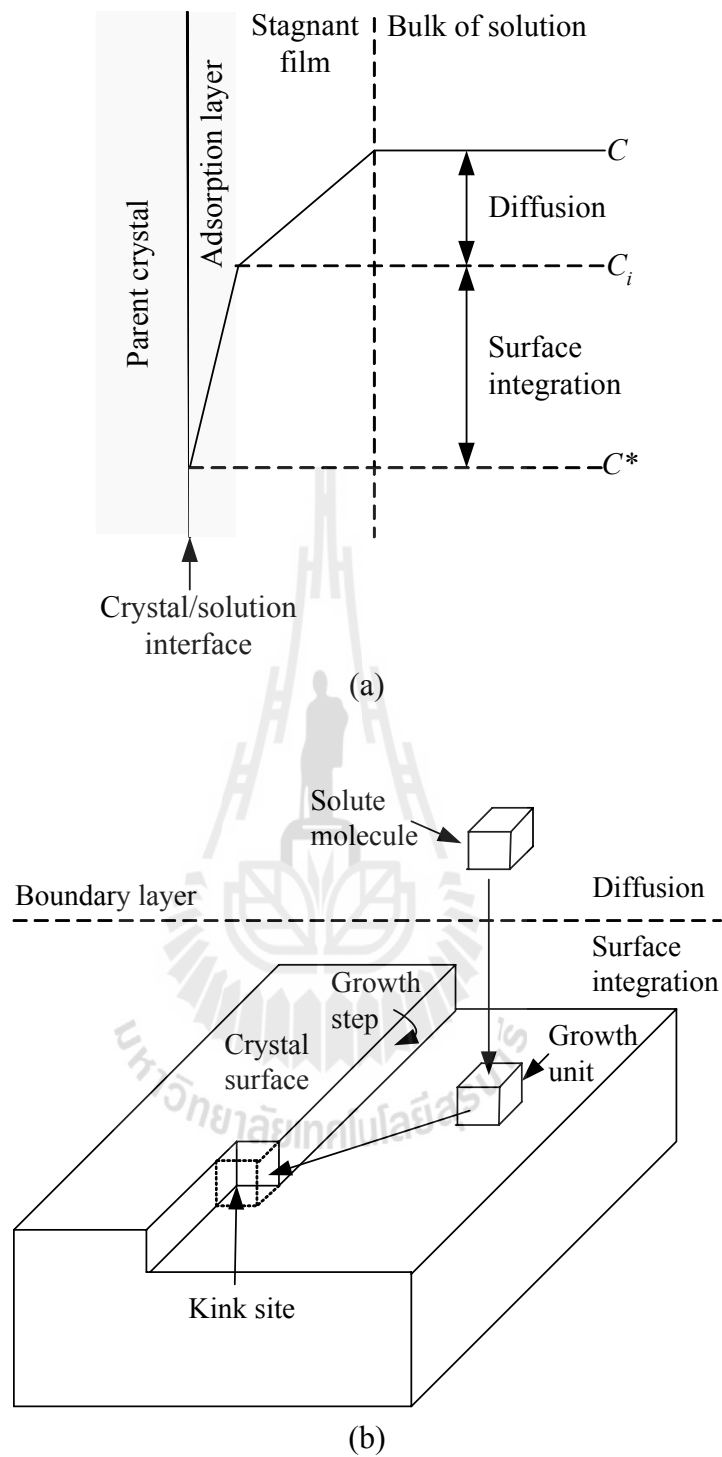


**Figure 4.1** The model representation of the concentration driving force (a), and the two-step crystal growth process (b).

The crystal growth rate can be described either as a mass deposition rate (i.e. a mass flux) or a rate of linear increase of a characteristic dimension (i.e. a velocity). Expressed as a velocity, the overall linear growth rate is

$$G = \frac{dL}{dt} \quad (4.1)$$

where  $t$  is the growth time (s) and  $L$  is the characteristic dimension that is increasing (m). The mass flux is equal to the crystal growth rate (as defined in equation (4.1)) multiplied by the density of the crystal. The mass deposition flux can be directly related to the overall linear growth rate through the relation

$$R_G = \frac{1}{A} \frac{dm}{dt} = 3 \frac{k_v}{k_a} \rho G = 3 \frac{k_v}{k_a} \rho \frac{dL}{dt} \quad (4.2)$$

where  $R_G$  is the mass deposition rate ( $\text{kg/m}^2 \cdot \text{s}$ ),  $m$  is the crystal mass (kg),  $A$  is the surface area of crystal ( $\text{m}^2$ ),  $k_v$  is the volume shape factor (-),  $k_a$  is the area shape factor (-), and  $\rho$  is the density of the crystal ( $\text{kg/m}^3$ ).

There are several theoretical models used to describe the mechanisms of crystal growth, and these have been reviewed in detail by Strickland-Constable (1968), Ohara and Reid (1973), and Mullin (2001).

### **Diffusion-reaction model**

As shown in Figure 4.1 (a), the growth is divided into two steps, i.e. diffusion of solute molecules from the bulk solution to the interface, with the rate

$$\frac{dm}{dt} = k_d A (C - C_i) \quad (4.3)$$

and subsequent insertion of molecules into the crystal surface (a reaction step), with a rate that must be equal to the diffusion step

$$\frac{dm}{dt} = k_r A (C_i - C^*)^r \quad (4.4)$$

Elimination of the unknown interfacial concentration  $C_i$  leads to

$$\frac{dm}{dt} = k_g A (C - C^*)^g \quad (4.5)$$

where  $k_d$  is a mass transfer coefficient (m/s),  $k_r$  is an integration rate constant (m/s), and  $k_g$  is the growth rate constant (m/s).

#### Surface integration models

There are several surface integration models which have been proposed. The first model is the *continuous growth model*. This is a model for a crystal surface which is rough on the molecular scale. For molecular compounds, the surface becomes rough when the step free energy becomes equal to zero at the roughening temperature. When a solute molecule arrives at the surface, it is immediately integrated, as depicted in Figure 4.1(b). For rough growth, crystal faces tend to become rounded and kinetic roughening is caused by growth at too high supersaturation. This growth always affects the crystal purity because impurity or solvent molecules are more easily incorporated (Kramer and van Rosmalen, 2009).

A second model is the *screw dislocation or Burton-Caberra-Frank (BCF) model*. This model is used to overcome the limitation of the continuous growth model (particularly in crystals where the thermodynamics suggest a very smooth

crystal surface) by recognizing the significance of the screw dislocation, which presents a continuous spiral during growth (Figure 4.2). When a screw dislocation occurs on the crystal surface, it continues to produce a self-repeating spiral step throughout the crystal growth period. This is a source of new steps, and provides for continuous incorporation of the growth units. This is the model for a molecularly very smooth crystal surface; the attachment of new molecules is very difficult without the ledge created by the spiral dislocation. Roughness is provided by the presence of step and kink sites. Steps at the crystal face are provided by screw dislocations where spiral growth takes place. The growth rate perpendicular to the surface,  $G$  (m/s), can be expressed as (Mullin, 2001; Randolph and Larson, 1988)

$$G = A_{BCF} \sigma^2 \tanh\left(\frac{B_{BCF}}{\sigma}\right) \quad (4.6)$$

where  $A_{BCF}$  and  $B_{BCF}$  are constants. In equation (4.6) the growth varies with the level of the supersaturation. At low supersaturation it leads to a parabolic relationship, but at high supersaturation it leads to a linear relationship.

Finally, the third common model used is the ***birth and spread model***. This is a model for a molecularly smooth surface; the growth rate is limited by the creation of new steps at the surface (Ohara and Reid, 1973). These steps are created by a mechanism of 2D nucleation followed by layer growth (Figure 4.3). This model is more likely to occur at high levels of supersaturation because a relatively high level of supersaturation is required for significant formation of 2D nuclei. The growth rate based on this model has been developed in the form (Jones, 2002; Garside et al., 2002)

$$G = A_{B+S} \sigma^p \exp\left(-\frac{B_{B+S}}{\sigma}\right) \quad (4.7)$$

where  $A_{B+S}$ ,  $p$ , and  $B_{B+S}$  are constants.

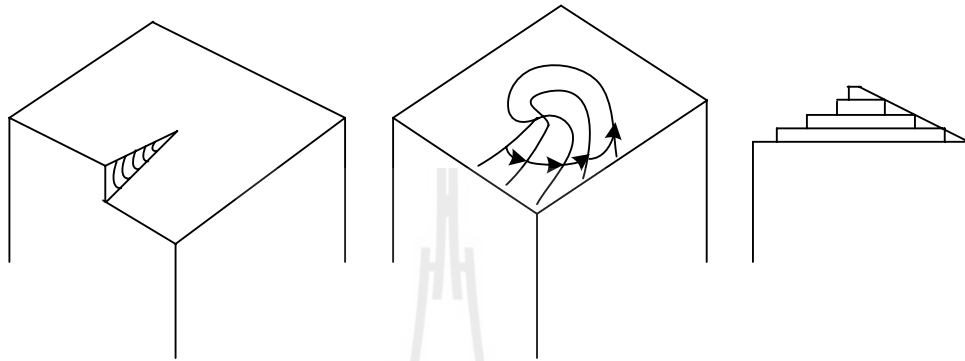


**Figure 4.2** Development of a crystal growth spiral starting from a screw dislocation.

(Adapted from Mullin, 2001)

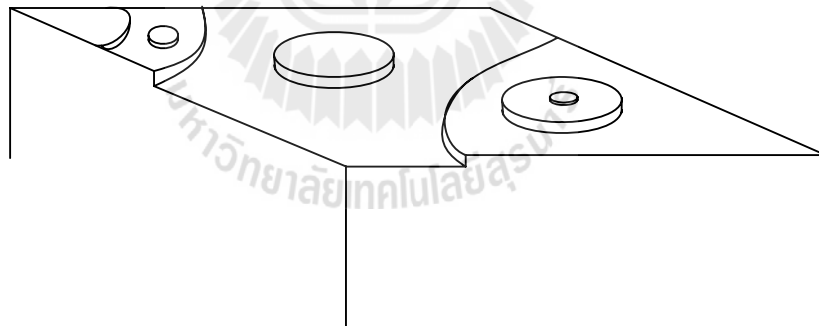


**Figure 4.3** Crystal growth arising from a surface nucleation (birth and spread)

mechanism. (Adapted from Jones, 2002)

### General growth expression

The difficulty of the previous theoretical models of crystal growth is that they can not yet predict crystal growth constants for a particular substance

*a priori*. Therefore, crystal growth rate data of industrial crystallization processes are usually correlated empirically with supersaturation using a power law model of the form (Myerson and Ginde, 2002)

$$G = K_G \sigma_G^n \quad (4.8)$$

where  $G$  is the growth rate (m/s),  $K_G$  is the growth rate constant (m/s), and  $n$  is the growth rate order. From the theoretical consideration above, for diffusion controlled growth (mass transfer controlled)  $n = 1$ , and for surface integration controlled growth  $n = 1 - 2$  (Flood, 2009).

The growth rate is temperature dependent. The relation between the growth kinetics and temperature is usually given by an Arrhenius relationship of the form (Mullin, 2001)

$$K_G = k_G^0 \exp\left[\frac{-E_G}{RT}\right] \quad (4.9)$$

where  $E_G$  is the activation energy of growth (kJ/mol),  $T$  is the temperature (K),  $k_G^0$  is a pre-exponential constant (m/s), and  $R$  is the ideal gas constant (8.314 J/mol·K). The activation energies are typically of the order of 10 - 20 kJ/mol for diffusion controlled growth and 40 - 60 kJ/mol for surface integration controlled growth (Kramer and van Rosmalen, 2009).

### 4.3.3 Crystal dissolution

There are two main steps of dissolution, surface reaction and detachment of the species followed by transfer of these species toward the bulk solution across the diffusion layer which surrounds the crystals. Normally surface

reaction and detachment of the species occurs at the crystal edges and at the pits, and the surface becomes easily roughened leading detachment to be a fast step, and diffusion to be the rate controlling step. Therefore, the dissolution rate expression is based on diffusion being the rate limiting step (Gougazeh et al., 2009; Kramer and van Rosmalen, 2009)

$$D = -\frac{dL}{dt} = -\frac{k_a}{3\rho k_v A} \frac{dm}{dt} = \frac{k_d k_a}{3\rho k_v} (C^* - C) \quad (4.10)$$

or by a combined diffusion and surface reaction rate, as given by equation (4.5) for growth, where the rate has a negative value for the change in mass, and there is a decreasing value of  $A$ . For practical use in industrial crystallization, dissolution rate data are usually correlated empirically with undersaturation using a power law model of the form (Gougazeh et al., 2009)

$$D = K_D \sigma_D^m \quad (4.11)$$

where  $D$  is the dissolution rate (m/s),  $K_D$  is the dissolution rate constant (m/s),  $\sigma_D$  is the relative undersaturation, and  $m$  is the dissolution rate order. From the theoretical consideration above, for diffusion controlled dissolution  $m = 1$ .

The dissolution rate is temperature dependent. The relation between the dissolution kinetics and temperature is usually given by Arrhenius relationship of the form (Gougazeh et al., 2009)

$$K_D = k_D^0 \exp\left[\frac{-E_D}{RT}\right] \quad (4.12)$$

where  $E_D$  is the activation energy of dissolution (kJ/mol),  $T$  is the temperature (K),  $k_D^0$  is a pre-exponential constant, and  $R$  is the ideal gas constant (8.314 J/mol·K).

## 4.4 Materials and Methods

### 4.4.1 Materials

DL-met (>99%, Acros Organics), NaOH (>97%, Carlo Erba), Na<sub>2</sub>CO<sub>3</sub> (>99.5%, Carlo Erba), HCl (37%, Carlo Erba) and deionized water were used without further purification. DL-met and deionized water were used to prepare the supersaturated and undersaturated solutions in all growth and dissolution experiments. Sodium methioninate (Na-Met) was also required for acidic precipitations of DL-met to prepare  $\alpha$ -DL-met. Aqueous solutions of Na-Met were prepared by the method previously described in Chapter II.

### 4.4.2 Apparatus

A 0.5 L batch crystallizer with a sealed glass lid to reduce solvent evaporation (Figure 2.9 in Chapter II) was used to measure the growth and dissolution rates. The slurry is continuously agitated at the required speed by a centrally located four-blade impeller driven by an overhead mixer. The crystallizer was placed inside a constant temperature water bath, where the temperature was controlled within  $\pm 0.5^\circ\text{C}$ .

250 mL and 500 mL glass beakers were used as batch crystallizers to prepare  $\alpha$ -DL-met and sodium methioninate (Na-Met) aqueous solutions, respectively. The temperature control and the agitation systems were the same as for the 0.5 L batch crystallizer.

#### 4.4.3 Preparation of the Polymorphic Forms of DL-Met

$\alpha$ -DL-met was prepared using reaction crystallization of Na-Met aqueous solutions with HCl as described in Chapter II.  $\gamma$ -DL-met was prepared by cooling crystallization of aqueous solutions of DL-met as described in Chapter II. The seed of pure  $\alpha$ -DL-met were obtained by collecting sieved crystals in the size range of 64 - 125  $\mu\text{m}$ . The seed of pure  $\gamma$ -DL-met were obtained by collecting sieved crystals in the size ranges of 180 - 250 and 250 - 300  $\mu\text{m}$ . Pure crystal polymorphs of each form were also characterized by X-ray powder diffractometry (XRPD) (Bruker axs, D5005).

The growth rate was assumed to be size independent growth, which has been the traditional assumption used. This has been investigated for other species, for example  $\alpha$ -L-glutamic acid (Schöll et al., 2007) and paracetamol (Mitchell, Ó'Ciardhá, and Frawley, 2011). Therefore, when considering the transformation kinetics, the growth rate of  $\alpha$ -DL-met (seed size: 64 - 125  $\mu\text{m}$ ) and the growth rate of  $\gamma$ -DL-met (seed size: 180 - 250  $\mu\text{m}$ ) can be reasonably compared with each other.

#### 4.4.4 Crystal Growth Rate Measurement

The growth kinetics of  $\gamma$ -DL-met were studied via seeded batch desupersaturation experiments using time dependent measurements of both particle size distributions (PSDs) and solute concentrations (Garside et al., 2002; Schöll et al., 2007). Experiments were performed at 10, 25, and 40 °C in a 0.5 L batch crystallizer agitated by a centrally located four-blade impeller driven by an overhead stirrer at 350 rpm, and performed within the secondary nucleation threshold (SNT) region to avoid nucleation. The solute concentration in the clear liquor was measured

periodically using dry substance determination (Garside et al., 2002), and the PSD of crystalline samples was measured using a Malvern Mastersizer (Malvern Instruments, Mastersizer/S). Volume percent distributions were converted mathematically to number density distributions in order to determine the number mean growth rate of the crystals, which is most suitable for use in population balance modeling. Nucleation was not detected in any seeded batch crystallization for growth determination. This was observed by the naked eye and also confirmed by the measurement of the PSD. Growth rate was determined as the time rate of change of the number mean crystal size.

Desupersaturation experiments were performed on supersaturated solutions within the SNT region that had previously been heated to 20 °C above the experimental temperature (this is also at least 5 °C above saturation temperature) for 30 to 40 min to ensure that no ghost nuclei remained in the solution. The solutions were then cooled to the experimental temperature, after which a quantity of dry seeds were fed to the crystallizer. A small volume of the suspension was sampled at particular times during the batch to determine the PSDs and solute concentration. All experiments were duplicated to determine reproducibility.

The growth experiments for  $\alpha$ -DL-met were studied using a similar method to the growth experiments for  $\gamma$ -DL-met, except the experiments were performed at 5, 15, and 25 °C. Experiments were performed within the area between the SNT of  $\gamma$ -DL-met (the stable polymorph) and the solubility of  $\alpha$ -DL-met, to avoid nucleation.

All experimental conditions for the growth experiments of  $\alpha$ -DL-met and  $\gamma$ -DL-met are shown Table 4.1.

**Table 4.1** Experimental conditions for the growth experiments. The seed size of  $\alpha$ -DL-met is 64 - 125  $\mu\text{m}$  and that of  $\gamma$ -DL-met is 180 - 250  $\mu\text{m}$ .

Exp. no.	$\sigma_{G0}$	Temperature ( $^{\circ}\text{C}$ )	Seed form	Seed mass (g)
1	0.091	10	$\gamma$	0.5
2	0.149	10	$\gamma$	0.5
3	0.091	25	$\gamma$	0.5
4	0.114	25	$\gamma$	0.5
5	0.072	25	$\gamma$	1.0
6	0.088	25	$\gamma$	1.0
7	0.094	25	$\gamma$	1.3
8	0.110	25	$\gamma$	1.3
9	0.051	40	$\gamma$	0.5
10	0.053	40	$\gamma$	0.5
11	0.080	5	$\alpha$	0.5
12	0.080	5	$\alpha$	0.5
13	0.059	15	$\alpha$	0.5
14	0.060	15	$\alpha$	0.5
15	0.036	25	$\alpha$	0.5
16	0.043	25	$\alpha$	0.5

#### 4.4.5 Crystal Dissolution Rate Measurement

The dissolution experiments were studied using a similar method to the growth experiments, except the experiments were performed at 10, 25, and 40 °C, and under the solubility of  $\gamma$ -DL-met. All experimental conditions for the dissolution experiments are shown in Table 4.2.

**Table 4.2** Experimental conditions for the dissolution experiments. The seed is only  $\gamma$ -DL-met.

Exp. no.	$\sigma_{D0}$	Temperature (°C)	Seed size	Seed mass (g)
1	0.116	10	250 - 300	1.50
2	0.116	10	250 - 300	1.50
3	0.066	25	180 - 250	1.50
4	0.069	25	180 - 250	1.50
5	0.082	25	250 - 300	1.50
6	0.067	25	250 - 300	1.51
7	0.051	40	250 - 300	1.80
8	0.054	40	250 - 300	1.81

In this work the dissolution rates of  $\alpha$ -DL-met and  $\gamma$ -DL-met as a function of undersaturation are assumed to be the same due to dissolution being considered as a single step (diffusion controlled) process. A bulk diffusion controlled process does not depend on the crystal structure at the surface (since diffusion occurs in the liquid phase where the molecule does not occur in a polymorphic form) but does depend on the level of undersaturation. The two forms should have the same

dissolution rate dependence on the undersaturation, but for a particular concentration of DL-met the two forms have different undersaturations since they have different solubilities. There is currently some debate about whether dissolution is really a two-step process, and hence this assumption is verified in Chapters V and VI.

Crystals of  $\alpha$ -DL-met prepared from reaction crystallization are very small, and it is impossible to accurately measure the dissolution rate of these crystals because the dissolution rate to zero size is very fast, and because the time rate of change in size for very small crystals is difficult to determine with high accuracy. Hence, in the current study dissolution rates were measured using  $\gamma$ -DL-met seed crystals only.

## 4.5 Results and Discussions

### 4.5.1 Crystal Growth Kinetics of $\alpha$ -DL-Met and $\gamma$ -DL-Met

Examples of PSDs from growth experiments of  $\alpha$ -DL-met and  $\gamma$ -DL-met at 25 °C are shown in Figures 4.4 and 4.5, respectively. The PSD is plotted on a log-scale to show that the volume-based PSD is a log-normal distribution, and hence appears as a normal distribution when size is plotted on a log-scale. The distribution was confirmed as log-normal by plotting the data on log-normal probability paper or fitting with log-normal distribution equation as shown in Appendix B. Photomicrographs of seed crystals and product crystals from a batch run of  $\alpha$ -DL-met and  $\gamma$ -DL-met at 25 °C are shown in Figures 4.6 and 4.7, respectively. The analysis showed that there is no nucleation occurring during the growth process because there is only one peak in the PSD and no particles smaller than the seed crystals are detected. The improved shape and features of the product crystals, as shown in

Figures 4.6 and 4.7, show that correct operation of the batch can lead to improved product quality. The PSD of product crystals obtained from growth showed only one peak, which indicates that the growth rate can be easily calculated from the change of the mean crystal size. The product crystals were also examined by XRPD analysis. The XRPD patterns of the product crystals were the same as the seed crystals; this indicates that there was no phase transformation during the growth processes during the relatively short batch times used. After the growth process of  $\alpha$ -DL-met the concentration reaches the solubility of  $\alpha$ -DL-met and then remains constant for some period of time. At this concentration  $\alpha$ -DL-met starts to transform to  $\gamma$ -DL-met. Therefore, the growth rate is measured from the time of seed addition until the concentration reaches the solubility of  $\alpha$ -DL-met. For  $\gamma$ -DL-met, after the growth process the concentration reaches the solubility of  $\gamma$ -DL-met and then remains constant. This indicates that  $\gamma$ -DL-met is the stable polymorphic form at these experimental temperatures (10 - 40 °C).

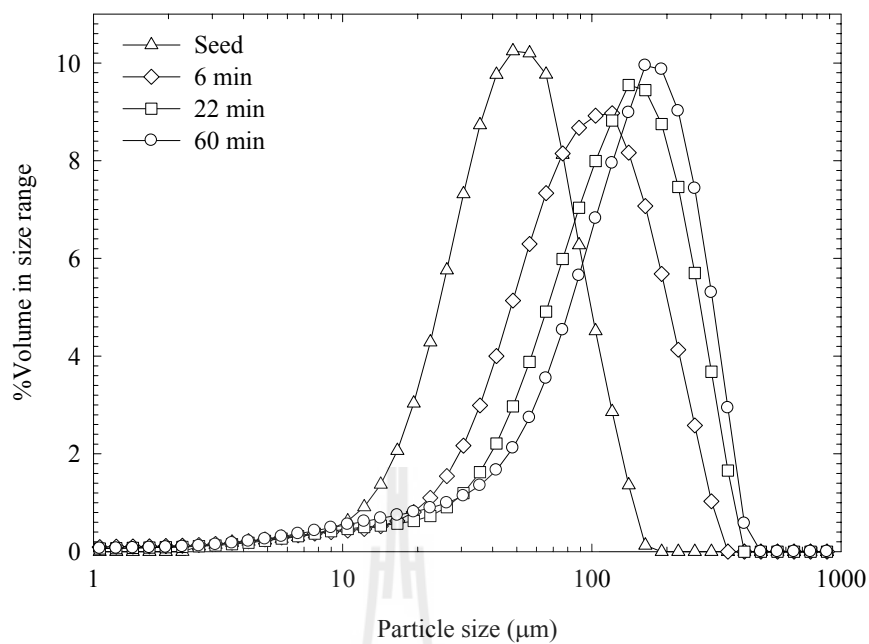


**Figure 4.4** Particle size distributions of seed and product crystals for the growth experiment of  $\alpha$ -DL-met at 25 °C and  $\sigma_{G0} = 0.043$ .

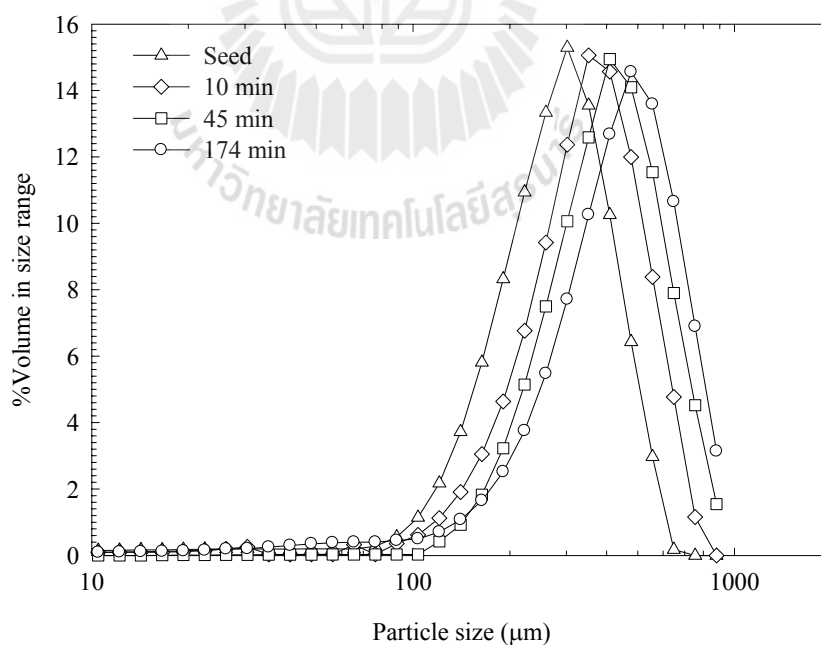


**Figure 4.5** Particle size distributions of seed and product crystals for the growth experiment of  $\gamma$ -DL-met at 25 °C and  $\sigma_{G0} = 0.114$ .

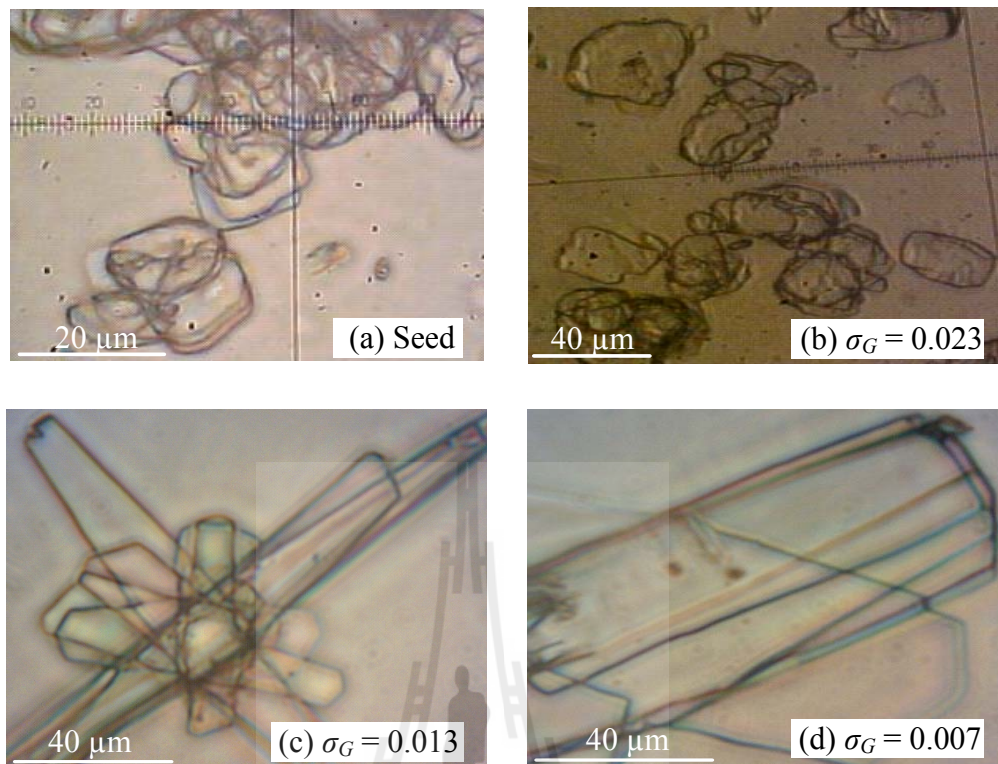


**Figure 4.6** Photomicrographs of seed crystals and product crystals from the growth experiment of  $\alpha$ -DL-met at 25 °C and  $\sigma_{G0} = 0.043$ .

A log-normal volume-based PSD indicates that the number distribution is also log-normal with the same geometric standard deviation (Allen, 1997). The number mean particle size may then be calculated from the following equation

$$\ln x_{NL} = \ln x_{mV} - 2.5 \ln^2 \sigma_g \quad (4.13)$$

where  $x_{NL}$  is the number mean crystal size,  $x_{mV}$  is the median of the volume distribution, and  $\sigma_g$  is the geometric standard deviation of the volume distribution. The PSDs of this work were confirmed by discretizing the volume density distribution into small elements (of 1 mm width), and calculating the number of particles in each element and then the number mean crystal size. The geometric standard deviation of

the volume distribution was constant over the time period of the experiment, indicating common history seed (Srisa-nga et al., 2006). Common History (CH) seed is a crystal population where the relative growth rate of a crystal is proportional to its size, and crystals of the same size have the same growth rate.

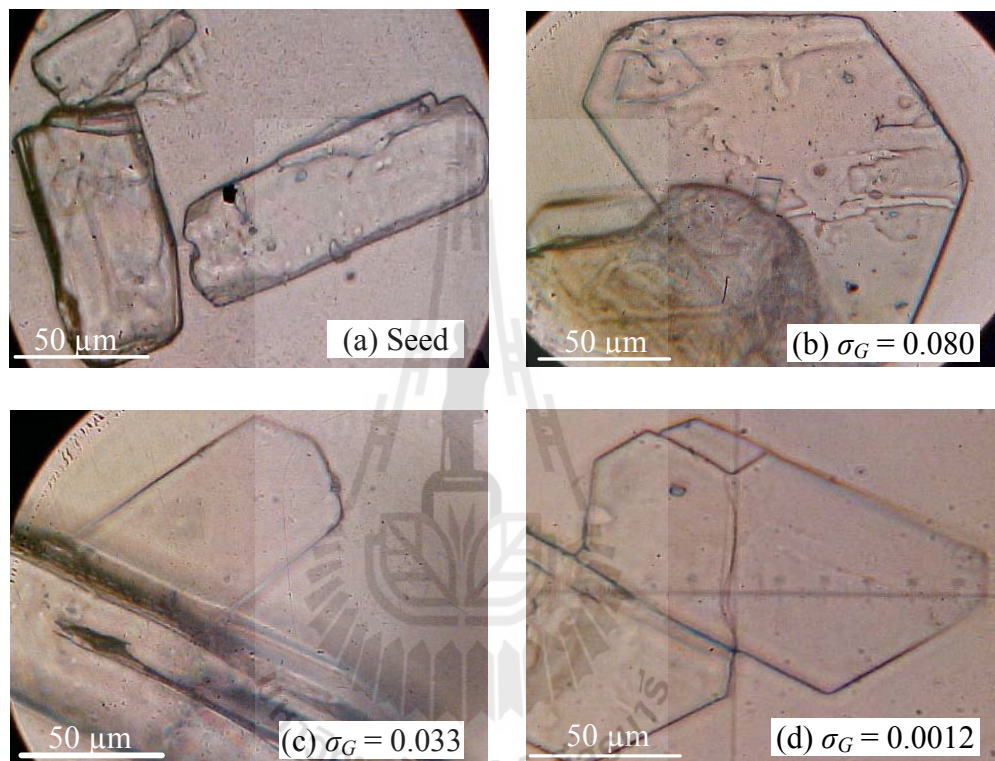


**Figure 4.7** Photomicrographs of seed crystals and product crystals from the growth experiment of  $\gamma$ -DL-met at 25 °C and  $\sigma_{G0} = 0.114$ .

The mean growth rate was determined as the time rate of change of the number mean crystal size. The number-basis was used to calculate the growth rate because the growth rate data can only be obtained from batch growth using the population balance, which is a number-based balance. If other mean sizes (i.e. the volume or mass mean sizes) are used then the result is not suitable for use in the

population balance, and therefore far less useful. The growth and dissolution rates can be calculated from the change of the number mean crystal size divided by the change of the time of each measurement, with these being correlated with the average of measured supersaturation at the same time period.

The technique for calculation the growth rates are shown in Table 4.3. The growth rate was calculated directly from the change of a smooth plot between the number mean crystal size and time of each measurement. Figure 4.8 is an example of this plot. These allow crystal growth rates to be determined as a function of relative supersaturation; crystal growth rates values are shown in column 7 of Table 4.3 and the corresponding relative supersaturation values are shown in column 4 of Table 4.3. Similar techniques are used for determining crystal growth rates as a function of relative supersaturation at all growth experiments for both  $\alpha$ -DL-met and  $\gamma$ -DL-met. As shown in Table 4.3,  $\sigma_G$  is the relatives supersaturation (-),  $\bar{L}$  is the number mean size ( $\mu\text{m}$ ), and  $t$  is the time (min).

**Table 4.3** Example for calculation of crystal growth rates as a function of relative supersaturation for experimental results of a batch run of  $\gamma$ -DL-met at 25 °C and initial supersaturation of 0.114.

$t$ (min)	$\Delta t$ (min)	$\sigma_G$ (-)	$\sigma_{G,average}$ (-)	$\bar{L}$ ( $\mu\text{m}$ )	$\Delta\bar{L}$ ( $\mu\text{m}$ )	$\bar{G} = \Delta\bar{L} / \Delta t$ ( $\mu\text{m}/\text{min}$ )
0		0.1093		175.86		
	2		0.1066		24.32	12.1580
2		0.1039		200.18		
	3		0.1001		11.70	3.8998
5		0.0963		211.88		
	5		0.0905		8.89	1.7794
10		0.0847		220.77		
	10		0.0750		13.26	1.3258
20		0.0652		234.03		
	10		0.0576		10.41	1.0410
30		0.0500		244.44		
	10		0.0440		8.20	0.8197
40		0.0380		252.64		
	10		0.0334		6.45	0.6454
50		0.0287		259.09		
	10		0.0250		5.08	0.5082
60		0.0213		264.17		
	10		0.0184		4.01	0.4002
70		0.0155		268.18		
	10		0.0133		3.15	0.3151
80		0.0110		271.33		
	20		0.0078		4.43	0.2217
100		0.0046		275.76		
	20		0.0027		2.74	0.1375
120		0.0007		278.51		

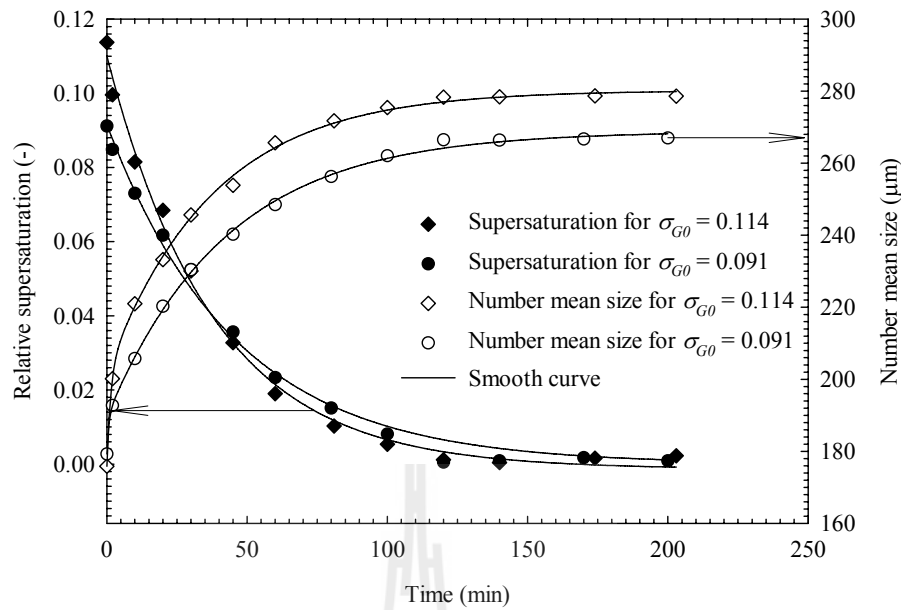


**Figure 4.8** Desupersaturation curves and time dependence of crystal sizes from a batch run of  $\gamma$ -DL-met at 25 °C with different initial supersaturation.

Figure 4.8 also shows the batch crystallization profiles for the condition of 0.5 g of  $\gamma$ -DL-met seed crystals having an average size of approximately 178  $\mu\text{m}$ , with the crystallization temperature being 25 °C and for initial relative supersaturations equal to 0.091 and 0.114. Figure 4.8 shows that an increase in the initial supersaturation results in an increase in the final mean crystal size. This is since the higher solute concentration in excess of the solubility leads to a higher amount of solute addition onto the same seed mass. In addition, experiments varying the seed mass (Figure 4.9) show that an increase of the total seed surface leads to a faster decrease in supersaturation, and smaller final crystal sizes. This is since the higher seed surface area results in an increased solid integration rate through crystal growth. The higher seed mass leads to a smaller average final crystal size since the same amount of solute is added to a larger number of seed crystals. The desupersaturation

rate increases with increasing temperature since the integration of solute into the crystal surface increases with increasing temperature (see Figure 4.10).

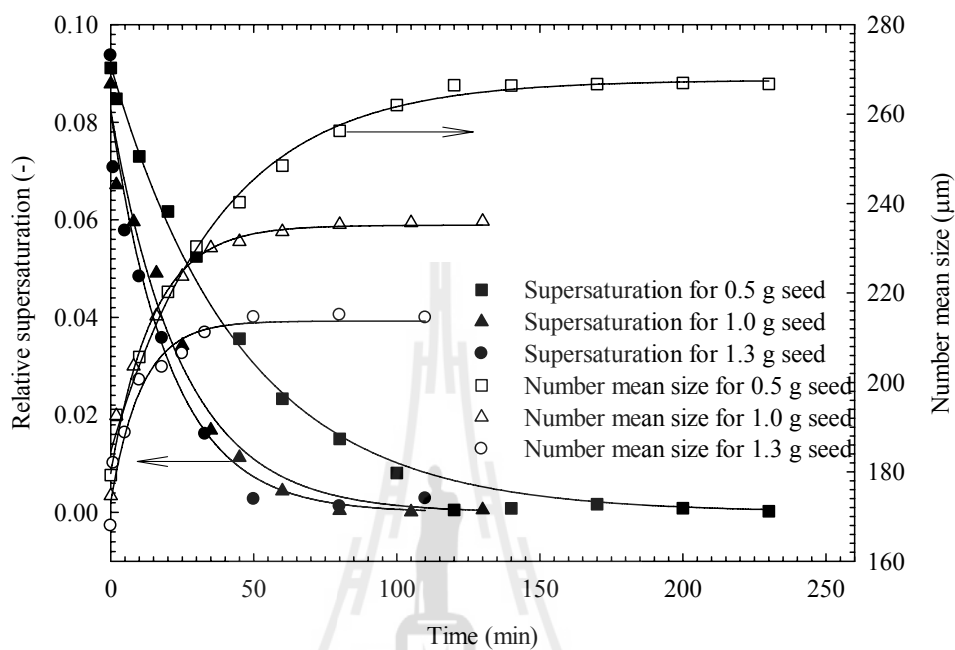


**Figure 4.9** Desupersaturation curves and time dependence of crystal sizes from a batch run of  $\gamma$ -DL-met at 25 °C with different seed masses.

The solid lines are given to guide the eye.

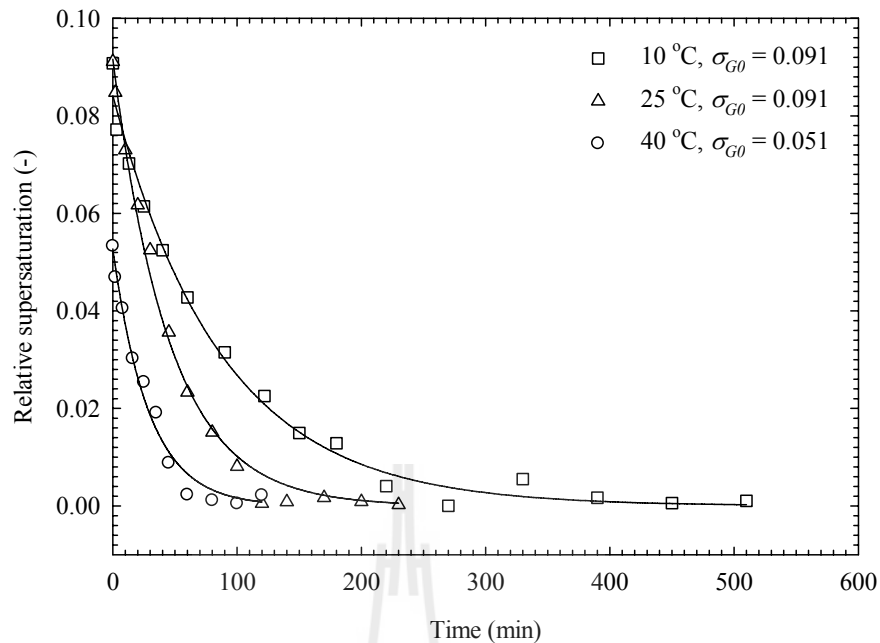


**Figure 4.10** Desupersaturation curves from a batch run of  $\gamma$ -DL-met at different temperatures. The solid lines are given to guide the eye.

The growth rates were calculated using the number mean crystal size. The crystal growth experiments allowed growth kinetics to be determined as a function of relative supersaturation, as shown in Figures 4.11, 4.12, and 4.13. It can be seen that, at constant temperature, the growth rates increase with increasing supersaturation. The results of the experiments with different initial supersaturation (Figures 4.11 and 4.12) agree very well for all but the first data points (for  $\alpha$ -DL-met experiments) and first three data points (for  $\gamma$ -DL-met experiments) of each experiment, where there were different growth rates predicted for the same supersaturation value. Similar results are seen at all experimental temperatures. Also the results of the experiments with different seed mass (Figure 4.13) agree very well for all but at early periods of the experiment, where there is some differences between data for different seed masses.

The explanation for the difference between the growth rates at early periods of the experiment is unknown, although earlier this has been noted in many other species, with the phenomenon initially being seen for fructose (Flood et al, 2000). Many explanations have been proposed for this behavior including initial fast crystal growth as seed crystals repair their surface; later crystal growth being slowed by slow surface adsorption of impurity molecules (Flood et al, 2000); and the effect of growth rate history on the crystal surface (Pantaraks and Flood, 2005; Pantaraks, Matsuoka, and Flood, 2007; Promraksa, Flood, and Schneider, 2009; Flood, 2010). As seen in Figures 4.6 and 4.7, at higher supersaturation levels (at beginning of the crystal growth) the crystals have rougher surface, while those at lower supersaturation levels the crystal surface becomes smoother. This is due to the effect of the growth history on the crystal surface, with crystals grown more quickly at higher supersaturation having a rougher surface than the seed crystals from which they were grown.

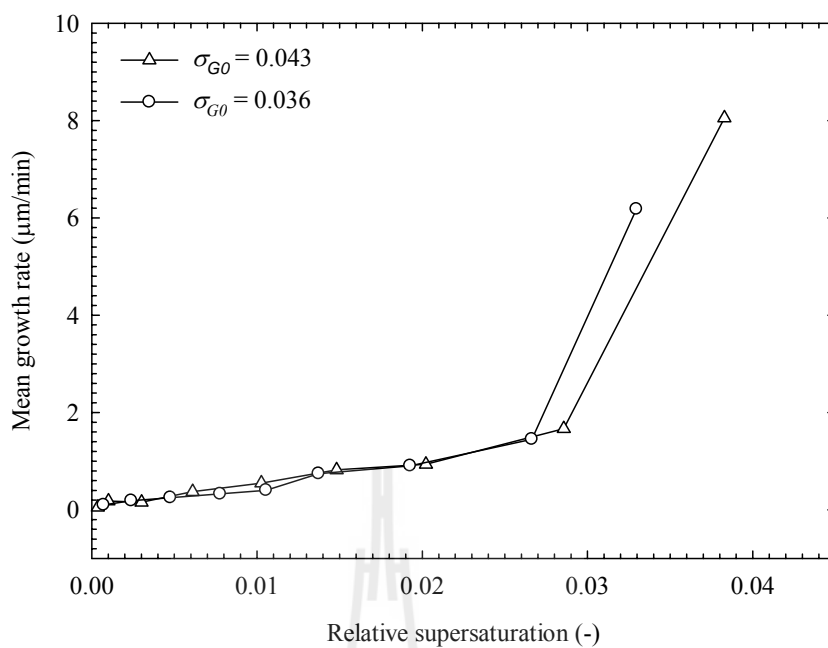


**Figure 4.11** Mean crystal growth rates for  $\alpha$ -DL-met as a function of relative supersaturation at  $25\text{ }^\circ\text{C}$  with different initial supersaturation.

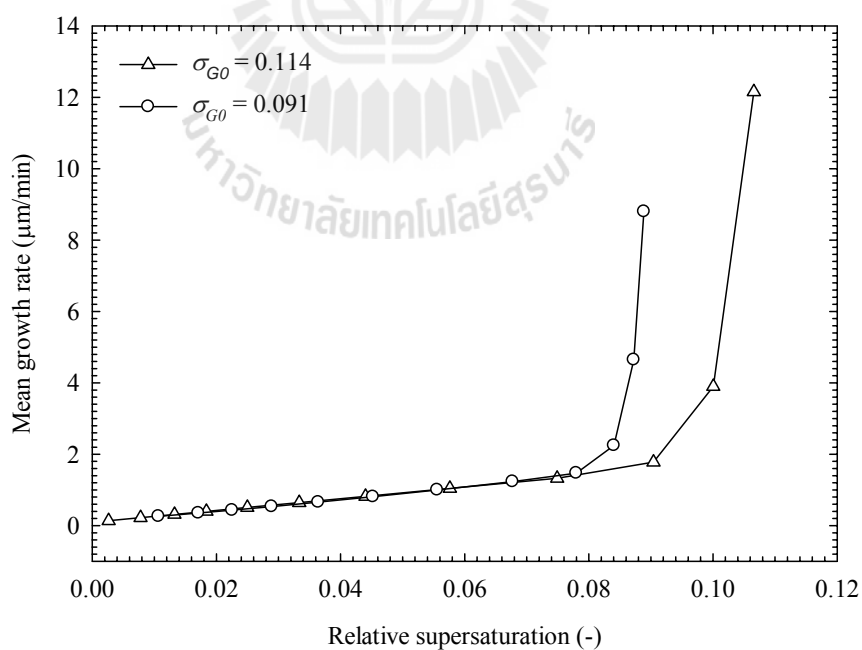


**Figure 4.12** Mean crystal growth rates for  $\gamma$ -DL-met as a function of relative supersaturation at  $25\text{ }^\circ\text{C}$  with different initial supersaturation.

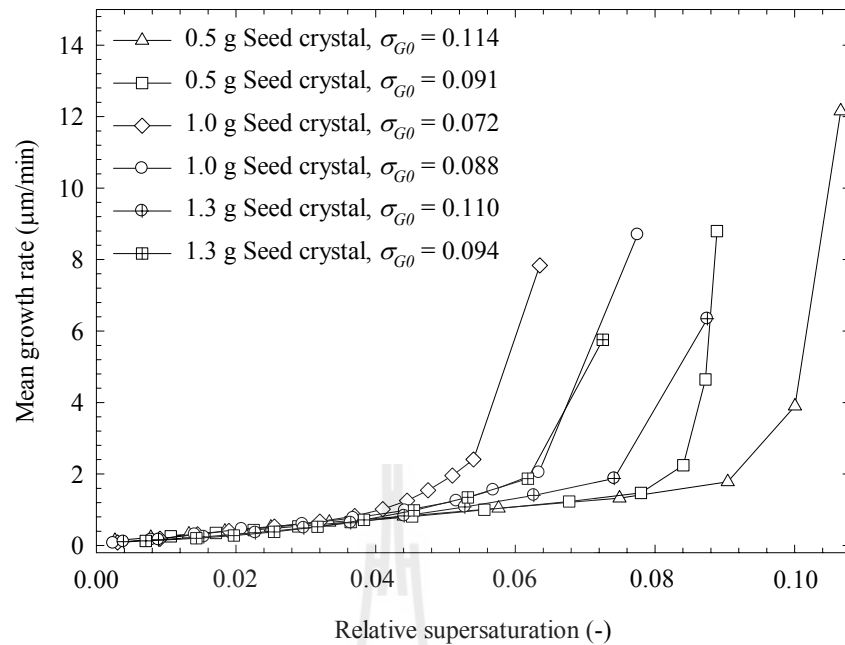


**Figure 4.13** Mean crystal growth rates for  $\gamma$ -DL-met as a function of relative supersaturation at 25 °C with different seed masses.

The unusually high growth rates during the early period of all experiments were ignored in subsequent analysis of crystallization kinetics. If three experiments are done with three different starting supersaturations, then three different growth rate values are obtained for the same supersaturation values. Of course this is physically impossible unless there is some other reason for it, and that reason is growth rate history as described above. The mean growth rates can be described for each set of conditions by the power-law model as expressed in equation (4.8). Therefore, in this work the mean growth rates (which were calculated using the method as shown in Table 4.3) can be expressed using the power-law model of the form

$$\bar{G} = \frac{\Delta \bar{L}}{\Delta t} = K_G \sigma_G^n \quad (4.14)$$

where  $\bar{G}$  is the mean growth rate ( $\mu\text{m}/\text{min}$ ). The experimental results for the growth of  $\alpha$ -DL-met and  $\gamma$ -DL-met were fitted with equation (4.14) and the results are shown in Figures 4.14 and 4.15 for  $\alpha$ -DL-met and  $\gamma$ -DL-met, respectively. The model fits the data well. The resulting equations show that the growth rate orders are unity for all conditions. The values of the growth rate constants obtained from the linear regression of the experimental data are shown in Table 4.5. The results indicate that the growth rate constants are strongly temperature dependent. The growth rate constants can be modeled by the Arrhenius relationship of equation (4.9). The growth rate constants of both  $\alpha$ -DL-met and  $\gamma$ -DL-met were fitted with equation (4.9), and the results are shown in Figure 4.21 together with the dissolution of  $\alpha$ -DL-met. The values of activation energy of growth obtained from the linear regression of the dissolution and growth rate constants are shown in Table 4.5.

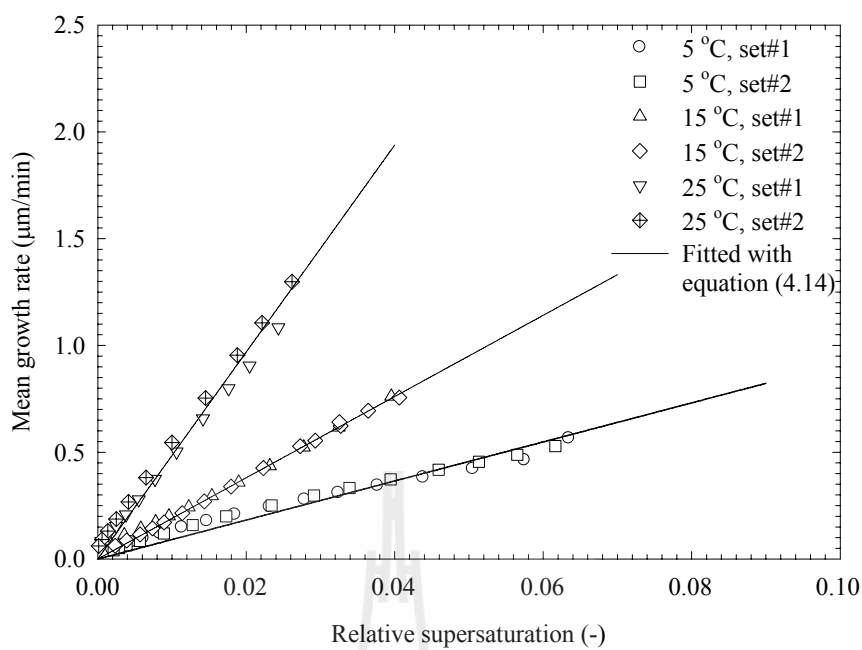


**Figure 4.14** Mean crystal growth rates of  $\alpha$ -DL-met as a function of relative supersaturation and temperature.

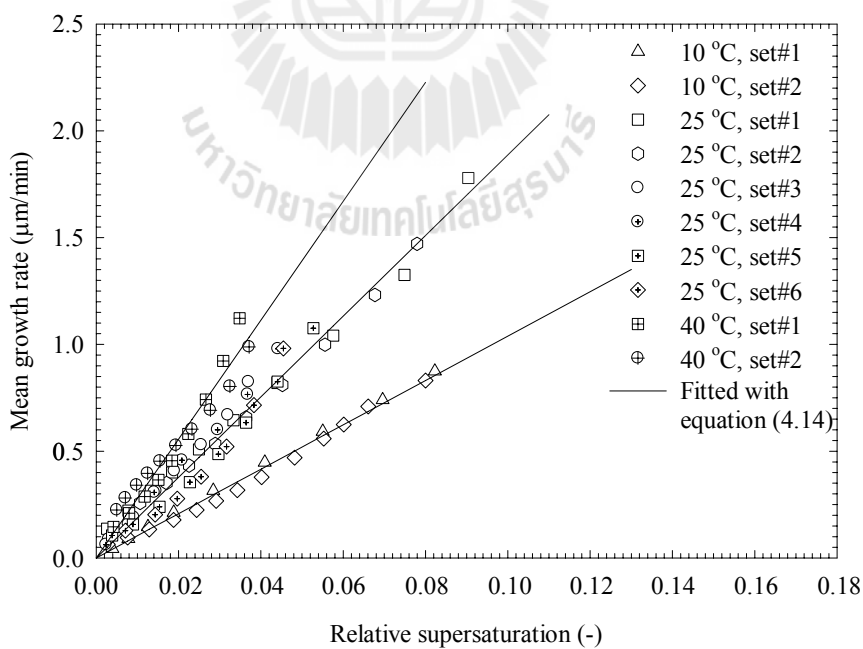


**Figure 4.15** Mean crystal growth rates of  $\gamma$ -DL-met as a function of relative supersaturation and temperature.

### 4.5.2 Crystal Dissolution Kinetics

Examples of PSDs from a dissolution experiment of  $\gamma$ -DL-met at 25 °C are shown in Figure 4.16. The PSD is plotted on a log-scale to show that the volume-based PSD is a log-normal distribution, and hence appears as a normal distribution when size is plotted on a log-scale. Photomicrographs of seed crystals and final crystals from dissolution experiments of  $\gamma$ -DL-met at 25 °C were also analyzed (Figure 4.17). The final crystals obtained from the dissolution processes showed only one peak, which indicates that the dissolution rates can be easily calculated from the change of the mean crystal size. The XRPD patterns of the final crystals were the same as the seed crystals; this indicates that there was no phase transformation during the dissolution processes during the relatively short batch times used.

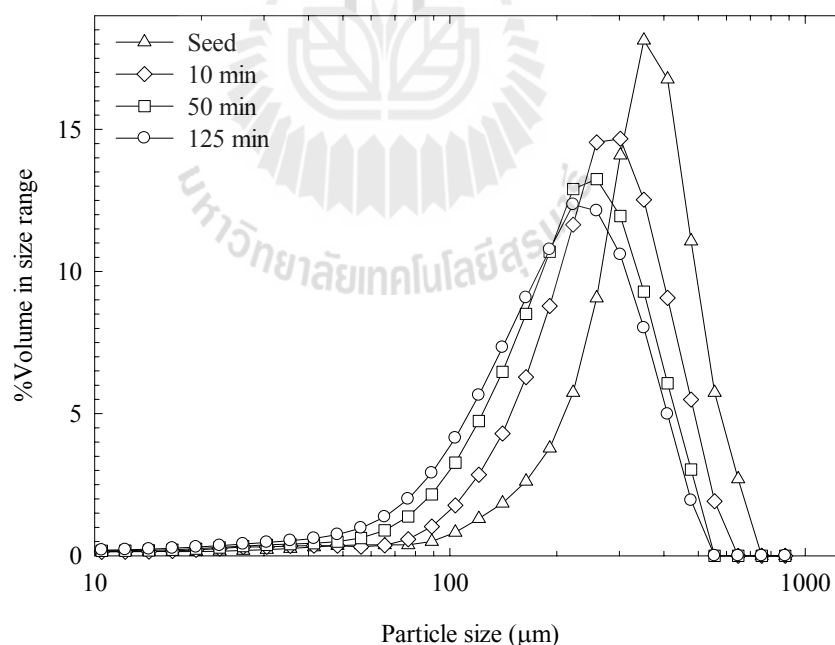


**Figure 4.16** Particle size distributions of seed and crystals in suspension vs time from a dissolution experiment of  $\gamma$ -DL-met at 25 °C and  $\sigma_{D0} = 0.082$ .

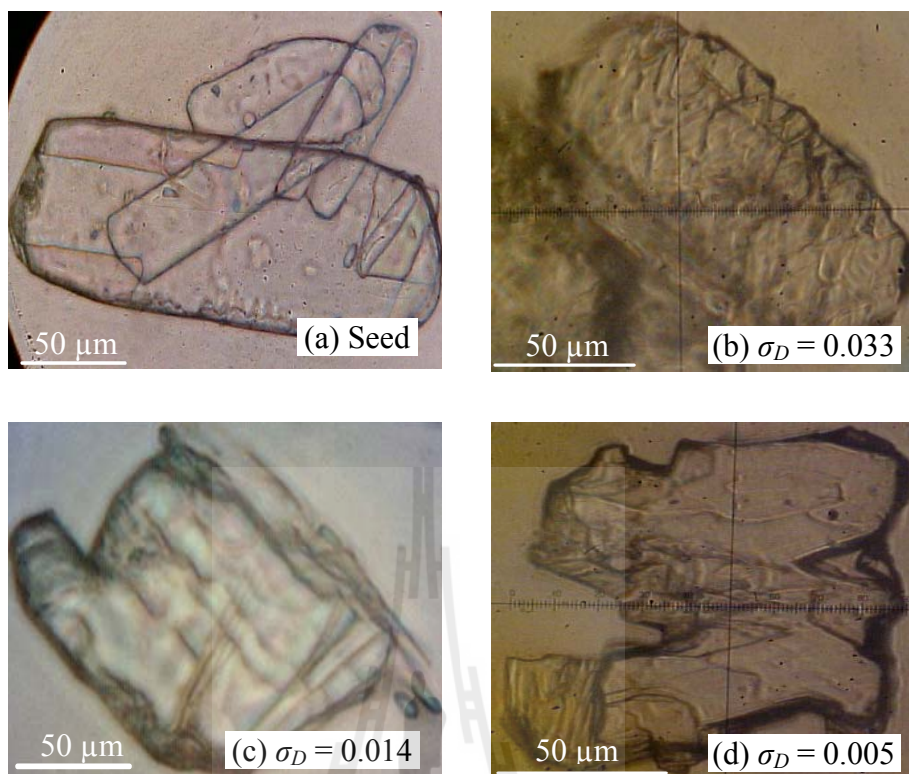


**Figure 4.17** Photomicrographs of seed and final crystals from dissolution experiment of  $\gamma$ -DL-met at 25 °C and  $\sigma_{D0} = 0.082$ .

The technique for calculating the dissolution rates are shown in Table 4.4. The dissolution rate was calculated directly from the change of a smooth plot between the number mean crystal size and the time of each measurement. Figure 4.18 is an example of this plot. The dissolution rates were calculated using the same technique for the growth rate as described in Section 4.5.1. These allow crystal dissolution rates to be determined as a function of relative undersaturation; crystal dissolution rates are the values in column 7 of Table 4.4, and the corresponding relative undersaturation are the values in column 4 of Table 4.4. Similar techniques are used for determining crystal dissolution rates as a function of relative

undersaturation for all experiments. As shown in Table 4.4,  $\sigma_D$  is the relative undersaturation (-),  $\bar{L}$  is the number mean size ( $\mu\text{m}$ ), and  $t$  is the time (min).

**Table 4.4** Example for calculation of crystal dissolution rates as a function of relative undersaturation for experimental results of a batch run of  $\gamma$ -DL-met at 25 °C and initial undersaturation of 0.082.

$t$ (min)	$\Delta t$ (min)	$\sigma_D$ (-)	$\sigma_{D,average}$ (-)	$\bar{L}$ ( $\mu\text{m}$ )	$\Delta\bar{L}$ ( $\mu\text{m}$ )	$\bar{D} = -\Delta\bar{L} / \Delta t$ ( $\mu\text{m}/\text{min}$ )
0		0.0820		208.03		
1	1	0.0424	0.0622	190.46	-17.57	17.5711
2	1	0.0353	0.0389	179.71	-10.75	10.7488
4	2	0.0321	0.0337	168.61	-11.10	5.5499
6	2	0.0302	0.0312	163.51	-5.10	2.5505
10	4	0.0264	0.0283	158.36	-5.15	1.2875
20	10	0.0191	0.0228	150.36	-8.00	0.7995
30	10	0.0139	0.0165	144.30	-6.06	0.6065
38	8	0.0109	0.0124	140.44	-3.86	0.4825
50	12	0.0076	0.0093	135.92	-4.52	0.3767
65	15	0.0050	0.0063	131.90	-4.02	0.2682
80	15	0.0035	0.0042	129.14	-2.76	0.1838
100	20	0.0023	0.0029	126.77	-2.37	0.1185

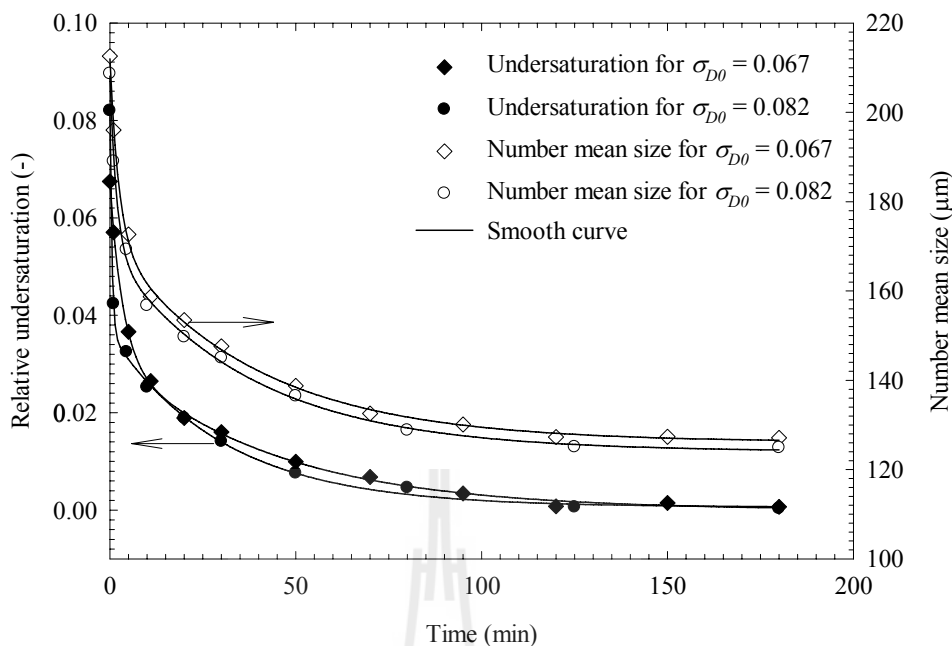


**Figure 4.18** Time dependence of undersaturation and crystal sizes from a batch run of  $\gamma$ -DL-met at 25 °C with different initial undersaturations.

The crystal dissolution experiments allowed dissolution kinetics to be determined as a function of relative undersaturation as shown in Figure 4.19. It can be seen that, at constant temperature, the dissolution rates of  $\gamma$ -DL-met increase with increasing undersaturation. The results of the experiments with different initial undersaturation agree very well for all but the first three data points of each experiment, where there were different dissolution rates predicted for the same undersaturation value. Similar results are seen at all experimental temperatures. This indicates that the initial dissolution rate of  $\gamma$ -DL-met at early periods of the experiment (at higher undersaturation) is significantly higher than would be expected from subsequent crystal dissolution (at lower undersaturation). This is a similar phenomenon as was found in the growth processes. This may be due to a change in the surface structure of the crystals as dissolution progressed; the seeds at the initial

undersaturation may have a rougher surface (on a microscopic scale) than they had after a period of dissolution, leading to a small difference in stability (see Figure 4.17).

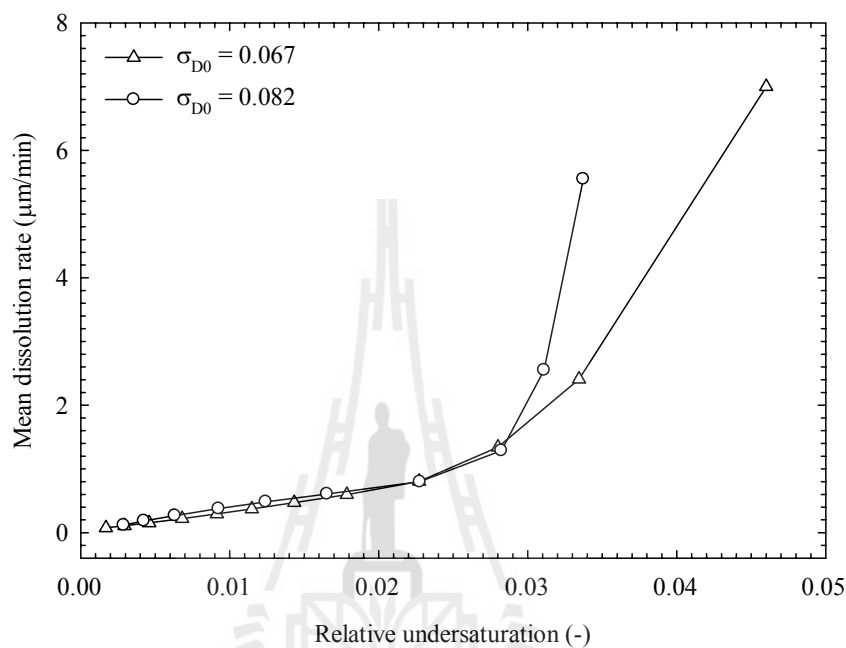


**Figure 4.19** Mean dissolution rates for  $\gamma$ -DL-met as a function of relative undersaturation at 25 °C with different initial undersaturation.

The initial crystal dissolution rates of all experiments were disregarded in subsequent analysis of dissolution kinetics. If three experiments are done with three different starting undersaturations, then three different dissolution rate values are obtained for the same undersaturation values. Of course this is physically impossible unless there is some other reason for it, and that reason is the surface roughness as described above. The mean dissolution rates can be described for each set of conditions by the power-law model as expressed in equations (4.10) and (4.11). Therefore, in this work the mean dissolution rates (which were calculated using the

method as shown in Table 4.4) can be expressed using the power-law model of the form

$$\bar{D} = -\frac{\Delta\bar{L}}{\Delta t} = K_D \sigma_D^m \quad (4.15)$$

where  $\bar{D}$  is the mean dissolution rate ( $\mu\text{m}/\text{min}$ ). The experimental results of the dissolution of  $\gamma$ -DL-met were fitted with equation (4.15), and the results are shown in Figure 4.20. The resulting equations show that the dissolution orders are unity for all conditions, as would be expected for a bulk diffusion controlled process. The values of the dissolution rate constants obtained from the linear regression of the experimental data are shown in Table 4.5. The results indicated that the dissolution rate constants are strongly temperature dependent. The dissolution rate constants can be modeled by the Arrhenius relationship as expressed in equation (4.12). The dissolution rate constants were fitted with equation (4.12), and the results are shown in Figure 4.21 together with the growth rate constants of  $\alpha$ -DL-met and  $\gamma$ -DL-met. The values of the activation energy of dissolution obtained from the linear regression of the dissolution rate constants are shown in Table 4.5.

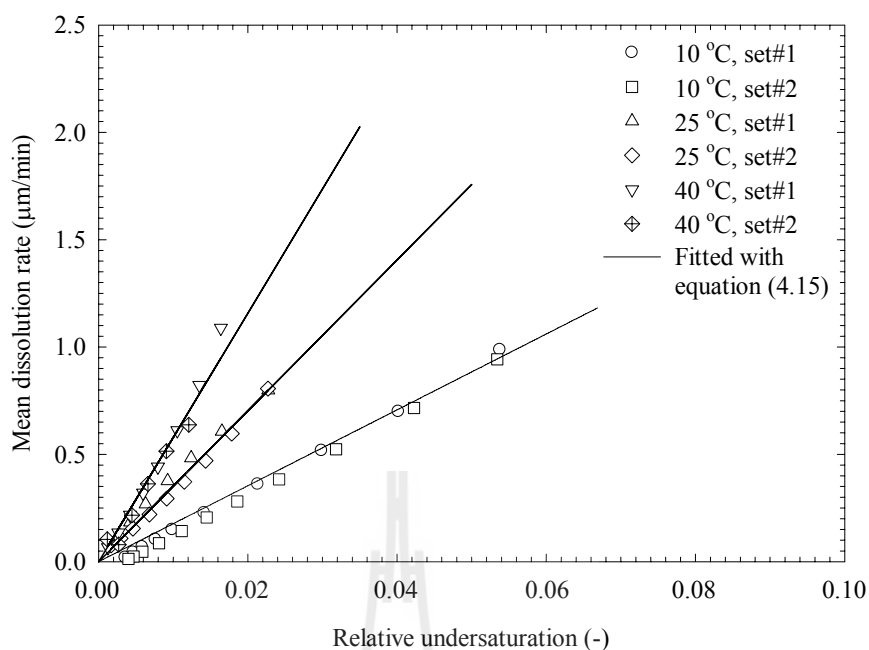


**Figure 4.20** Mean dissolution rates of  $\gamma$ -DL-met as a function of relative undersaturation and temperature.

**Table 4.5** Dissolution and growth kinetic parameters of the polymorphs of DL-met.

Temperature (°C)	$\gamma$ -DL-met				$\alpha$ -DL-met	
	$K_G$ ( $\mu\text{m}/\text{min}$ )	$E_G$ (kJ/mol)	$K_D$ ( $\mu\text{m}/\text{min}$ )	$E_D$ (kJ/mol)	$K_G$ ( $\mu\text{m}/\text{min}$ )	$E_G$ (kJ/mol)
5	-	24.26	-	29.16	9.11	56.00
10	10.39		16.93			
15	-		-			
25	18.87		35.13			
40	27.83		57.87		-	

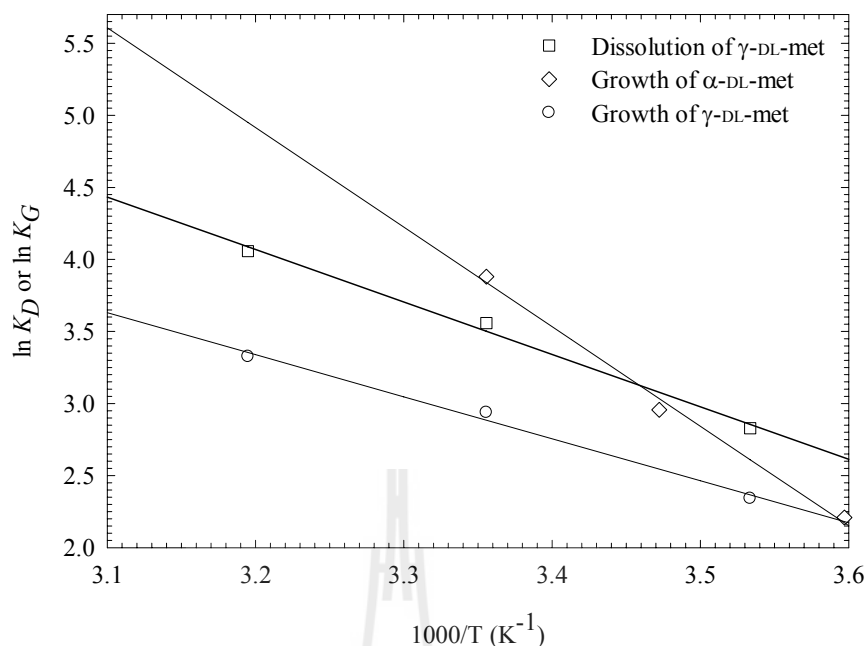


**Figure 4.21** An Arrhenius plot of the growth rate and dissolution rate constants for DL-met for determination of the activation energy of crystal growth and dissolution.

Moreover, in the dissolution kinetics experiments, the dissolution rate of two different sets of seed crystals, in the size ranges of 180 - 250 and 250 - 300  $\mu\text{m}$  were measured at 25 °C to determine if any size dependence was found in the dissolution rate. The results showed that the dissolution rates of both seed sizes are the same (see Figure 2.22). The growth rate is also size independent growth as described in Section 4.4.3. Therefore, when considering the transformation kinetics, the growth rate of  $\alpha$ -DL-met (seed size: 64 - 125  $\mu\text{m}$ ), the dissolution rates of  $\gamma$ -DL-met (when the dissolution rates of  $\alpha$ -DL-met and  $\gamma$ -DL-met as a function of undersaturation are assumed to be the same) (seed size: 250 - 300  $\mu\text{m}$ ), and the growth rate of  $\gamma$ -DL-met (seed size: 180 - 250  $\mu\text{m}$ ) can be reasonably compared with each other.

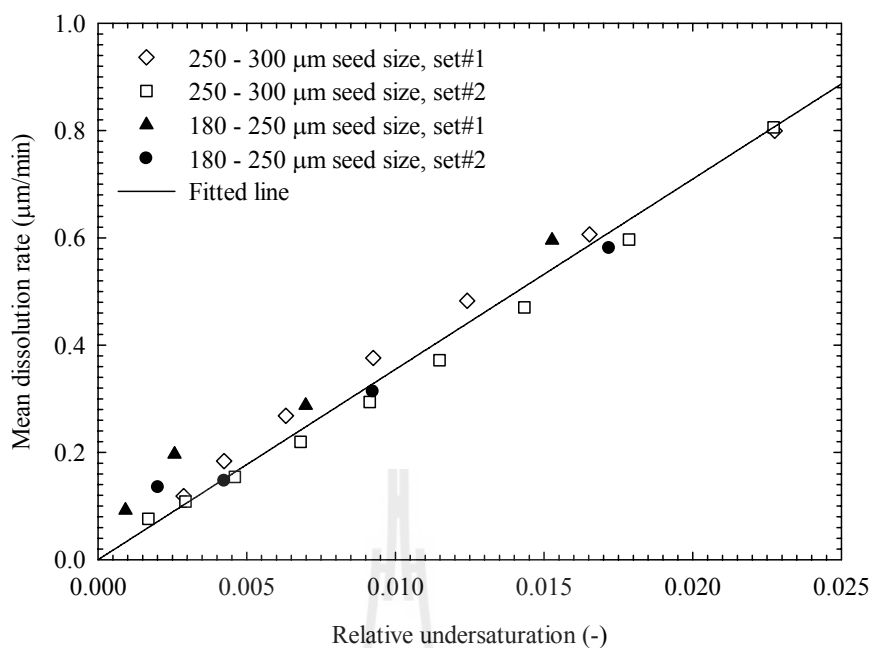


**Figure 4.22** Mean dissolution rates of  $\gamma$ -DL-met as a function of relative undersaturation at 25 °C with different seed sizes.

### 4.5.3 Discussion

The SMT is usually the most important process in crystallization of polymorphs from solution. If  $\alpha$ -DL-met crystals are put in a saturated aqueous solution, a SMT from  $\alpha$ -DL-met to  $\gamma$ -DL-met will take place. The dissolution of  $\alpha$ -DL-met and growth of  $\gamma$ -DL-met are the main kinetics of SMT. Table 4.5 shows that the dissolution rate constants of  $\gamma$ -DL-met are higher than the growth rate constants of  $\gamma$ -DL-met at all temperatures studied. Assuming that the dissolution process is mass transfer controlled and that therefore the two polymorphs have the same dissolution kinetics, the dissolution rate of  $\alpha$ -DL-met is faster than the growth rate of  $\gamma$ -DL-met. This conclusion is similar to the SMT of other crystalline substances, for example, L-histidine (Kitamura, 1993), taltireline (Maruyama, Ooshima, and Kato, 1999),

L-glutamic acid (Dharmayat et al., 2008; Ono et al., 2004; Schöll et al., 2006), and carbamazepine (Qu et al., 2006). From the results in the current chapter we cannot be sure of the validity of this conclusion. The uncertainty is also since the dissolution rates of  $\alpha$ -DL-met and  $\gamma$ -DL-met as a function of undersaturation of this work are assumed to be the same due to dissolution being considered as a single step (diffusion controlled), and hence the dissolution rates were measured using  $\gamma$ -DL-met seed crystals only. The assumption is checked in Chapters V and VI and more conclusions are also described in those chapter. Moreover, the growth rate of the  $\alpha$ -DL-met is also faster than the growth rate of  $\gamma$ -DL-met, except at low temperature. The crystallization kinetics of the metastable polymorphs are usually faster than the stable polymorphs when the metastable polymorphs appear first and then transform to a more stable polymorphs (Ono et al., 2004; Jiang, ter Horst, and Jansens, 2008; Roelands et al., 2006).

#### 4.6 Conclusions

In this work, the kinetics of the processes which contribute to the rate of transformation between the polymorphs have been studied. The growth and dissolution kinetics of the two polymorphs were measured between 5 and 40 °C in an agitated batch crystallizer. The initial growth rate (at higher supersaturation) is significantly higher than subsequent crystal growth (at lower supersaturation). During the early periods of the experiments there were much larger growth rates than that would be expected from extrapolation of the data determined during the later time periods. This is due to the effect of the growth history on the crystal surface, with crystals grown more quickly at higher supersaturation having a rougher surface on a

microscopic level than the seed crystals they were grown from. At all temperatures studied, the growth rate orders of both  $\alpha$ -DL-met and  $\gamma$ -DL-met are 1. The dissolution rate order of  $\alpha$ -DL-met is also 1. The growth and dissolution rate constants increase with increasing temperature and follow an Arrhenius relationship. At all temperatures studied, the growth rate of  $\alpha$ -DL-met and the dissolution rate of  $\gamma$ -DL-met are faster than the growth rate of the  $\gamma$ -DL-met for equivalent driving forces.

#### 4.7 References

- Allen, T. (1997). **Particle size measurement: Volume 1 powder sampling and particle size measurement** (5<sup>th</sup> ed.). London: Chapman&Hall.
- Chakraborty, D., and Bhatia, S.K. (1996a). Formation and aggregation of polymorphs in continuous precipitation. 1. Mathematical modeling. **Ind. Eng. Chem. Res.** 35(6): 1985-1994.
- Chakraborty, D., and Bhatia, S.K. (1996b). Formation and aggregation of polymorphs in continuous precipitation. 2. Kinetics of CaCO<sub>3</sub> precipitation. **Ind. Eng. Chem. Res.** 35(6): 1995-2006.
- Cornel, J., Lindenberg, C., and Mazzotti, M. (2009). Experimental characterization and population balance modeling of the polymorph transformation of L-glutamic acid. **Cryst. Growth Des.** 9(1): 243-252.
- Dharmayat, S., Hammond, R.B., Lai, X., Ma, C., Purba, E., Roberts, K.J., Chen, Z-P., Martin, E., Morris, J., and Bytheway, R. (2008). An examination of the kinetics of the solution-mediated polymorphic phase transformation between  $\alpha$ - and  $\beta$ -forms of L-glutamic acid as determined using online powder X-ray diffraction. **Cryst. Growth Des.** 8(7): 2205-2216.

- Flood, A.E. (2009). **Industrial crystallization from solution: A primer**. Thailand: Suranaree University of Technology.
- Flood, A.E. (2010). Feedback between crystal growth rates and surface roughness, **CrystEngComm** 12(2): 313-323.
- Flood, A.E., Johns, M.R., and White, E.T. (2000). Crystal growth rates and dispersion for D-fructose from aqueous ethanol. **AIChE J.** 46(2): 239-246.
- Garside, J., Mersmann, A., and Nyvlt, J. (2002). **Measurement of crystal growth and nucleation rates** (2<sup>nd</sup> ed.). UK: Institute of Chemical Engineering.
- Glade, H., Ilyaskarov, A.M., and Ulrich, J. (2004). Determination of crystal growth kinetics using ultrasonic technique. **Chem. Eng. Technol.** 27(4): 736-740.
- Gougazeh, M., Omar, W., and Ulrich, J. (2009). Growth and dissolution kinetics of potassium sulfate in pure solutions and in the presence of Cr<sup>3+</sup> ions. **Cryst. Res. Technol.** 44(11): 1205-1210.
- Gutjahr, A., Dabringhaus, H., and Lacmann, R. (1996a). Studies of the growth and dissolution kinetics of the CaCO<sub>3</sub> polymorphs calcite and aragonite I. Growth and dissolution rates in water. **J. Cryst. Growth** 158(3): 296-309.
- Gutjahr, A., Dabringhaus, H., and Lacmann, R. (1996b). Studies of the growth and dissolution kinetics of the CaCO<sub>3</sub> polymorphs calcite and aragonite II. The influence of divalent cation additives on the growth and dissolution rates. **J. Cryst. Growth** 158(3): 310-315.
- Hurley, L.A., Jones, A.G., and Drummond, J.N. (1997). Growth and dissolution kinetics of cyanazine crystals in aqueous ethanol solutions. **J. Cryst. Growth** 172(3-4): 499-507.

- Jiang, S., ter Horst, J.H., and Jansens, P.J. (2008). Concomitant polymorphism of *o*-aminobenzoic acid in antisolvent crystallization. **Cryst. Growth Des.** 8(1): 37-43.
- Jones, A.G. (2002). **Crystallization process systems** (1<sup>st</sup> ed.). Oxford: Butterworth-Heinemann.
- Kitamura, M. (1993). Crystallization behavior and transformation kinetics of L-histidine polymorphs. **J. Chem. Eng. Jpn.** 26(3): 303-307.
- Kitamura, M. (2009). Strategy for control of crystallization of polymorphs, **CrystEngComm.** 11(6): 949-964.
- Kitamura, M., Furukawa, H., and Asaeda, M. (1994). Solvent effect of ethanol on crystallization and growth process of L-histidine polymorphs. **J. Cryst. Growth** 141(1-2): 193-199.
- Kitamura, M., and Ishizu, T. (1998). Kinetic effect of L-phenylalanine on growth process of L-glutamic acid polymorph. **J. Cryst. Growth** 192(1-2): 225-235.
- Kitamura, M., and Ishizu, T. (2000). Growth kinetics and morphological change of polymorphs of L-glutamic acid. **J. Cryst. Growth** 209(1): 138-145.
- Kramer, H.J.M., and van Rosmalen, G.M. (2009). Crystallization. In: I.A., Wilson and C.F., Poole (ed.). **Handbook of methods and instrumentation in separation science volume 2** (pp 1-20). London: Academic Press.
- Maruyama, S., Ooshima, H., and Kato, J. (1999). Crystal structures and solvent-mediated transformation of taltireline polymorphs. **Chem. Eng. J.** 75(3): 193-200.

- Mitchell, N.A., Ó'Ciardhá, C.T., and Frawley, P.J. (2011). Estimation of the growth kinetics for the cooling crystallization of paracetamol and ethanol solutions. **J. Cryst. Growth** 328(1): 39-49.
- Mullin, J.W. (2001). **Crystallization** (4<sup>th</sup> ed.). Oxford: Butterworth-Heinemann.
- Myerson, A.S., and Ginde, R. (2002). Crystals, crystal growth, and nucleation. In: A.S. Myerson (ed.). **Handbook of industrial crystallization** (2<sup>nd</sup> ed., pp 33-65). USA: Butterworth-Heinemann.
- Ohara, M., and Reid, R.C. (1973). **Modeling crystal growth rates from solution**. Englewood Cliffs: Prentice-Hall.
- Ono, T., Kramer, H.J.M., ter Horst, J.H., and Jansens, P.J. (2004). Process modeling of the polymorphic transformation of L-glutamic acid. **Cryst. Growth Des.** 4(6): 1161-1167.
- Pantaraks, P., and Flood, A.E. (2005). Effect of growth rate history on current crystal growth: A second look at surface effects on crystal growth rates. **Cryst. Growth Des.** 5(1): 365-371.
- Pantaraks, P., Matsuoka, M., and Flood, A.E. (2007). Effect of growth rate history on current crystal growth. 2: Crystal growth of sucrose,  $KAl(SO_4)_2 \cdot 12H_2O$ ,  $KH_2PO_4$ , and  $K_2SO_4$ . **Cryst. Growth Des.** 7(12): 2635-2642.
- Prasad, K.V.R., Ristic, R.I., Sheen, D.B., and Sherwood, J.N. (2002). Dissolution kinetics of paracetamol single crystals. **Int. J. Pharm.** 238(1-2): 29-41.
- Promraksa, A., Flood, A.E., and Schneider, P.A. (2009). Measurement and analysis of the dextran partition coefficient in sucrose crystallization. **J. Cryst. Growth** 311(14): 3667-3673.

- Qu, H., Louhi-Kultanen, M., Rantanen, J., and Kallas, J. (2006). Solvent-mediated phase transformation kinetics of an anhydrate/hydrate system. **Cryst. Growth Des.** 6(9): 2053-2060.
- Randolph, A.D., and Larson, M.A. (1988). **Theory of particulate processes: Analysis and techniques of continuous crystallization** (2<sup>nd</sup> ed.). California: Academic Press.
- Roelands, C.P.M., Jiang, S., Kitamura, M., ter Horst, J.H., Kramer, H.J.M., and Jansens, P.J. (2006). Antisolvent crystallization of the polymorphs of L-histidine as a function of supersaturation ratio and of solvent composition. **Cryst. Growth Des.** 6(4): 955-963.
- Schöll, J., Bonalumi, D., Vicum, L., and Mazzotti, M. (2006). In situ monitoring and modeling of the solvent-mediated polymorphic transformation of L-glutamic acid. **Cryst. Growth Des.** 6(4): 881-891.
- Schöll, J., Lindenberg, C., Vicum, L., Brozio, J., and Mazzotti, M. (2007). Precipitation of  $\alpha$ -L-glutamic acid: determination of growth kinetics. **Faraday Discuss.** 136:247-264.
- Srisa-nga, S., Flood, A.E., and White, E.T. (2006). The secondary nucleation threshold and crystal growth of  $\alpha$ -glucose monohydrate in aqueous solution. **Cryst. Growth Des.** 6(3): 795-801.
- Strickland-Constable, R.F. (1968). **Kinetics and mechanism of crystallization**. London: Academic Press.
- Tanrikulu, S.Ü., Eroğlu, I., Bulutcu, A.N., and Özkar, S. (1998). The growth and dissolution of ammonium perchlorate crystals in a fluidized bed crystallizer. **J. Cryst. Growth** 194(2): 220-227.

# CHAPTER V

## POLYMORPHIC TRANSFORMATION OF DL-METHIONINE IN AQUEOUS SOLUTION: EXPERIMENTATION

### 5.1 Abstract

In this work, the solution-mediated transformation (SMT) of  $\alpha$ -DL-met into  $\gamma$ -DL-met in water at 25 °C via a seeded batch crystallization process was studied by measurement of the change of the solute concentration and the fraction of  $\gamma$ -DL-met in the crystal phase with time during the crystallization process. The solute concentration was measured off-line using the dry substance method since this is recognized as the most accurate method for concentration determination. The fraction of  $\gamma$ -DL-met was measured off-line by XRPD by setting a calibration curve using the internal standard method. The internal standard method was done by setting up a calibration curve using mixtures of  $\alpha$ -DL-met,  $\gamma$ -DL-met, and NaCl, where NaCl was the internal standard. The mechanism of the SMT was interpreted to be a two step process, consisting of the dissolution process of  $\alpha$ -DL-met and the crystallization process (nucleation and growth) of  $\gamma$ -DL-met. The dissolution of  $\alpha$ -DL-met is the rate controlling step during the transformation. The transformation time for the case where the seed was added to a supersaturated solution within the SNT region is longer than the case where the seed was added to a supersaturated solution above the SNT region.

## 5.2 Introduction

When the driving force is created in a solution of a polymorphic compound, the system tends to minimize its free energy. Theoretically, this leads to the crystallization of the stable polymorph. However, if the crystallization kinetics of the metastable polymorph are faster the compound may crystallize into this metastable polymorph first. Eventually the metastable polymorph should transform into the stable one (Roelands, 2005). This phenomenon of formation of the kinetically controlled polymorph over the thermodynamically favored form is known as Ostwald's rule of stages (Threlfall, 2003). This rule is based on observation and is not a physical law (Roelands et al., 2006); it is often incorrect, particularly in cases where the solution is either below the solubility of the metastable polymorph, or below the nucleation threshold of the metastable polymorph. Moreover, if both polymorphs crystallize at similar rates a mixture of the two polymorphs is initially obtained; this is called concomitant polymorphism (Bernstein, Davey, and Henck, 1999).

The metastable polymorph will transform to the stable polymorph via solid-state transformation (SST) (O'Brien, Timmins, Williams, and York, 2004; Jiang, Jansens, and ter Horst, 2010a) or solution-mediated transformation (SMT) (Schöll, Bonalumi, Vicum, and Mazzotti, 2006; Jiang, Jansens, and ter Horst, 2010b). In the case of true SST the crystal lattice transforms into the different arrangement, for instance when the temperature is raised. Studies of SST are important, for example the sudden appearance or disappearance of a polymorphic form in pharmaceutical products can lead to serious consequences if the transformation occurs in the dosage forms (Vippagunta, Brittain, and Grant, 2001). The transformation in the solid state is often much slower than in the solution. For the SMT the transformation of the

metastable polymorph into the stable polymorph occurs when a liquid phase surrounds the crystals. SMT consists of the nucleation and crystal growth of the stable polymorph and the dissolution of the metastable polymorph. There are two mechanisms that could control the transformation rate: either the dissolution rate of the metastable polymorph is limiting or the crystallization rate of the stable polymorph is limiting (Mangin, Puel, and Veessler, 2009). SMT is found in the crystallization of polymorphic compounds in solution. Crystallization with seeding (which is commonly found in industrial crystallization) is the easy way to study the SMT mechanisms. However, the SMT can be studied via unseeded crystallization where the metastable polymorph forms first, followed by transformation to the more stable polymorph (Ostwald's rule). Therefore, crystallization processes involving polymorphs consist of the competitive nucleation and crystal growth of the polymorphs, and the transformation from the metastable to the stable polymorph. In this work the focus is on the SMT of the polymorphs of DL-methionine (DL-met).

To study the mechanisms of SMT and identify which mechanism is the limiting step the polymorphic composition of the slurry has to be followed in time in combination with the concentration of the solute in the solution. For example, the SMT of the metastable  $\alpha$  polymorph of L-glutamic acid was studied by Garti and Zour (1997), by Ono, Kramer, ter Horst, and Jansens, (2004), by Schöll et al., (2006), and by Dharmayat et al. (2008). In all studies the aqueous suspension was stirred in an agitated crystallizer. It was concluded that the growth rate of the stable  $\beta$  polymorph was the rate controlling step during the transformation processes. In addition, the experimental results of Garti and Zour (1997) showed that the transformation could be inhibited by the addition of surfactants. Kitamura (1993) found that the dissolution

rate constant of the metastable B polymorph of L-histidine was nearly six times larger than the growth rate constant of the stable A polymorph, which indicated the transformation process in aqueous solution was growth controlled. The SMT of the metastable  $\alpha$  polymorph of taltireline to the stable  $\beta$  polymorph in water at 10 °C was studied by Maruyama, Ooshima, and Kato, (1999). It was found that the growth rate of the stable  $\beta$  polymorph was the rate controlling step during the transformation process, and the coexistence of methanol promoted the transformation rate. Qu, Louhi-Kultanen, Rantanen, and Kallas (2006) found that the crystallization (nucleation and growth) of dihydrate form (CBZH) of carbamazepine was the rate controlling step for the transformation of anhydrous form (CBZA) into CBZH in water-ethanol mixed solvent.

Usually, the transformation rate is controlled by the growth rate of the stable polymorph as described in the above examples. However, the transformation rate can be controlled by the dissolution rate of the metastable polymorph. For example, the transformation rate of the metastable  $\beta$  polymorph of glycine to the stable  $\alpha$  polymorph in water-ethanol mixed solvent was limited by the slow dissolution rate of the metastable  $\beta$  polymorph (Ferrari, Davey, Cross, Gillon, and Towler, 2003). In this work it was concluded that increased attrition of the metastable polymorph created additional surface area which facilitated the rate-limiting dissolution process.

The experiment to study the SMT can be performed by monitoring the transformation of the metastable polymorph to the stable polymorph during the crystallization. Monitoring the transformation involves measuring the change of the supersaturation (or solute concentration) and polymorphic fraction with time during the crystallization process. Several methods have been used to measure the solute

concentration during the SMT experiments, for example the dry substance method (Qu et al., 2006; Roelands et al., 2006; Jiang, ter Horst, and Jansens, 2008), using UV spectroscopy (Kitamura, 1993; Garti and Zour, 1997; Lu, Wang, Yang, and Ching, 2007), and using HPLC (Maruyama et al., 1999). There are many analytical methods which have been used for measuring the polymorphic fraction off-line, for example Raman spectroscopy (Ono, Kramer et al., 2004; Qu et al., 2006; Roelands et al., 2006), X-ray powder diffractometry (XRPD) (Kitamura 1993; Garti and Zour, 1997; Maruyama et al., 1999; Kitamura and Sugimoto, 2003), and Fourier transform infrared spectroscopy (FT-IR) (Ferrari et al., 2003; Lu et al., 2007). However, for this purpose there are at least two techniques have been applied in-situ during crystallization: XRPD (Davis et al., 2003; Hammond, Lai, Roberts, Thomas, and White, 2004; Dharmayat et al., 2008) and Raman spectroscopy (Ono, ter Horst, and Jansens, 2004; Qu et al., 2006; Schöll et al., 2006; Jiang et al., 2010b). During the crystallization experiment simultaneous in-situ measurements and off-line measurements of the polymorphs fraction were done by Ono, ter Horst et al. (2004) and by Qu et al. (2006), and the two techniques showed good agreement.

All of the above techniques are accurate enough for determining the solute concentration and polymorphic fraction during the crystallization process. The accuracy depends on the performance of each equipment, and the reliability and robustness of the sampling techniques, data analysis, etc. Usually, off-line handling rather than in-situ measurements may be the cause of the observed deviations. However, the studies of Ono, ter Horst et al. (2004) and Qu et al. (2006) showed that the off-line result is accurate enough for this purpose as described above. Therefore,

in this work the dry substance method was used to determine the solute concentration and XRPD was used for measuring the polymorphic fraction off-line.

The aim of this work is to study the SMT of the metastable  $\alpha$ -DL-methionine ( $\alpha$ -DL-met) to the stable  $\gamma$ -DL-methionine ( $\gamma$ -DL-met) in aqueous solution at 25 °C. The polymorphic transformation was studied by measuring the changes of the polymorphic fraction and the solute concentration with time during the crystallization process. The off-line measurements of the solute concentration and polymorphic fraction were measured by the dry substance method and XRPD, respectively.

### 5.3 Theory

The transformation of polymorphs can be carried out only from the less stable polymorphs to the most stable one. During crystallization from solution of a polymorphic compound the phase transformation phenomena are often promoted by the liquid phase surrounding the crystals. This is usually called solution-mediated transformation (SMT).

If the polymorphic system is far away from the transformation temperature, as shown in Figure 5.1(a), the metastable polymorph (polymorph II) has a higher solubility than the stable polymorph (polymorph I). Initially, the solution at concentration  $C_i$  and temperature  $T$  is supersaturated with respect to both polymorphs. For Ostwald's rule of stages, when the crystallization kinetics, determined by both the nucleation rate and the growth rate, of polymorph II are faster than that of polymorph I, polymorph II crystals will initially nucleate and grow (Jiang et al., 2010b; Roelands, 2005). The solute concentration  $C_i$  drops to the solubility of polymorph II,  $C_{II}^*$ . This is since the crystal growth is of polymorph II. At this point,

the solution is saturated with respect to polymorph II while still supersaturated with respect to polymorph I. This corresponds with the beginning of region 1 in Figure 5.1(b), where the supersaturation ratios  $S_I$  of polymorph I and  $S_{II}$  of polymorph II are a function of time, and both the supersaturation ratios decrease because of the decrease of the solute concentration  $C_i$ .

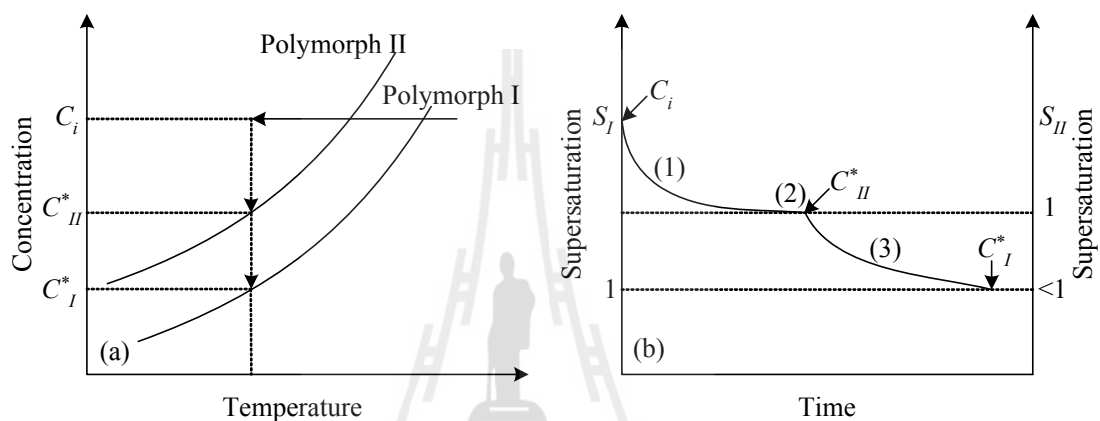


**Figure 5.1** Thermodynamic and kinetic features of the SMT: (a) typical solubility curves of a monotropically related stable polymorph (polymorph I) and metastable polymorph (polymorph II), (b) general features of the time dependence of supersaturation ratios in a SMT.

(Adapted from Jiang et al., 2010b)

Because the solution is still supersaturated with respect to polymorph I, polymorph I crystals start nucleating and growing, and polymorph II start dissolving when the supersaturation ratio of polymorph II becomes  $S_{II} < 1$ . This is the start of SMT, which consists of the nucleation and crystal growth of the stable polymorph and the dissolution of the metastable polymorph (Jiang et al., 2010b; Schöll et al., 2006). The solute concentration is balanced by the decrease in the solute concentration due to

the growth of polymorph I crystals and the increase the solute concentration due to the dissolution of polymorph II crystals. In many cases, the phase transformation is a growth-controlled transformation. During the transformation the solute concentration  $C_i$  is maintained at or close to the solubility  $C_{II}^*$  of polymorph II because the dissolution of polymorph II crystals is rapid enough to maintain the solution concentration  $C_i$ . This coincides with region 2 in Figure 5.1(b) which the supersaturation ratio  $S_I$  remains at a plateau value of  $S_I \approx C_{II}^* / C_I^*$ .

The solute concentration (or supersaturation ratio) remains constant until polymorph II crystals have completely dissolved. The solute concentration starts to decrease upon the further growth of polymorph I crystals, and the whole transformation process is complete when the solute concentration  $C_i$  reaches the solubility  $C_I^*$  of polymorph I. At this point the supersaturation ratio of polymorph I  $S_I = 1$ , and supersaturation ratio of polymorph II becomes  $S_{II} < 1$ . This is indicated as region 3 in Figure 5.1(b).

It is important to note that if the phase transformation is a growth-controlled transformation, the concentration profile corresponds to curve (1) in Figure 5.2 where the plateau of solute concentration is located in the vicinity of the solubility of the metastable polymorph (Mangin et al., 2009). This indicates the growth rate constant is much smaller than the dissolution rate constant. If the solute concentration drops immediately to the solubility of the stable polymorph (as shown curve (2) in Figure 5.2), the phase transformation is a dissolution-controlled transformation. This indicates the dissolution rate constant of the metastable polymorph is much smaller than that the growth rate constant of the stable polymorph.

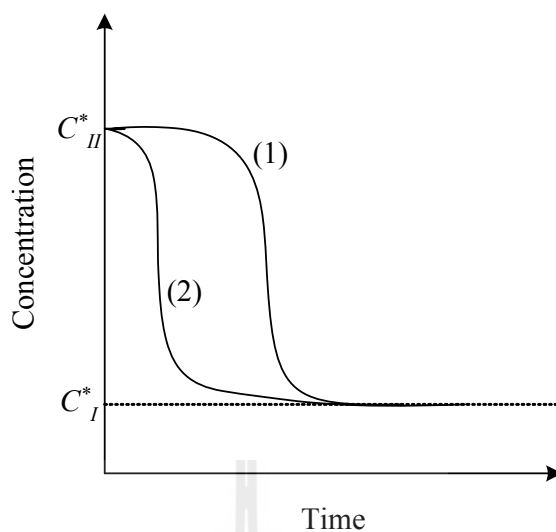


**Figure 5.2** Concentration as a function of time during SMT: curve (1) growth-controlled transformation, curve (2) dissolution-controlled transformation. (Adapted from Mangin et al., 2009)

## 5.4 Experimental Methods

### 5.4.1 Materials

DL-met (>99%, Acros Organics), NaOH (>97%, Carlo Erba), Na<sub>2</sub>CO<sub>3</sub> (>99.5%, Carlo Erba), HCl (37%, Carlo Erba) and deionized water were used without further purification. DL-met and deionized water were used to prepare the supersaturated solutions in all SMT experiments. Sodium methioninate (Na-Met) was also required for acidic precipitations of DL-met to prepare  $\alpha$ -DL-met. Aqueous solutions of Na-Met were prepared by the method previously described in Chapter II.

### 5.4.2 Apparatus

A 0.5 L batch crystallizer with a sealed glass lid to reduce solvent evaporation (Figure 2.9 in Chapter II) was used to study the SMT. The slurry is continuously agitated at the set speed by a centrally located four-blade impeller driven

by an overhead stirrer. The crystallizer was placed inside a constant temperature water bath, where the temperature was controlled within  $\pm 0.5^\circ\text{C}$ .

250 mL and 500 mL glass beakers were used as batch crystallizers to prepare  $\alpha$ -DL-met and sodium methioninate (Na-Met) aqueous solutions, respectively. The temperature control and the agitation systems were the same as for the 0.5 L batch crystallizer.

#### **5.4.3 Preparation of Polymorph**

$\alpha$ -DL-met was prepared using reaction crystallization of Na-Met aqueous solutions with HCl as described in Chapter II. The obtained pure  $\alpha$ -DL-met with the size range of 64 - 250  $\mu\text{m}$  was used as seed.

#### **5.4.4 Analysis of the Polymorphic Fraction**

X-ray powder diffractometry (XRPD) (Bruker axs, D5005) was used for the measurement of the polymorphic content during crystallization (or polymorphic transformation experiments). XRPD have been used to quantify the polymorphic crystalline material off-line in the literature (Takahashi, Takenishi, and Nagashima, 1962; Kitamura 1993; Garti and Zour, 1997; Maruyama et al., 1999; Kitamura and Sugimoto, 2003). This method is based on a calibration curve using prepared polymorphic mixtures as dry powder. Takahashi et al. (1962) showed that an exponential calibration line was obtained from the direct method (a binary mixture of the two polymorphs), while a linear calibration line was obtained from the internal standard method (mixtures of the two polymorphs with a known amount of the internal standard). This indicates that the internal standard method is more efficient and more accurate than the direct method. A suitable internal standard should have satisfactory purity, sharp diffraction lines, and a suitable line free from interference

and superposition (Takahashi et al., 1962). In this work the internal standard is NaCl.

The XRPD patterns of NaCl,  $\alpha$ -DL-met, and  $\gamma$ -DL-met are shown in Figure 5.3.

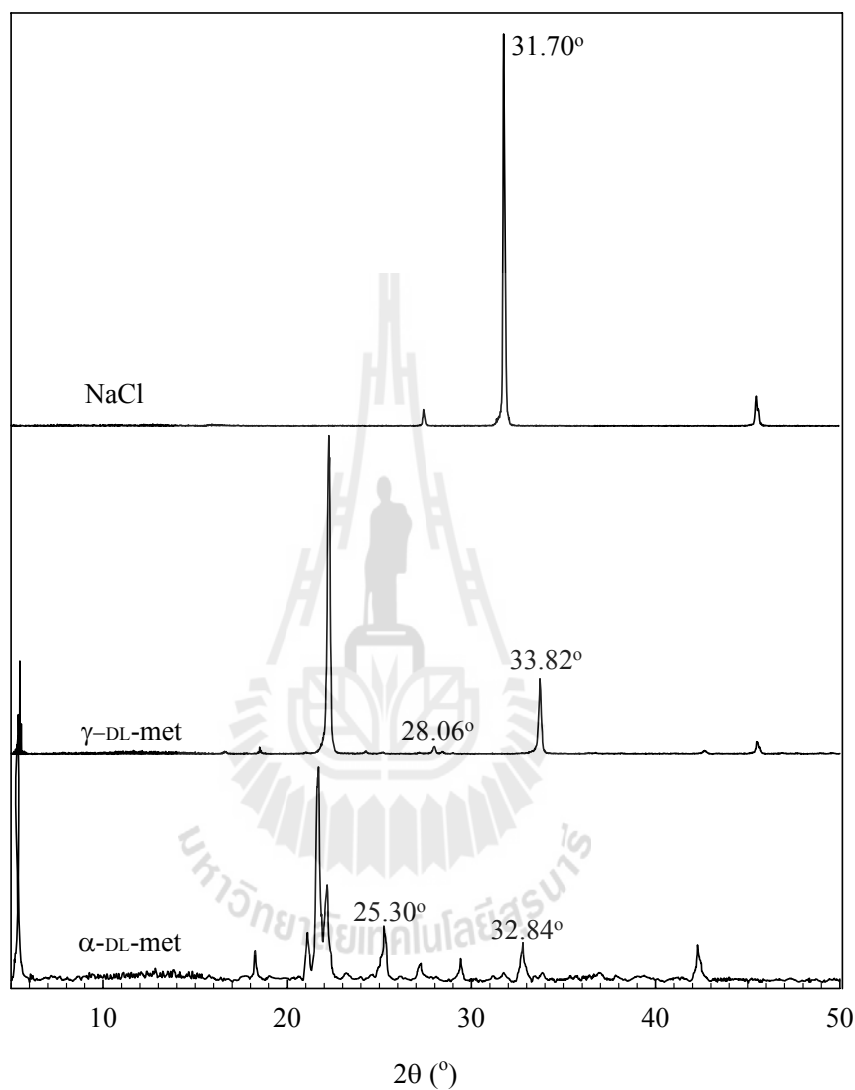


**Figure 5.3** XRPD patterns for  $\alpha$ -DL-met,  $\gamma$ -DL-met, and NaCl.

From Figure 5.3, the characteristic peaks are at  $2\theta = 31.7^\circ$  for NaCl,  $2\theta = 25.3^\circ$  and  $32.84^\circ$  for  $\alpha$ -DL-met, and  $2\theta = 28.06^\circ$  and  $33.82^\circ$  for  $\gamma$ -DL-met. The following equations were used for construction the calibration lines.

Based on peak intensities:

$$Y_I = \frac{\left[ \frac{I_{\gamma,33.82^\circ} + I_{\gamma,28.06^\circ}}{I_{N,31.7^\circ}} + \left( 1 - \frac{I_{\alpha,32.84^\circ}}{I_{N,31.7^\circ}} \right) + \left( 1 - \frac{I_{\alpha,25.3^\circ}}{I_{N,31.7^\circ}} \right) \right]}{4} \quad (5.1)$$

Based on area of the peaks:

$$Y_A = \frac{\left[ \frac{A_{\gamma,33.82^\circ} + A_{\gamma,28.06^\circ}}{A_{N,31.7^\circ}} + \left( 1 - \frac{A_{\alpha,32.84^\circ}}{A_{N,31.7^\circ}} \right) + \left( 1 - \frac{A_{\alpha,25.3^\circ}}{A_{N,31.7^\circ}} \right) \right]}{4} \quad (5.2)$$

where  $I$  is the characteristic peak intensity,  $A$  is the area under curve of the characteristic peak, and  $Y$  is the calculation factor. The calibration curves were thus obtained from plotting  $Y$  against the concentration of  $\gamma$ -DL-met in standard samples. The standard samples were prepared as mixtures of the two polymorphs and NaCl, in various mass fractions with a constant mass of NaCl. These fractions are shown in Table 5.1. The mixing was done in a mortar by hand, with grinding for more than 10 min. The mixing should be done softly to avoid the transformation of the metastable  $\alpha$ -DL-met to the stable  $\gamma$ -DL-met due to the heat effect from grinding.

**Table 5.1** Compositions of the synthetic mixtures for the multi-component system.

Note that the weight percent of  $\gamma$ -DL-met is based on the binary mixture of  $\alpha$ -DL-met and  $\gamma$ -DL-met.

Replicate no.	Weight and weight percent of sample			
	$\alpha$ -DL-met (g)	$\gamma$ -DL-met (g)	NaCl (g)	$\gamma$ -DL-met (wt.%)
1	0.0000	1.0003	0.5000	100
	0.0999	0.9004	0.5000	90
	0.2003	0.8004	0.5001	80
	0.3503	0.6501	0.5004	65
	0.5000	0.5000	0.4999	50
	0.6502	0.3499	0.5002	35
	0.8002	0.2001	0.5000	20
	0.8999	0.0998	0.5003	10
	1.0000	0.0000	0.5000	0
2	0.0000	1.0002	0.5002	100
	0.1000	0.8997	0.5001	90
	0.2001	0.8001	0.4999	80
	0.3503	0.6502	0.5006	65
	0.5001	0.5000	0.5000	50
	0.6502	0.3503	0.5000	35
	0.8000	0.2004	0.4999	20
	0.9000	0.1000	0.5003	10
	1.0004	0.0000	0.5005	0

**Table 5.1** (continued)

Replicate no.	Weight and weight percent of sample			
	$\alpha$ -DL-met (g)	$\gamma$ -DL-met (g)	NaCl (g)	$\gamma$ -DL-met (wt.%)
3	0.0000	0.9999	0.5004	100
	0.0999	0.9000	0.5003	90
	0.2001	0.8004	0.5000	80
	0.3501	0.6500	0.5003	65
	0.5003	0.5000	0.5002	50
	0.6501	0.3500	0.5000	35
	0.8001	0.2000	0.5000	20
	0.9002	0.1004	0.5001	10
	0.9999	0.0000	0.5001	0

#### 5.4.5 Polymorphic Transformation Experiments

The polymorphic transformation experiments were studied by seeded batch crystallization. There are two distinct experiments (as shown in Table 5.2): (1) seed crystals were added to a supersaturated solution where the supersaturation level is above the secondary nucleation threshold (SNT) for  $\gamma$ -DL-met, and (2) seed crystals were added to a supersaturated solution where the supersaturation level is in the SNT for  $\gamma$ -DL-met. All experiments were performed at 25 °C in a 0.5 L batch crystallizer agitated by a centrally located four-blade impeller driven by an overhead stirrer at 350 rpm. The solute concentration in the clear liquor was measured periodically using dry substance determination (Garside, Mersmann, and Nyvlt,

2002). In addition, the solid fraction in wt.% was measured periodically using the calibration curve which is given in Section 5.4.4.

**Table 5.2** Experimental conditions of the polymorphic transformation experiments where the seed is  $\alpha$ -DL-met. SNT indicates the SNT for  $\gamma$ -DL-met.

Exp. no.	Amount of seed (g)	$C_0$ (g DL-met/ kg water)	$S_{\alpha,0}$	$S_{\gamma,0}$	Level of $C_0$
1	1	40.50	1.14	1.20	above SNT
2	1	40.50	1.14	1.20	above SNT
3	1	40.50	1.14	1.20	above SNT
4	1	40.50	1.14	1.20	above SNT
5	2	37.00	1.04	1.10	in SNT
6	2	37.00	1.04	1.10	in SNT
7	2	37.00	1.04	1.10	in SNT

At the beginning of all experiments, the supersaturated solutions were prepared by dissolving DL-met in deionized water at 55 °C (at least 20 °C above saturation temperature) for 30 to 40 min to ensure that no ghost nuclei remained in the solution. After complete dissolution of the solid material the solutions were then cooled to the experimental temperature, which was then held constant throughout the process, and a quantity of dry seeds was fed to the crystallizer. A small volume of the suspension was sampled at particular times during the batch to determine the solid fraction and the solute concentration.

The experimental conditions are shown in Table 5.2, where  $C_0$  is the initial concentration, and  $S_{\alpha,0}$  and  $S_{\gamma,0}$  are the initial supersaturations with respect to  $\alpha$ -DL-met and  $\gamma$ -DL-met, respectively.

#### 5.4.6 Characterization of Uncertainty

Wherever uncertainty is indicated in this chapter the uncertainty is represented by 90% confidence interval (see Appendix A).

### 5.5 Results and Discussions

#### 5.5.1 Analysis of the Polymorphic Fraction

The obtained XRPD patterns for the reference mixture samples (for replicate number 1) are shown in Figure 5.4. This shows that the characteristic peaks of each polymorph and NaCl do not overlap (in the case of pure  $\alpha$ -DL-met or  $\gamma$ -DL-met). The characteristic peaks of  $\alpha$ -DL-met and  $\gamma$ -DL-met overlapped for the mixture samples. It is observed that as the fraction of  $\gamma$ -DL-met changes the height and area of the characteristic peaks change correspondingly. Therefore, quantitative analysis can be done by a calibration line which was constructed from the overlapped peak intensities, or areas under the characteristic peaks of each polymorph, as described in Section 5.4.4. This illustrates how the characteristic peaks of each polymorph change with the polymorphic fraction. These indicate that XRPD can be used to analyze the quantitative of the solid composition of polymorphic forms during the transformation process well.

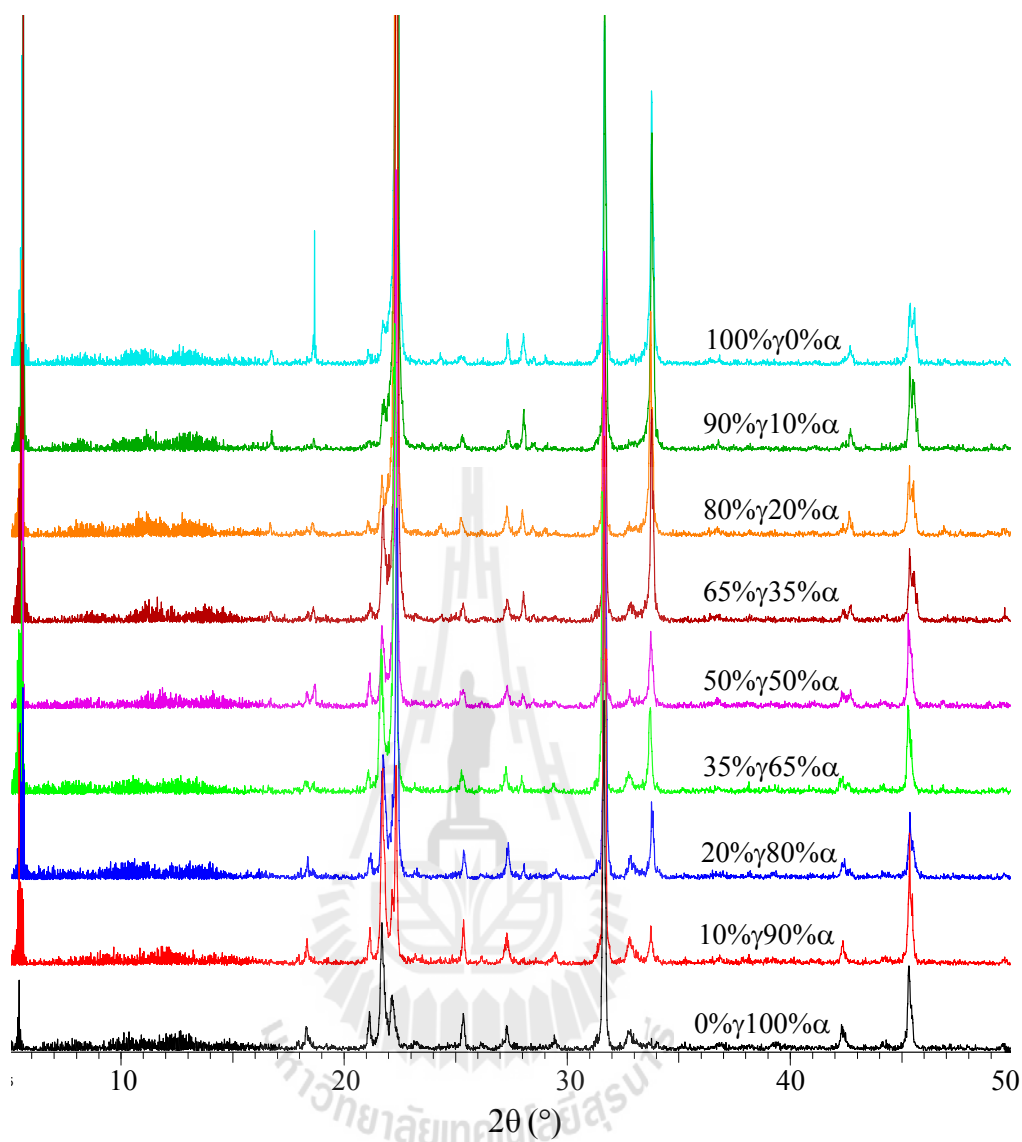


**Figure 5.4** XRPD patterns (5 - 50° 2 $\theta$ ) of various compositions of  $\alpha$ -DL-met,  $\gamma$ -DL-met, and NaCl.

The plots of the calculated factor  $Y$  against the fraction of  $\gamma$ -DL-met in the standard samples are shown in Figures 5.5 (for  $Y_I$ ) and 5.6 (for  $Y_A$ ). The linear relationships are

$$Y_I = 0.2992w + 0.4521 \quad (5.3)$$

$$Y_A = 0.3322w + 0.4405 \quad (5.4)$$

where  $w$  is the mass fraction of  $\gamma$ -DL-met (wt.%) and the mass fraction of  $\alpha$ -DL-met is  $1 - w$ . The calibration line (Figures 5.5 and 5.6) exhibits good linearity over the entire concentration range studied. The rmsd values for the fitting equation of  $Y_I$  and  $Y_A$  are 0.0098 and 0.0109, and R-squared values are 0.9944 and 0.9945, respectively. These two figures suggest that the calibration line applied in this work for the quantification of the polymorphic mixture of DL-met via XRPD is practical. These two equations were used to determine the polymorphic fractions of  $\gamma$ -DL-met obtained during the polymorphic transformation experiments. The fraction  $w$  is the average value that is obtained from equations (5.3) and (5.4).

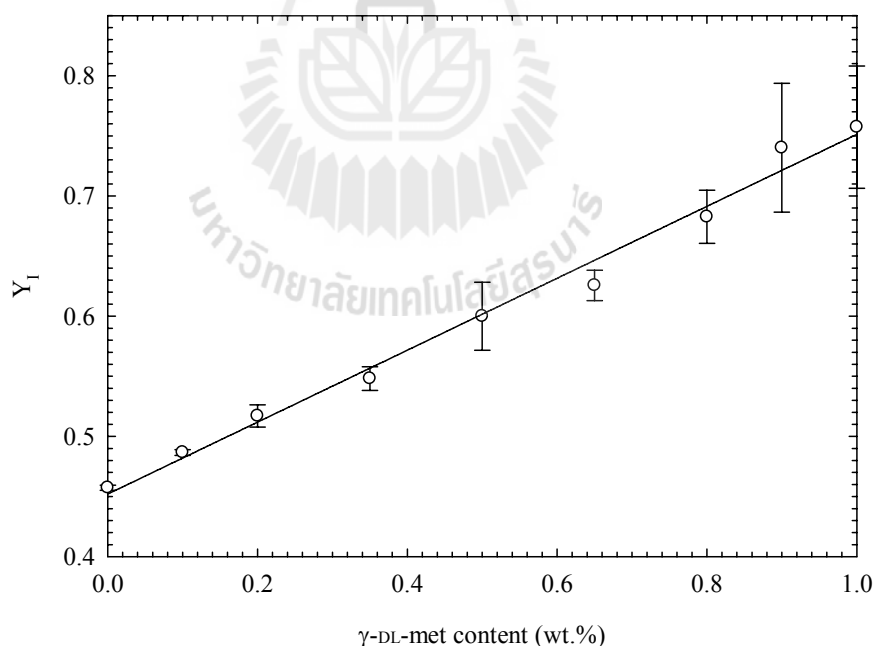


**Figure 5.5** The calibration curve for analysis of the fraction of  $\gamma$ -DL-met based on the peak intensities. XRPD measurements (circle) and the fit (solid line).

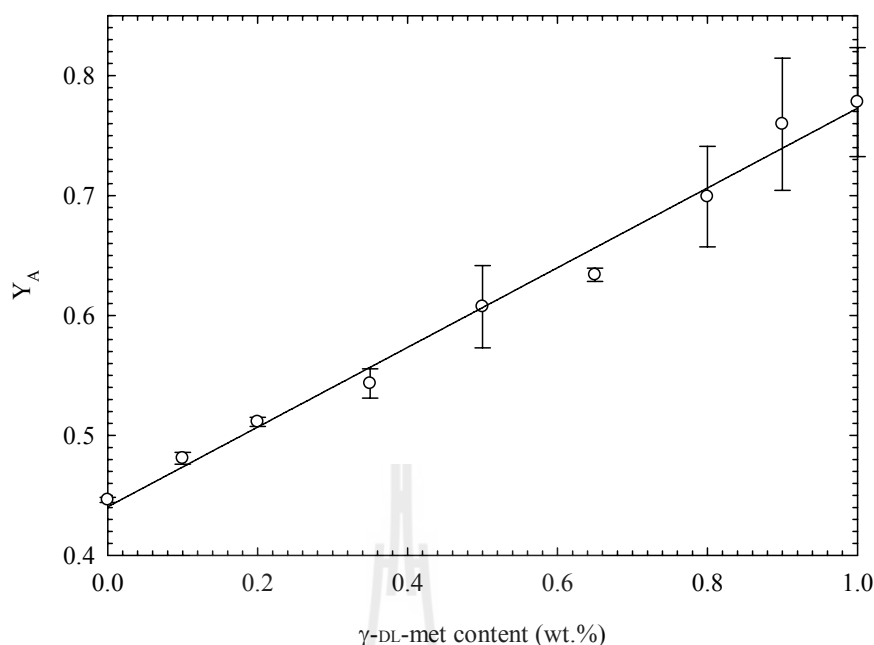


**Figure 5.6** The calibration curve for analysis of the fraction of  $\gamma$ -DL-met based on the area of the peaks. XRPD measurements (circle) and the fit (solid line).

### 5.5.2 Polymorphic Transformation

Figure 5.7 shows the typical change in the XRPD patterns of the product crystals relative to the crystallization time from the seeded batch crystallization at 25 °C and  $C_0 = 40.5$  g DL-met/kg water (for which the initial supersaturation level is above the SNT for  $\gamma$ -DL-met). It was found that the characteristic peak heights of each polymorph (e.g. peaks at 32.84° for  $\alpha$ -DL-met and 33.82° for  $\gamma$ -DL-met) gradually changed with crystallization time because of the spontaneous generation of  $\gamma$ -DL-met and the transformation of polymorphs during crystallization process. The characteristic peaks for  $\gamma$ -DL-met increase with crystallization time, while the characteristic peaks for  $\alpha$ -DL-met decrease with crystallization time. This indicates that there is a transformation of  $\alpha$ -DL-met into  $\gamma$ -DL-met during the crystallization process. Therefore, according to the SMT

mechanism of the polymorphs (Mangin et al., 2009; Jiang et al., 2010b), the stable  $\gamma$ -DL-met is nucleated, and then simultaneously the metastable  $\alpha$ -DL-met is dissolved and the stable  $\gamma$ -DL-met is grown. Figure 5.7 also shows that the characteristic peaks of  $\gamma$ -DL-met appear clearly at 1 h. This leads to the conclusion that  $\gamma$ -DL-met is nucleated at or close to 1 h. This indicates that there is an induction time for nucleation of  $\gamma$ -DL-met. Only  $\gamma$ -DL-met was nucleated because only  $\gamma$ -DL-met was found to nucleate during the crystallization of DL-met from aqueous solution (Matsuoka, Yamanobe, Tezuka, Takiyama, and Ishii, 1999). The resulting peaks indicate the amount of  $\alpha$ -DL-met and  $\gamma$ -DL-met in the solid (which can be calculated from equations (5.3) and (5.4)) present as a function of crystallization time, as shown in Figure 5.8.

The SMT is a complex process because there are several mechanisms, including the dissolution of the metastable polymorph and the nucleation and growth of the stable polymorph, which are both involved in the transformation. The comparison of the solute concentration profile and the solid phase composition measured using XRPD allows for the identification of the mechanisms during the transformation. The measured solute concentration and the solid phase composition ( $\gamma$ -DL-met fraction) obtained from the seeded batch crystallization at 25 °C and  $C_0 = 40.5$  g DL-met/kg water (where the initial supersaturation level is above the SNT for  $\gamma$ -DL-met) are shown in Figure 5.8. A magnification of the rapid decrease in the solute concentration in the range of 0 - 60 min is shown in Figure 5.9.

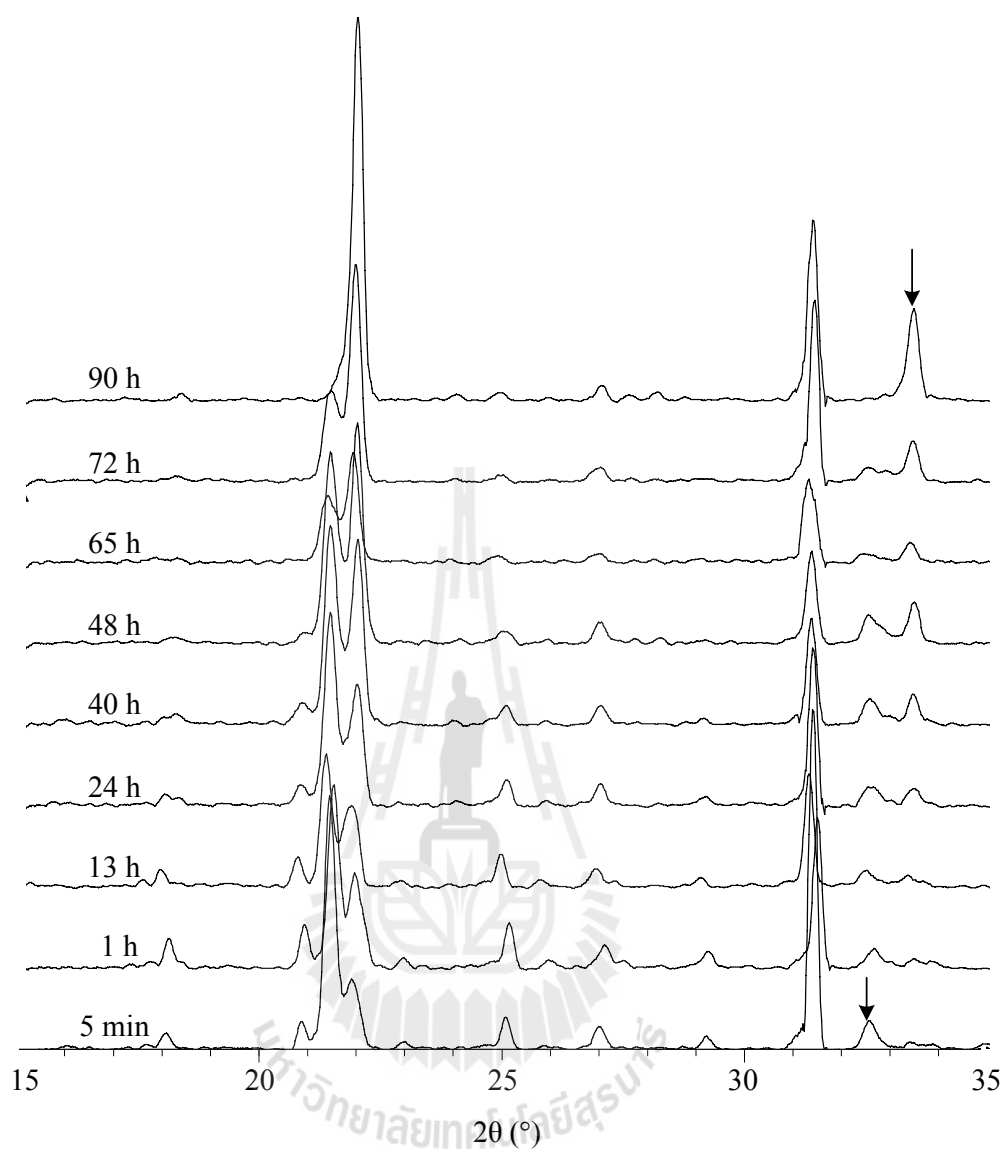


**Figure 5.7** XRPD patterns of the solid mixture taken at various times during the polymorphic transformation of  $\alpha$ -DL-met into  $\gamma$ -DL-met at 25 °C and  $C_0 = 40.5$  g DL-met/kg water.

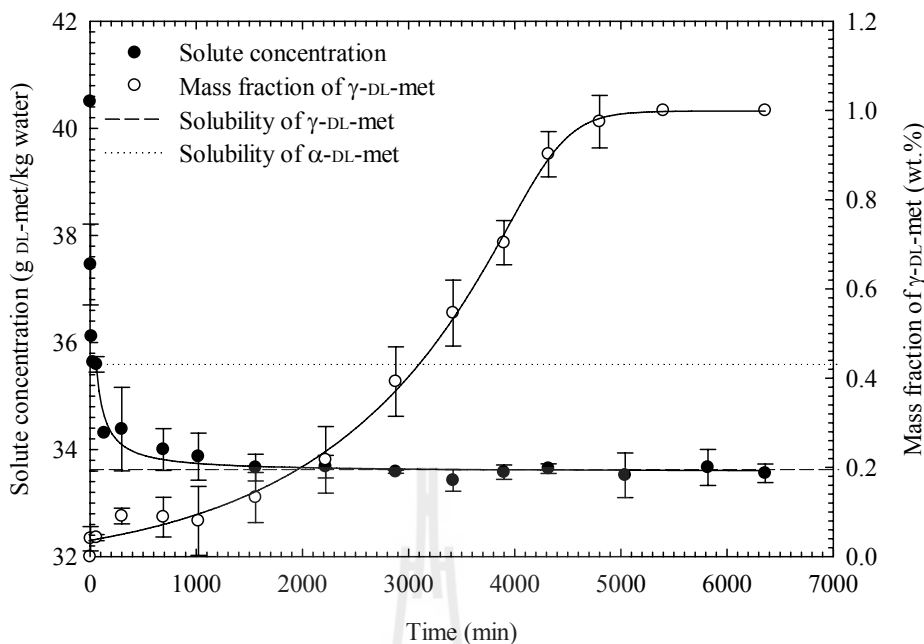


**Figure 5.8** Solute concentration and fraction of  $\gamma$ -DL-met in the crystal phase during the polymorphic transformation of  $\alpha$ -DL-met into  $\gamma$ -DL-met at 25 °C and  $C_0 = 40.5$  g DL-met/kg water. The solid lines are given to guide the eye.

Figure 5.8 clearly illustrates the transformation process where  $\alpha$ -DL-met seeds have been added to the supersaturated solution. Initially, the solute concentration is supersaturated with respect to both polymorphs, and  $\alpha$ -DL-met crystals were seeded. The growth of  $\alpha$ -DL-met initially occurs since crystals of this polymorph are already present in the solution. This leads to a drop in the solute concentration, to the solubility of  $\alpha$ -DL-met, within 30 min (Figure 5.9). At this point, the solution is saturated with respect to  $\alpha$ -DL-met, while still being supersaturated with respect to  $\gamma$ -DL-met. The solute concentration is maintained at, or close to, the solubility of  $\alpha$ -DL-met during a short period (30 min).

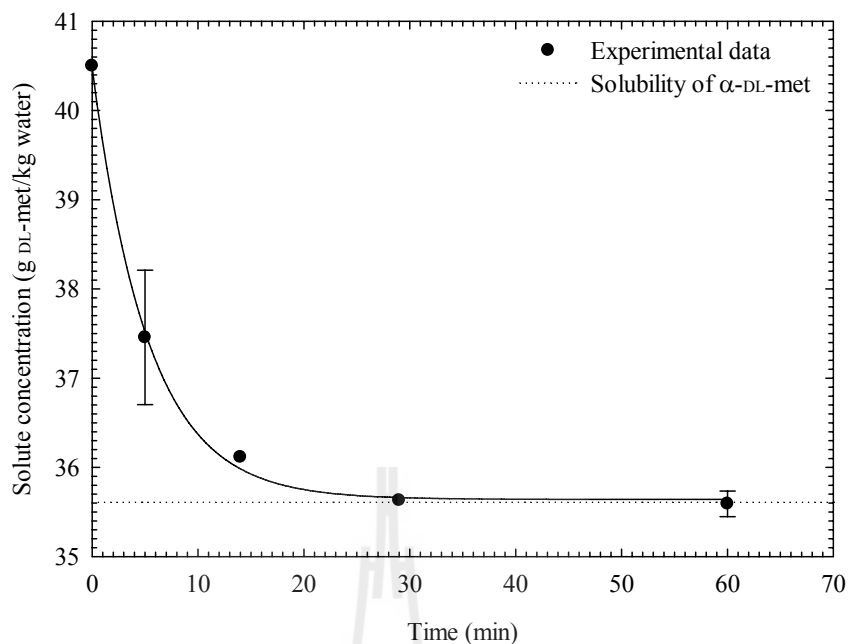


**Figure 5.9** The magnification of the solute concentration in Figure 5.8 in the range of 0 - 60 min. The solid line is given to guide the eye.

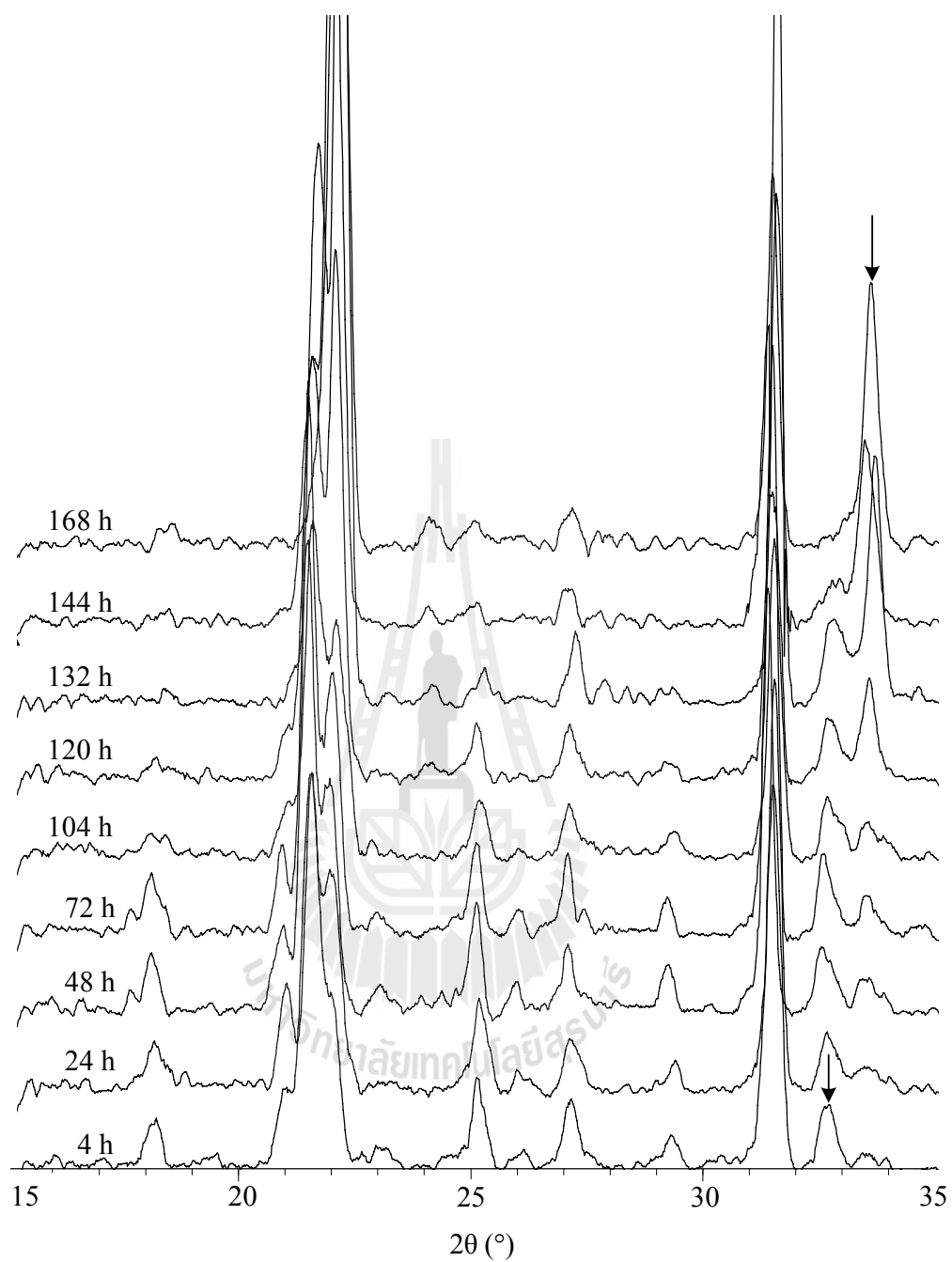
Since the solution is still supersaturated with respect to  $\gamma$ -DL-met,  $\gamma$ -DL-met crystals start nucleating and growing, and  $\alpha$ -DL-met start dissolving as the solute concentration drops lower than the solubility of  $\alpha$ -DL-met ( $S_\alpha < 1$ ). This is the start of the SMT of  $\alpha$ -DL-met into  $\gamma$ -DL-met, which consists of the nucleation and crystal growth of the stable  $\gamma$ -DL-met and the dissolution of the metastable  $\alpha$ -DL-met. This also indicates that the induction time for nucleation of  $\gamma$ -DL-met is approximately 30 min. As shown in Figure 5.8, the amount of  $\gamma$ -DL-met begins to increase at this point. The increase in solute concentration due to dissolution of  $\alpha$ -DL-met is balanced by the decrease in the solute concentration due to the growth of  $\gamma$ -DL-met crystals at this point. The dissolution of  $\alpha$ -DL-met crystals is rapid enough to maintain the solute concentration for only a short period of time (30 min). After that the solute concentration drops rapidly to the solubility of  $\gamma$ -DL-met within the crystallization time

of 1,400 - 2,000 min, while the transformation still occurs continually (the fraction of  $\gamma$ -DL-met still increases). After 2,000 min the transformation still occurs until the fraction of  $\gamma$ -DL-met reaches 1 (complete transformation) at approximately 5,400 min. The solute concentration is maintained at or close to the solubility of  $\gamma$ -DL-met. This means that from 60 min until 5,400 min the dissolution of  $\alpha$ -DL-met crystals is not rapid enough to maintain the solute concentration at or close to the solubility of  $\alpha$ -DL-met. This can demonstrate that the dissolution rate of  $\alpha$ -DL-met is slower than the crystallization rate of  $\gamma$ -DL-met. The transformation process in this period depends on the simultaneous growth of  $\gamma$ -DL-met and the dissolution of  $\alpha$ -DL-met. The supersaturated solution is created by the slower dissolution of  $\alpha$ -DL-met, but the solute concentration drop is more rapid due to the faster growth of  $\gamma$ -DL-met. These two processes are occurred simultaneously until the  $\alpha$ -DL-met crystals are completely dissolved, which means that the transformation is complete. The transformation time in this case is approximately 5,400 min.

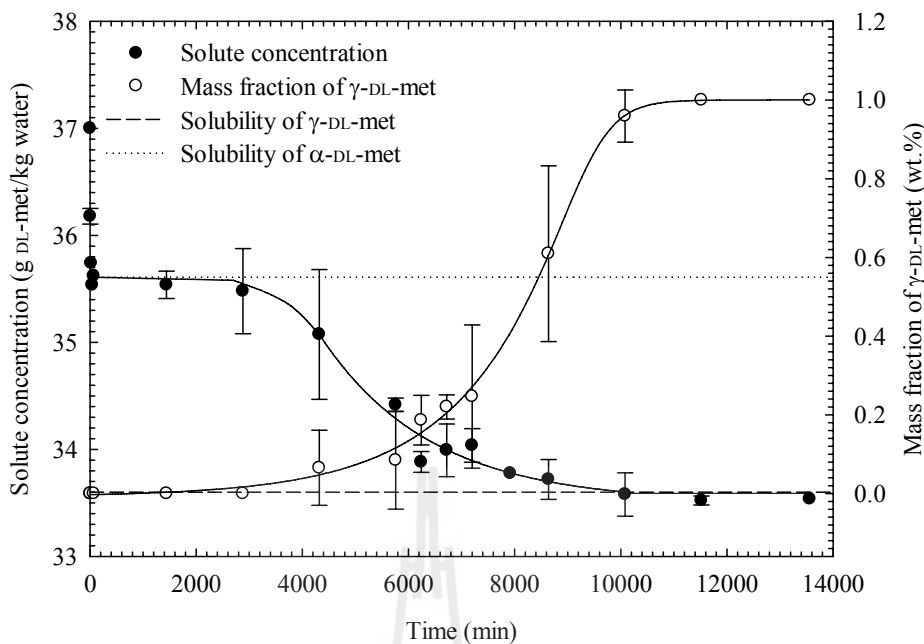
The results in the case where  $\alpha$ -DL-met crystals were seeded to a supersaturated solution where the supersaturation level is within the SNT for  $\gamma$ -DL-met are shown Figures 5.10-12. Figure 5.10 shows the typical change in the XRPD patterns for this case. There is noise (or a lot of the small peaks) in the XRPD patterns. A possible explanation is a reduction in the performance of the XRPD in Suranaree University of Technology. After the changes to the machine the XRPD works, and patterns of sample are the same as previous measurements, but there is some noise in the spectra and all peak intensities are reduced. However, the ratios of the peak or peak areas are still the same. This indicates that the quantification of the polymorphic fraction still works.

Figure 5.10 shows that the change in the XRPD patterns is similar to the previous case, but the transformation time is longer. It seems that the nucleation of  $\gamma$ -DL-met does not start during the initial period which indicates that the transformation does not occur during this period either. This can be confirmed from the fact that the characteristic peaks of  $\gamma$ -DL-met appear clearly at around 2 - 3 days (48 - 72 h). This indicates that there is an induction time which is required for the nucleation of  $\gamma$ -DL-met. This is reasonable because the seed was added to the supersaturated solution where the supersaturation level is within the SNT of  $\gamma$ -DL-met.

The measured solute concentration and the solid phase composition (fraction of  $\gamma$ -DL-met) obtained from the seeded batch crystallization at 25 °C and  $C_0 = 37.0$  g DL-met/kg water (where the initial supersaturation level is within the SNT for  $\gamma$ -DL-met) are shown in Figure 5.11. The magnification of the rapid decrease of the solute concentration in Figure 5.11, in the range of 0 - 70 min, is shown in Figure 5.12.



**Figure 5.10** XRPD patterns of the solid mixture taken at various times during the polymorphic transformation of  $\alpha$ -DL-met into  $\gamma$ -DL-met at 25 °C and  $C_0 = 37.0$  g DL-met/kg water.



**Figure 5.11** Solute concentration and fraction of  $\gamma$ -DL-met in the crystal phase during the polymorphic transformation of  $\alpha$ -DL-met into  $\gamma$ -DL-met at 25 °C and  $C_0 = 37.0$  g DL-met/kg water. The solid lines are given to guide the eye.

Figure 5.11 clearly illustrates the transformation process where  $\alpha$ -DL-met seeds are added to the supersaturated solution. Since the seed was added to a supersaturated solution within the SNT region, there is an induction time for the nucleation of  $\gamma$ -DL-met. As shown in Figure 5.11, the induction time (the time where the fraction of  $\gamma$ -DL-met starts to increase from zero) is more than 2 days (2,880 min); due to the measurement uncertainty the induction time is around 2 - 3 days.

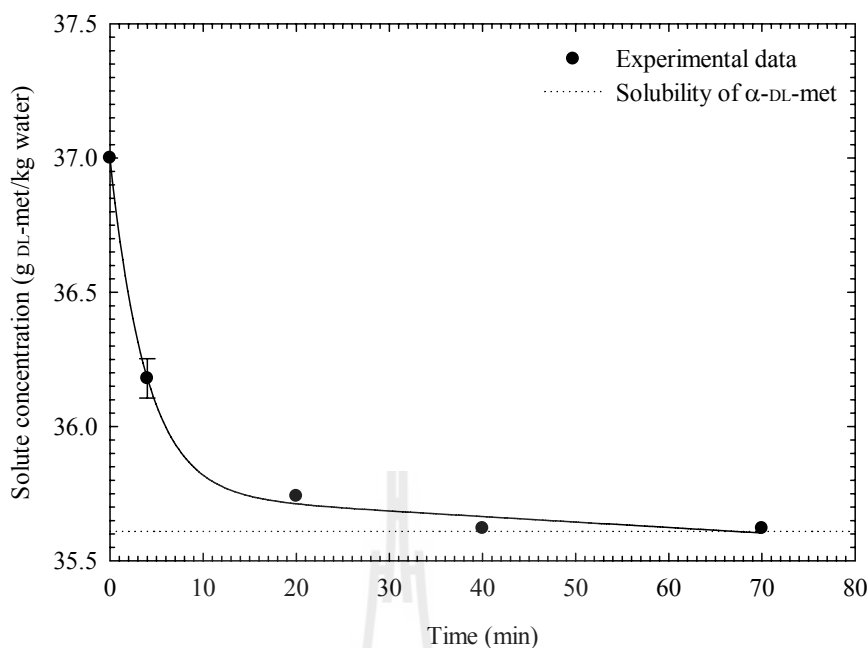


**Figure 5.12** The magnification of the solute concentration in Figure 5.11 in the range of 0 - 70 min. The solid line is given to guide the eye.

As shown in Figure 5.11, initially the solute is supersaturated with respect to both polymorphs, and  $\alpha$ -DL-met crystals were seeded. However the initial supersaturated solution is within the SNT region so that the only growth of  $\alpha$ -DL-met was occurred initially. This leads to the solute concentration dropping to the solubility of  $\alpha$ -DL-met within 40 min (Figure 5.12). At this point, the solution is in equilibrium with respect to  $\alpha$ -DL-met, and the solution will remain at this equilibrium until the crystallization time reaches the induction time for the nucleation of  $\gamma$ -DL-met (around 2 - 3 days). When the system reaches this induction time,  $\gamma$ -DL-met crystals start nucleating (the fraction of  $\gamma$ -DL-met starts to increase from zero) and growing, which causes  $\alpha$ -DL-met to start dissolving when the supersaturation ratio of  $\alpha$ -DL-met becomes  $S_\alpha < 1$ . This is the start of the SMT of  $\alpha$ -DL-met into  $\gamma$ -DL-met, where the behavior of the SMT is similar to the previous case. The solute concentration is

balanced by the decrease in the solute concentration due to the growth of  $\gamma$ -DL-met crystals and the increase the solute concentration due to the dissolution of  $\alpha$ -DL-met crystals. In this case, after the start of the transformation, the solute concentration drops slowly to the solubility of  $\gamma$ -DL-met (not remaining constant at the solubility of  $\alpha$ -DL-met), while the fraction of  $\gamma$ -DL-met increases slowly until it reaches 1 (complete transformation). This can be explained in a similar way to the previous case. Namely, the dissolution rate of  $\alpha$ -DL-met is slower than the growth rate of  $\gamma$ -DL-met. Therefore, the transformation process depends on the simultaneous growth of  $\gamma$ -DL-met and the dissolution of  $\alpha$ -DL-met. These two processes simultaneously occur until  $\alpha$ -DL-met crystals are completely dissolved, which means that the transformation is complete. In this case, the transformation is complete at approximately 8 days (11,520 min). The transformation time is around 5 - 6 days, which is the time between the induction time and the complete transformation time. The transformation time is longer than the previous case due to a slower crystallization of  $\gamma$ -DL-met.

### 5.5.3 Discussion

The transformation experiments showed the SMT of  $\alpha$ -DL-met into  $\gamma$ -DL-met at 25 °C is a dissolution controlled process, where the mass transfer of solute to the growing phase rapidly depletes the solute concentration to the value consistent with the minimum level of supersaturation required to maintain the growth of the stable polymorph (Dharmayat et al., 2008). This is since the solute concentration drops immediately to the solubility of the stable polymorph as shown in Figures 5.8 and 5.11. In the literature there are a lot of studies showing that the growth of the stable polymorph was the limiting step, for example L-glutamic acid (Garti and Zour, 1997; Ono, Kramer et al., 2004; Schöll et al., 2006; Dharmayat et al., 2008),

L-histidine (Kitamura, 1993), taltireline (Maruyama et al., 1999), and carbamazepine (Qu et al., 2006). The SMT of glycine is at least one example where the dissolution of the metastable polymorph was the limiting step (Ferrari et al., 2003).

The conclusion here indicates that the assumption behind the dissolution measurement in Chapter IV is not true. Namely, in Chapter IV the dissolution rates were measured based on  $\gamma$ -DL-met seed crystals and then assuming the same dissolution rate for both  $\alpha$ -DL-met and  $\gamma$ -DL-met due to the dissolution being considered as a single step (a diffusion controlled process). This result showed that the dissolution rate of  $\alpha$ -DL-met was faster than the growth rate of  $\gamma$ -DL-met. But the results of the SMT experiments in this chapter showed that the dissolution rate of  $\alpha$ -DL-met is slower than the growth rate of  $\gamma$ -DL-met. Therefore, in reality the dissolution rate of  $\alpha$ -DL-met is slower than  $\gamma$ -DL-met based on the result of this chapter. This leads to the conclusion that the dissolution process of the polymorphs of DL-met is a two step process. These are the surface reaction and the detachment of the species followed by transfer of these species toward the bulk solution across the diffusion layer which surrounds the crystals (Kramer and van Rosmalen, 2009). The value of the dissolution rate constant of  $\alpha$ -DL-met at 25 °C was estimated from the simulation of the SMT process as shown in Chapter VI.

## 5.6 Conclusions

The kinetics of the SMT of  $\alpha$ -DL-met into  $\gamma$ -DL-met in water at 25 °C via seeded batch crystallization process was studied by the change of the solute concentration and  $\gamma$ -DL-met fraction with time during the crystallization process. The solute concentration profile was measured by off-line sampling using the dry

substance method. Off-line quantitative measurement of the fraction of  $\gamma$ -DL-met in suspension was accomplished with XRPD by setting up a calibration curve using the mixtures of  $\alpha$ -DL-met,  $\gamma$ -DL-met, and NaCl. NaCl was the internal standard sample and the composition was fixed to a constant value. A linear calibration line was obtained. The SMT is a two step process, consisting of the dissolution process of  $\alpha$ -DL-met and the crystallization process (nucleation and growth) of  $\gamma$ -DL-met. The dissolution of  $\alpha$ -DL-met is the rate controlling step during the transformation since the solute concentration drops immediately to the solubility of the stable  $\gamma$ -DL-met at the start of the transformation. The transformation time for the case where the seed was added to the supersaturated solution in the SNT region is longer than the case in which the seed was added to the supersaturated solution above the SNT region. There is the induction time for the nucleation of  $\gamma$ -DL-met for the first case, but for the second case  $\gamma$ -DL-met is nucleates quickly (there is little or no induction time).

## 5.7 References

- Bernstein, J., Davey, R.J., and Henck, J.O. (1999). Concomitant polymorphs. **Angew. Chem. Int. Ed.** 38(23): 3440-3461.
- Davis, T.D., Morris, K.R., Huang, H., Peck, G.E., Stowell, J.G., Eisenhauer, B.J., Hilden, J.L., Gibson, D., and Byrn, S.R. (2003). *In situ* monitoring of wet granulation using online X-ray powder diffraction. **Pharm. Res.** 20(11): 1851-1857.

- Dharmayat, S., Hammond, R.B., Lai, X., Ma, C., Purba, E., Roberts, K.J., Chen, Z-P., Martin, E., Morris, J., and Bytheway, R. (2008). An examination of the kinetics of the solution-mediated polymorphic phase transformation between  $\alpha$ - and  $\beta$ -forms of L-glutamic acid as determined using online powder X-ray diffraction. **Cryst. Growth Des.** 8(7): 2205-2216.
- Ferrari, E.S., Davey, R.J., Cross, W.I., Gillon, A.L., and Towler, C.S. (2003). Crystallization in polymorphic systems: The solution-mediated transformation of  $\beta$  to  $\alpha$  glycine. **Cryst. Growth Des.** 3(1): 53-60.
- Garside, J., Mersmann, A., and Nyvlt, J. (2002). **Measurement of crystal growth and nucleation rates** (2<sup>nd</sup> ed.). UK: Institute of Chemical Engineering.
- Garti, N., and Zour, H. (1997). The effect of surfactants on the crystallization and polymorphic transformation of glutamic acid. **J. Cryst. Growth** 172(3-4): 486-498.
- Hammond, R.B., Lai, X., Roberts, K.J., Thomas, A., and White, G. (2004). Application of in-process X-ray powder diffraction for the identification of polymorphic forms during batch crystallization reactions. **Cryst. Growth Des.** 4(5): 943-948.
- Jiang, S., Jansens, P.J., and ter Horst, J.H. (2010a). Mechanism and kinetics of the polymorphic transformation of o-aminobenzoic acid. **Cryst. Growth Des.** 10(5): 2123-2128.
- Jiang, S., Jansens, P.J., and ter Horst, J.H. (2010b). Control over polymorph formation of o-aminobenzoic acid. **Cryst. Growth Des.** 10(6): 2541-2547.

- Jiang, S., ter Horst, J.H., and Jansens, P.J. (2008). Concomitant polymorphism of o-aminobenzoic acid in antisolvent crystallization. **Cryst. Growth Des.** 8(1): 37-43.
- Kitamura, M. (1993). Crystallization behavior and transformation kinetics of L-histidine polymorphs. **J. Chem. Eng. Jpn.** 26(3): 303-307.
- Kitamura, M., and Sugimoto, M. (2003). Anti-solvent crystallization and transformation of thiazole-derivative polymorphs-I: effect of addition rate and initial concentrations. **J. Cryst. Growth** 257(1-2): 177-184.
- Kramer, H.J.M., and van Rosmalen, G.M. (2009). Crystallization. In: I.A., Wilson and C.F., Poole (ed.). **Handbook of methods and instrumentation in separation science volume 2** (pp 1-20). London: Academic Press.
- Lu, J., Wang, X-J., Yang, X., and Ching, C-B. (2007). Polymorphism and crystallization of famotidine. **Cryst. Growth Des.** 7(9): 1590-1598.
- Mangin, D., Puel, F., and Veessler, S. (2009). Polymorphism in processes of crystallization in solution: A practical review. **Org. Process Res. Dev.** 13(6): 1241-1253.
- Maruyama, S., Ooshima, H., and Kato, J. (1999). Crystal structures and solvent-mediated transformation of taltireline polymorphs. **Chem. Eng. J.** 75(3): 193-200.
- Matsuoka, M., Yamanobe, M., Tezuka, N., Takiyama, H., and Ishii, H. (1999). Polymorphism, morphologies and bulk densities of DL-methionine agglomerate crystals. **J. Cryst. Growth** 198-199: 1299-1306.

- O'Brien, L.E., Timmins, P., Williams, A.C., and York, P. (2004). Use of in situ FT-Raman spectroscopy to study the kinetics of the transformation of carbamazepine polymorphs. **J. Pharm. Biomed. Anal.** 36 (2): 335-340.
- Ono, T., Kramer, H.J.M., ter Horst, J.H., and Jansens, P.J. (2004). Process modeling of the polymorphic transformation of L-glutamic acid. **Cryst. Growth Des.** 4(6): 1161-1167.
- Ono, T., ter Horst, J.H., and Jansens, P.J. (2004). Quantitative measurement of the polymorphic transformation of L-glutamic acid using in-situ Raman spectroscopy. **Cryst. Growth Des.** 4 (3): 465-469.
- Qu, H., Louhi-Kultanen, M., Rantanen, J., and Kallas, J. (2006). Solvent-mediated phase transformation kinetics of an anhydrate/hydrate system. **Cryst. Growth Des.** 6(9): 2053-2060.
- Roelands, C.P.M. (2005). **Polymorphism in precipitation process**. Ph.D. thesis, Delft University of Technology, The Netherlands.
- Roelands, C.P.M., Jiang, S., Kitamura, M., ter Horst, J.H., Kramer, H.J.M., and Jansens, P.J. (2006). Antisolvent crystallization of the polymorphs of L-histidine as a function of supersaturation ratio and of solvent composition. **Cryst. Growth Des.** 6(4): 955-963.
- Schöll, J., Bonalumi, D., Vicum, L., and Mazzotti, M. (2006). In situ monitoring and modeling of the solvent-mediated polymorphic transformation of L-glutamic acid. **Cryst. Growth Des.** 6(4): 881-891.
- Takahashi, H., Takenishi, T., and Nagashima, N. (1962). Quantitative analysis of mixtures of L-glutamic acid polymorphs by X-ray diffraction. **Bull. Chem. Soc. Jpn.** 35 (6): 923-926.

Threlfall, T. (2003). Structural and thermodynamic explanations of Ostwald's rule.

**Org. Process Res. Dev.** 7(6): 1017-1027.

Vippagunta, S.R., Brittain, H.G., and Grant, D.J.W. (2001). Crystalline solids.

**Adv. Drug Del. Rev.** 48(1): 3-26.



# CHAPTER VI

## POLYMORPHIC TRANSFORMATION OF DL-METHIONINE IN AQUEOUS SOLUTION: MODELING

### 6.1 Abstract

Models of the crystallization and the solution-mediated transformation (SMT) of the metastable  $\alpha$ -DL-met into the stable  $\gamma$ -DL-met in water at 25 °C were developed using the concept of the population balance equation (PBE). The growth, dissolution, and nucleation kinetic expressions obtained in Chapters III and IV were used in the models. It was found that the PBE models did not satisfactorily describe the SMT process of DL-met when the measured crystallization and dissolution kinetics were used; there were large mismatches between the simulation and experimental results. Improving the model of the dissolution kinetics of  $\alpha$ -DL-met (which in fact appear different to those of the  $\gamma$ -form) enabled these mismatches to be lowered, and this was done by re-estimating only a single dissolution kinetic parameter  $K_{D\alpha}$ . The result showed that the dissolution rate constant of  $\alpha$ -DL-met is smaller than the growth rate constant of  $\gamma$ -DL-met. Based on this result and the profiles of the solute concentration, the SMT is a dissolution controlled process in this system. The result confirms that the dissolution rates of  $\alpha$ -DL-met and  $\gamma$ -DL-met are not the same, and therefore that the dissolution mechanism of the polymorphs of DL-met is a two step process.

## 6.2 Introduction

The transformation of the polymorph can be carried out only from the less stable polymorph to the more stable one. During solids processing, in particular during suspension crystallization processes, the presence of a liquid phase often promotes the occurrence of the phase transformation. This is usually called solution-mediated transformation (SMT) (Mangin, Puel, and Veessler, 2009). The basic phenomena involved in SMT consists of the nucleation and crystal growth of the stable polymorph and the dissolution of the metastable polymorph (Jiang, Jansens, and ter Horst, 2010; Dharmayat et al., 2008). There are two mechanisms that could control the transformation rate: either the dissolution of the metastable polymorph or the growth rate of the stable polymorph (Mangin, et al., 2009; Roelands, 2005). The growth of the stable polymorph is limiting if during the transformation the solute concentration remains at the solubility level of the metastable polymorph. On the other hand, if the solute concentration drops immediately to the solubility level of the stable polymorph the dissolution rate of the metastable polymorph is limiting.

The easy way to study the SMT mechanism is crystallization with seeding, which is commonly found in industrial crystallization. The SMT process can be also studied via unseeded crystallization in which the metastable polymorph forms first, which is followed by transformation to the more stable polymorph (Ostwald's rule). Therefore, crystallization processes involving polymorphs consist of the competitive nucleation and crystal growth of the polymorphs, and the transformation from the metastable to the stable polymorph. To study the mechanisms of SMT and identify which mechanism is the limiting step the polymorphic composition of the slurry has

to be followed in time, in combination with the concentration of the solute in the solution.

To control the formation of a desired polymorphic form, the crystallization kinetics and the kinetics of the SMT process should be known, as well as the effect of the processing conditions on the kinetics (Morris, Griesser, Eckhardt, and Stowell, 2001). The experimental study of the polymorph crystallization and the SMT process to find the optimal operating conditions is expensive and time consuming. Adequate process simulations will shorten the required time. Moreover, process simulations will help to understand the mechanisms of the polymorph crystallization and the SMT, and give valuable information on the process parameters which are difficult to determine experimentally. Therefore, in this work both the experiment and process simulation were studied. The experimental study of the SMT of  $\alpha$ -DL-met into  $\gamma$ -DL-met is described in Chapter V. The validation of the experimental and simulation methods is evaluated in this chapter.

The population balance equation (PBE) model is an appropriate method to simulate the crystallization and SMT processes. It can be used for a wide range of objectives, for example to describe the behavior of the crystallization and SMT of the polymorphs, to estimate the unknown parameters characterizing the phenomena involved, and to determine the mechanisms which govern the transformation. The PBE model can be used for this purpose in at least two ways, either where the kinetic rate expression of each mechanism is estimated from a combination of the PBE model and the results from SMT experiments, or by separately distinguishing each mechanism experimentally and then combining them within the PBE model. After the validation of the PBE model with the SMT experiment, this allows for a deeper

understanding of the SMT process and, for faster and more robust process development of the polymorphic systems (Schöll, Bonalumi, Vicum, and Mazzotti, 2006).

There are numbers of publications that employed the combination of the PBE model and SMT experiments to estimate the kinetic parameters of the SMT process. For example, Ono, Kramer, ter Horst, and Jansens (2004) presented the PBE model for the SMT of *L*-glutamic acid from the  $\alpha$ -polymorph to the  $\beta$ -polymorph. Unseeded batch cooling crystallizations were used to investigate the SMT process. The process was modeled only in the SMT region (after the nucleation of the  $\alpha$ -polymorph). Therefore, only the kinetic parameters representing the SMT process, which consisted of the dissolution of the metastable  $\alpha$ -polymorph and the secondary nucleation and subsequent growth of the stable  $\beta$ -polymorph, were estimated. Primary nucleation of the  $\beta$ -polymorph was neglected because the maximum value of the supersaturation ratio of the  $\beta$ -polymorph was not sufficient for primary nucleation. The simulation was used to obtain the crystal size distribution of the different polymorphs which is difficult or impossible to obtain experimentally.

The SMT of *L*-glutamic acid from the  $\alpha$ -polymorph to  $\beta$ -polymorph was also studied by Schöll, Bonalumi et al. (2006). The whole of the unseeded batch crystallization experiment data (which included the SMT process) were combined with the PBE model. All kinetic parameters, which included the kinetics of the nucleation and growth of both polymorphs, were estimated. The dissolution process of the metastable  $\alpha$ -polymorph was estimated from Sherwood correlation. There are the differences in the estimated kinetic parameters representing the SMT process between this work and the work of Ono et al. (2004). In particularly, in this work the

surface nucleation of the stable  $\beta$ -polymorph on the surface of the metastable  $\alpha$ -polymorph was considered and this is the major impact on the transformation process. Both groups estimated the kinetic parameters by fitting the model without validation that the parameters found represent the real kinetics. Therefore there is no way of knowing which is better.

The same system studied by Schöll, Bonalumi et al. (2006) was simulated by Cornel, Lindenberg, and Mazzotti (2009). In this study, only the secondary nucleation (surface and attrition based nucleation) of the stable  $\beta$ -polymorph was estimated from the simulation. The growth rate of the stable  $\beta$ -polymorph was determined from the independent seeded batch desupersaturation experiments. The growth and nucleation kinetic parameters of the metastable  $\alpha$ -polymorph were collected from experimental results in the literature (Schöll, Lindenberg, Vicum, Brozio, and Mazzotti, 2007; Lindenberg and Mazzotti, 2009). The dissolution process of the metastable  $\alpha$ -polymorph was estimated from Sherwood correlation. This study indicates that surface and attrition based nucleation of the stable  $\beta$ -polymorph governs the transformation. The growth and nucleation rates that were presented in this study show some discrepancy with the studies of Schöll, Bonalumi et al. (2006) and Ono et al. (2004). The work of Schöll, Bonalumi et al. (2006) can be used to analyze and understand the details of the transformation process behavior better than the other two works. This is since the different kinetics (except the nucleation kinetics) were measured independently, and the range of the operating conditions are wider than the other two works, for example the effect of stirring and seed mass.

The combination of the PBE model and the SMT experiment were also applied to study systems in which there are more than two polymorphs. For example,

the SMT of three polymorphs of D-mannitol was investigated and simulated by Cornel, Kidambi, and Mazzotti (2010). All kinetic parameters, which included the kinetics of the nucleation, growth, and dissolution of  $\alpha$ - and  $\beta$ -polymorphs, and the nucleation and growth of  $\gamma$ -polymorph, were estimated from the simulation. This study showed that the experimental results obtained and their simulation allowed prediction of the behavior of the SMT process.

There is at least one publication that applied the kinetic expressions of each mechanism to the PBE model. For example, Févotte, Alexandre, and Nida (2007) applied the growth and nucleation kinetic expressions of the stable anhydrous citric acid (aCA) and the dissolution kinetic expression of the metastable monohydrate citric acid (mCA), which were obtained independently from experiments (Caillet, Sheibat-Othman, and Févotte, 2007) to the PBE model of the SMT of aCA to mCA and then compared this with the SMT experimental results. The results showed mismatches between the simulations and experiments, and the mismatches increased with decreasing seed amounts. The modification of the nucleation kinetic of the stable mCA to be the secondary nucleation (based on aCA interparticles impacts or birth of mCA particles on aCA surface) reduced the mismatches between the simulations and experiments.

As described above, applying the kinetic parameters of all the relevant crystallization and dissolution processes to PBE models of the SMT process has not yet been proven to agree with experiments performed to measure the SMT. The main drawback of this technique is that the results can be skewed by incorrect parameter estimation of other parameters such as the crystal growth rate kinetics, which may lead to non-realistic estimates of nucleation rates. Due to the disadvantage of this

technique, in this work the crystallization (nucleation and growth) and dissolution kinetics of each polymorph were experimentally determined in Chapter III and IV and then were applied to PBE model of SMT in this chapter in order to estimate the time of the transformation, polymorphic fraction profile, concentration profile, etc., which were compared with the results from SMT experiment in Chapter V.

## 6.3 Theory

### 6.3.1 Population Balance

The population balance equation (PBE) is a widely used tool in engineering, including crystallization, comminution, precipitation, polymerization, aerosol and emulsion processes, among others (Kumar, 2006). The PBE is an equation of continuity for discrete entities having a particular characteristic or characteristics. In crystallization, the population consists of the particles or crystals within the crystallization unit (or a particular subsection of the unit) and the characteristic of most significance is the particle size based on a particular linear dimension.

In practice, crystallizations are carried out in one or more regions that can each be considered to be well mixed. In this case the PBE may be averaged over the spatial region of interest. The full form of the PBE for well-mixed system is given by (Randolph and Larson, 1988; Flood, 2009)

$$\frac{\partial n}{\partial t} + n \frac{\partial(\log V)}{\partial t} + \frac{\partial(Gn)}{\partial L} = \sum \frac{Q_{in,i} n_{in,i}}{V} - \sum \frac{Q_{out,i} n_{out,i}}{V} + B - D \quad (6.1)$$

The number density distribution ( $\#/m^3 \cdot m$ ) is defined as

$$n = \frac{dN}{dL} \quad (6.2)$$

where  $N$  is the cumulative number distribution ( $\#/m^3$ ) as a function of particle size,  $L$  (m),  $G$  is the crystal growth rate (m/s),  $B$  is the birth term ( $\#/m^3 \cdot m \cdot s$ ),  $D$  is the death term ( $\#/m^3 \cdot m \cdot s$ ),  $Q_{in,i}$  is the flow rate of the inlet stream  $i$  ( $m^3/s$ ),  $Q_{out,i}$  is the flow rate of the outlet stream  $i$  ( $m^3/s$ ),  $V$  is the crystallizer volume ( $m^3$ ), and  $t$  is the time (s). Note that the parameters are no longer functions of the spatial variables because the system is assumed to be uniform across the entire (well-mixed) spatial region.

For a batch crystallizer with size independent crystal growth, there are no inlet or outlet streams, and it can be assumed that there are no birth or death terms in the system and no volume change on crystallization. The full form of the PBE becomes

$$\frac{\partial n}{\partial t} + G \frac{\partial n}{\partial L} = 0 \quad (6.3)$$

The first term in equation (6.3) describes the change in the number density over time and the second term accounts for the difference in number of crystals entering and leaving a size class  $\partial L$  due to crystal growth.

For crystallizations of the polymorphic compounds the PBE has to be applied for each of the polymorphs so that the equation (6.3) becomes

$$\frac{\partial n_i}{\partial t} + G_i \frac{\partial n_i}{\partial L} = 0 \quad (6.4)$$

where  $i$  denotes the  $i^{\text{th}}$  polymorph.

### 6.3.2 Mass Balance

The growth of crystals reduces the supersaturation of the solution. This is due to the addition of dissolved solute to the surface of the crystals. The rate of this consumption depends on the solution supersaturation (which determines growth and nucleation kinetics), the total particle count, and the size distribution. Therefore, a mass balance for the crystallization system is written for the phase change. That is, the rate at which solute is lost from the solution phase must be equal to the rate at which mass is transferred to the solid phase. The solute mass balance is given by

$$C(t) = C_0 + C_{s,0} - C_{s,t} \quad (6.5)$$

where  $C_0$  is the initial solute concentration ( $\text{kg/m}^3$ ),  $C_{s,0}$  is the seed crystal concentration ( $\text{kg/m}^3$ ), and  $C_{s,t}$  is the mass concentration of the crystal at time  $t$  ( $\text{kg/m}^3$ ), i.e. a suspension density. The change of the solute concentration at time  $t$  ( $\text{kg/m}^3$ ), which is a function of the solution supersaturation (due to the crystal growth), the total particle count, and the size distribution is given by (Wey and Karpinski, 2002; Scully, 2010)

$$\frac{dC}{dt} = -3\rho k_v G \int_0^{\infty} nL^2 dL \quad (6.6)$$

where  $\rho$  is the crystal density ( $\text{kg/m}^3$ ) and  $k_v$  is the volume shape factor.

For the crystallization of the polymorphic compound the mass balance (equations (6.5) and (6.6)) become

$$C(t) = C_0 + \sum_i C_{i,s,0} - \sum_i C_{i,s,t} \quad (6.7)$$

$$\frac{dC}{dt} = -3 \sum_i \rho_i k_{v,i} G_i \int_0^{\infty} n_i L^2 dL \quad (6.8)$$

There is only one solute concentration for the liquid phase since both polymorphs crystallize from the same molecule.

### 6.3.3 Method of Moments

Based on the fact that the equations describing the system typically involve partial differential equation in the PBE, an integral equation that represents the mass of crystal as a function of the crystal population density, and an algebraic equation for the calculation of the growth rate from the concentration of the solute (which is dependent on the mass of crystal), it is typically impossible to find analytical solutions for most realistic cases.

Randolph and Larson (1988) proposed the method of moments to reduce the dimensionality of the system by taking different averages of the number density with respect to  $L$ , for example by finding the moments about the origin for the distribution. This results in the partial differential equation representing the PBE to be converted to a series of ordinary differential equations, which simplifies the solution greatly. This method can be applied to the PBE for the completely mixed system (equation (6.1)), which is first order in time ( $t$ ) and first order in length ( $L$ ), which reduces to a series of ordinary differential equations in time only.

It should be noted that some information about the system will be lost if the moment form of the PBE is solved. After the moment form of the PBE is solved, then the key engineering properties of the system can be determined (for example the total number of crystals, the average crystal size, the total surface area of crystal, and the total volume and mass of crystals) however there is not

sufficient information to fully describe the number density distribution at each point in time. However, this is not a significant drawback because in the engineering sense the engineering properties of the system alone are sufficient to make design and operational decisions (Flood, 2009).

The definition of the  $j^{\text{th}}$  moment of the function  $f(L)$  about the origin for a distribution is given by (Randolph and Larson, 1988)

$$\mu_j = \int_{-\infty}^{\infty} L^j f(L) dL \quad (6.9)$$

In the case of the well-mixed system, the number density distribution which is a function of time and particle size (i.e.  $n(t, L)$ ), determines the moment forms. Taking the moments of the distribution will present different averaging over the length variable,  $L$ , thus producing a series of moments  $\mu_j(t, L)$  [ $j = 0, 1, 2, \dots, \infty$ ].

$$\mu_j(t, L) = \int_0^{\infty} L^j n(L) dL \quad (6.10)$$

Note that the lower limit on the integral may only take a non-negative value because the independent variable in the integral is the particle size.

The transformation of the PBE (equation (6.1)) into the moment form can be done by multiplying each term in equation (6.1) by  $L^j$  and then integrating over the entire range of the distribution, zero to infinity. Finally, the full form of the PBE in the moment form of the well-mixed system, when the growth is size independent, is given by (Randolph and Larson, 1988; Flood, 2009)

$$\frac{\partial \mu_j}{\partial t} + \mu_j \frac{\partial(\log V)}{\partial t} - 0^j J - jG\mu_{j-1} = \sum \frac{Q_{in,i} \mu_{j,(in,i)}}{V} - \sum \frac{Q_{out,i} \mu_{j,(out,i)}}{V} + \bar{B}_j - \bar{D}_j \quad (6.11)$$

where  $\mu_j$  is the  $j^{\text{th}}$  moment around the origin ( $\# \cdot \text{m}^j / \text{m}^3$ ), and  $J$  is the nucleation rate ( $\# / \text{m}^3 \cdot \text{s}$ ).

For a batch crystallizer with size independent crystal growth, assuming no birth and death terms considered in the system, and no volume change on crystallization. The balances are

$$\frac{d\mu_j}{dt} = 0^j J + jG\mu_{j-1} \quad (6.12)$$

The equations for the first four moments can be simplified to the following equations.

$$\frac{d\mu_0}{dt} = J \quad (6.13)$$

$$\frac{d\mu_1}{dt} = G\mu_0 \quad (6.14)$$

$$\frac{d\mu_2}{dt} = 2G\mu_1 \quad (6.15)$$

$$\frac{d\mu_3}{dt} = 3G\mu_2 \quad (6.16)$$

Solving the above four equations gives knowledge of the zeroth, first, second, and third moments, which represents knowledge of the total number of crystals, the

average crystal size, the total surface area of crystal, and the total volume and mass of crystals respectively. The number mean particle size can be calculated by

$$\bar{L} = \frac{\mu_1}{\mu_0} \quad (6.17)$$

and the solid concentration is calculated by

$$C_s = \rho k_v \mu_3 \quad (6.18)$$

For the crystallization of polymorphic compounds the moment form of the PBE equation (6.12)) becomes

$$\frac{d\mu_{i,j}}{dt} = 0^j J_i + j G_i \mu_{i,j-1} \quad (6.19)$$

#### 6.3.4 Numerical Solution of the Ordinary Differential Equations

In this work Euler's method (or the first-order method) (Chapra and Canale, 2006) was used to solve all the time derivatives of the moment equations.

This method is devoted to solving ordinary differential equations of the form

$$\frac{dy}{dx} = f(x, y) \quad (6.20)$$

This differential equation is used to estimate the slope in the form of first derivative at  $x_i$ . This means that the slope at the beginning of the interval is taken as an approximation of the average slope over the whole interval (Figure 6.1). The slope at  $x_i$  is estimated from the first derivative (Figure 6.1) as in equation (6.21).

$$\text{slope at } x_i = \left. \frac{dy}{dx} \right|_{(y_i, x_i)} = \frac{y_{i+1} - y_i}{x_{i+1} - x_i} = \frac{y_{i+1} - y_i}{h} \quad (6.21)$$

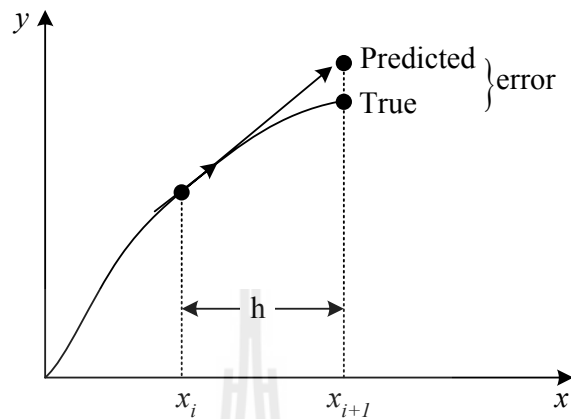


**Figure 6.1** Euler's method.

After the comparison of equations (6.20) and (6.21), the following relationship is obtained.

$$y_{i+1} = y_i + f(x_i, y_i)h \quad (6.22)$$

where  $h$  is the step size. This equation means that a new value of  $y$  can be predicted using the slope  $(f(x_i, y_i))$  to extrapolate linearly over the step size. This indicates that the solution of  $y$  can be calculated initially using the initial value of  $y_i$  at  $x_i$  and then the new value  $y_{i+1}$  is calculated from the step size  $h$ . From Figure 6.1, the accuracy of this method depends on the step size; if the step size is a very small value then the solution should be very accurate.

## 6.4 Modeling Methods

### 6.4.1 Mathematical Development

#### Model assumptions

1. In this work the studies of the SMT of  $\alpha$ -DL-met into  $\gamma$ -DL-met in aqueous solutions were simulated using seeded batch crystallizations at 25 °C (the batch system is shown in Figure 6.2). The system is considered to be a well-mixed system, the growth is size independent growth, and it can also be assumed that there is no volume change due to crystallization, and no agglomeration or breakage (birth and death terms) in the crystallizer.

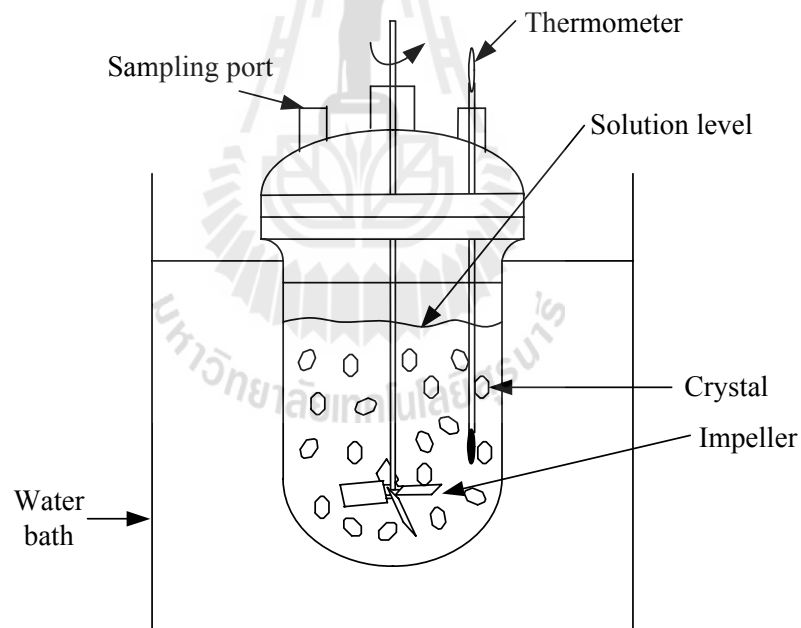


**Figure 6.2** Seeded batch crystallization system.

2. The seed crystals of  $\alpha$ -DL-met were considered to be mono-sized particles. This means that all particles of seed have the same size, and the total number of particles (or  $\mu_0$ ) is constant until the particles have completely dissolved.

3. Both the nucleation and growth of  $\gamma$ -DL-met were applied in the mathematical models. However, only the growth and dissolution of  $\alpha$ -DL-met were considered in the mathematical models. The nucleation of  $\alpha$ -DL-met was not considered because only  $\gamma$ -DL-met was seen to crystallize from clear aqueous solutions (Matsuoka, Yamanobe, Tezuka, Takiyama, and Ishii, 1999), suggesting that the nucleation threshold must be large for  $\alpha$ -DL-met.

4. The aqueous solutions were considered to be dilute solutions because very low amounts of the solute dissolved in water; for example the initial solute concentrations (40.5 or 37.0 g DL-met/kg water) used and the solubility of  $\alpha$ -DL-met (35.63 g DL-met/kg water) and  $\gamma$ -DL-met (33.6 g DL-met/kg water), was less than 5 %. Therefore, the density of the solution was assumed to be the density of water.

5. The solute and solid concentration profiles as shown in Figure 5.8 or 5.11 in Chapter V are the key properties which were used to describe the behavior of the SMT of  $\alpha$ -DL-met into  $\gamma$ -DL-met in aqueous solutions. Therefore, the solute concentration in equation (6.7) and the solid concentration in equation (6.18) together with the differential equations of the first four moments are sufficient for modeling the SMT of this system.

### Mathematical models

The following are the mathematical models for describing the behavior of the crystallization and SMT of  $\alpha$ -DL-met into  $\gamma$ -DL-met in aqueous solutions at 25 °C with seeding of  $\alpha$ -DL-met crystals.

For  $\alpha$ -DL-met, the time derivative of the 0<sup>th</sup> moment can be calculated as

$$\frac{d\mu_{\alpha,0}}{dt} = 0 \quad \text{for all } t \text{ where } \mu_{\alpha,1} > 0 \quad (6.23)$$

$$\mu_{\alpha,0} = 0 \quad \text{for all other } t \quad (6.24)$$

The first of these equations is equal to zero because the mono-sized seed of  $\alpha$ -DL-met crystals leads to the total number of particles (or  $\mu_{\alpha,0}$ ) being constant until the particles have completely dissolved ( $\mu_{\alpha,0} = 0$  when  $\mu_{\alpha,1} = 0$  or  $\bar{L}_\alpha = 0$ ) and the fact that there is no nucleation of  $\alpha$ -DL-met.

The time derivative of the 1<sup>st</sup> moment of  $\alpha$ -DL-met can be calculated as

$$\frac{d\mu_{\alpha,1}}{dt} = \begin{cases} -D_\alpha \mu_{\alpha,0}, & \text{if } S_\alpha < 1 \\ G_\alpha \mu_{\alpha,0}, & \text{if } S_\alpha > 1 \end{cases} \quad (6.25)$$

where  $S$  is the supersaturation ratio and  $D$  is the dissolution rate (m/s). Again based on the mono-sized crystals, the 2<sup>nd</sup> and 3<sup>rd</sup> moments of  $\alpha$ -DL-met can be calculated as

$$\mu_{\alpha,2} = \mu_{\alpha,0} \bar{L}_\alpha^2 \quad (6.26)$$

$$\mu_{\alpha,3} = \mu_{\alpha,0} \bar{L}_\alpha^3 \quad (6.27)$$

The number mean crystal size and the solid concentration of  $\alpha$ -DL-met can be calculated using equations (6.28) and (6.29) respectively.

$$\bar{L}_\alpha = \frac{\mu_{\alpha,1}}{\mu_{\alpha,0}} \quad (6.28)$$

$$C_{\alpha,s} = \rho_\alpha k_{\alpha,v} \mu_{\alpha,3} \quad (6.29)$$

For  $\gamma$ -DL-met, the time derivative of the 0<sup>th</sup> moment can be calculated as

$$\frac{d\mu_{\gamma,0}}{dt} = \begin{cases} 0, & \text{if } S_\gamma \leq 1 \\ J_\gamma, & \text{if } t \geq t_{ind} \text{ and } S_\gamma > 1 \end{cases} \quad (6.30)$$

where  $t_{ind}$  is the induction time for the nucleation of  $\gamma$ -DL-met. The time derivative of the 1<sup>st</sup>, 2<sup>nd</sup>, and 3<sup>rd</sup> moments of  $\gamma$ -DL-met can be calculated using equations (6.31), (6.32), and (6.33) respectively.

$$\frac{d\mu_{\gamma,1}}{dt} = G_\gamma \mu_{\gamma,0} \quad (6.31)$$

$$\frac{d\mu_{\gamma,2}}{dt} = 2G_\gamma \mu_{\gamma,1} \quad (6.32)$$

$$\frac{d\mu_{\gamma,3}}{dt} = 3G_\gamma \mu_{\gamma,2} \quad (6.33)$$

The number mean crystal size and the solid concentration of  $\gamma$ -DL-met and the solute concentration can be calculated using equations (6.34), (6.35), and (6.36) respectively.

$$\bar{L}_\gamma = \frac{\mu_{\gamma,1}}{\mu_{\gamma,0}} \quad (6.34)$$

$$C_{\gamma,s} = \rho_\gamma k_{\gamma,v} \mu_{\gamma,3} \quad (6.35)$$

$$C(t) = C_0 + C_{\alpha,s,0} - C_{\alpha,s} - C_{\gamma,s} \quad (6.36)$$

The mass fraction of  $\gamma$ -DL-met ( $w_\gamma$ ) is calculated as

$$w_\gamma = \frac{C_{\gamma,s}}{C_{\alpha,s} + C_{\gamma,s}} \quad (6.37)$$

When the initial solid concentration of  $\gamma$ -DL-met,  $C_{\gamma,s,0}$ , is equal to zero (no seed of  $\gamma$ -DL-met).

#### 6.4.2 Crystallization and Dissolution Kinetics

This section considers the equations that describe the crystallization and polymorphic transformation of DL-met within the mathematical model developed in the above section. This includes the growth, nucleation, and dissolution kinetics.

The kinetic expressions of the nucleation of  $\gamma$ -DL-met is collected from Chapter III, the growth of  $\gamma$ -DL-met and the growth and dissolution of  $\alpha$ -DL-met are collected from Chapter IV. The units of all parameters in those chapters are converted to the units which are shown in this chapter. The expressions of these kinetics are shown below.

$$J_\gamma = \begin{cases} 0, & \text{if } S_\gamma \leq 1 \\ AS_\gamma \exp\left(\frac{-B}{\ln^2 S_\gamma}\right), & \text{if } t \geq t_{ind} \text{ and } S_\gamma > 1 \end{cases} \quad (6.38)$$

$$G_\gamma = \begin{cases} 0, & \text{if } S_\gamma \leq 1 \\ K_{G\gamma}(S_\gamma - 1), & \text{if } t \geq t_{ind} \text{ and } S_\gamma > 1 \end{cases} \quad (6.39)$$

$$G_\alpha = \begin{cases} 0, & \text{if } S_\alpha \leq 1 \\ K_{G\alpha}(S_\alpha - 1), & \text{if } S_\alpha > 1 \end{cases} \quad (6.40)$$

$$D_\alpha = \begin{cases} 0, & \text{if } S_\alpha \geq 1 \\ K_{D\alpha}(1 - S_\alpha), & \text{if } S_\alpha < 1 \end{cases} \quad (6.41)$$

where  $J$  is the nucleation rate ( $\#/m^3 \cdot s$ ),  $G$  is the growth rate (m/s), and  $D$  is the dissolution rate (m/s).

**Table 6.1** Crystallization and dissolution kinetic parameters.

Mechanism	Kinetic parameter	Value of kinetic parameter
$\gamma$ -DL-met nucleation	$A$	$3.4700 \times 10^{11} \text{ \#/m}^3 \cdot \text{s}$
	$B$	0.0813 (-)
$\gamma$ -DL-met growth	$K_{G\gamma}$	$3.1450 \times 10^{-7} \text{ m/s}$
$\alpha$ -DL-met growth	$K_{G\alpha}$	$8.0767 \times 10^{-7} \text{ m/s}$
$\alpha$ -DL-met dissolution	$K_{D\alpha}$	$5.8550 \times 10^{-7} \text{ m/s}$

### 6.4.3 Material Properties for the Mathematical Model

The physical properties of the polymorphs used in the models are shown in Table 6.2. As described in the model assumption number 4, the density of the solution was assumed to be the density of water, which at 25 °C is approximately equal to 1,000 kg/m<sup>3</sup>.

**Table 6.2** The physical properties of the polymorphs used in the models.

Physical property	$\alpha$ -DL-met	$\gamma$ -DL-met
Solubility in water at 25 °C, $C^*$ (kg/m <sup>3</sup> )	35.63	33.60
Crystal density, $\rho$ (kg/m <sup>3</sup> )	1,340	1,340
Volume shape factor, $k_v$ (based on spherical average length as the measured crystal size) (-)	0.524	0.524
Area shape factor, $k_a$ (based on spherical average length as the measured crystal size) (-)	3.142	3.142

### 6.4.4 Initial Conditions

The initial conditions for numerical solution of the mathematical models are shown in Table 6.3 and 6.4. Due to the mono-sized seed approximation for  $\alpha$ -DL-met the first four moment were calculated as  $N_{\alpha,0}$ ,  $N_{\alpha,0}\bar{L}_{\alpha,0}$ ,  $N_{\alpha,0}\bar{L}_{\alpha,0}^2$ , and  $N_{\alpha,0}\bar{L}_{\alpha,0}^3$ , respectively for the initial values of  $\mu_{\alpha,0}$ ,  $\mu_{\alpha,1}$ ,  $\mu_{\alpha,2}$ , and  $\mu_{\alpha,3}$ . The larger induction time in Table 6.4 is due to the smaller initial supersaturation in this experiment.

**Table 6.3** Initial conditions for the model at 25 °C with initial solute concentration of 40.5 kg/m<sup>3</sup> and the induction time in the period of 0 - 30 min.

Initial condition	$\alpha$ -DL-met	$\gamma$ -DL-met
Solid concentration, $C_s$ (kg/m <sup>3</sup> )	2.0	0.0
Mean crystal size, $\bar{L}_0$ (m)	$145.623 \times 10^{-6}$	0.0
Zero moment, $\mu_0$ (#/m <sup>3</sup> )	921,404,220	0.0
First moment, $\mu_1$ (#·m/m <sup>3</sup> )	$1.3418 \times 10^5$	0.0
Second moment, $\mu_2$ (#·m <sup>2</sup> /m <sup>3</sup> )	19.5395	0.0
Third moment, $\mu_3$ (#·m <sup>3</sup> /m <sup>3</sup> )	0.0028	0.0

**Table 6.4** Initial conditions for the model at 25 °C with initial solute concentration of 37.0 kg/m<sup>3</sup> and the induction time is in the period of 2 - 3 days.

Initial condition	$\alpha$ -DL-met	$\gamma$ -DL-met
Solid concentration, $C_s$ (kg/m <sup>3</sup> )	4.0	0.0
Mean crystal size, $\bar{L}_0$ (m)	$145.623 \times 10^{-6}$	0.0
Zero moment, $\mu_0$ (#/m <sup>3</sup> )	1,842,808,440	0.0
First moment, $\mu_1$ (#·m/m <sup>3</sup> )	$2.6837 \times 10^5$	0.0
Second moment, $\mu_2$ (#·m <sup>2</sup> /m <sup>3</sup> )	39.0825	0.0
Third moment, $\mu_3$ (#·m <sup>3</sup> /m <sup>3</sup> )	0.0057	0.0

#### 6.4.5 Numerical Solution Procedures

The ordinary differential equations (6.23), (6.25), and (6.30) to (6.33) combined with the algebraic equations (6.24), (6.26) to (6.29) and (6.34) to (6.41) were solved numerically using the initial values of the first four moment (included the

initial mean crystal size), solid concentrations, and solute concentration as shown in Tables 6.3 and 6.4 using MATLAB 7. The ordinary differential equations were solved using Euler's method as described in Section 6.3.4.

The solution procedure is outlined as follows

1. The solution starts by inputting the simulation time (total time), time step, induction time, initial moment data, initial mean crystal sizes, initial solid concentrations, and initial solute concentration.

2. The initial run inputs the rates that are used at time  $t = 0$ . This includes calculating the initial supersaturations, growth rates, nucleation rate, and dissolution rate of the polymorphs. Values of the solubility, crystals densities, and shape factors of the polymorphs and the induction time are also input.

3. For the remaining time steps, the growth, nucleation, and dissolution rates of the polymorphs are calculated. These values are used to work out the change in the moments over time using equations (6.23), (6.25), and (6.30) to (6.33). These equations are solved by Euler's method (equation (6.22)) together with the initial values of each moment.

4. The new values of  $\mu_{\alpha,0}$  and  $\mu_{\alpha,1}$  are then used to calculate  $\bar{L}_{\alpha}$  in equation (6.28), and this size is then used to calculate  $\mu_{\alpha,2}$  in equation (6.26) and  $\mu_{\alpha,3}$  in equation (6.27). The value of  $\mu_{\alpha,3}$  is then used to calculate  $C_{\alpha,s}$  in equation (6.29). The new values of  $\mu_{\gamma,0}$  and  $\mu_{\gamma,1}$  are used to calculate  $\bar{L}_{\gamma}$  in equation (6.34). The new value of  $\mu_{\gamma,3}$  is used to calculate  $C_{\gamma,s}$  in equation (6.35). The values of  $C_{\alpha,s}$  and  $C_{\gamma,s}$  are then used to calculate  $C(t)$  in equation (6.36) and  $w_{\gamma}$  in equation (6.37). The new values of  $\mu_{\alpha,0}$ ,  $\mu_{\alpha,1}$ ,  $\mu_{\gamma,0}$ ,  $\mu_{\gamma,1}$ ,  $\mu_{\gamma,2}$ , and  $\mu_{\gamma,3}$  are also used as the initial values of these moments for the next time step.

The accuracy of Euler's method depends on the time step. Therefore, the optimum time step has to be evaluated. The optimum time step was evaluated by changing the time step until the change in the solution is small or there is no change. The two adjacent time steps that give little or no change in the solution contain the optimum time step, but of these two the time step that has the maximum time step scale should be used to reduce the calculation time. In this work, the solution in terms of the solute concentration during the first 60 min (which changes rapidly) was selected to optimize the time step. The values of the simulated solute concentration obtained from various time steps are shown in Figure 6.3. Considering Figure 6.3, it can be seen that the solute concentration profiles of the time step of 1 to 30 s have only small differences, so that the time step of 30 s is selected to simulate the crystallization and SMT of  $\alpha$ -DL-met into  $\gamma$ -DL-met.

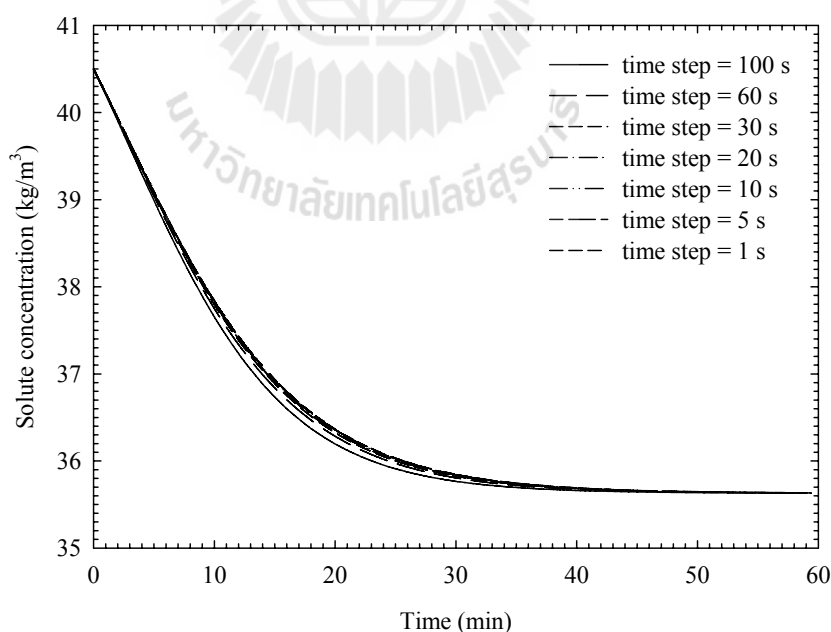


**Figure 6.3** The simulated solute concentration profiles during the first 60 min for the simulation at 25 °C with initial solute concentration of 40.5 kg/m<sup>3</sup>.

#### 6.4.6 Parameter Estimation

As the results from Chapter V, the SMT process is dissolution controlled which indicates that the dissolution rate constant of  $\alpha$ -DL-met should be smaller than the growth rate constant of  $\gamma$ -DL-met. Unfortunately, in Chapter IV the dissolution rates were measured based on  $\gamma$ -DL-met seed crystals and then assuming the same dissolution rate for both  $\alpha$ -DL-met and  $\gamma$ -DL-met due to the dissolution being considered as a single step (diffusion controlled). This result showed that the growth rate constant of  $\gamma$ -DL-met was smaller than the dissolution rate constant of  $\alpha$ -DL-met. This means that the results in Chapter V indicate the assumption in Chapter IV is not true. Therefore, in this chapter the dissolution rate of  $\alpha$ -DL-met was estimated from the combination of the modeling method in this chapter with the SMT experimental data obtained from Chapter V. Considering equation (6.41), only the parameter  $K_{D\alpha}$  has to be estimated. However, the induction times (for both the experiment with  $C_0 = 40.5 \text{ kg/m}^3$  and  $C_0 = 37.0 \text{ kg/m}^3$ ) obtained from Chapter V are not consistent with earlier measurements so that the induction time have to be estimated also. The induction time measurements have very wide scatter, so that the estimated parameters are likely to lie within the scatter of the measured values; however it appears that the mean of the scattered values is not a good estimate for the modeling. These parameters were estimated using a nonlinear optimization algorithm to minimize the sum of square errors between the experimental and the simulated values of the solute concentration  $C$  and the mass fraction of  $\gamma$ -DL-met  $w_\gamma$ . The sum of square errors (SSE) is written as

$$SSE = \sum_{i=1}^{N_e} \sum_{j=1}^{N_{d,i}} (C_{i,j}^{\text{exp}} - C_{i,j}^{\text{sim}})^2 + \sum_{i=1}^{N_e} \sum_{j=1}^{N_{d,i}} (w_{i,j}^{\text{exp}} - w_{i,j}^{\text{sim}})^2 \quad (6.42)$$

where  $N_e$  is the number of experiments, and  $N_{d,i}$  is the number of the data points per experiment.  $C^{exp}$  and  $C^{sim}$  are the experimental and simulated solute concentrations, respectively, and  $w^{exp}$  and  $w^{sim}$  are the experimental and simulated mass fraction of  $\gamma$ -DL-met, respectively. The experimental data given in Figure 5.8 and 5.11 in Chapter V were used for the optimization. The MATLAB nonlinear unconstrained multivariable optimization algorithm *fminsearch* was used to minimize equation (6.42) by varying the parameter  $K_{D\alpha}$  and the induction times.

## 6.5 Results and Discussions

In the first part of the modeling all of the kinetic parameters obtained from Chapter III and IV were applied to the PBE models. The simulated and experimental solute concentrations and fractions of  $\gamma$ -DL-met are shown in Figures 6.4 to 6.7. The estimated induction times for the case of  $C_0 = 40.5$  and  $37.0 \text{ kg/m}^3$  are 15 min and 2.5 days, respectively.

It can be seen that there are very large mismatches between the models and experiments as shown in Figures 6.4 and 6.6, particularly the mismatch is large for the mass fraction of  $\gamma$ -DL-met. The mismatch for the case of  $C_0 = 40.5 \text{ kg/m}^3$  (which is outside the nucleation threshold for  $\gamma$ -DL-met) is larger than the case of  $C_0 = 37.0 \text{ kg/m}^3$ . However, the trends of the solute concentrations and mass fractions of  $\gamma$ -DL-met are similar to the experimental results. This indicates the mathematical model developed in this work can be used to describe the SMT process of DL-met. The simulated transformation times are faster than the experimental times. The simulated transformation time for the case of  $C_0 = 40.5 \text{ kg/m}^3$  is 262.5 min while the experimental transformation time is around 5,400 min. In the case of  $C_0 = 37.0 \text{ kg/m}^3$ ,

the simulated transformation time is 5,827 min while the experimental transformation time is around 11,520 min.

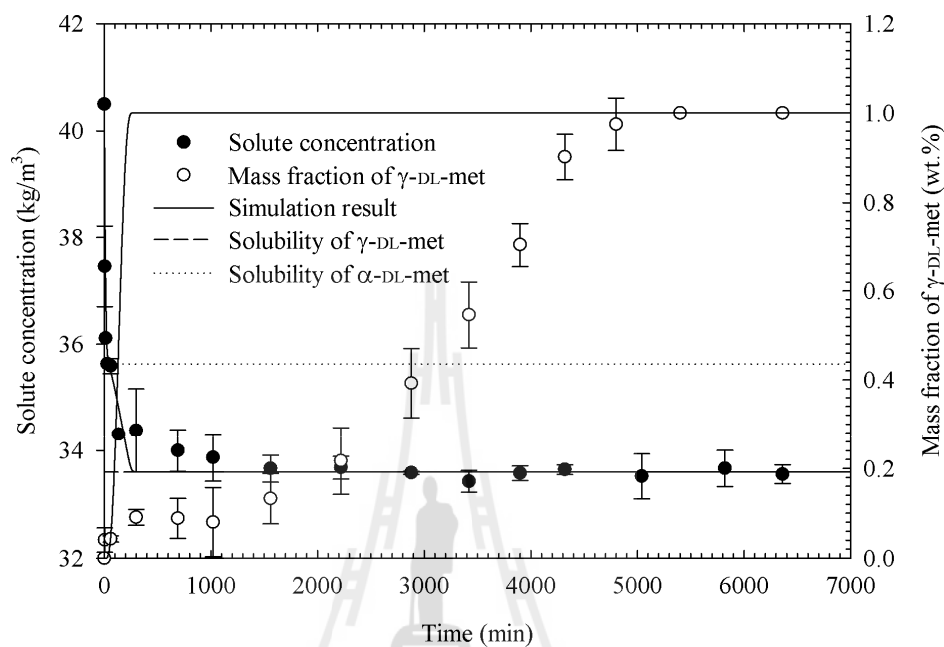


**Figure 6.4** Comparison between simulated and experimental solute concentration and fraction of  $\gamma$ -DL-met in the crystal phase during the polymorphic transformation of  $\alpha$ -DL-met into  $\gamma$ -DL-met at 25 °C and  $C_0 = 40.5 \text{ kg/m}^3$ . The dissolution kinetics obtained from Chapter IV were applied to the simulation.

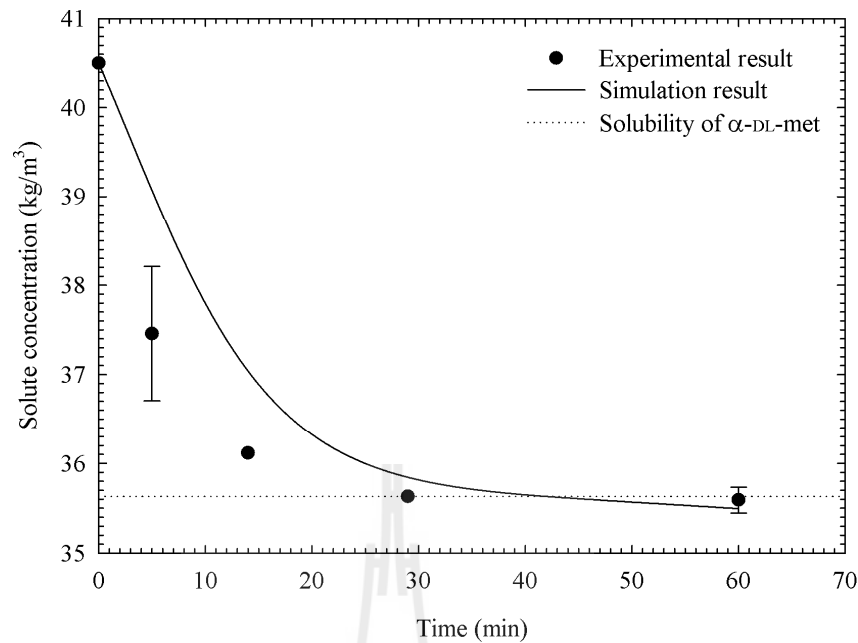


**Figure 6.5** The magnification of the comparison between simulated and experimental solute concentration in Figure 6.4 on the range of 0 - 60 min.

The large mismatches between the simulation and experimental results may be due to the incorrect the dissolution rates of  $\alpha$ -DL-met obtained from Chapter IV, which were measured based on the assumption that the same dissolution rate would be obtained for both  $\alpha$ -DL-met and  $\gamma$ -DL-met due to dissolution being considered as a single step (diffusion controlled) process, and only the dissolution rates of  $\gamma$ -DL-met were measured. This result shows that the dissolution rate constants of  $\alpha$ -DL-met are larger than the growth rate constants of  $\gamma$ -DL-met, which indicates the growth of  $\gamma$ -DL-met is the limiting step for the SMT process. However, the experimental results of the SMT in Chapter V show that the dissolution of  $\alpha$ -DL-met is the limiting step which indicates the dissolution rate constant of  $\alpha$ -DL-met is smaller than the growth rate constant of  $\gamma$ -DL-met. This means that the dissolution rates obtained from

Chapter IV are not the real dissolution rates of  $\alpha$ -DL-met which may result in the large mismatches between the models and experiments. These mismatches may be decreased by using the real dissolution rate of  $\alpha$ -DL-met in the mathematical models. In this work these mismatches will be decreased by estimation of the dissolution kinetic parameter (the parameter  $K_{D\alpha}$ ) from the combination of the PBE models and SMT experimental data while the other kinetics were unchanged.

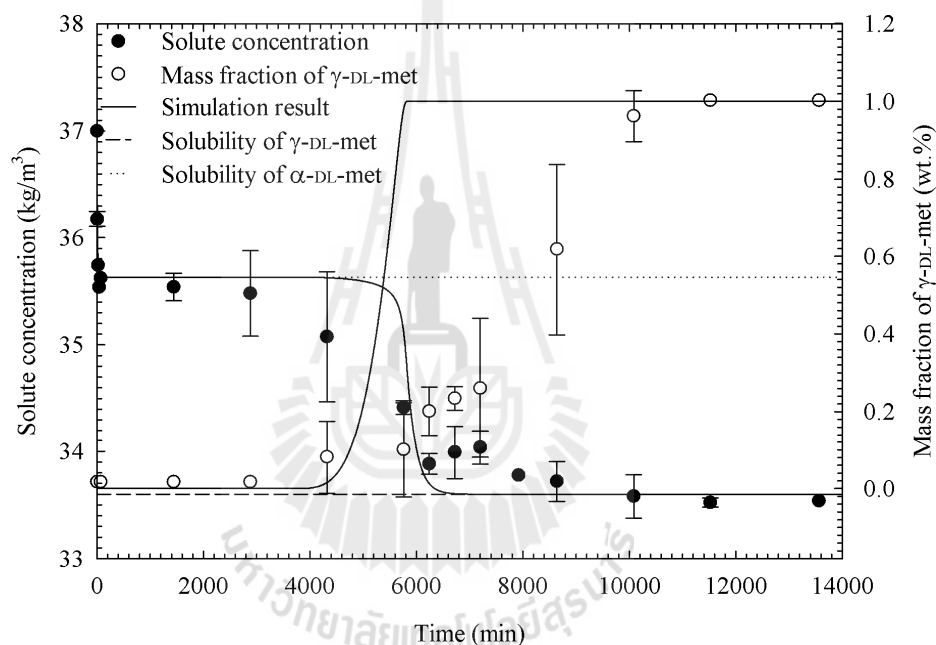


**Figure 6.6** Comparison between simulated and experimental solute concentration and fraction of  $\gamma$ -DL-met in the crystal phase during the polymorphic transformation of  $\alpha$ -DL-met into  $\gamma$ -DL-met at 25 °C and  $C_0 = 37.0 \text{ kg/m}^3$ . The dissolution kinetics obtained from Chapter IV were applied to the simulation.

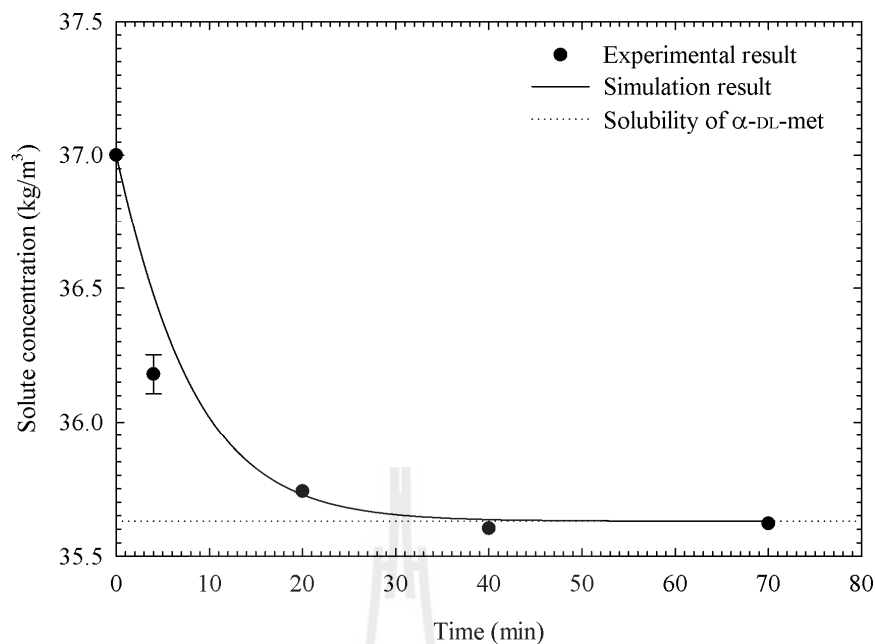


**Figure 6.7** The magnification of the comparison between simulated and experimental solute concentration in Figure 6.6 on the range of 0 - 70 min.

In the second part of the models, all of the kinetic parameters obtained from Chapter III and IV were applied to the modeling except the dissolution kinetics of  $\alpha$ -DL-met. The dissolution kinetic of  $\alpha$ -DL-met (the parameter  $K_{D\alpha}$ ) and the induction times were estimated from the combination of the PBE models and SMT experimental data using the optimization technique as shown in Section 6.4.6. The estimated induction times for the case of  $C_0 = 40.5$  and  $37.0 \text{ kg/m}^3$  are 25 min and 3 days, respectively, and the estimated  $K_{D\alpha}$  is  $7.4766 \times 10^{-9} \text{ m/s}$ .

The estimated values of  $K_{D\alpha}$  and the induction times were applied to the PBE models. The simulated and experimental solute concentrations and fractions of  $\gamma$ -DL-met of this part are shown in Figures (6.8) to (6.11). It can be seen that the mismatches between the modeling and experiments decrease. Both the profiles of

simulated solute concentrations and fractions of  $\gamma$ -DL-met agree with the experimental data. However, there are still some deviations between the simulation and experimental results. This deviation may be due to primary nucleation kinetic of  $\gamma$ -DL-met used in the model (which was collected from Chapter III) which was measured at higher supersaturation (higher than 1.17 or the solute concentration is higher than  $39.3 \text{ kg/m}^3$ ) while the nucleation of  $\gamma$ -DL-met in the SMT process occurred at the solubility of  $\alpha$ -DL-met ( $35.63 \text{ kg/m}^3$ ). This means that the supersaturation in the SMT process is insufficient for the primary nucleation of  $\gamma$ -DL-met crystals. Moreover, Ono et al. (2004), Févotte et al. (2007), and Cornel et al. (2009) proposed that secondary nucleation of the stable polymorph (based on the metastable interparticles impacts or birth of the stable polymorph on the surface of the metastable polymorph) should be accounted for in the SMT process instead of primary nucleation. Therefore, changes in nucleation kinetics based on these two reasons may reduce these deviations between the simulation and experimental results.

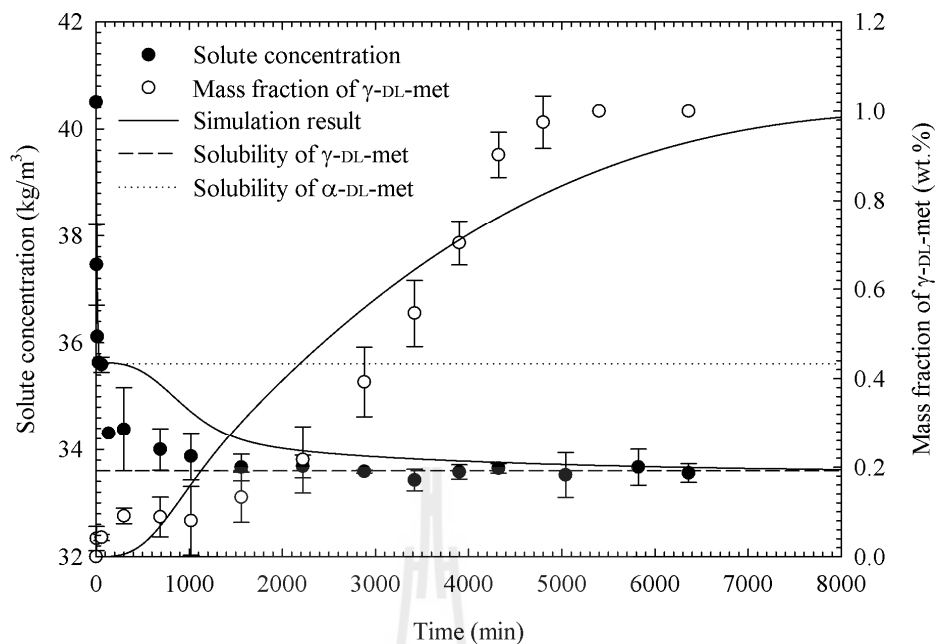


**Figure 6.8** Comparison between simulated and experimental solute concentration and fraction of  $\gamma$ -DL-met in the crystal phase during the polymorphic transformation of  $\alpha$ -DL-met into  $\gamma$ -DL-met at 25 °C and  $C_0 = 40.5 \text{ kg/m}^3$ . The dissolution kinetics were estimated from the combination of the modeling method with the SMT experimental data.

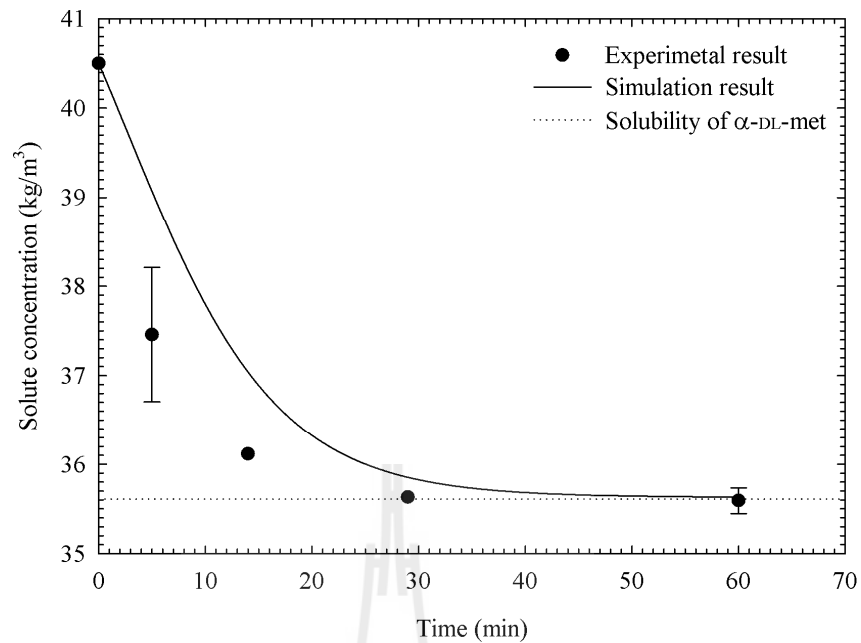


**Figure 6.9** The magnification of the comparison between simulated and experimental solute concentration in Figure 6.8 on the range of 0 - 60 min.

Figures 6.5, 6.7, 6.9, and 6.11 show the simulated solute concentration profiles in the period of 0 - 70 min for both cases do not change with the change of the value of  $K_{D\alpha}$ . This is since only the growth of  $\alpha$ -DL-met occurs in this period and this has no dependence on the dissolution rate parameter (see more detail in Chapter V).

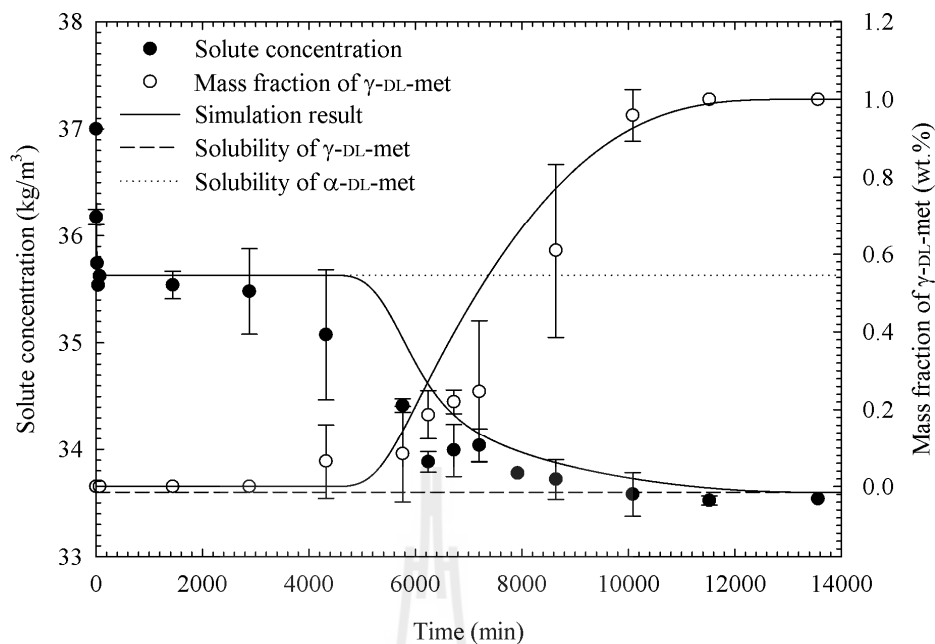


**Figure 6.10** Comparison between simulated and experimental solute concentration and fraction of  $\gamma$ -DL-met in the crystal phase during the polymorphic transformation of  $\alpha$ -DL-met into  $\gamma$ -DL-met at 25 °C and  $C_0 = 37.0 \text{ kg/m}^3$ . The dissolution kinetics were estimated from the combination of the modeling method with the SMT experimental data.

The plots of the first four moments ( $\mu_0$ ,  $\mu_1$ ,  $\mu_2$ , and  $\mu_3$ ) for each polymorph for the case when the dissolution kinetic parameter was estimated are shown in Appendix C. These moments are related to the total number of crystals, the average crystal size, the total surface area of crystal, and the total volume and mass of crystals. Therefore, these data can be used to describe and understand the crystallization and SMT process better.

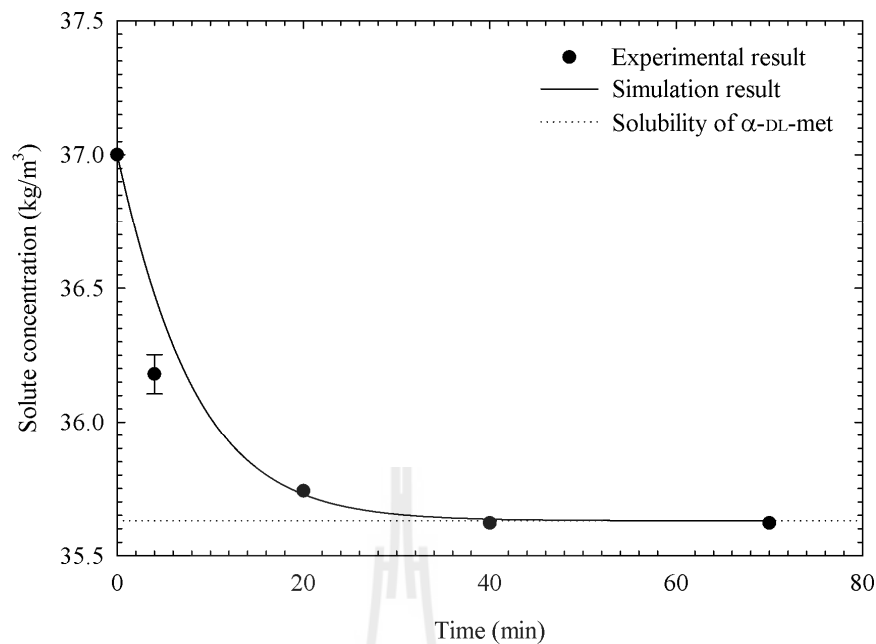


**Figure 6.11** The magnification of the comparison between simulated and experimental solute concentration in Figure 6.10 on the range of 0 - 70 min.

The kinetic expressions of the growth of  $\gamma$ -DL-met (equation (6.39)) and the dissolution of  $\alpha$ -DL-met (equation (6.41)) are a linear function of the driving force (concentration difference) for the growth or dissolution. Therefore, at the same level of driving force the estimated  $K_{D\alpha}$  value of  $7.4766 \times 10^{-9}$  m/s and the measured  $K_{G\gamma}$  value of  $3.1450 \times 10^{-7}$  m/s have to be compared for indicating the controlling process. This comparison shows the estimated  $K_{D\alpha}$  value is far lower than the measured  $K_{G\gamma}$  value, which indicates the dissolution of  $\alpha$ -DL-met is the limiting step. The simulated and experimental solute concentrations also confirm that the dissolution of  $\alpha$ -DL-met is the limiting step (see details in Chapter V). Therefore, both the results obtained from Chapter V and this chapter confirms that the dissolution kinetics of  $\alpha$ -DL-met and  $\gamma$ -DL-met are not the same. The assumption (in Chapter IV) that the dissolution of

DL-met polymorphs is a single step (diffusion controlled) is not true. The real mechanism of the dissolution must consist of a surface reaction and the detachment of the species followed by transfer of these species toward the bulk solution across the diffusion layer which surrounds the crystals, as discussed in a recent study (Kramer and van Rosmalen, 2009).

The model proved that the kinetic parameters obtained from the experiments performed on a single polymorphic form can be used to describe the whole crystallization and SMT process. The agreement between the simulation and the experimental results depends on the accuracy of the experimental method to obtain kinetic parameters, or the use of appropriate kinetics in the model. In the best possible case the kinetic parameters could be estimated from experiments that are independent from the SMT experiments, however this was not possible here; in particular a single parameter in the dissolution rate kinetics needed to be estimated based on the SMT results. The combination of the experiments and models helps to understand and predict the crystallization and SMT behaviors.

## 6.6 Conclusions

The population balance equation (PBE) model for crystallization and the SMT of the metastable  $\alpha$ -DL-met into the stable  $\gamma$ -DL-met in water at 25 °C was derived and validated using the SMT experimental data obtained from Chapter V. The results showed that there are large mismatches between the simulation and experimental results. Particularly above the nucleation threshold there were large deviations between the simulation results and the experimental results. Improvement of the simulation results could be achieved by improving the dissolution kinetics of

$\alpha$ -DL-met. This was done by estimating the dissolution kinetic parameter  $K_{D\alpha}$ . The simulation results showed that the estimated  $K_{D\alpha}$  value at 25 °C is  $7.4766 \times 10^{-9}$  m/s which indicates that the dissolution rate constant of  $\alpha$ -DL-met is smaller than the growth rate constant of  $\gamma$ -DL-met. The results indicate that the PBE can be used to describe the whole crystallization and SMT process. This result together with the profiles of the solute concentration leads to the conclusion that the SMT in this system is a dissolution controlled process. This result also confirms that the dissolution rates of  $\alpha$ -DL-met and  $\gamma$ -DL-met are not the same and the dissolution mechanism of the polymorphs of DL-met is a two steps process. This includes the surface reaction and the detachment of the species, and followed by transfer of these species toward the bulk solution across the diffusion layer which surrounds the crystals.

## 6.7 References

- Caillet, A., Sheibat-Othman, N., and Févotte, G. (2007). Crystallization of monohydrate citric acid. 2. Modeling through population balance equations. **Cryst. Growth Des.** 7(10): 2088-2095.
- Chapra, S.C., and Canale, R.P. (2006). **Numerical methods for engineers** (5<sup>th</sup> ed.). Singapore: McGraw-Hill.
- Cornel, J., Kidambi, P., and Mazzotti, M. (2010). Precipitation and transformation of the three polymorphs of D-mannitol. **Ind. Eng. Chem. Res.** 49(12): 5854-5862.
- Cornel, J., Lindenberg, C., and Mazzotti, M. (2009). Experimental characterization and population balance modeling of the polymorph transformation of L-glutamic acid. **Cryst. Growth Des.** 9(1): 243-252.

- Dharmayat, S., Hammond, R.B., Lai, X., Ma, C., Purba, E., Roberts, K.J., Chen, Z-P., Martin, E., Morris, J., and Bytheway, R. (2008). An examination of the kinetics of the solution-mediated polymorphic phase transformation between  $\alpha$ - and  $\beta$ -forms of L-glutamic acid as determined using online powder X-ray diffraction. **Cryst. Growth Des.** 8(7): 2205-2216.
- Févotte, G., Alexandre, C., and Nida, S.O. (2007). A population balance model of the solution-mediated phase transition of citric acid. **AIChE J.** 53(10): 2578-2589.
- Flood, A.E. (2009). **Industrial crystallization from solution: A primer.** Thailand: Suranaree University of Technology.
- Jiang, S., Jansens, P.J., and ter Horst, J.H. (2010). Control over polymorph formation of o-aminobenzoic acid. **Cryst. Growth Des.** 10(6): 2541-2547.
- Kramer, H.J.M., and van Rosmalen, G.M. (2009). Crystallization. In: I.A., Wilson and C.F., Poole (ed.). **Handbook of methods and instrumentation in separation science volume 2** (pp 1-20). London: Academic Press.
- Kumar, J. (2006). **Numerical approximations of population balance equations in particulate systems.** Ph.D. thesis, Otto-von-Guericke-University, Germany.
- Lindenberg, C., and Mazzotti, M. (2009). Effect of temperature on the nucleation kinetics of  $\alpha$ -L-glutamic acid. **J. Cryst. Growth** 311(4): 1178-1184.
- Mangin, D., Puel, F., and Veessler, S. (2009). Polymorphism in processes of crystallization in solution: A practical review. **Org. Process Res. Dev.** 13(6): 1241-1253.

- Matsuoka, M., Yamanobe, M., Tezuka, N., Takiyama, H., and Ishii, H. (1999). Polymorphism, morphologies and bulk densities of DL-methionine agglomerate crystals. **J. Cryst. Growth** 198-199: 1299-1306.
- Morris, K.R., Griesser, U.J., Eckhardt, C.J., and Stowell, J.G. (2001). Theoretical approaches to physical transformations of active pharmaceutical ingredients during manufacturing processes. **Adv. Drug. Del. Rev.** 48(1): 91-114.
- Ono, T., Kramer, H.J.M., ter Horst, J.H., and Jansens, P.J. (2004). Process modeling of the polymorphic transformation of L-glutamic acid. **Cryst. Growth Des.** 4(6): 1161-1167.
- Randolph, A.D., and Larson, M.A. (1988). **Theory of particulate processes: Analysis and techniques of continuous crystallization** (2<sup>nd</sup> ed.). California: Academic Press.
- Roelands, C.P.M. (2005). **Polymorphism in precipitation process**. Ph.D. thesis, Delft University of Technology, The Netherlands.
- Schöll, J., Bonalumi, D., Vicum, L., and Mazzotti, M. (2006). In situ monitoring and modeling of the solvent-mediated polymorphic transformation of L-glutamic acid. **Cryst. Growth Des.** 6(4): 881-891.
- Schöll, J., Lindenberg, C., Vicum, L., Brozio, J., and Mazzotti, M. (2007). Precipitation of  $\alpha$  L-glutamic acid: determination of growth kinetics. **Faraday Discuss.** 136:247-264.
- Scully, J. (2010). **Numerical simulation of the L-glutamic acid polymorphic system**. Ph.D. thesis, University of Limerick, Ireland.

Wey, J.S., and Karpinski, P.H. (2002). Batch crystallization. In: A.S. Myerson (ed.).  
**Handbook of industrial crystallization** (2<sup>nd</sup> ed., pp 231-248). USA:  
Butterworth-Heinemann.



## CHAPTER VII

### CONCLUSIONS AND RECOMMENDATIONS

#### 7.1 Conclusions

Polymorphs are crystalline solids which are chemically identical but have different crystal structures. Each polymorph has its own mechanical, thermal, physical, and chemical properties, such as compressibility, melting point, crystal habit, color, density, dissolution rate, and solubility. Polymorphism gives the scientist or engineer a chance to select the form which best matches the needs of the product. On the other hand, polymorphism is sometimes an undesired phenomenon because the different properties of different polymorphs can make variable materials that do not meet the prescribed specifications when the system is not polymorphically pure in the desired polymorph. Usually, the unstable polymorph is not acceptable from the point of view of obtaining polymorphically pure compounds suitable for sale, particular in the food industry and other material products. On the other hand, in the field of pharmaceuticals, metastable polymorphs may be more desirable than the stable one. Therefore, the production of specific and well-defined polymorphs is important in a variety of industrial applications.

It is advantageous to choose the proper polymorph for the desired application. Therefore, in the crystallization processes involving polymorphs, the formation of the desired polymorph has to be controlled and such a process should be robust and reproducible. The formation of the polymorph is usually determined by thermodynamics,

and crystallization and dissolution kinetics, and transformation kinetics. Thermodynamics are used to identify whether the phase is the stable or metastable, while kinetics determine how fast these phases can be crystallized at a certain driving force. Therefore, to control polymorphism, the thermodynamics and kinetics in a crystallization process should be understood, predicted, and controlled. This thesis focuses on the understanding and prediction of the thermodynamics, kinetics, and transformation behavior of the polymorphs of DL-methionine (DL-met). The following conclusions can be made for this thesis.

1. Polymorphically pure crystals of the two commonly known polymorphs of DL-met,  $\alpha$ -DL-met and  $\gamma$ -DL-met, were prepared by reaction crystallization of sodium methioninate (Na-Met) aqueous solutions with HCl, and cooling crystallization of aqueous solutions of DL-met, respectively. The solubility of both  $\alpha$ -DL-met and  $\gamma$ -DL-met in water increases with increasing temperature, and the solubility of  $\alpha$ -DL-met is higher than that of  $\gamma$ -DL-met as expected from a metastable polymorph. The melting temperature and enthalpy of fusion of  $\gamma$ -DL-met are higher than those of  $\alpha$ -DL-met. The Gibbs free energy of  $\alpha$ -DL-met is higher than  $\gamma$ -DL-met. The solubility data, DSC thermograms and Gibbs free energies of the two polymorphs strongly suggest that the system is a monotropic polymorph system where  $\gamma$ -DL-met is the stable polymorph while  $\alpha$ -DL-met is the metastable polymorph for all temperatures below the melting points of the compounds. The solubility data was used as the basic information to design the experiments of the crystallization (nucleation and growth kinetics measurements) and transformation processes.

2. The secondary nucleation threshold (SNT) of  $\gamma$ -DL-met in aqueous solution was determined in an agitated batch system prior to the crystal growth experiments to ensure no nucleation would take place in the crystallizer. The weakly temperature dependent of the width of the SNT was found. Slightly smaller induction times were found at higher temperatures. The direct determination of the rate of nucleation based on measurements of particle (crystal) counts as a function of time was used to determine the nucleation rates of  $\gamma$ -DL-met in aqueous solution for the temperature range 18 - 35 °C. The nucleation rates were found to exponentially increase with respect to the supersaturation of DL-met and increase with increasing temperature. The measured nucleation kinetics can be described by the classical nucleation theory (CNT) and allowing approximate interfacial energies to be estimated by fitting the measured data to CNT.

3. The growth and dissolution rates of  $\gamma$ -DL-met and the growth rates of  $\alpha$ -DL-met in aqueous solution were measured in an agitated batch crystallizer for the temperature range 5 - 40 °C. The growth rates were measured within the SNT region. The growth history of the crystal surface, where the crystals grown more quickly at higher supersaturation have a rougher surface on a microscopic level than the seed crystals they were grown from, results in the initial growth rate (during the first 20 min of the batch) being significantly higher than subsequent crystal growth. There is no effect of the seed mass on the growth rates. The growth rates were a linear function of the relative supersaturation of DL-met in the system. The dissolution rate was a linear function of the relative undersaturation of DL-met in the system. The growth and dissolution rate constants increase with increasing temperature and follow an Arrhenius relationship.

4. The solution-mediated transformation (SMT) of  $\alpha$ -DL-met into  $\gamma$ -DL-met in water at 25 °C was studied via a seeded batch crystallization process. The change of the solute concentration and the fraction of  $\gamma$ -DL-met with time during the crystallization process were used to describe the behavior of the SMT. Off-line XRPD quantitative measurement was used to determine the fraction of  $\gamma$ -DL-met in suspension. The SMT process consists of the dissolution process of  $\alpha$ -DL-met and the crystallization process (nucleation and growth) of  $\gamma$ -DL-met. The transformation is a dissolution controlled process, where the mass transfer of solute to the growing phase rapidly depletes the solute concentration to a value consistent with the minimum level of supersaturation required to maintain the growth of the stable polymorph. This since the dissolution rate of the metastable polymorph is relatively slow. The transformation time is also quite slow. The transformation rate is faster if the initial solute concentration is higher, particularly if it is above the nucleation threshold of the stable polymorph. This study shows that the crystallization and dissolution kinetics are very important and helpful to understand and control crystallization processes involving polymorphs.

5. The combination of the population balance equation (PBE) models and the experimental results of the SMT of  $\alpha$ -DL-met into  $\gamma$ -DL-met in water at 25 °C were investigated. The experimented growth, dissolution, and nucleation kinetics were accounted for in the models. It was found that there were large mismatches between the simulation and experimental results if kinetic parameters were taken from experiments not involving SMT. Improving the model of the dissolution kinetics of  $\alpha$ -DL-met (which in fact appear different to those of the  $\gamma$ -form) enabled these mismatches to be lowered, and this was done by re-estimating only a single

dissolution kinetic parameter  $K_{D\alpha}$ . The estimated dissolution rate constant of  $\alpha$ -DL-met is smaller than the growth rate constant of  $\gamma$ -DL-met. This result together the profiles of the solute concentration also confirm that the SMT is dissolution controlled process in this system.

## 7.2 Recommendations

The following recommendations may help for a deeper understanding of the SMT process, and also useful for future studies of the phenomenon of SMT.

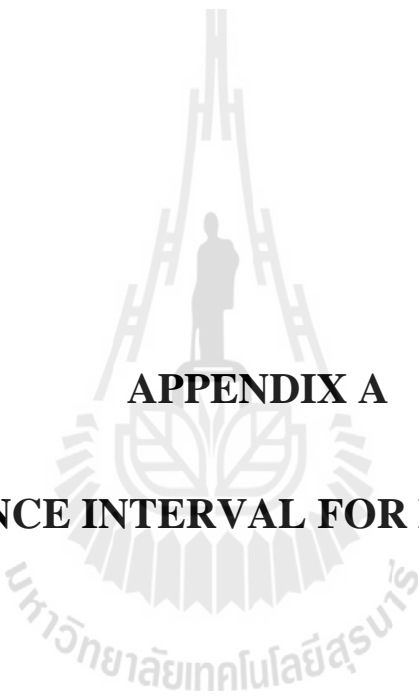
1. The dissolution rate of  $\alpha$ -DL-met is an important kinetic parameter for describing the SMT process, but this was not measured independently of the SMT in this work. This is since the crystals of  $\alpha$ -DL-met prepared from reaction crystallization are very small, and it is impossible to accurately measure the dissolution rate of these crystals because the dissolution rate to zero size is very fast, and because the time rate of change in size for very small crystals is difficult to determine with high accuracy. There are ways to prepare a larger size of the crystals of  $\alpha$ -DL-met which can be used to measure the dissolution rate; for example growth of the crystals that were obtained from the reaction crystallization to a larger size. However, the dissolution rate for  $\alpha$ -DL-met at 25 °C was estimated from a combination of the PBE models with the SMT experimental results in the present work. Therefore, the dissolution rate of  $\alpha$ -DL-met may be measured in future work; and this could be compare with the value estimated in the present work.

2. The nucleation rate of  $\alpha$ -DL-met was not studied because the crystallization and SMT processes were performed in aqueous solutions in which only  $\gamma$ -DL-met crystallized. However, if the crystallization and SMT processes are studied in sodium

methioninate (Na-Met) aqueous solution all kinetics should be studied. This is since the reaction crystallization from Na-Met aqueous solution produces  $\alpha$ -DL-met first, and this form then transforms to  $\gamma$ -DL-met. Therefore, the whole process will be described by the nucleation kinetics of  $\alpha$ -DL-met and  $\gamma$ -DL-met, the growth kinetics of  $\alpha$ -DL-met and  $\gamma$ -DL-met, and the dissolution kinetics of  $\alpha$ -DL-met. This should be studied further.

3. Usually, the SMT process occurs at the solubility of the metastable polymorph. This indicates that the supersaturation in the SMT process is insufficient for the primary nucleation of the stable  $\gamma$ -DL-met crystals. Therefore, the secondary nucleation (based on the metastable interparticle impacts or birth of the stable polymorph on the surface of the metastable polymorph) of the stable  $\gamma$ -DL-met polymorph should be accounted for in the SMT process instead of primary nucleation. This may reduce the deviation between the simulation and experimental results.

4. For the further work, all the kinetic parameters of the whole crystallization and SMT process should be estimated from the combination of the simulation and SMT experiment. This may help to prove the agreement between the estimates values and the values obtained from the experiments performed on a single polymorphic form.



**APPENDIX A**

**CONFIDENCE INTERVAL FOR MEAN VALUES**

## A.1 Confidence Interval for Mean Values

In this work all uncertainty limits, and the upper- and lower-confidence bounds of the error bar plots for the mean (average) values were calculated based on the 90% confidence level. Since all sample sizes in this work are small (less than 30 samples per sample), confidence intervals for mean are calculated by using a probability density function called the t-distribution (Doebelin, 1995; Montgomery and Runger, 2004). It should be noted that for a large sample size (more than or equal to 30 samples), the t-distribution becomes close to the z-distribution (the standard normal distribution).

The confidence interval for the mean value is defined as (Doebelin, 1995; Montgomery and Runger, 2004)

$$\text{Confidence interval} \equiv \bar{x} \pm t_{\alpha/2, n-1} \frac{s}{\sqrt{n}} \quad (\text{A.1})$$

where the mean value ( $\bar{x}$ ) and the standard deviation ( $s$ ) of the sample are given by

$$\bar{x} = \frac{\sum_{i=1}^n x_i}{n} \quad (\text{A.2})$$

$$s = \left[ \frac{\sum_{i=1}^n (x_i - \bar{x})^2}{n-1} \right]^{1/2} \quad (\text{A.3})$$

Note that  $x_i - \bar{x}$  is the distance of an individual point from the mean which is a measure of the scatter.  $n$  is the number of samples and  $t$  is the percentage point of the

t-distribution (see Table A.1).  $1 - \alpha$  is the confidence coefficient, for example  $\alpha = 0.1$  for a 90% confidence interval ( $100(1-\alpha)\%$ ). The t-distribution has an adjustable parameter  $\nu$ , the degrees of freedom. In this case  $\nu = n - 1$ . If we look at the  $t$  table (Table A.1) the  $t$  value is located in the  $(n - 1)^{\text{st}}$  row and the  $\alpha/2$  column for a 2-trail interval. If  $n = 5$  and  $\alpha = 0.1$ , this value is 2.132. Assume that we have a 5-point data set with  $\bar{x} = 53$  and  $s = 8.77$ , and we choose 90% confidence interval (see Table A.1),

$$\text{Confidence interval} = 53 \pm 2.132 \frac{8.77}{\sqrt{5}} = 53 \pm 8.36 \quad (\text{A.4})$$

This means that the best estimate of  $\bar{x}$  is 53, and the true value is somewhere between 44.64 and 61.36.

**Table A.1** Percentage points  $t_{\alpha,\nu}$  of the t-distribution.

$\alpha \backslash \nu$	0.100	0.050	0.025	0.010	0.005
1	3.078	6.314	12.706	31.821	63.657
2	1.866	2.920	4.303	6.965	9.925
3	1.638	2.353	3.182	4.541	5.841
4	1.533	2.132	2.776	3.747	4.604
5	1.476	2.015	2.571	3.365	4.302
6	1.440	1.943	2.447	3.143	3.707
7	1.415	1.895	2.365	2.998	3.499
8	1.397	1.860	2.306	2.896	3.355

Note: The full form of this table can be found in a number of references

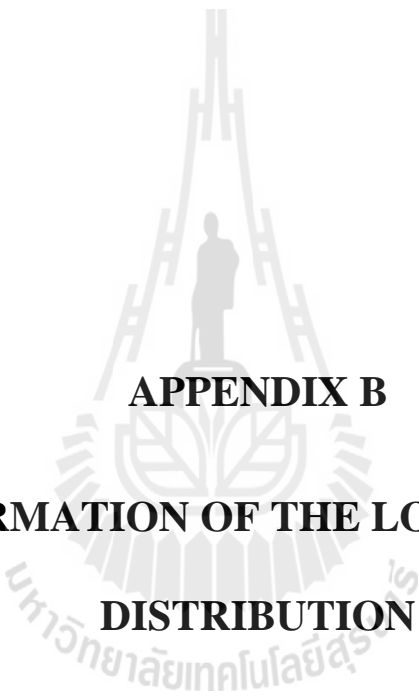
(Doebelin, 1995; Montgomery and Runger, 2004).

## A.2 References

Doebelin, E.O. (1995). **Engineering experimentation: Planning, execution and reporting**. Singapore: McGraw-Hill.

Montgomery, D.C., and Runger, G.C. (2004). **Applied statistics and probability for engineers** (3<sup>rd</sup> ed.). India: John Wiley & Sons.





**APPENDIX B**  
**CONFIRMATION OF THE LOG-NORMAL**  
**DISTRIBUTION**

## B.1 Confirmation of the Log-Normal Distribution

The particle size distribution (PSD) can be confirmed as a log-normal distribution by fitting the data with the log-normal distribution equation or plotting the data on log-normal probability paper. In this appendix, these two methods are described.

The log-normal distribution equation is given by (Flood, 2009)

$$f(L) = \frac{a}{L} \exp \left[ -0.5 \left( \frac{(\ln L - \ln L')}{b} \right)^2 \right] \quad (\text{B.1})$$

when

$$a = \frac{1}{\sqrt{2\pi} \ln \sigma_g} \quad (\text{B.2})$$

$$b = \ln \sigma_g \quad (\text{B.3})$$

where  $f(L)$  is the density distribution,  $L$  is the particle size,  $L'$  is the median of the distribution, and  $\sigma_g$  is the geometric standard deviation of the distribution. Therefore, after the data are fitted with the log-normal distribution equation, the  $L'$  and  $\sigma_g$  can be estimated. The PSD of the product crystals obtained at 45 min for the growth experiment of  $\gamma$ -DL-met at 25 °C and  $\sigma_{G0} = 0.114$  (as shown in Figure 4.5 in Chapter IV) is used to be an example for this fitting. The PSD is shown in Table B.1 and fitted with equation (B.1) which is shown in Figure B.1. Figure B.1 shows the PSD is fitted well with the log-normal distribution equation, which the estimated value of  $\sigma_g$  is equal to 1.51.

**Table B.1** Particle size distribution of product crystals obtained at 45 min for the growth experiment of  $\gamma$ -DL-met at 25 °C and  $\sigma_{G0} = 0.114$ .

Particle size ( $\mu\text{m}$ )	%Volume in size range	%Volume undersize
18.0000	0.0000	0.0000
24.0000	0.0000	0.0000
30.0000	0.0000	0.0000
40.0000	0.0000	0.0000
55.0000	0.0000	0.0000
80.0000	0.0000	0.0000
103.5775	0.0312	0.0312
120.6678	0.4409	0.4720
140.5780	0.9609	1.4329
163.7733	1.8982	3.3311
190.7959	3.3519	6.6830
222.2773	5.3429	12.0259
258.9530	7.7865	19.8124
301.6802	10.4517	30.2642
351.4575	13.0734	43.3375
409.4479	15.5232	58.8607
477.0068	14.6431	73.5038
555.7130	11.9846	85.4885
647.4056	8.2039	93.6924
754.2275	4.6996	98.3920
878.6750	1.6080	100.0000

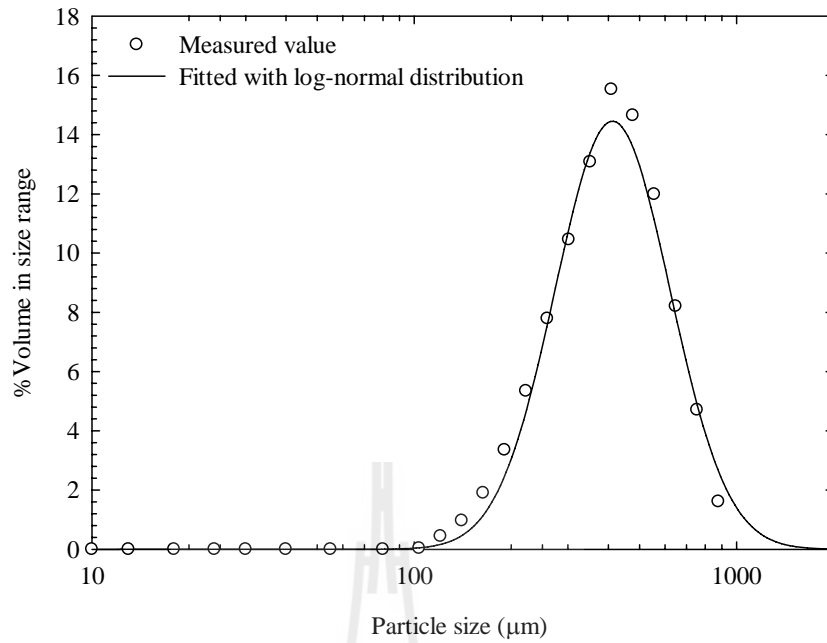


**Figure B.1** Particle size distribution of product crystals obtained at 45 min for the growth experiment of  $\gamma$ -DL-met at 25 °C and  $\sigma_{G0} = 0.114$ .

The distribution can also be confirmed by plotting the data on log-normal probability paper. If the plot is linear the distribution is a log-normal distribution. The value of  $\sigma_g$  can be read from the graph, and is given by (Allen, 1997)

$$\ln \sigma_g = \ln L_{84} - \ln L_{50} = \ln L_{50} - \ln L_{16} \quad (\text{B.4})$$

or

$$\sigma_g = \frac{L_{84}}{L_{50}} = \frac{L_{50}}{L_{16}} \quad (\text{B.5})$$

where  $L_{16}$ ,  $L_{50}$ , and  $L_{84}$  are the sizes at 16, 50, and 84 percent undersize, respectively.

The data in Table B.1 are plotted on the log-normal probability paper as shown in

Figure B.2. The curve is linear, and the estimated value of  $\sigma_g$  is equal to 1.49 which is close to the value obtained from the fitting with the log-normal distribution equation (~1.32% lower). To reduce the calculation time all values of  $\sigma_g$  that were obtained in this thesis were estimated from fitting the log-normal distribution equation.

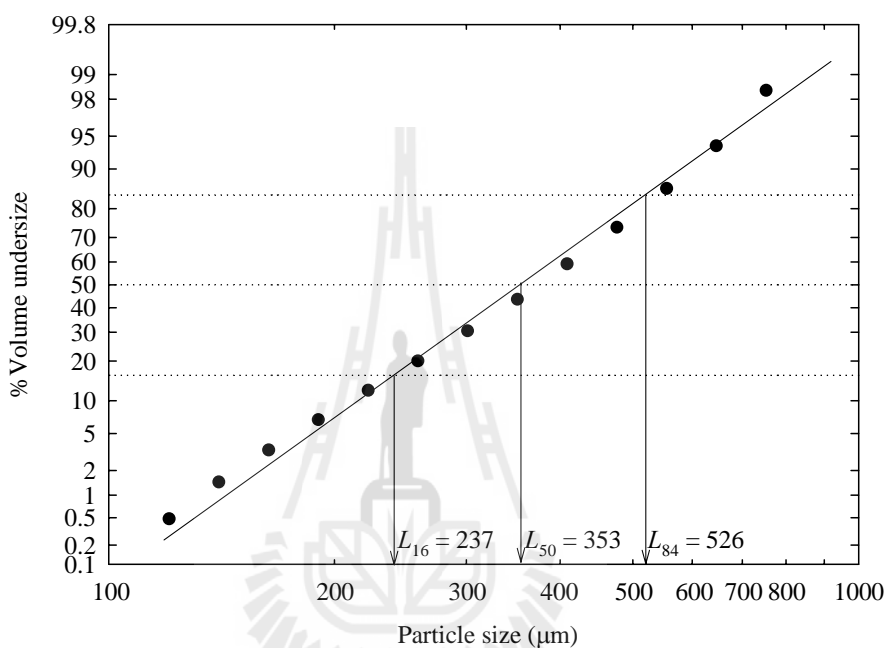
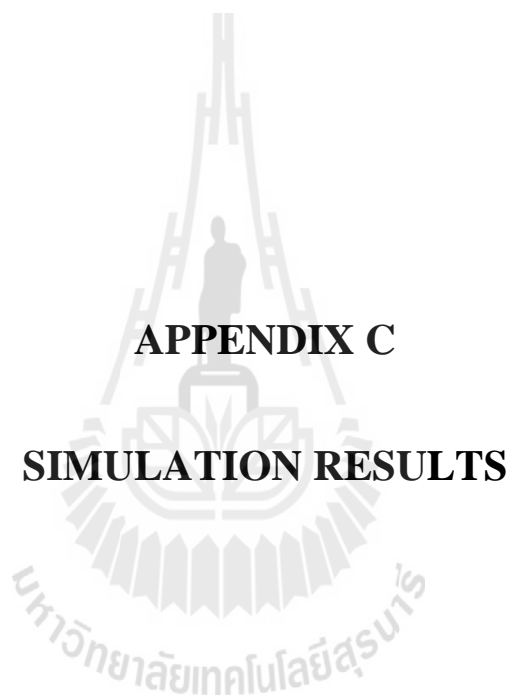


**Figure B.2** Plot of the PSD of product crystals obtained at 45 min for the growth experiment of  $\gamma$ -DL-met at 25 °C and  $\sigma_{G0} = 0.114$  on log-normal probability paper.

## B.2 References

- Allen, T. (1997). **Particle size measurement: Volume 1 powder sampling and particle size measurement** (5<sup>th</sup> ed.). London: Chapman&Hall.
- Flood, A.E. (2009). **Industrial crystallization from solution: A primer**. Thailand: Suranaree University of Technology.



**APPENDIX C**

**SIMULATION RESULTS**

The plots of the change of  $\mu_0$ ,  $\mu_1$ ,  $\mu_2$ , and  $\mu_3$  for each polymorph are shown in this appendix. These can be used to describe and understand the crystallization and solution-mediated transformation (SMT) process better. For example for  $\alpha$ -DL-met, during the SMT process  $\mu_{\alpha,0}$  (Figure C.1 or Figure C.9) which represents the total number of particles is constant until the particles have completely dissolved ( $\mu_{\alpha,0} = 0$ ) or the completeness of the SMT. This is due to the seed crystals of  $\alpha$ -DL-met were considered to be mono-sized particles. The value of  $\mu_{\alpha,1}$  (Figure C.2 or Figure C.10) which is related to the average particle size ( $\bar{L} = \mu_{\alpha,1} / \mu_{\alpha,0}$ ) decreases with respect to time until it reaches zero when the particles have completely dissolved. However, at the early period the average particle size increases with respect to time. This is since only the growth of  $\alpha$ -DL-met occurred in this period. The profiles of  $\mu_{\alpha,2}$  (Figure C.3 or Figure C.11) and  $\mu_{\alpha,3}$  (Figure C.4 or Figure C.12) are similar trends with  $\mu_{\alpha,1}$ . These two moments are related to the total surface area of crystals, and the total volume and mass of crystals, respectively.

For  $\gamma$ -DL-met, the total number of particle,  $\mu_{\gamma,0}$ , (Figure C.5 or Figure C.13) increases rapidly at the start of the SMT until it reaches the constant value. This is due to the occurrence of the nucleation of  $\gamma$ -DL-met at the start of the SMT. After that the solute concentration drops to the level that the supersaturation is not sufficient for the nucleation, and then the nucleation is stopped which leads to the total number of particle is a constant value. After the start of SMT, the values of  $\mu_{\gamma,1}$  (Figure C.6 or Figure C.14),  $\mu_{\gamma,2}$  (Figure C.7 or Figure C.15), and  $\mu_{\gamma,3}$  (Figure C.8 or Figure C.16) increase with respect to time due to the growth of  $\gamma$ -DL-met. The full details of the SMT process are described based on the change of the solute concentration and the fraction of  $\gamma$ -DL-met in Chapter V.

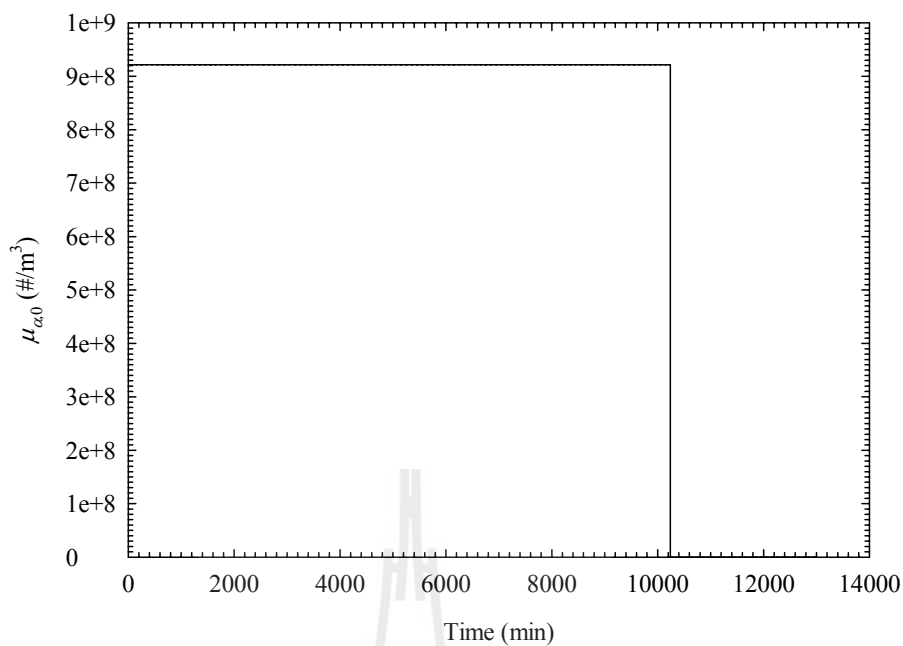


**Figure C.1** The change of  $\mu_{\alpha,0}$  with time during the SMT of  $\alpha$ -DL-met into  $\gamma$ -DL-met at 25 °C,  $C_0 = 40.5 \text{ kg/m}^3$  and  $K_{D\alpha} = 7.4766 \times 10^{-9} \text{ m/s}$ .

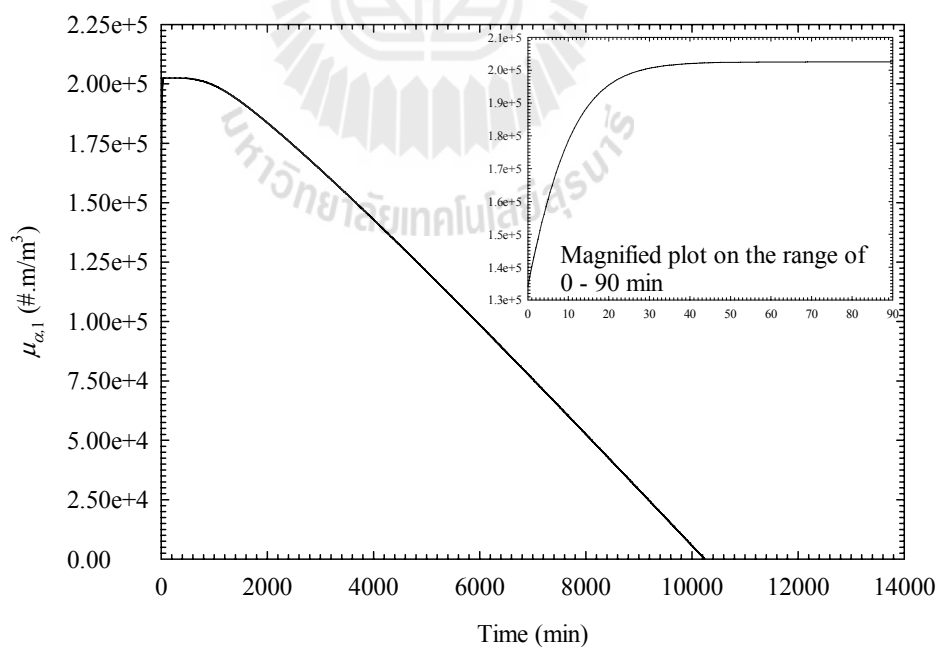


**Figure C.2** The change of  $\mu_{\alpha,1}$  with time during the SMT of  $\alpha$ -DL-met into  $\gamma$ -DL-met at 25 °C,  $C_0 = 40.5 \text{ kg/m}^3$  and  $K_{D\alpha} = 7.4766 \times 10^{-9} \text{ m/s}$ .

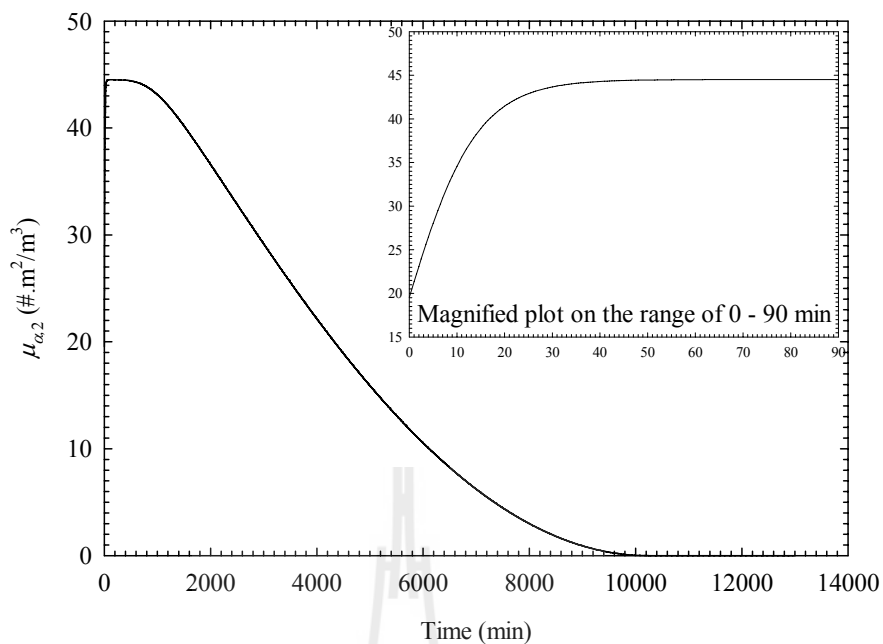


**Figure C.3** The change of  $\mu_{\alpha,2}$  with time during the SMT of  $\alpha$ -DL-met into  $\gamma$ -DL-met at 25 °C,  $C_0 = 40.5 \text{ kg/m}^3$  and  $K_{D\alpha} = 7.4766 \times 10^{-9} \text{ m/s}$ .

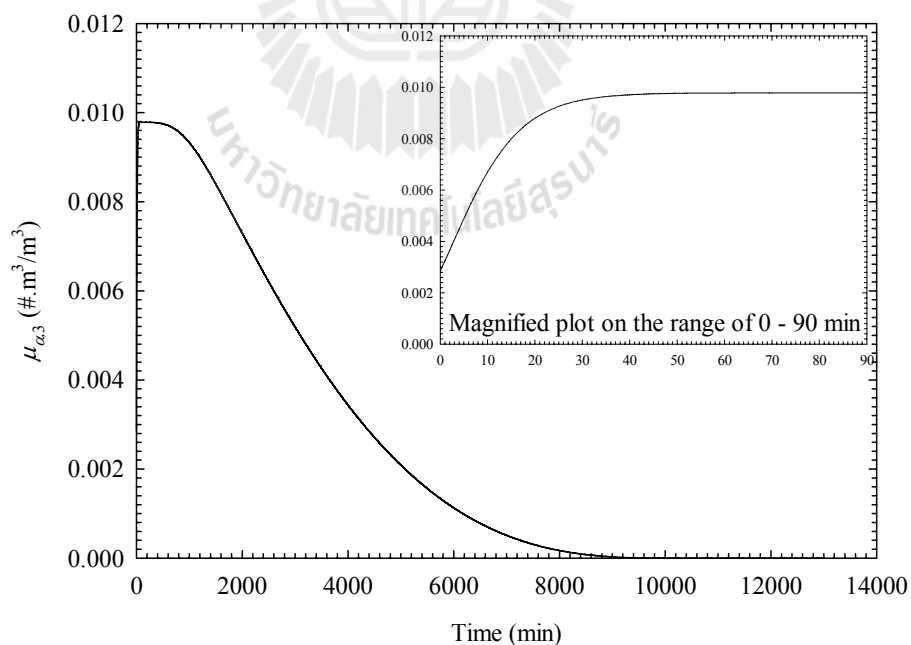


**Figure C.4** The change of  $\mu_{\alpha,3}$  with time during the SMT of  $\alpha$ -DL-met into  $\gamma$ -DL-met at 25 °C,  $C_0 = 40.5 \text{ kg/m}^3$  and  $K_{D\alpha} = 7.4766 \times 10^{-9} \text{ m/s}$ .

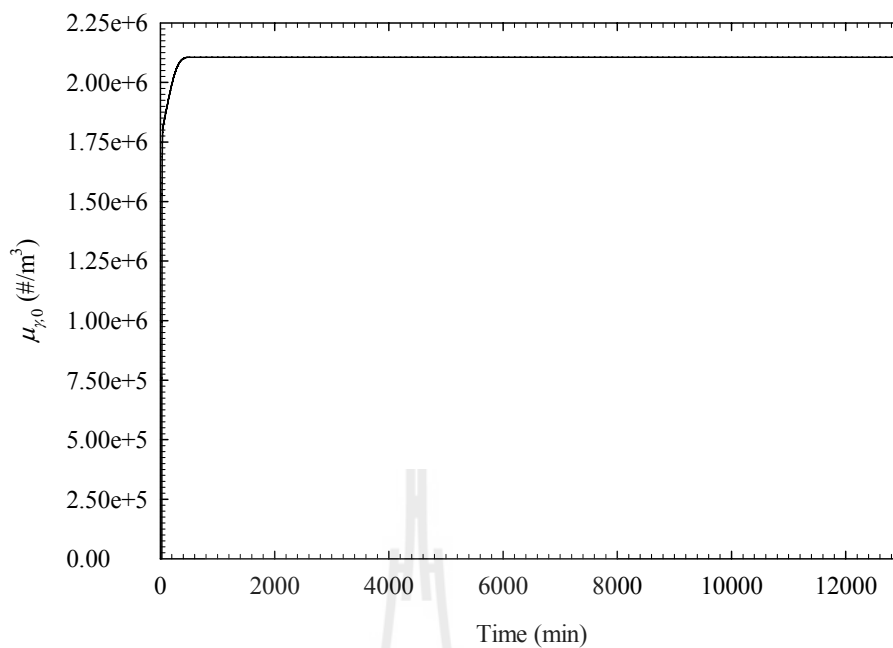


**Figure C.5** The change of  $\mu_{\gamma,0}$  with time during the SMT of  $\alpha$ -DL-met into  $\gamma$ -DL-met at 25 °C,  $C_0 = 40.5 \text{ kg/m}^3$  and  $K_{D\alpha} = 7.4766 \times 10^{-9} \text{ m/s}$ .

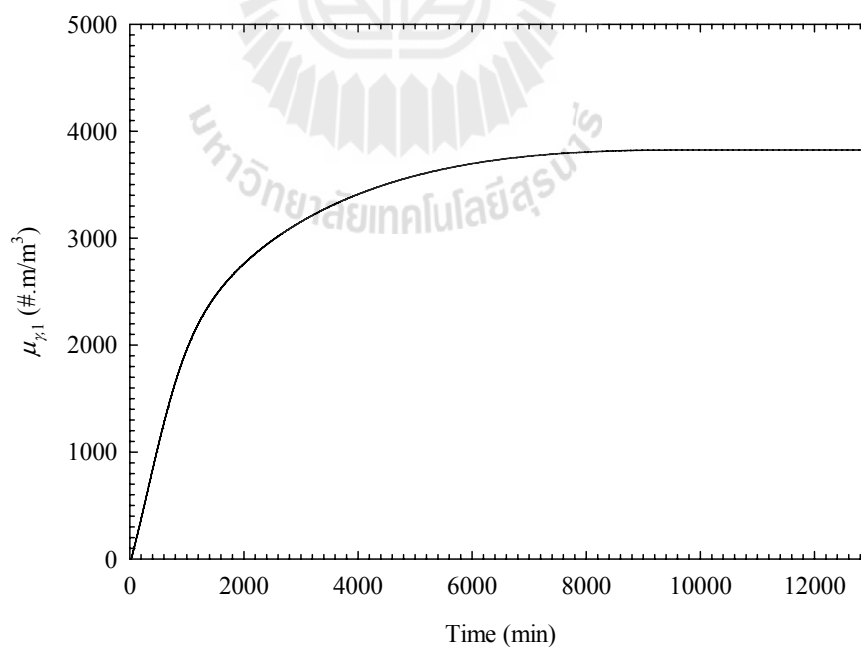


**Figure C.6** The change of  $\mu_{\gamma,1}$  with time during the SMT of  $\alpha$ -DL-met into  $\gamma$ -DL-met at 25 °C,  $C_0 = 40.5 \text{ kg/m}^3$  and  $K_{D\alpha} = 7.4766 \times 10^{-9} \text{ m/s}$ .

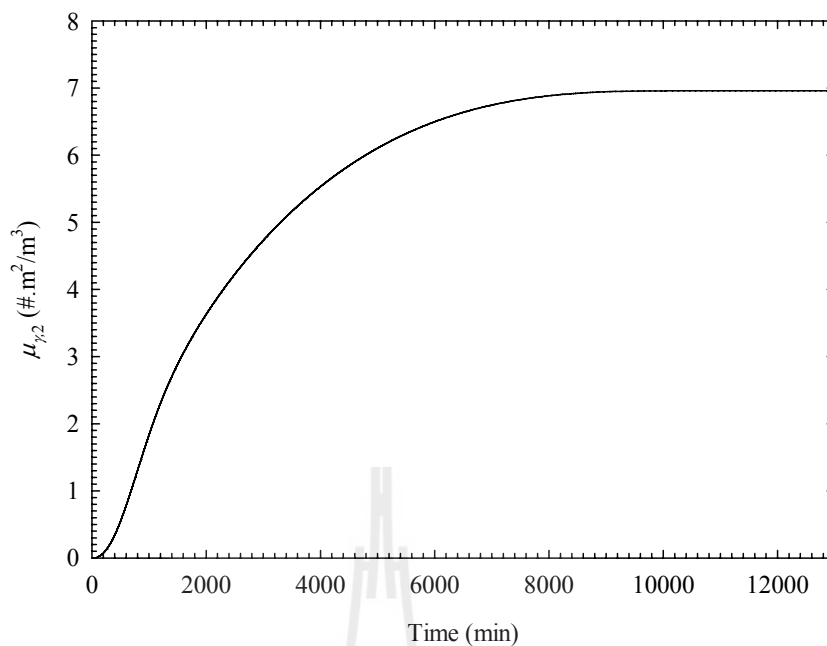


**Figure C.7** The change of  $\mu_{\gamma,2}$  with time during the SMT of  $\alpha$ -DL-met into  $\gamma$ -DL-met at 25 °C,  $C_0 = 40.5 \text{ kg/m}^3$  and  $K_{D\alpha} = 7.4766 \times 10^{-9} \text{ m/s}$ .

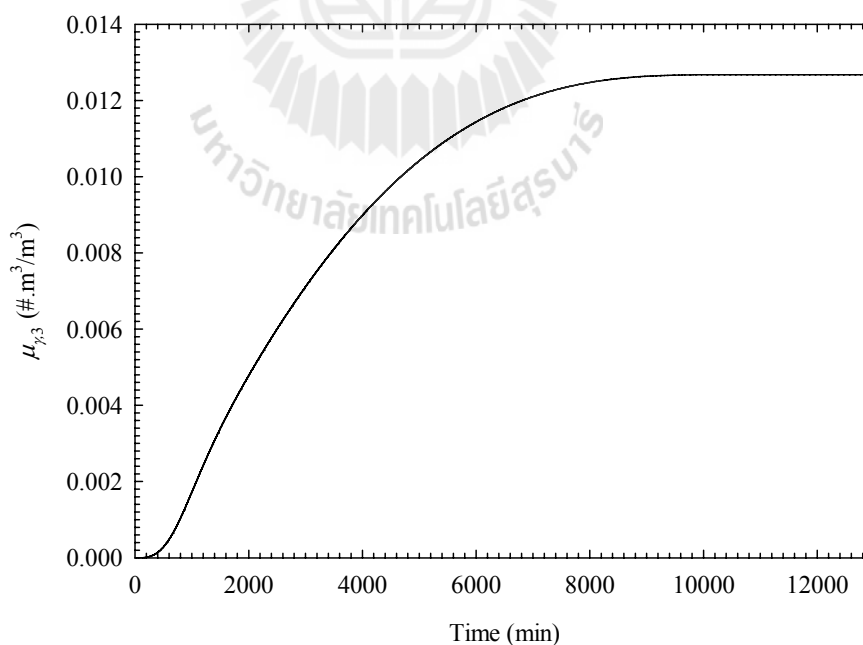


**Figure C.8** The change of  $\mu_{\gamma,3}$  with time during the SMT of  $\alpha$ -DL-met into  $\gamma$ -DL-met at 25 °C,  $C_0 = 40.5 \text{ kg/m}^3$  and  $K_{D\alpha} = 7.4766 \times 10^{-9} \text{ m/s}$ .

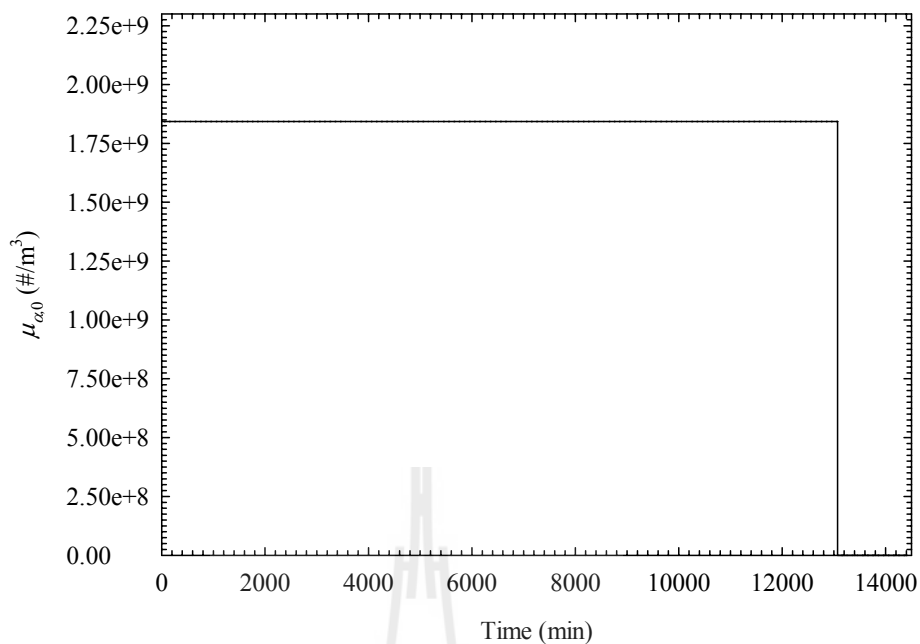


**Figure C.9** The change of  $\mu_{\alpha,0}$  with time during the SMT of  $\alpha$ -DL-met into  $\gamma$ -DL-met at 25 °C,  $C_0 = 37.0 \text{ kg/m}^3$  and  $K_{D\alpha} = 7.4766 \times 10^{-9} \text{ m/s}$ .

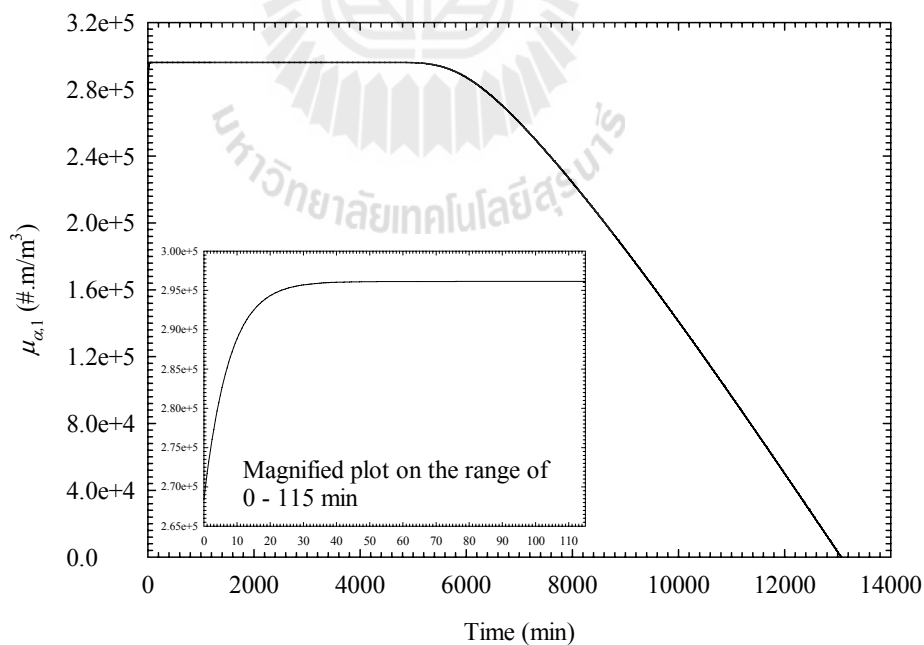


**Figure C.10** The change of  $\mu_{\alpha,1}$  with time during the SMT of  $\alpha$ -DL-met into  $\gamma$ -DL-met at 25 °C,  $C_0 = 37.0 \text{ kg/m}^3$  and  $K_{D\alpha} = 7.4766 \times 10^{-9} \text{ m/s}$ .

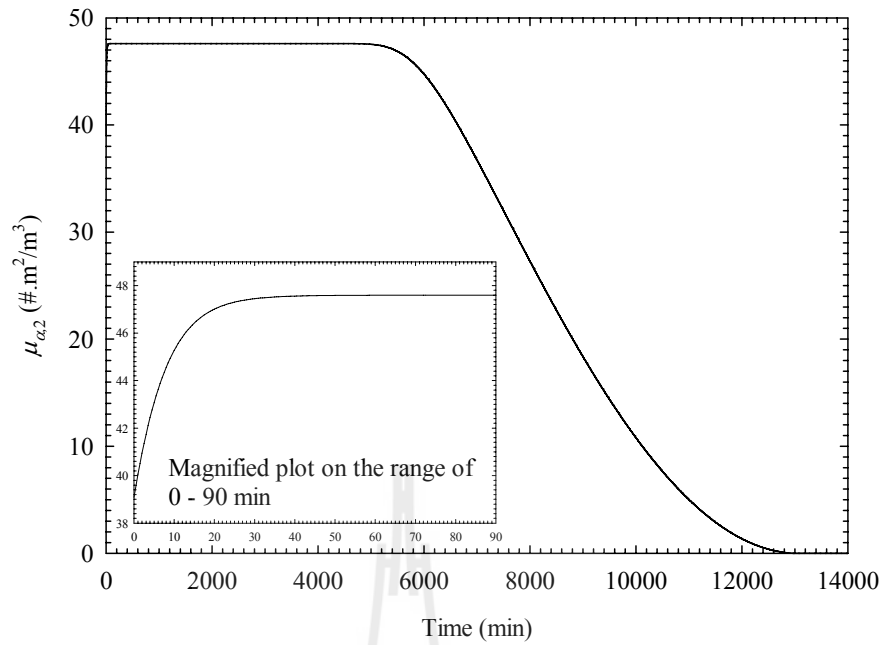


**Figure C.11** The change of  $\mu_{\alpha,2}$  with time during the SMT of  $\alpha$ -DL-met into  $\gamma$ -DL-met at 25 °C,  $C_0 = 37.0 \text{ kg/m}^3$  and  $K_{D\alpha} = 7.4766 \times 10^{-9} \text{ m/s}$ .

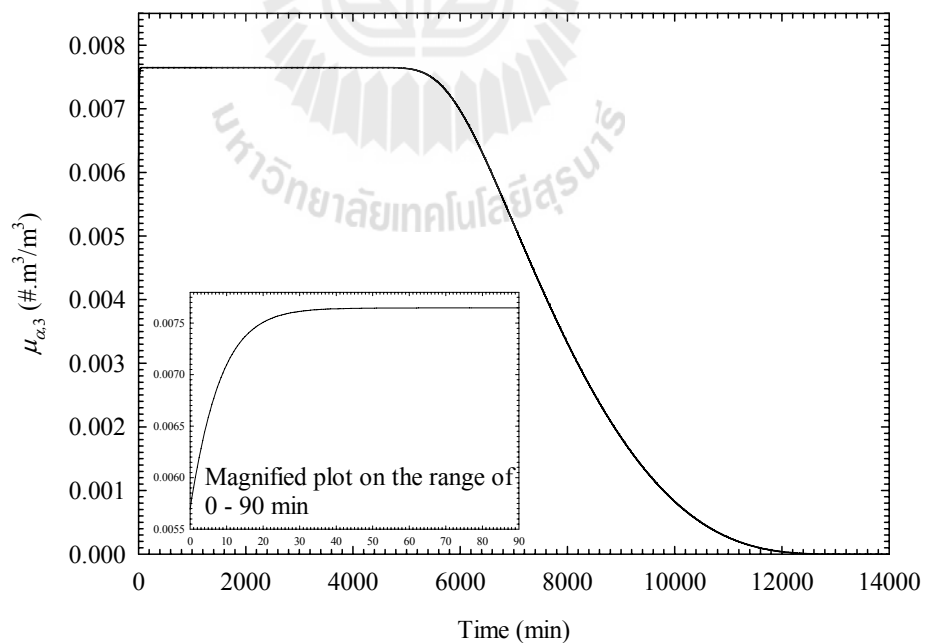


**Figure C.12** The change of  $\mu_{\alpha,3}$  with time during the SMT of  $\alpha$ -DL-met into  $\gamma$ -DL-met at 25 °C,  $C_0 = 37.0 \text{ kg/m}^3$  and  $K_{D\alpha} = 7.4766 \times 10^{-9} \text{ m/s}$ .

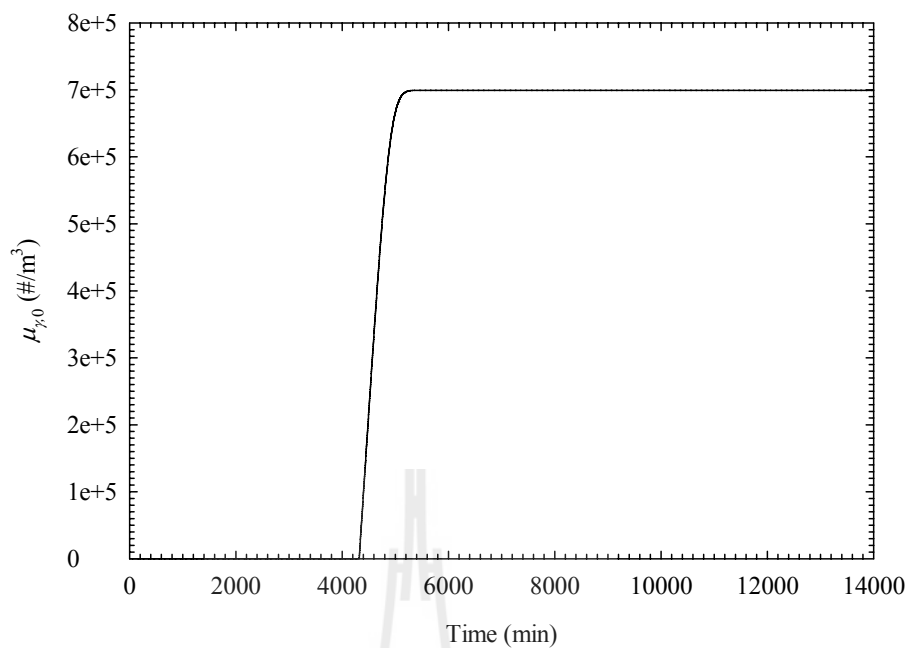


**Figure C.13** The change of  $\mu_{\gamma,0}$  with time during the SMT of  $\alpha$ -DL-met into  $\gamma$ -DL-met at 25 °C,  $C_0 = 37.0 \text{ kg/m}^3$  and  $K_{D\alpha} = 7.4766 \times 10^{-9} \text{ m/s}$ .

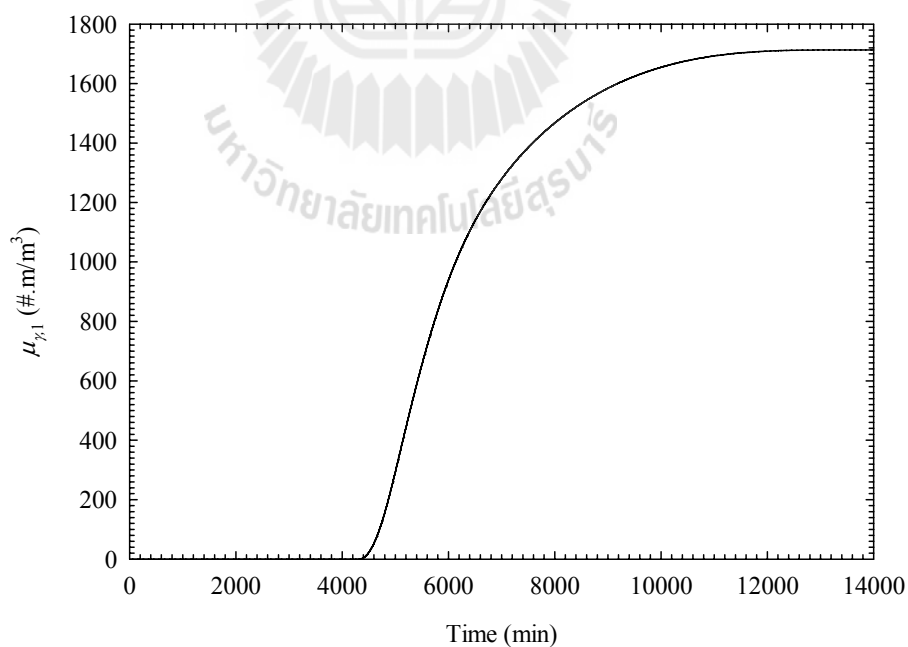


**Figure C.14** The change of  $\mu_{\gamma,1}$  with time during the SMT of  $\alpha$ -DL-met into  $\gamma$ -DL-met at 25 °C,  $C_0 = 37.0 \text{ kg/m}^3$  and  $K_{D\alpha} = 7.4766 \times 10^{-9} \text{ m/s}$ .

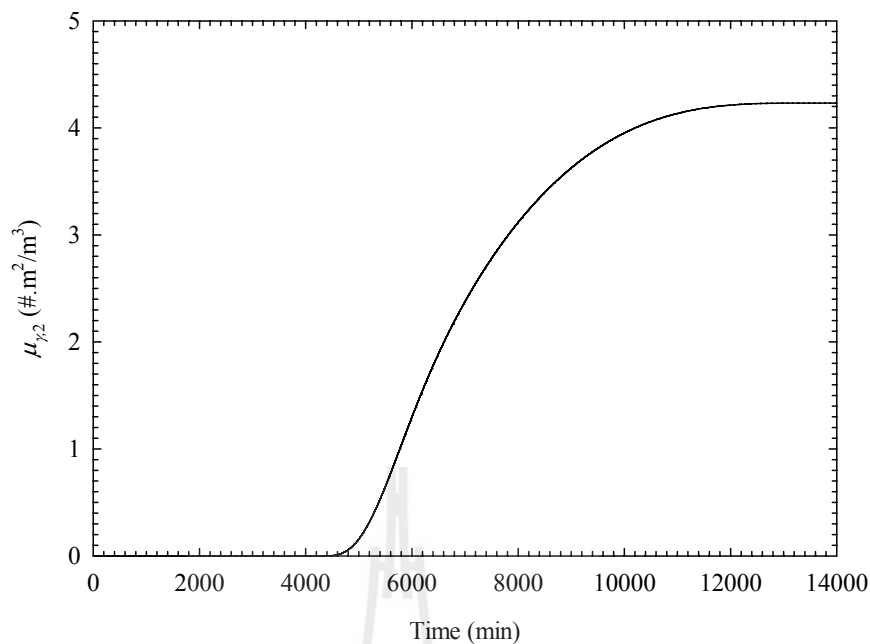


**Figure C.15** The change of  $\mu_{\gamma,2}$  with time during the SMT of  $\alpha$ -DL-met into  $\gamma$ -DL-met at 25 °C,  $C_0 = 37.0 \text{ kg/m}^3$  and  $K_{D\alpha} = 7.4766 \times 10^{-9} \text{ m/s}$ .

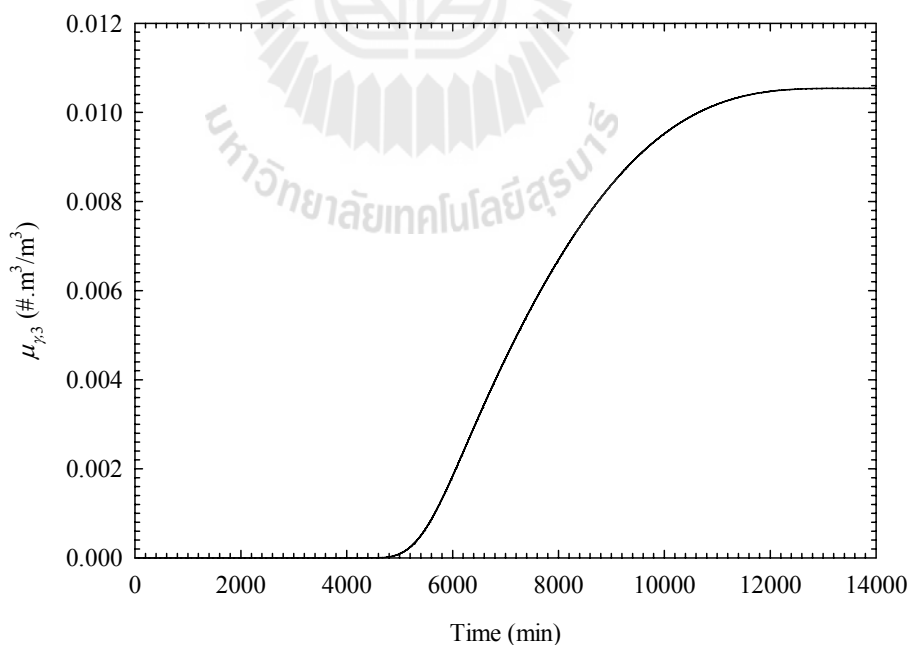
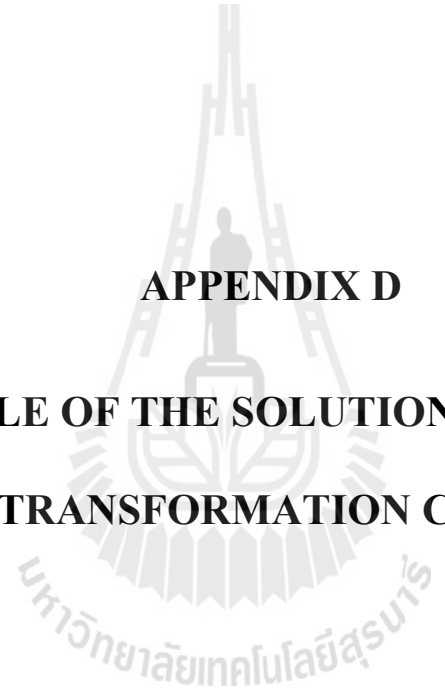


**Figure C.16** The change of  $\mu_{\gamma,3}$  with time during the SMT of  $\alpha$ -DL-met into  $\gamma$ -DL-met at 25 °C,  $C_0 = 37.0 \text{ kg/m}^3$  and  $K_{D\alpha} = 7.4766 \times 10^{-9} \text{ m/s}$ .



**APPENDIX D**

**EXAMPLE OF THE SOLUTION-MEDIATED  
TRANSFORMATION CODE**

The example of MATLAB code for simulating the solution-mediated transformation (SMT) of polymorphs of DL-met is shown below.

**Main code (SMT\_DL\_MET.m)**

```

%%%%%%%%%%%%%%%%%%%%%%%%%%%%%%%%%%%%%%%%%%%%%%%%%%%%%%%%%%%%%%%%%%%%%%%%
%%% Main Code – The Simulation of the SMT of DL-Methionine
%%%%%%%%%%%%%%%%%%%%%%%%%%%%%%%%%%%%%%%%%%%%%%%%%%%%%%%%%%%%%%%%%%%%%%%%

clc

clear all

tic

format long e

run initial_mom;           %input the initial moments

%%Specific simulation time which unit is sec

it=1;                     % iteration number

t_end=7*24*60*60;        %end time

t_inc=30;                 %time step

time=(t_inc*[0:t_end/t_inc]);

time(end)=[];

%%Run code once to get initial rate

run constants;

m=ma;                     % 1 means the calculation apply to alpha moment

run alpha_growth;        %calculate the growth of alpha

run alpha_dissolution;   %calculate the dissolution of alpha

```

```

run gamma_nuc;           %calculate the nucleation of gamma
run gamma_growth;       %calculate the growth of gamma
run dmj_dt;             %calculate the change in moment
ma0(it+1)=ma0(it)+(dma0_dt(it)*t_inc);
ma1(it+1)=ma1(it)+(dma1_dt(it)*t_inc);
if ma0(it+1)<=0||ma1(it+1)<=0    %calculate the mean particle size
    La_mean(it+1)=0;
else
    La_mean(it+1)=ma1(it+1)/ma0(it+1);
end
ma2(it+1)=ma0(it+1)*La_mean(it+1)^2;
ma3(it+1)=ma0(it+1)*La_mean(it+1)^3;
ca(it+1)=crystal_density*kva*ma3(it+1); %calculate the solid concentration of alpha
m=mg;                    %2 means the calculation apply to gamma moment
run alpha_growth;
run alpha_dissolution;
run gamma_nuc;
run gamma_growth;
run dmj_dt;
mg0(it+1)=mg0(it)+(dmg0_dt(it)*t_inc);
mg1(it+1)=mg1(it)+(dmg1_dt(it)*t_inc);
mg2(it+1)=mg2(it)+(dmg2_dt(it)*t_inc);
mg3(it+1)=mg3(it)+(dmg3_dt(it)*t_inc);
cg(it+1)=crystal_density*kvg*mg3(it+1);%cal. the solid concentration of gamma

```

```

c(it+1)=c(1)+cs-ca(it+1)-cg(it+1);      %calculate the solute concentration
xg(it+1)=cg(it+1)/(cg(it+1)+ca(it+1));   %calculate the mass fraction of gamma
if mg0(it+1)<=0||mg1(it+1)<=0           %calculate the mean particle size
    Lg_mean(it+1)=0;
else
    Lg_mean(it+1)=mg1(it+1)/mg0(it+1);
end
%%Loop code for all time steps to obtain evolution of system
for it=2:t_end/t_inc;
    m=ma;
    run alpha_growth;
    run alpha_dissolution;
    run gamma_nuc;
    run gamma_growth;
    run dmj_dt;
    ma0(it+1)=ma0(it)+(dma0_dt(it)*t_inc);
    ma1(it+1)=ma1(it)+(dma1_dt(it)*t_inc);
    if ma0(it+1)<=0||ma1(it+1)<=0
        La_mean(it+1)=0;
    else
        La_mean(it+1)=ma1(it+1)/ma0(it+1);
    end
    ma2(it+1)=ma0(it+1)*La_mean(it+1)^2;
    ma3(it+1)=ma0(it+1)*La_mean(it+1)^3;

```

```

ca(it+1)=crystal_density*kva*ma3(it+1);

m=mg;

run alpha_growth;

run alpha_dissolution;

run gamma_nuc;

run gamma_growth;

run dmj_dt;

mg0(it+1)=mg0(it)+(dmg0_dt(it)*t_inc);
mg1(it+1)=mg1(it)+(dmg1_dt(it)*t_inc);
mg2(it+1)=mg2(it)+(dmg2_dt(it)*t_inc);
mg3(it+1)=mg3(it)+(dmg3_dt(it)*t_inc);
cg(it+1)=crystal_density*kvg*mg3(it+1);
c(it+1)=c(1)+cs-ca(it+1)-cg(it+1);
xg(it+1)=cg(it+1)/(cg(it+1)+ca(it+1));
if mg0(it+1)<=0||mg1(it+1)<=0
    Lg_mean(it+1)=0;
else
    Lg_mean(it+1)=mg1(it+1)/mg0(it+1);
end

it

end

%% Last entry set to zero to ensure equal vector length
ma0(end)=[]; ma1(end)=[]; ma2(end)=[]; ma3(end)=[]; mg0(end)=[]; mg1(end)=[];
mg2(end)=[]; mg3(end)=[]; ca(end)=[]; cg(end)=[]; c(end)=[]; xg(end)=[];

```

```
La_mean(end)=[]; Lg_mean(end)=[];
```

### Initial moment (initial\_mom.m)

```
%%%%%%%%%%%%%%%%%%%%%%%%%%%%%%%%%%%%%%%%%%%%%%%%%%%%%%%%%%%%%%%%%%%%%%%%%
```

```
%%Initial Moment
```

```
%%%%%%%%%%%%%%%%%%%%%%%%%%%%%%%%%%%%%%%%%%%%%%%%%%%%%%%%%%%%%%%%%%%%%%%%%
```

```
ma=1; % 1 means the calculation apply to alpha moment
```

```
ma0=921404220;
```

```
ma1=921404220*145.623e-6;
```

```
ma2=921404220*(145.6234e-6)^2;
```

```
ma3=921404220*(145.623e-6)^3;
```

```
La_mean=ma1/ma0;
```

```
mg=2; % 2 means the calculation apply to gamma moment
```

```
mg0=0;
```

```
mg1=0;
```

```
mg2=0;
```

```
mg3=0;
```

```
Lg_mean=0; % this means no particles in the initial stage
```

### Constants and initial concentrations (constants.m)

```
%%%%%%%%%%%%%%%%%%%%%%%%%%%%%%%%%%%%%%%%%%%%%%%%%%%%%%%%%%%%%%%%%%%%%%%%%
```

```
%% Constants and Initial Concentrations
```

```
%%%%%%%%%%%%%%%%%%%%%%%%%%%%%%%%%%%%%%%%%%%%%%%%%%%%%%%%%%%%%%%%%%%%%%%%%
```

```
c(1)=40.5; % initial solute concentration in kg/m3
```

```
cs=2; % initial solid concentration in kg/m3
```

```

ca(1)=2;           %initial solid concentration of alpha in kg/m3
cg(1)=0;           %initial solid concentration of gamma in kg/m3
xg(1)=0;           %initial mass fraction of gamma
cai=35.63;         %solubility at 25 degree C in of alpha in kg/m3
cgi=33.60;         %solubility at 25 degree C in of alpha in kg/m3
crystal_density=1340; %crystal density in kg/m3 and both forms are the same
kva=0.524;         %volume shape factor for alpha and assume spherical nuclei
kvg=0.524;         %volume shape factor for gamma and assume spherical nuclei
kaa=3.142;         %area shape factor for alpha and assume spherical nuclei
kag=3.142;         %area shape factor for gamma and assume spherical nuclei
KDa=5.8550e-7;    %dissolution rate constant of alpha in m/s
KGa=8.0767e-7;    %growth rate constant of alpha in m/s
KGg=3.1450e-7;    %growth rate constant of gamma in m/s
A=3.4700e+11;     %pre-exp. factor for nucleation kinetic of gamma in #/m3/s
B=0.0813;         %thermodynamic parameter for nucleation kinetic of gamma
t_ind=25*60;      %induction time for nucleation of gamma in sec

```

### **Growth of $\alpha$ -DL-met (alpha\_growth.m)**

```

%%%%%%%%%%%%%%%%%%%%%%%%%%%%%%%%%%%%%%%%%%%%%%%%%%%%%%%%%%%%%%%%%%%%%%%%
%%% Alpha Growth
%%%%%%%%%%%%%%%%%%%%%%%%%%%%%%%%%%%%%%%%%%%%%%%%%%%%%%%%%%%%%%%%%%%%%%%%
sa(it)=c(it)/cai;      %supersaturation with respect to alpha
for m=mg               %ignore alpha growth if solving gamma moments
    G_alpha(it,1)=0;

```

end

if sa(it)<=1

    G\_alpha(it,1)=0;

else

    G\_alpha(it,1)=KGa\*(sa(it)-1);

end

### **Dissolution of $\alpha$ -DL-met (alpha\_dissolution.m)**

%%%

%%% Alpha Dissolution

%%%

sa(it)=c(it)/cai;                      % supersaturation with respect to alpha

if sa(it)>=1||ca(it)<=0

    D\_alpha(it,1)=0;

else

    D\_alpha(it,1)=KDa\*(1-sa(it));

End

### **Nucleation of $\gamma$ -DL-met (gamma\_nuc.m)**

%%%

%%% Gamma Nucleation

%%%

sg(it)=c(it)/cgi;                      % supersaturation with respect to gamma

for m=ma                                % ignore alpha nucleation if solving gamma moments

    J\_gamma(it,1)=0;

```

end

if sg(it)<=1
    J_gamma(it,1)=0;
elseif it>=( t_ind /t_inc)+1 & sg(it)>1
    J_gamma(it,1)=A*sg(it)*exp(-B/((log(sg(it)))^2));
else
    J_gamma(it,1)=0;
end

```

### **Growth of $\gamma$ -DL-met (gamma\_growth.m)**

```

%%%%%%%%%%%%%%%%%%%%%%%%%%%%%%%%%%%%%%%%%%%%%%%%%%%%%%%%%%%%%%%%%%%%%%%%
%%% Gamma Growth
%%%%%%%%%%%%%%%%%%%%%%%%%%%%%%%%%%%%%%%%%%%%%%%%%%%%%%%%%%%%%%%%%%%%%%%%
sg(it)=c(it)/cgi;           %supersaturation with respect to gamma
for m=ma                    %ignore alpha growth if solving gamma moments
    G_gamma(it,1)=0;
end

if sg(it)<=1
    G_gamma(it,1)=0;
elseif it>=(t_ind/t_inc)+1 & sg(it)>1
    G_gamma(it,1)=KGg*(sg(it)-1);
else
    G_gamma(it,1)=0;
end

```

**Rate of change of moment (dmj\_dt.m)**

```
%%%%%%%%%%%%%%%%%%%%%%%%%%%%%%%%%%%%%%%%%%%%%%%%%%%%%%%%%%%%%%%%%%%%%%%%%
```

```
%%% Calculation Rate of Change of Moments
```

```
%%%%%%%%%%%%%%%%%%%%%%%%%%%%%%%%%%%%%%%%%%%%%%%%%%%%%%%%%%%%%%%%%%%%%%%%%
```

```
%% Calculatre the rate of change of alpha moments
```

```
if ma1(it)>0
```

```
    ma0(it)=921404220;
```

```
    dma0_dt(it)=0;
```

```
else
```

```
    ma0(it)=0;
```

```
    dma0_dt(it)=0;
```

```
end
```

```
dma1_dt(it)=G_alpha(it)*ma0(it)-D_alpha(it)*ma0(it);
```

```
%% Calculatre the rate of change of gamma moments
```

```
if it>=(t_ind/t_inc)+1
```

```
    dmj0_dt(it)=J_gamma(it);
```

```
else
```

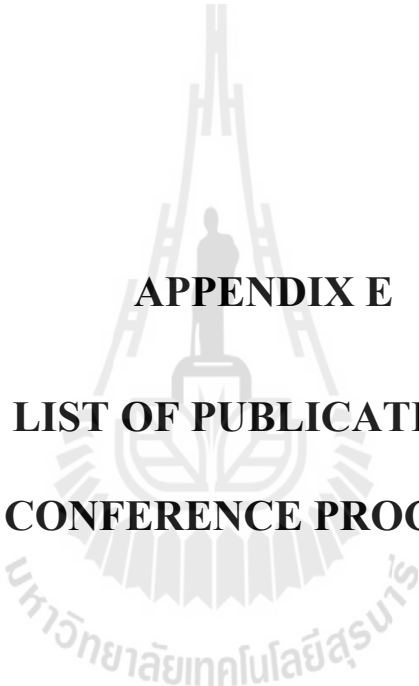
```
    dmj0_dt(it)=0;
```

```
end
```

```
dmj1_dt(it)=G_gamma(it)*mj0(it);
```

```
dmj2_dt(it)=2*G_gamma(it)*mj1(it);
```

```
dmj3_dt(it)=3*G_gamma(it)*mj2(it);
```



**APPENDIX E**  
**LIST OF PUBLICATIONS**  
**AND CONFERENCE PROCEEDINGS**

## Referred Journals

Wantha, L. and Flood, A.E. (2011). **Crystal growth rates and secondary nucleation threshold for  $\gamma$ -DL-methionine in aqueous solution.** Journal of Crystal Growth 318(1): 117-121.

Wantha, L. and Flood, A.E. (2011). **Growth and dissolution kinetics of  $\alpha$  and  $\gamma$  polymorphs of DL-methionine.** Journal of Crystal Growth. (Article in Press)

## Conference Proceedings

Wantha, L. and Flood, A.E. (2011). **Nucleation kinetics of the  $\gamma$  polymorph of DL-methionine.** 18<sup>th</sup> BIWIC International Workshop on Industrial Crystallization. Delft, The Netherlands.

Wantha, L. and Flood, A.E. (2010). **Kinetics of crystallization of  $\alpha$ -DL-methionine.** 17<sup>th</sup> Regional Symposium on Chemical Engineering (RSCE2010). Bangkok, Thailand.

Wantha, L. and Flood, A.E. (2009). **Thermodynamics and kinetics of crystallization of the polymorphs of DL-methionine.** 16<sup>th</sup> BIWIC International Workshop on Industrial Crystallization. Lappeenranta, Finland.

Wantha, L. and Flood, A.E. (2009). **An investigation of the secondary nucleation threshold and growth of  $\gamma$ -DL-methionine in aqueous solution.** 19<sup>th</sup> Thailand Chemical Engineering and Applied Chemistry Conference. Kanchanaburi, Thailand.

Wantha, L. and Flood, A.E. (2008). **Polymorphism and thermodynamics of DL-methionine.** 18<sup>th</sup> Thailand Chemical Engineering and Applied Chemistry Conference. Pattaya, Thailand.

## Conference Abstracts

- Wantha, L. and Flood, A.E. (2011). **Crystallization kinetics of polymorphs of DL-methionine.** The Commission on Higher Education Congress IV. Chonburi, Thailand.
- Wantha, L. and Flood, A.E. (2011). **Growth and dissolution kinetics of  $\alpha$  and  $\gamma$  polymorphs of DL-methionine.** 5<sup>th</sup> Asian Conference on Crystal Growth and Crystal Technology (CGCT-5). Suntec, Singapore.
- Wantha, L. and Flood, A.E. (2010). **Crystal growth rates for  $\gamma$ -DL-methionine in aqueous solution.** 16<sup>th</sup> International Conference on Crystal Growth (ICCG-16). Beijing, People's Republic of China.
- Wantha, L. and Flood, A.E. (2010). **Crystal growth and dissolution rates for  $\alpha$ -DL-methionine in aqueous solution.** 14<sup>th</sup> International Summer School on Crystal Growth (ISSCG-14). Dalian, People's Republic of China.
- Wantha, L. and Flood, A.E. (2009). **Polymorphism and kinetics of crystallization of DL-methionine.** International Symposium of East Asian Young Scientists Follow-up Program on Environment- and Bio-Engineering. Hyogo, Japan.
- Wantha, L. and Flood, A.E. (2009). **Polymorphism and polymorphic transformation of DL-methionine crystals.** 42<sup>nd</sup> IUPAC Congress: Chemistry Solutions. Glasgow, UK.
- Wantha, L. and Flood, A.E. (2008). **Polymorph characterization and solubility measurement of DL-methionine.** The Commission on Higher Education Congress I. Chonburi, Thailand.



## Crystal growth rates and secondary nucleation threshold for $\gamma$ -DL-methionine in aqueous solution

Lek Wantha, Adrian E. Flood\*

School of Chemical Engineering, Suranaree University of Technology, 111 University Avenue, Muang District, Nakhon Ratchasima 30000, Thailand

### ARTICLE INFO

Available online 18 November 2010

#### Keywords:

- A1. Secondary nucleation threshold
- A2. Batch crystallization
- A2. Growth from solution
- B1.  $\gamma$ -DL-Methionine

### ABSTRACT

The Secondary Nucleation Threshold (SNT) of  $\gamma$ -DL-methionine (DL-met) in aqueous solution was measured for the temperature range 10–61 °C. The width of the SNT is weakly temperature dependent with slightly smaller induction times at higher temperatures. Seeded batch crystallizations of  $\gamma$ -DL-met were performed isothermally at 10, 25, and 40 °C in an agitated batch crystallizer, and within the SNT region to avoid nucleation. The effect of the initial supersaturation and seed mass on crystal growth were also studied at 25 °C. The initial growth rate (during the first 20 min of the batch) is significantly higher than subsequent crystal growth, a phenomenon previously seen with other species. The measured growth rates are independent of seed mass, as expected, for the usable portion of the growth rate data. The growth rates were found to linearly depend on the relative supersaturation of the total DL-met in the system. The growth rate constants increase with increasing temperature and follow an Arrhenius relationship. The growth kinetics of the  $\gamma$ -DL-met will be used to study in order to begin characterization of the polymorphic transformations and the overall crystallization rate of DL-met.

© 2010 Elsevier B.V. All rights reserved.

### 1. Introduction

Polymorphism occurs when a compound can exist in more than one crystalline form [1]. These crystalline forms contain the same molecules but have a different arrangement of molecules within the crystalline lattice. Polymorphs can have different mechanical, thermal, physical, and chemical properties, which greatly influence their suitability for a wide variety of uses, particularly for pharmaceutical products, and affects their suitability for further processing.

Crystallization processes where polymorphs form may consist of competitive nucleation, crystal growth, and the transformation from the metastable to the stable form. In most cases, the most important factor for the control of polymorphic crystallization is the nucleation process. However, the mechanism of each elementary step in the crystallization process needs to be clear in relation to the operational conditions in order to selectively crystallize polymorphs. The most important process in crystallization of polymorphs is Solution-Mediated Transformation (SMT) which consists of the dissolution of the metastable form and the growth of the stable form [2].

The crystal growth process is described by two successive mechanisms, mass transfer (by diffusion or convection) of solute molecules from the bulk solution to the crystal surface and

integration of solute molecules into the surface (a reaction step) [3]. Crystals can grow without significant birth of new crystals (nuclei) in a metastable zone which is often exhibited by supersaturated solutions. When the supersaturation is sufficiently high, secondary nucleation in the presence of prior crystals occurs; the limit of this regime is referred to as the metastable limit for secondary nucleation [4] or the Secondary Nucleation Threshold (SNT), depending on the method of measurement. The secondary nucleation threshold is the upper limit of the metastable zone with regard to secondary nucleation. Nucleation is typically avoided or minimized in crystallization processes because it is difficult to control and gives a bad product size distribution. In batch processes the operation is usually undertaken in the metastable zone, and crystallization is initiated through the addition of seed crystals, thus avoiding large amounts of nucleation.

DL-methionine (DL-met) is an essential amino acid in the human diet, and is also used as dietary component in poultry and animal feeds. It is also used in active pharmaceutical ingredients, and as a precursor to other amino acids. DL-met has previously been shown to exhibit polymorphism and exists in the solid phase as  $\alpha$ -DL-met,  $\beta$ -DL-met, and  $\gamma$ -DL-met [5,6].  $\alpha$ -DL-met and  $\beta$ -DL-met forms are almost equally stable [5], and the crystal structures of each polymorph are known [7]. Single crystals of both forms were grown from an ethanol–water solution by slow evaporation and occur as soft plates.  $\beta$ -DL-met was discovered accidentally while attempting to grow  $\alpha$ -DL-met crystals of greater plate thickness. Moreover,  $\alpha$ -DL-met crystals can be obtained by the reaction crystallization of aqueous solutions of sodium methioninate

\* Corresponding author. Tel.: +66 44224497; fax: +66 44224609.  
E-mail address: [adrianf@g.sut.ac.th](mailto:adrianf@g.sut.ac.th) (A.E. Flood).

(Na-met) using liquid acids such as hydrochloric, acetic, nitric, sulfuric, or formic acids [6]. Matsuoka et al. [6] reported the third polymorph,  $\gamma$ -DL-met, as well as its preparation method and crystal structure.  $\gamma$ -DL-met crystals were obtained by reaction crystallization of aqueous solutions of Na-Met with a solid benzoic acid, or by cooling crystallization of aqueous solutions of DL-met.

The transformation of DL-met crystals in solution has been reported to consist of the Solid-State Transformation (SST) of  $\gamma$ -DL-met to  $\alpha$ -DL-met in the charged crystals and Solvent-Mediated Transformation (SMT) of  $\alpha$ -DL-met to  $\gamma$ -DL-met, which is caused by the dissolution of  $\alpha$ -DL-met and crystal growth of  $\gamma$ -DL-met [8]. This indicates that the crystallization kinetics (particularly dissolution of  $\alpha$ -DL-met and growth of  $\gamma$ -DL-met) for the polymorphs produced also have to be studied in order to characterize the phase transformation in the system.

There is no published data on the SNT and crystal growth kinetics of  $\gamma$ -DL-met in aqueous solution. Therefore, in the present study the growth rate of the  $\gamma$ -DL-met in aqueous solution was measured to attempt to begin to characterize the polymorphic transformation in solution. The SNT of this system was determined to ensure that the system is operated under convenient non-nucleating conditions.

## 2. Materials and methods

### 2.1. Materials

DL-met (>99%, Acros Organics) and deionized water were used to prepare the supersaturated solution in all experiments.  $\gamma$ -DL-met was prepared by cooling crystallization of aqueous solutions of DL-met as follows. DL-met (21 g) was dissolved in 350 mL of water in a 0.5 L batch crystallizer maintained above 60 °C. This solution was continuously agitated by an overhead stirrer at 300 rpm, and the solution was cooled and maintained at 25 °C, after which the crystals were removed and filtered. Since these crystals were too large for use as seed crystals a further crystallization was performed. The solution at 25 °C was heated to 30 °C, then cooled to 5 °C and held at this temperature for 24 h. After 24 h, the suspension was filtered, washed, and dried.  $\gamma$ -DL-met was identified using X-ray powder diffractometry (Bruker axs, D5005). The pure  $\gamma$ -DL-met crystals were sieved, and the cut between 180 and 250  $\mu$ m was used as seeds for crystal growth rate measurement.

### 2.2. Secondary nucleation threshold measurement

Secondary nucleation threshold experiments were performed at 10, 25, 40, and 61 °C in a 0.5 L batch crystallizer for a range of supersaturated solutions containing  $\gamma$ -DL-met seed crystals using a method similar to that of Srisa-nga et al. [4]. A series of supersaturated solutions were prepared and heated to 20 °C above the experimental temperature for a period of 30 to 40 min to ensure that no ghost nuclei remained in the solution. Approximately 3 mg of sieved  $\gamma$ -DL-met crystals, 75–105  $\mu$ m in size, was added to each solution to induce secondary nucleation. Nucleation was observed by the naked eye at particular time intervals, with nucleation being indicated by precipitation or clouding due to the very fine nuclei particles. The clouding occurring in the experiments was clearly visible and the distinction between solutions that had precipitated at a particular measurement time and those had not precipitated was clear. The highest concentration solution that had not nucleated at a particular time and the lowest concentration that had nucleated were both recorded. All experiments were duplicated to check reproducibility.

### 2.3. Crystal growth rate measurement

The growth kinetics of  $\gamma$ -DL-met were studied via seeded batch desupersaturation experiments using time dependent measurements of both Particle Size Distributions (PSDs) and solute concentrations [9,10]. Experiments were performed at 10, 25, and 40 °C in a 0.5 L batch crystallizer agitated at 350 rpm by an overhead stirrer, and performed within the SNT region to avoid nucleation. The solute concentration in the clear liquor was measured periodically using dry substance determination [10], and the PSD of crystalline samples was measured using a Malvern Mastersizer/E (Malvern Instrument, Mastersizer S). Volume percent distributions were converted mathematically to number density distributions in order to determine the number mean growth rate of the crystals, which is most suitable for use in population balance modeling. Nucleation was not detected in any seeded batch crystallization for growth determination. Growth rate was determined as the time rate of change of the number mean crystal size.

Desupersaturation experiments were performed on supersaturated solutions within the SNT region that had previously been heated to 20 °C above the experimental temperature for a period of 30 to 40 min to ensure that no ghost nuclei remained in the solution. The solutions were then cooled to the experimental temperature, after which a quantity of dry seeds were fed to the crystallizer. A small volume of the suspension was sampled at particular times during the batch to determine the PSDs and solute concentration. All experiments were duplicated to determine reproducibility.

## 3. Results and discussion

### 3.1. Secondary nucleation threshold

The effect of induction time on the measured SNT at different temperatures is shown in Fig. 1. In this figure, the upper point on each vertical line represents the lowest absolute supersaturation that had nucleated and the lower point represents the highest absolute supersaturation that had not nucleated. This means that the true value of the SNT must lie between these two points. The mean value of these two points is an approximation for the true SNT at this experimental time. This figure shows the time dependence of the SNT, with the SNT decreasing as the induction time increases. In

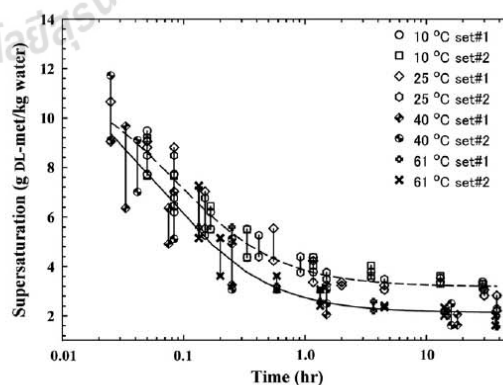


Fig. 1. The time dependence of the secondary nucleation zone width based on DL-met concentrations at temperatures of 10, 25, 40, and 61 °C. The dashed line represents the model for data at 10 and 25 °C. The solid line represents the model for 40 and 61 °C.

terms of absolute supersaturation, initial time SNT is about 11.8 g of DL-met/kg of water for 10 and 25 °C, and 12.1 g of DL-met/kg of water for 40 and 61 °C. At large induction times, greater than 50 h, the SNT is about 3.2 g of DL-met/kg of water for 10 and 25 °C, and 2.2 g of DL-met/kg of water for 40 and 61 °C. After 2 days there were still some solutions of low supersaturation which had not nucleated.

Since the SNTs at temperatures of 10 and 25, and 40 and 61 °C do not overlap when plotted in terms of absolute value of supersaturation, the induction time dependence of the SNT is plotted separately. This indicates that temperature has an effect on the SNT over the range of temperatures that DL-met is likely to be crystallized.

The data in Fig. 1 were fitted with a hyperbolic decay with three parameters. Eqs. (1) and (2) show the fitted equations, where  $C$  represents the total DL-met concentration (g of DL-met/kg of water) for the SNT,  $C^*$  is the solubility, and  $t_{ind}$  is the observation time in hours.

$$C - C^* = 3.1828 + \frac{0.7266}{0.0845 + t_{ind}} \quad (\text{For } 5^\circ\text{C} < T < 40^\circ\text{C}) \quad (1)$$

$$C - C^* = 2.1287 + \frac{0.6519}{0.0651 + t_{ind}} \quad (\text{For } 40^\circ\text{C} < T < 70^\circ\text{C}) \quad (2)$$

The solubility data of  $\alpha$ -DL-met and  $\gamma$ -DL-met in the temperature range of 5–70 °C has been measured previously [11] and is plotted as a function of temperature in Fig. 2. The solubility of  $\gamma$ -DL-met (g of DL-met/kg of water) was fitted using a cubic polynomial with the result shown in Eq. (3), where  $T$  represents the experimental temperature in °C.

$$C^* = 18.23 + 5.053 \times 10^{-1}T + 2.436 \times 10^{-3}T^2 + 8.410 \times 10^{-5}T^3 \quad (3)$$

Substitution of Eq. (3) into Eq. (1) gives the SNT concentration as a function of time between 5 and 40 °C, and substitution of Eq. (3) into Eq. (2) gives the SNT concentration as a function of time between 40 and 70 °C.

The induction time dependence of SNT of  $\gamma$ -DL-met in aqueous solution is shown in Fig. 2. SNT shows limitations on either the operating concentration or the batch time to ensure that nuclei are not formed, so it is very important for control of seeded batch crystallizations. For example, when the crystallization is performed at 25 °C and the operating time is within 1 h, the initial concentration that can operate without a significant birth of new crystals is up to 37 g of DL-met/kg of water.

The SNT of  $\alpha$ -DL-met was not measured in this work since experiments were performed in regions where only the  $\gamma$ -form will

nucleate. The SNT technique used by Lu et al. [12] is appropriate for the metastable form. However, growth experiments for the  $\alpha$ -form can only be performed within the area between the SNT of  $\gamma$ -DL-met and the solubility of  $\alpha$ -DL-met. This is reasonable for the temperature range 5–35 °C.

### 3.2. Crystal growth kinetics

An example of PSDs from a batch run at 25 °C is shown in Fig. 3. The PSD is plotted on a log-scale to show that the volume-based PSD is a log-normal distribution, and hence appears as a normal distribution on a log-scale. Photomicrographs of seed crystals and product crystals from a batch run at 25 °C were also analyzed. These indicated that there is no nucleation occurring during the growth process because there is only one peak in the PSD and no particles smaller than the seed crystals. PSDs of product crystals are uniform, which lead to a good product quality.

The morphology of  $\gamma$ -DL-met is thin rod-like, prism-like, or plate-like having a hexagonal cross section [6,13]. For this study the shape of the seed crystals ( $\gamma$ -DL-met crystals) obtained from an aqueous solution is plate-like having a hexagonal cross section, but the shape is not perfect. After the growth process the morphology of the crystals has not changed, but the shape is more perfect than the seed crystals. This means that there is no phase transformation during the growth of the  $\gamma$ -DL-met crystals in aqueous solution. Similar results are seen at all experimental temperatures (10, 25, and 40 °C), which indicates that  $\gamma$ -DL-met is the stable polymorphic form at these temperatures. The improved shape and features of the product crystals show that correct operation of the batch can lead to improved product quality.

A log-normal volume-based PSD indicates that the number distribution is also log-normal with the same geometric standard deviation [14]. The number mean size may then be calculated from the following equation:

$$\ln X_{NL} = \ln X_{mV} - 2.5 \ln^2 \sigma_g \quad (4)$$

where  $X_{NL}$  is the number mean crystal size,  $X_{mV}$  is the median of the volume distribution, and  $\sigma_g$  is the geometric standard deviation of the volume distribution. The PSDs of this work were confirmed by discretizing the volume density distribution into small elements (of 1  $\mu\text{m}$  width), and calculating the number of particles in each element and number mean crystal size. The geometric standard deviation of the volume distribution was constant over the time

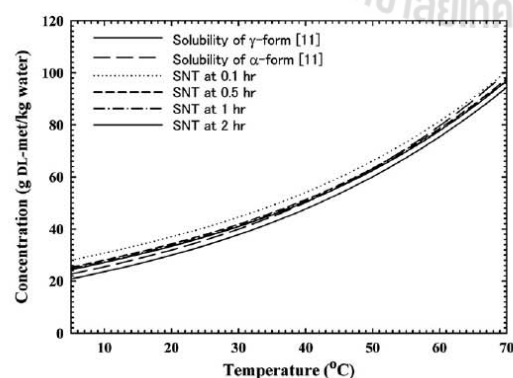


Fig. 2. Secondary nucleation thresholds for  $\gamma$ -DL-met at operating times of 0.1, 0.5, 1.0, and 2.0 h.

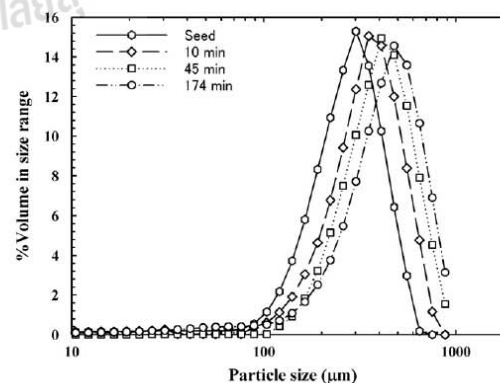


Fig. 3. Particle size distributions of seed and product crystals from a batch run at 25 °C and  $\sigma_0 = 0.11$ .

period of the experiment, indicating common history seed [4]. The mean growth rate was determined as the time rate of change of the number mean crystal size. The growth rate was calculated directly from the slope of a plot between the number mean crystal size and time of each measurement. Fig. 4 is an example of this plot.

Fig. 4 also shows the batch crystallization profiles for the condition of 0.5 g of  $\gamma$ -DL-met seed crystals having an average size of approximately 178  $\mu\text{m}$ , with the crystallization temperature being 25 °C and for initial relative supersaturations ( $\sigma$ ) equal to 0.09 and 0.11. Fig. 4 shows that an increase in the initial supersaturation results in an increase in the final crystal sizes. This is since the higher solute concentration in excess of the solubility leads to a higher amount of solute addition onto the same seed mass. In addition, experiments varying the seed mass show that an increase of the total seed surface leads to a faster decrease in supersaturation, and smaller final crystal sizes. This is since the higher seed surface area results in an increased solid integration rate through crystal growth. The higher seed mass leads to a smaller final crystal sizes since the same amount of solute is added to a larger number of seed crystals. The desupersaturation rate increases with increasing temperature since the integration of solute into the crystal surface increases with increasing temperature.

The growth rates were calculated using the number mean crystal size. The crystal growth experiments allowed growth kinetics to be determined as a function of relative supersaturation, as shown in Figs. 5 and 6. It can be seen that, at constant temperature, the growth rates increase with increasing supersaturation. The results of the experiments with different initial supersaturation (Fig. 5) agree very well for all but the first three data points of each experiment, where there were different growth rates predicted for the same supersaturation value. Also the results of the experiments with different seed mass (Fig. 6) agree very well for all but at early periods of the experiment, where there is some differences between data for different seed masses.

The explanation for the difference between the growth rates at early periods of the experiment is unknown, although earlier this has been noted in many other species, with the phenomenon initially being seen for fructose [15]. Many explanations have been proposed for this behavior including initial fast crystal growth as seed crystals repair their surface; later crystal growth being slowed by slow surface adsorption of impurity molecules [15]; and the effect of growth rate history on the crystal surface [16–19].

The unusually high growth rates during the early period of all experiments were ignored in subsequent analysis of crystallization kinetics. The growth kinetics can be described for each set of conditions by the power-law model [20]

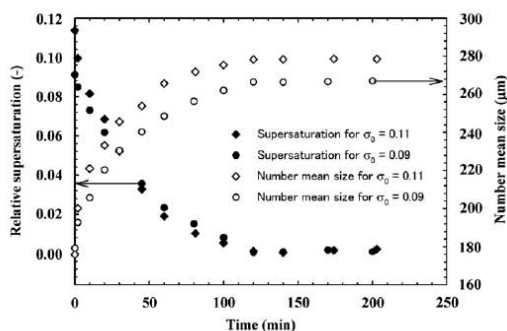


Fig. 4. Desupersaturation curves and time dependence of crystal sizes from a batch run at 25 °C with different initial supersaturations.

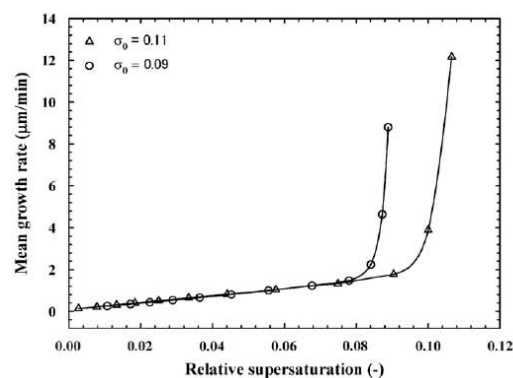


Fig. 5. Mean crystal growth rates for  $\gamma$ -DL-met as a function of relative supersaturation at 25 °C with different initial supersaturations.

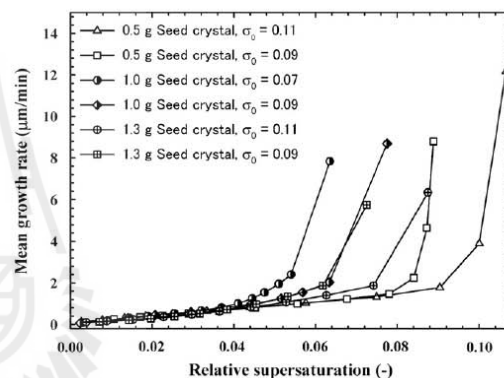


Fig. 6. Mean crystal growth rates for  $\gamma$ -DL-met as a function of relative supersaturation at 25 °C with different seed masses.

$$\bar{G} = K_G \sigma^n \quad (5)$$

where  $\bar{G}$  is the mean growth rate in  $\mu\text{m}/\text{min}$ ,  $K_G$  is the growth rate constant in  $\mu\text{m}/\text{min}$ ,  $\sigma$  is the relative supersaturation, and  $n$  is the growth rate order. The experimental data were fitted using Eq. (5), with the result shown in Fig. 7. The resulting equations show that the growth rate order is unity for all conditions. The values of growth rate constant ( $K_G$ ) obtained from linear regression of the experimental data (Fig. 7) are 10.39, 18.87, and 27.83  $\mu\text{m}/\text{min}$ , respectively, for 10, 25, and 40 °C. This indicates that the growth rate constant is strongly temperature dependent. The growth rate constant can be modeled by Arrhenius relationship of the form [21]

$$K_G = k_G \exp\left[\frac{-E_G}{RT}\right] \quad (6)$$

where  $E_G$  is the activation energy of growth in  $\text{kJ}/\text{mol}$ ,  $T$  is the temperature in  $\text{K}$ , and  $R$  is the ideal gas constant (8.314  $\text{J}/\text{mol}/\text{K}$ ). The results (Fig. 8) indicate an activation energy of growth for  $\gamma$ -DL-met of 24.26  $\text{kJ}/\text{mol}$ .

The value of the growth rate order is very important in understanding the controlling mechanism. In general, a growth rate order of  $n=1$  indicates that mass transfer becomes more important as a rate controlling mechanism and a growth rate order between 1 and

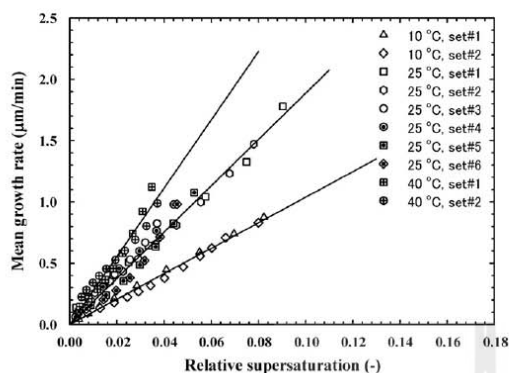


Fig. 7. Mean crystal growth rates of  $\gamma$ -DL-met as a function of relative supersaturation and temperature.

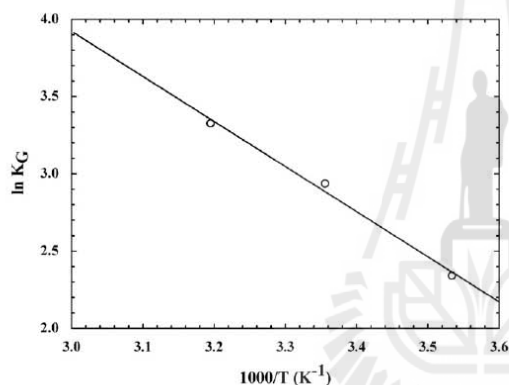


Fig. 8. An Arrhenius plot of the growth rate constant for DL-met for determination of the activation energy of crystal growth.

2 indicate that the surface integration step is more pronounced [21]. In the case of  $\gamma$ -DL-met growth at all temperature studied, with growth rate order of 1, indicates that the mass transfer process plays an important role in explaining the growth process.

Further work needs to be performed in order to characterize both the crystal growth and dissolution kinetics of the  $\alpha$ -form of DL-met, and also the nucleation rates of the two polymorphs in order to fully characterize the phase transitions in the system.

#### 4. Conclusions

The SNT of  $\gamma$ -DL-met in aqueous solution decreases with increasing induction time. The SNT in these measurement units is temperature independent for all induction times. The crystallization of  $\gamma$ -DL-met from aqueous solution should be operated within the SNT region if nucleation is to be avoided. The initial growth rate (at higher supersaturation) is significantly higher than subsequent crystal growth (at lower supersaturation). During the early periods of the experiments there were much larger growth rates than that would be expected from extrapolation of the data determined during the later time periods. This is due to the effect of

the growth history on the crystal surface, with crystals grown more quickly at higher supersaturation having a rougher surface on a microscopic level than the seed crystals they were grown from. The crystal growth rate orders are 1, and the growth rate constants are temperature dependent, and follow an Arrhenius relationship with an activation energy of 24.26 kJ/mol. Further crystal nucleation, growth, and dissolution experiments will be performed on the  $\alpha$ -form. This should allow a complete model of the SMT between the polymorphs to be achieved.

#### Acknowledgement

The authors acknowledge the support of the Commission on Higher Education, Thailand through the program of Strategic Scholarships for Frontier Research Network for the Ph.D. Program Thai Doctoral degree for the support of LW and for the research funding.

#### References

- [1] D.J.W. Grant, Theory and Origin of Polymorphism, in: H.G. Brittain (Ed.), Polymorphism in Pharmaceutical Solids, Drugs and the Pharmaceutical Sciences, Marcel Dekker, New York, 1999, pp. 1–34 Vol. 95.
- [2] M. Kitamura, Strategy for control of crystallization of polymorphs, CrystEngComm, 11 (2009) 949–964.
- [3] A.D. Randolph, M.A. Larson, Theory of Particulate Processes: Analysis and Techniques of Continuous Crystallization, second ed., Academic Press, California, 1988.
- [4] S. Srisa-nga, A.E. Flood, E.T. White, The secondary nucleation threshold and crystal growth of  $\alpha$ -glucose monohydrate in aqueous solution, Cryst. Growth Des. 6 (2006) 795–801.
- [5] A.M. Mathieson, The crystal structures of the dimorphs of DL-methionine, Acta Cryst. 5 (1952) 332–341.
- [6] M. Matsuoka, M. Yamanobe, N. Tezuka, H. Takiyama, H. Ishii, Polymorphism, morphologies and bulk densities of DL-methionine agglomerate crystals, J. Cryst. Growth 198–199 (1999) 1299–1306.
- [7] T. Taniguchi, Y. Takaki, K. Sakurai, The crystal structures of the  $\alpha$ - and  $\beta$ -forms of DL-methionine, Bull. Chem. Soc. Jpn. 53 (1980) 803–804.
- [8] M. Yamanobe, H. Takiyama, M. Matsuoka, Polymorphic transformation of DL-methionine crystals in aqueous solution, J. Cryst. Growth 237–239 (2002) 2221–2226.
- [9] J. Schöll, Nucleation, growth, and solid phase transformations during precipitation processes, Ph.D. thesis, Swiss Federal Institute of Technology Zurich, Zurich, Switzerland, 2006.
- [10] J. Garside, A. Mersmann, J. Nyvlt, Measurement of crystal growth and nucleation rates, second ed., Institute of Chemical Engineering, UK, 2002.
- [11] L. Wantha, A.E. Flood, Thermodynamics and Kinetics of crystallization of the polymorphs of DL-methionine, in: M. Louhi-Kultanen, H. Hatakka (Eds.), Proceedings of the 16th International Workshop on Industrial Crystallization: BIWIC 2009, Lappeenranta University of Technology, Finland, 2009, pp. 173–180.
- [12] J. Lu, X.-J. Wang, X. Yang, C.-B. Ching, Polymorphism and crystallization of famotidine, Cryst. Growth Des. 7 (2007) 1590–1598.
- [13] M. Yamanobe-Hada, A. Ito, H. Shindo, Study of spontaneous cleavage and change in surface structure of DL-methionine crystals, J. Cryst. Growth 275 (2005) e1739–e1743.
- [14] T. Allen, Particle size measurement: Volume 1 Powder Sampling and Particle Size Measurement, fifth ed., Chapman & Hall, London, 1997.
- [15] A.E. Flood, M.R. Johns, E.T. White, Crystal growth rates and dispersion for D-fructose from aqueous ethanol, AIChE J. 46 (2000) 239–246.
- [16] P. Pantarakas, A.E. Flood, Effect of growth rate history on current crystal growth: A second look at surface effects on crystal growth rates, Cryst. Growth Des. 5 (2005) 365–371.
- [17] P. Pantarakas, M. Matsuoka, A.E. Flood, Effect of growth rate history on current crystal growth. 2: Crystal growth of sucrose,  $KAl(SO_4)_2 \cdot 12H_2O$ ,  $KH_2PO_4$ , and  $K_2SO_4$ , Cryst. Growth Des. 7 (2007) 2635–2642.
- [18] A. Promraksa, A.E. Flood, P.A. Schneider, Measurement and analysis of the dextran partition coefficient in sucrose crystallization, J. Cryst. Growth 311 (2009) 3667–3673.
- [19] A.E. Flood, Feedback between crystal growth rates and surface roughness, CrystEngComm 12 (2010) 313–323.
- [20] A.S. Myerson, R. Ginde, Crystals, crystal growth, and nucleation, in: A.S. Myerson (Ed.), Handbook of Industrial Crystallization, second ed., Butterworth-Heinemann, USA, 2002, pp. 33–65.
- [21] J.W. Mullin, Crystallization, fourth ed., Butterworth-Heinemann, Oxford, 2001.



Contents lists available at SciVerse ScienceDirect

Journal of Crystal Growth

journal homepage: [www.elsevier.com/locate/jcrysgr](http://www.elsevier.com/locate/jcrysgr)

## Growth and dissolution kinetics of $\alpha$ and $\gamma$ polymorphs of DL-methionine

Lek Wantha, Adrian E. Flood\*

School of Chemical Engineering, Suranaree University of Technology, 111 University Avenue, Muang District, Nakhon Ratchasima 30000, Thailand

### ARTICLE INFO

#### Keywords:

A1. Dissolution  
 A1. Polymorphism  
 A2. Growth from solution  
 B1.  $\alpha$ -DL-Methionine  
 B1.  $\gamma$ -DL-Methionine

### ABSTRACT

Growth kinetics of the two common polymorphs of DL-methionine ( $\alpha$ -DL-met),  $\alpha$ -DL-met and  $\gamma$ -DL-met, and dissolution kinetics of  $\gamma$ -DL-met, were studied in aqueous solution as part of an attempt to complete an *a-priori* model of the solution-mediated transformation (SMT) of polymorphs in this system, which will then be compared to measured rates of polymorph transformation. The growth rates of  $\alpha$ -DL-met and  $\gamma$ -DL-met were found to be linearly dependent on the relative supersaturation of DL-met in the system. The dissolution rate of  $\gamma$ -DL-met was found to linearly depend on the relative undersaturation of DL-met in the system. Both the growth and dissolution rate constants are temperature dependent and follow an Arrhenius relationship. At all temperatures studied, both the growth rate of  $\alpha$ -DL-met and the dissolution rate of  $\gamma$ -DL-met are faster than the growth rate of  $\gamma$ -DL-met, indicating that if the dissolution is a diffusion controlled process, then the SMT of the polymorphs of DL-met is likely to be controlled by the growth rate of  $\gamma$ -DL-met.

© 2011 Elsevier B.V. All rights reserved.

### 1. Introduction

Crystallization processes, which include transformation of polymorphs consist of the competitive nucleation and crystal growth of the polymorphs, and the transformation from the metastable form to the stable form, usually via a solution-mediated transformation (SMT), which consists of the nucleation and crystal growth of the stable form and the dissolution of the metastable form. To understand and control polymorph formation, the mechanism of each elementary step in the crystallization process needs to be understood and be able to be modeled for inclusion in crystal population balances for each polymorph involved in the transformation.

Crystal growth from solution is a two step process [1]. The first step is the mass transfer (by diffusion and/or convection) of solute molecules from the bulk solution to the surface of the growing crystal. The second step is the adsorption of solute molecules to the surface of the crystal, and integration of the adsorbed molecules into the crystal lattice if they find a suitable integration site via a surface diffusion mechanism before they desorb. The growth rate depends on the level of driving force for crystal growth, which is the supersaturation. Crystals can grow without significant birth of new crystals (nuclei) in a region, which lies between the saturation and nucleation limits, called the metastable zone, which is time dependent.

Dissolution has traditionally been considered as a one step process, which is diffusion controlled. The dissolution rate depends

on the level of the driving force for dissolution, which is the undersaturation.

DL-methionine (DL-met) is an essential amino acid, which has previously been shown to exhibit polymorphism and exists in the solid phase as  $\alpha$ -DL-met,  $\beta$ -DL-met, and  $\gamma$ -DL-met [2,3]. The SMT of DL-met has been studied by Yamanobe et al. [4], which showed that the transformation of  $\alpha$ -DL-met to  $\gamma$ -DL-met occurs via the dissolution of  $\alpha$ -DL-met and crystal growth of  $\gamma$ -DL-met. To improve understanding of the behavior of the polymorphic crystallization of DL-met, growth kinetics, dissolution kinetics, and nucleation kinetics need to be studied. The crystal growth rates of  $\gamma$ -DL-met have been reported in a previous study [5], as have nucleation kinetics for  $\gamma$ -DL-met [6]. In the present study, the growth and dissolution kinetics of  $\alpha$ -DL-met and  $\gamma$ -DL-met were measured and analyzed using batch experiments containing substantial populations of crystals. Similar data can also be obtained using results from measurements in a small growth cell under a microscope [7,8] however this technique may be more time consuming if a large number of crystals are analyzed to obtain the extent of growth rate dispersion. The influence of the supersaturation and temperature on crystal growth, and undersaturation and temperature on dissolution, were investigated. The solubility data used for the calculation of supersaturation and undersaturation of the two polymorphs was from a recent study [5]. The results in the current article will be used with the results of the nucleation study in order to *a-priori* model the SMT of the methionine polymorphs with population balances, and compare the model to measured rates of transformation; this will be discussed in a later article. Previous research has shown that population balance models can be used to fit mechanistic models of nucleation, dissolution and growth in SMT systems, however it is also important to show how accurate the population balance models are when measured data are used to describe the fundamental mechanisms.

\* Corresponding author. Tel.: +66 44224497; fax: +66 44224609.  
 E-mail address: [adrianfl@gsut.ac.th](mailto:adrianfl@gsut.ac.th) (A.E. Flood).

## 2. Materials and methods

### 2.1. Materials

$\alpha$ -DL-met (>99%, Acros Organics), NaOH (>97%, Carlo Erba),  $\text{Na}_2\text{CO}_3$  (>99.5%, Carlo Erba), and HCl (37%, Carlo Erba) were used without further purification. Deionized water was used to prepare all solutions. Sodium methioninate (Na-met) was also required for acidic precipitations of  $\alpha$ -DL-met to prepare  $\alpha$ -DL-met. Aqueous solutions of Na-met were prepared by a method previously described [9]. 50 g of  $\alpha$ -DL-met and 13.5 g of NaOH were dissolved in 166.5 mL of water, with the addition of 20 g of  $\text{Na}_2\text{CO}_3$ . After mixing, solutions were stirred with a magnetic stirrer for 6 h, and about 150 mL of water was removed from the solution by distillation; the precipitate formed was separated by filtration over a hot (>100 °C) 8  $\mu\text{m}$  filter by a vacuum pump. The filtrate contained 71% sodium methioninate.

### 2.2. Preparation of the polymorphic forms of $\alpha$ -DL-met

$\alpha$ -DL-met was prepared using reaction crystallization of Na-met aqueous solutions as follows: concentrated HCl (37%) was fed slowly into diluted Na-met aqueous solutions (80 mL of 71% Na-met aqueous solution diluted by 40 mL of water) in a 250 mL glass beaker at 35 °C. The mixed solutions were continuously agitated by a centrally located four-blade impeller driven by an overhead stirrer at 300 rpm. The pH of the solutions reached the isoelectric point of  $\alpha$ -DL-met (pH=5.7–5.9) after the full amount of HCl was added. The resulting crystals were collected by filtration and dried over silica gel.  $\gamma$ -DL-met was prepared by cooling crystallization of aqueous solutions of  $\alpha$ -DL-met, which has been described in a previous paper [5]. The seed of pure  $\alpha$ -DL-met were obtained by collecting sieved crystals in the size range of 64–125  $\mu\text{m}$ . The seed of pure  $\gamma$ -DL-met were obtained by collecting sieved crystals in the size ranges of 180–250 and 250–300  $\mu\text{m}$ . Pure crystal polymorphs of each form were also characterized by X-ray powder diffractometry (XRPD) (Bruker axs, D5005).

### 2.3. Crystal growth and dissolution rates measurement

The growth kinetics of  $\alpha$ -DL-met were studied via seeded batch desupersaturation experiments, as described in a previous paper [5]. The experiments were performed at 5, 15, and 25 °C in a 0.5-L stirred glass crystallizer agitated by a centrally located four-blade impeller driven by an overhead stirrer at 350 rpm. Experiments were performed within the area between the secondary nucleation threshold (SNT) of  $\gamma$ -DL-met (the stable polymorph) and the solubility of  $\alpha$ -DL-met, to avoid nucleation [5]. Concentration was measured periodically using dry substance determination [10], and the particle size distribution (PSD) of crystalline samples was measured using a Malvern Mastersizer/S (Malvern Instrument, Mastersizer S). Volume percent distributions were converted mathematically to number density distributions in order to determine the number mean growth rate of the crystals, which is most suitable for use in population balance modeling [5,11]. Nucleation was not detected in any seeded batch crystallizations for growth rate determination. Growth rate was determined as the time rate of change of the number mean crystal size using a number of experiments using different seeds and different starting supersaturation values. Crystal growth rate at a particular supersaturation was measured to  $\pm 0.05 \mu\text{m}/\text{min}$  (95% confidence).

The dissolution experiments for  $\gamma$ -DL-met were studied using a similar method to the growth experiments, except the experiments were performed at 10, 25, and 40 °C, and under the

solubility of  $\gamma$ -DL-met. The dissolution rate at a particular undersaturation was measured to  $\pm 0.07 \mu\text{m}/\text{min}$  (95% confidence).

## 3. Results and discussion

### 3.1. Growth and dissolution kinetics of the polymorphic forms

Examples of PSDs from dissolution and growth experiments at 25 °C are shown in Figs. 1 and 2, respectively. The PSD is plotted on a log-scale to show that the volume-based PSD is a log-normal distribution, and hence appears as a normal distribution on a log-scale. Photomicrographs of seed crystals and product crystals from growth, and final crystals from dissolution experiments at 25 °C were also analyzed. The analysis showed that there is no nucleation occurring during the growth process because there is only one peak in the PSD and no particles smaller than the seed crystals. Good quality product crystals were obtained because these are uniform PSDs. The product crystals obtained from growth and the final crystals obtained from the dissolution processes showed only one peak, which indicates that the growth

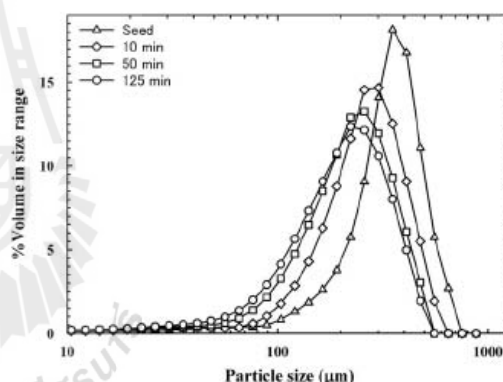


Fig. 1. Particle size distributions of seed and final crystals from a dissolution experiment at 25 °C.

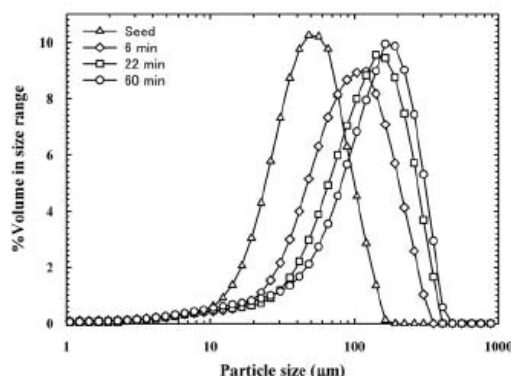


Fig. 2. Particle size distributions of seed and product crystals from a growth experiment at 25 °C.

and dissolution rates can be easily calculated from the change of the mean crystal size. The product and final crystals were also examined by XRPD analysis. The XRPD patterns of the product and final crystals were the same as the seed crystals; this indicates that there was no phase transformation during the growth and dissolution processes during the relatively short batch times used. After the growth process of  $\alpha$ -DL-met the concentration reaches the solubility of  $\alpha$ -DL-met and then remains constant for some period of time. At this concentration  $\alpha$ -DL-met starts to transform to  $\gamma$ -DL-met. Therefore the growth rate is measured from the time of seed addition until the concentration reaches the solubility of  $\alpha$ -DL-met.

A log-normal volume-based PSD indicates that the number distribution is also log-normal with the same geometric standard deviation [11]. The number mean crystal size was calculated using a method described in a previous paper [5]. The mean growth and dissolution rates were determined as the change of the number mean crystal size with time. The number-basis was used to calculate the growth rate because the growth rate data can only be obtained from batch growth using the population balance, which is a number-based balance. If other mean sizes (i.e. the volume or mass mean sizes) are used then the result is not suitable for use in the population balance, and therefore far less useful. The growth and dissolution rates can be calculated from the slope of the plot between the number mean crystal size and the time of each measurement, with these being correlated with the measured supersaturation at the same time point.

The crystals of  $\alpha$ -DL-met prepared by precipitation of the aqueous solutions of Na-met are small and partly aggregated, which makes them unsuited for determination of average dissolution rates. At the same undersaturation values used for  $\gamma$ -DL-met the  $\alpha$ -DL-met crystals dissolved too quickly for the determination of the dissolution rate to any suitable accuracy, and the time rate of change in the mean size of the crystals changed too rapidly to measure. Where the undersaturation was small enough that dissolution was sufficiently slow the concentration is so close to the solubility of  $\alpha$ -DL-met that the undersaturation cannot be predicted to sufficient accuracy. Hence, in the current study dissolution rates were measured using  $\gamma$ -DL-met seed crystals only.

In a preliminary model of the SMT the dissolution rates of  $\alpha$ -DL-met and  $\gamma$ -DL-met as a function of undersaturation may be assumed to be the same based on the assumption that dissolution is a single step (diffusion controlled) process. A bulk diffusion controlled process does not depend on the crystal structure at the surface (since diffusion occurs in the liquid phase where the molecule does not occur in a polymorphic form). The assumption of common dissolution kinetics does not mean that the dissolution rates of the two forms will be the same at the same concentration of DL-met, however: the two forms will have different undersaturation levels for a particular value of the DL-met concentration, since they have a different solubility. There is currently some debate about whether dissolution is really a two step process, and hence this assumption will be verified in later work. It is quite possible that this assumption is not sufficiently accurate; confirmation of the validity of this assumption can be demonstrated when SMT data for the transformation of  $\alpha$ -DL-met to  $\gamma$ -DL-met is compared to the population balance model.

The crystal growth of either of the two polymorphs is a two step process (mass transfer to the surface of the crystal, and a reaction step, which integrates the solute into the crystal surface) [1], and therefore the growth kinetics of the two forms will not be the same. The second step (solute integration into the lattice) depends on the characteristics of the surface of the crystal, and therefore on the crystal structure of the polymorph.

The crystal dissolution experiments allowed dissolution kinetics to be determined as a function of relative undersaturation and the dissolution rates of  $\gamma$ -DL-met increased linearly with increasing undersaturation, as expected. The crystal growth experiments allowed growth kinetics to be determined as a function of relative supersaturation and the growth rates of  $\alpha$ -DL-met also increased with increasing supersaturation. The initial growth rates of  $\alpha$ -DL-met (the first one or two growth rate data points) are significantly higher than expected based on extrapolation of data from subsequent crystal growth measurements, as was found previously in the case of  $\gamma$ -DL-met [5]. This is due to the effect of the growth history on the crystal surface, with crystals grown more quickly at higher supersaturation having a rougher surface than the seed crystals they were grown [12–15]. A similar phenomenon was also found in the dissolution experiments of  $\gamma$ -DL-met; that is the initial dissolution rate of  $\gamma$ -DL-met at early periods of the experiment (at higher undersaturation) is significantly higher than would be expected from subsequent crystal dissolution (at lower undersaturation). This may be due to a change in the surface structure of the crystals as dissolution progressed; the seeds at the initial undersaturation may have a rougher surface (on a microscopic scale) than they had after a period of dissolution, leading to a small difference in thermodynamic stability due to the increased surface energy of the rougher crystals.

The growth rate was assumed to be size independent growth, which has been the traditional assumption used. This has been investigated for other species, for example  $\alpha$ -L-glutamic acid [16]. The dissolution rate of two different sets of seed crystals, in the size ranges of 180–250 and 250–300  $\mu\text{m}$  were measured at 25 °C to determine if any size dependence was found in the dissolution rate. The results showed that the dissolution rates of both seed sizes are the same. Therefore, when considering the transformation kinetics, the growth rate of  $\alpha$ -DL-met (seed size: 64–125  $\mu\text{m}$ ), the dissolution rates of  $\gamma$ -DL-met (seed size: 250–300  $\mu\text{m}$ ), and the growth rate of  $\gamma$ -DL-met (seed size: 180–250  $\mu\text{m}$ ) [5] can be reasonably compared with each other.

The initial crystal dissolution and growth rates of all experiments were disregarded in subsequent analysis of crystallization kinetics. The growth and dissolution kinetics were described for each set of conditions by the power-law model [17,18]

$$\bar{D} = K_D \sigma_D^m \quad (1)$$

$$\bar{G} = K_G \sigma_G^n \quad (2)$$

where  $\bar{D}$  and  $\bar{G}$  are the mean dissolution and growth rates in  $\mu\text{m}/\text{min}$ , respectively;  $K_D$  and  $K_G$  are the dissolution and growth rate constants in  $\mu\text{m}/\text{min}$ , respectively;  $\sigma_D$  and  $\sigma_G$  are the relative undersaturation and supersaturation, respectively;  $m$  and  $n$  are the dissolution and growth rates orders, respectively. The experimental results of the dissolution of  $\gamma$ -DL-met and growth of  $\alpha$ -DL-met were fitted with Eqs. (1) and (2), and the results are shown in Figs. 3 and 4. The resulting equations show that the dissolution and growth rate order are unity for all conditions. The values of the dissolution and growth rate constants obtained from the linear regression of the experimental data are shown in Table 1. The results indicated that the dissolution and growth rate constants are strongly temperature dependent. The dissolution and growth rate constants can be modeled by Arrhenius relationship of the form [18,19]

$$K_D = k_D \exp\left(\frac{-E_D}{RT}\right) \quad (3)$$

$$K_G = k_G \exp\left(\frac{-E_G}{RT}\right) \quad (4)$$

where  $E_D$  and  $E_G$  are the activation energies of dissolution and growth in J/mol, respectively;  $T$  is the temperature in K, and  $R$  is the ideal gas constant (8.314 J/mol/K). The dissolution rate constant of  $\gamma$ -DL-met and growth rate constant of  $\alpha$ -DL-met were fitted with Eqs. (3) and (4), and the results are shown in Fig. 5 together with the growth of  $\gamma$ -DL-met [5]. The values of activation energy of dissolution and growth obtained from the linear regression of the dissolution and growth rate constants are shown in Table 1.

### 3.2. Discussion

The SMT is usually the most important process in crystallization of polymorphs from solution. If  $\alpha$ -DL-met crystals are put in a saturated aqueous solution, a SMT from  $\alpha$ -DL-met to  $\gamma$ -DL-met will take place. The dissolution of  $\alpha$ -DL-met and growth of  $\gamma$ -DL-met are the main kinetics of SMT. Table 1 shows that the dissolution rate constants of  $\alpha$ -DL-met (assuming they are similar to the dissolution rates of  $\gamma$ -DL-met) are likely to be larger than the growth rate constants of  $\gamma$ -DL-met at all temperatures studied. Therefore, the rate of the SMT is likely to be controlled by the growth of  $\gamma$ -DL-met. This conclusion is similar to the SMT of other crystalline substances, for example, L-histidine [20], and L-glutamic acid [21]. Moreover, the growth rate constant of  $\alpha$ -DL-met is larger than the growth rate constant of  $\gamma$ -DL-met, except at low temperature. This is reasonable because the crystallization kinetics of the metastable forms should be faster than the stable forms when the metastable forms appear first and then transform to more stable forms [21,22], although the increased crystallization rates of the metastable form could also be due to larger nucleation rates for the metastable form rather than larger growth rates. Nucleation rates in general have a larger effect on the overall rate of crystallization of a species since differences in nucleation rate can have very large effects on the population density of crystals in the system, however in many cases the differences in growth rates are sufficiently large that differences in the growth kinetics are more significant. For instance it has been shown that, for an equal supersaturation, the growth rate of  $\alpha$ -glycine (the metastable polymorph) is 500 times faster than the growth rate of  $\gamma$ -glycine (the stable polymorph) [23].

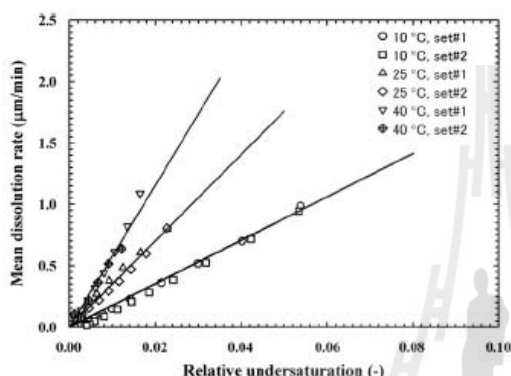


Fig. 3. Mean dissolution rates of  $\alpha$ -met as a function of relative undersaturation and temperature.

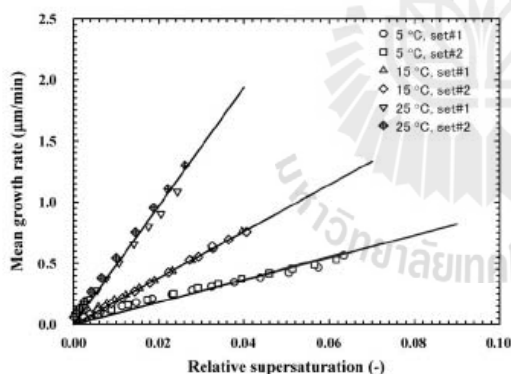


Fig. 4. Mean crystal growth rates of  $\alpha$ - $\alpha$ -met as a function of relative supersaturation and temperature.

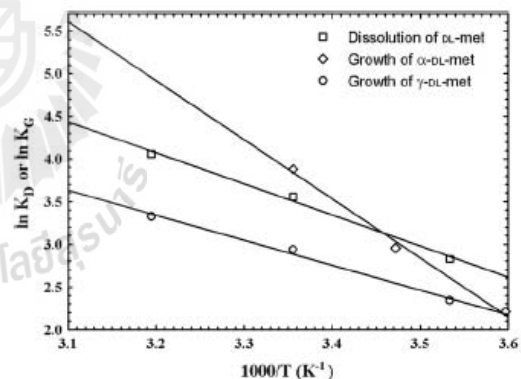


Fig. 5. An Arrhenius plot of the growth rate and dissolution rate constants for  $\alpha$ -met for determination of the activation energy of crystal growth and dissolution.

**Table 1**  
Dissolution and growth kinetic parameters of the polymorphs of  $\alpha$ -met.

Temperature (°C)	$\alpha$ - $\alpha$ -met		$\gamma$ - $\alpha$ -met <sup>a</sup>		$\alpha$ -met <sup>b</sup>	
	$K_G$ ( $\mu\text{m}/\text{min}$ )	$E_G$ (kJ/mol)	$K_G$ ( $\mu\text{m}/\text{min}$ )	$E_G$ (kJ/mol)	$K_D$ ( $\mu\text{m}/\text{min}$ )	$E_D$ (kJ/mol)
5	9.11	56.00	–	24.26	–	29.16
10	–	–	10.39	–	16.93	–
15	19.23	–	–	–	–	–
25	48.46	–	18.87	–	35.13	–
40	–	–	27.83	–	57.87	–

<sup>a</sup> Data from [5].

<sup>b</sup> Dissolution kinetics of  $\alpha$ - $\alpha$ -met or  $\gamma$ - $\alpha$ -met are assumed to be the same.

#### 4. Conclusion

In this work, the kinetics of the processes which contribute to the rate of transformation between the polymorphs have been studied. The growth kinetics of the two polymorphs and the dissolution kinetics of  $\gamma$ -DL-met were measured between 5 and 40 °C in an agitated batch crystallizer. At all temperatures studied, the growth rate orders of both  $\alpha$ -DL-met and  $\gamma$ -DL-met are 1. The dissolution rate order of  $\gamma$ -DL-met is also 1. The growth and dissolution rate constants increase with increasing temperature and follow an Arrhenius relationship. At all temperatures studied, the growth rate constant for  $\alpha$ -DL-met and the dissolution rate constant for  $\gamma$ -DL-met are larger than the growth rate constant for  $\gamma$ -DL-met, indicating that, based on the assumption that the two forms have the same dissolution rate kinetics, the SMT of the polymorph of DL-met may be controlled by the growth of  $\gamma$ -DL-met.

#### Acknowledgments

The authors acknowledge the support of the Commission on Higher Education, Thailand through the program Strategic Scholarships for Frontier Research Network for the Ph.D. Program Thai Doctoral degree for the support of LW. Research funding was also provided by the SUT Research Fund, Grant no. SUT7-706-51-36-31.

#### References

- [1] A.D. Randolph, M.A. Larson, *Theory of Particulate Processes: Analysis and Techniques of Continuous Crystallization*, second ed., Academic Press, California, 1988.
- [2] A.M. Mathieson, The crystal structures of the dimorphs of  $\alpha$ -methionine, *Acta Crystallographica* 5 (1952) 332–341.
- [3] M. Matsuoka, M. Yamanobe, N. Tezuka, H. Takiyama, H. Ishii, Polymorphism, morphologies and bulk densities of  $\alpha$ -methionine agglomerate crystals, *Journal of Crystal Growth* 198–199 (1999) 1299–1306.
- [4] M. Yamanobe, T. Takiyama, M. Matsuoka, Polymorphic transformation of  $\alpha$ -methionine crystals in aqueous solution, *Journal of Crystal Growth* 237–239 (2002) 2221–2226.
- [5] L. Wantha, A.E. Flood, Crystal growth rates and secondary nucleation threshold for  $\gamma$ - $\alpha$ -methionine in aqueous solution, *Journal of Crystal Growth* 318 (2011) 117–121.
- [6] L. Wantha, A.E. Flood, Nucleation kinetics of the  $\gamma$ -polymorph of  $\alpha$ -methionine, in: J.H. ter Horst (Ed.), *Proceedings of BIWIC 2011*, IOS Press, Delft, 2011, pp. 302–307.
- [7] R. Dowling, R.J. Davey, R.A. Curtis, G. Han, S.K. Poomachary, P.S. Chow, R.B.H. Tan, Acceleration of crystal growth rates: an unexpected effect of tailor-made additives, *Chemical Communications* 46 (2010) 5924–6926.
- [8] G. Han, S.K. Poomachary, P.S. Chow, R.B.H. Tan, Understanding growth morphology changes of  $\gamma$ -glycine and  $\alpha$ -alanine polar crystals in pure aqueous solutions, *Crystal Growth and Design* 10 (2010) 4883–4889.
- [9] K. Huthmacher, W. Binder, H.J. Hasselbach, M. Korfer, L. Rohland, H.C. Alt, H. Kniessel, Process for the preparation of aqueous sodium methioninate solutions and use of those solutions in the production of a granulate, U.S. 6,126,972, October 3, 2000.
- [10] J. Garside, A. Mersmann, J. Nyvlt, *Measurement of Crystal Growth and Nucleation Rates*, second ed., Institute of Chemical Engineering, UK, 2002.
- [11] T. Allen, *Particle Size Measurement*, fifth ed., Powder Sampling and Particle Size Measurement, Volume 1, Chapman & Hall, London, 1997.
- [12] P. Pantarak, A.E. Flood, Effect of growth rate history on current crystal growth: A second look at surface effects on crystal growth rates, *Crystal Growth and Design* 5 (2005) 365–371.
- [13] P. Pantarak, M. Matsuoka, A.E. Flood, Effect of growth rate history on current crystal growth. 2: Crystal growth of sucrose,  $\text{KAl}(\text{SO}_4)_2 \cdot 12 \text{H}_2\text{O}$ ,  $\text{KH}_2\text{PO}_4$ , and  $\text{K}_2\text{SO}_4$ , *Crystal Growth and Design* 7 (2007) 2635–2642.
- [14] A. Promraksa, A.E. Flood, P.A. Schneider, Measurement and analysis of the dextran partition coefficient in sucrose crystallization, *Journal of Crystal Growth* 311 (2009) 3667–3673.
- [15] A.E. Flood, Feedback between crystal growth rates and surface roughness, *Crystal Engineering Communications* 12 (2010) 313–323.
- [16] J. Schöll, C. Lindenberg, L. Vicum, J. Brozio, M. Mazzotti, Precipitation of  $\alpha$ -L-glutamic acid: determination of growth kinetics, *Faraday Discussions* 136 (2007) 247–264.
- [17] A.S. Myerson, R. Ginde, Crystals, crystal growth, and nucleation, in: A.S. Myerson (Ed.), *Handbook of Industrial Crystallization*, second ed., Butterworth-Heinemann, USA, 2002, pp. 33–65.
- [18] M. Gougazeh, W. Omar, J. Ulrich, Growth and dissolution kinetics of potassium sulfate in pure solutions and in the presence of  $\text{Cr}^{3+}$  ions, *Crystal Research and Technology* 44 (2009) 1205–1210.
- [19] J.W. Mullin, *Crystallization*, fourth ed., Butterworth-Heinemann, Oxford, 2001.
- [20] M. Kitamura, Crystallization behavior and transformation kinetics of L-histidine polymorphs, *Journal of Chemical Engineering of Japan* 26 (1993) 303–307.
- [21] T. Ono, H.J.M. Kramer, J.H. ter Horst, P.J. Jansens, Process modeling of the polymorphic transformation of L-glutamic acid, *Crystal Growth and Design* 4 (2004) 1161–1167.
- [22] S. Jiang, J.H. ter Horst, P.J. Jansens, Concomitant polymorphism of o-aminobenzoic acid in antisolvent crystallization, *Crystal Growth and Design* 8 (2008) 37–43.
- [23] J.W. Chew, S.N. Black, P.S. Chow, R.B.H. Tan, K.J. Carpenter, Stable polymorphs: difficult to make and difficult to predict, *Crystal Engineering Communications* 9 (2007) 128–130.

## Nucleation Kinetics of the $\gamma$ Polymorph of DL-Methionine

L. Wantha, A. E. Flood

School of Chemical Engineering, Suranaree University of Technology, Institute of Engineering, 111 University Avenue, Muang District, Nakhon Ratchasima 30000, Thailand.

adrianfl@g.sut.ac.th

*Nucleation kinetics of  $\gamma$ -DL-methionine ( $\gamma$ -DL-met) were measured in aqueous solution using direct determination of the rate of nucleation based on measurements of particle (crystal) counts as a function of time. The number of crystals appearing in a microdroplet were counted by observation under a microscope. The nucleation rates increase with increasing temperature, and were found to exponentially increase with respect to the supersaturation of DL-met. The measured nucleation kinetics follow the trends expected from Classical Nucleation Theory (CNT) allowing approximate interfacial energies to be estimated by fitting the measured data to CNT.*

### 1. Introduction

Crystallization processes which include transformation between polymorphs consist of the competitive nucleation and crystal growth of the polymorphs and the transformation from the metastable form to the stable form, usually via a solution mediated mechanism. The mechanism of each elementary step in the crystallization process needs to be understood to predict and control polymorph formation. This analysis has been already begun in the current system with results on the crystal growth rates and secondary nucleation threshold of  $\gamma$ -DL-met [1].

Determination of the nucleation rate is of key importance for the development of process models that can be used for process design and optimization. This is a difficult step in crystallization process design and development. Numerous techniques for determination of the nucleation rate for crystallization process have been proposed in the literature, for example methods using combined particle (crystal) counting and process time measurements [2,3], mixed-suspension mixed-product removal (MSMPR) experiments in combination with particle size distribution (PSD) measurements [4], induction time measurements [5,6] and metastable zone experiments [7]. An overview about the difference of these techniques can be found elsewhere [4].

In this work, a previously developed method [2], which is based on the use of particle (crystal) counts in microdroplets as a function of time, was used to determine the nucleation kinetics of  $\gamma$ -DL-met in aqueous solution. The effects of supersaturation and temperature on the nucleation rates were studied.

### 2. Experimental Methods

A saturated solution at the temperature under consideration was prepared at a temperature  $T_0$  (see Fig. 1), chosen to prevent nucleation of crystals. To prepare this solution, a known amount of DL-met was dissolved in 300 mL of water in a 0.5 L batch crystallizer agitated at 350 rpm by an overhead stirrer maintained at a constant temperature,  $T_0$ . Note that  $T_0$  is at least 20 °C above  $T_{sat}$ .

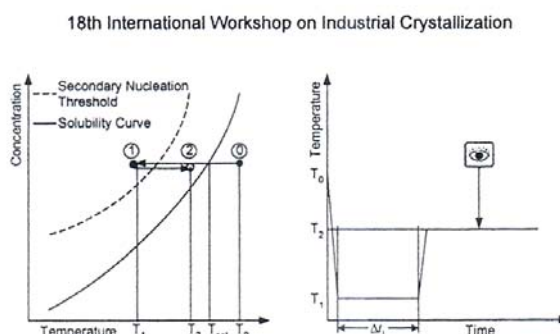


**Fig. 1:** Position in the phase diagram and temperature profile during a nucleation experiment.

The direct determinations of the rate of nucleation are described as follows. The principle of this technique is illustrated in Fig. 1 and the experiment setup is illustrated in Fig. 2. A solution droplet with a volume of  $0.2 \mu\text{L}$  (prepared using a micropipette) at  $T_0$  was placed in the nucleation cell at which was maintained at the selected  $T_1$ . This temperature was such that the nucleation process was initiated at the desired supersaturation level. After a specific time interval ( $\Delta t_1$ ) for nucleation, the temperature  $T_1$  was raised to a temperature  $T_2$  at which the supersaturation was at a sufficiently low level to prevent further nucleation, but allowed existing crystals to grow to a visible size. During this stage the numbers of crystals that appeared in the solution droplet was counted using observation under a microscope. After plotting the total number of crystals detected in the droplet as a function of  $\Delta t_1$ , the nucleation rate was determined from the slope of this plot as  $\Delta t_1$  approaches zero divided by the volume of the solution droplet. Note that the times to change the temperature from  $T_0$  to  $T_1$  and  $T_1$  to  $T_2$  depend on the thermal property of the material of the nucleation cell and the size of droplet. In this case the times were about 5-10 sec because of the very small size of droplet. At a high nucleation temperature,  $35^\circ\text{C}$  for this work, inert liquid paraffin was used to cover the solution droplet to reduce the effect of the liquid evaporation due to very small size of the droplet.

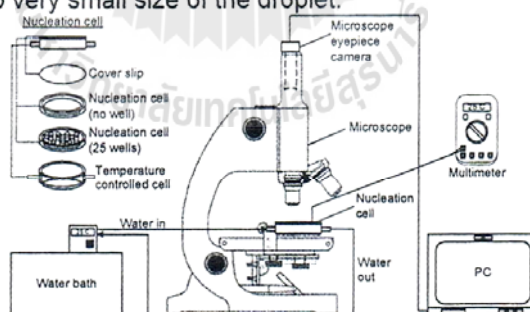


**Fig. 2:** Schematic of the experiment setup. The nucleation cell is made from acrylic and wells are flat-bottom.

### 3. Results and Discussion

Crystals obtained from cooling crystallization from aqueous solutions of DL-met have previously been found to be the  $\gamma$ -polymorph ( $\gamma$ -DL-met) [8], and this work obtains the same polymorph using identification by X-ray powder diffractometry (Bruker axs, D5005).

The nucleation rates of  $\gamma$ -DL-met in aqueous solution were determined for three different temperatures: 18, 25 and  $35^\circ\text{C}$ , and at each temperature the nucleation

rate was determined at various values of supersaturation. For each value of the initial supersaturation the number of crystals that appeared in the solution droplet was counted at 4-6 values of the nucleation time  $\Delta t_1$ , and for each value of  $\Delta t_1$  the measurements were performed with 3-6 replicates. For each value of  $\Delta t_1$  the number of crystals was counted at particular times during the growth stage, and stopped when the number of crystals did not change with time. The number of crystals detected at the end of this period is the number of crystals nucleated during  $\Delta t_1$ ; the experiment must be performed in this way since newly nucleated crystals are too small to be detected until growth to a visible size has occurred. The growth occurs at a supersaturation within the metastable zone (for the time period of the measurement) and hence no new nuclei are formed during the growth period. Fig. 3 illustrates photomicrographs of crystals nucleated in a droplet from a measurement at 18 °C and  $S = 1.37$ . The number of crystals nucleated during  $\Delta t_1$  are 47, 84, 114, and 124 crystals respectively for nucleation times of 10, 15, 40, and 60 seconds. During the measurement the shape and size of droplet did not change, which indicates that evaporation from the solution droplet did not occur during nucleation measurement.

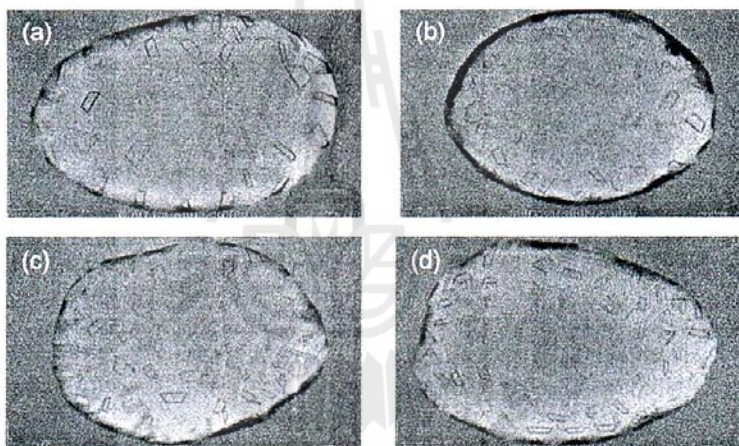


**Fig. 3:** Micrographs of crystals nucleated in a droplet at various nucleation times; measurement at 18 °C and  $S = 1.37$ : 10 s (a), 15 s (b), 40 s (c), 60 s (d).

Fig. 4, 5, and 6 show that the mean number of nucleated crystals increases with increasing nucleation time and supersaturation for the nucleation rate measurements at 18, 25, and 35 °C, respectively. The plots start from zero crystals (no nucleation) at  $\Delta t_1 = 0$  because the measurement start with a clear solution. At higher nucleation time the mean number of nucleated crystals approach to constant value because the solution concentration approaches the metastable limit due to the crystal growth during the experiment. Usually, for each  $\Delta t_1$  measurement the crystals that appeared in the solution droplet consist of the new crystals formed and crystals that grow to larger size. To cancel the effect of the change in supersaturation due to growth the nucleation rate should be determined for the earlier stages (at small values of  $\Delta t_1$ ) of the measurement. This also indicates that the nucleation rate is measured at constant concentration because at very small  $\Delta t_1$  the concentration is nearly constant because the number of nuclei produced is small. The nucleation rate is determined from the slope of these plots as  $\Delta t_1$  approaches zero divided by the volume of the solution droplet ( $dN/dt \cdot V^{-1}$ ). To reduce the difficulty of the determination the plots were fitted with an exponential rise to a maximum:  $N = a(1 - e^{-bt})$ , which fits the

available data very well. This equation gives  $dN/dt = abe^{-bt}$  and therefore  $dN/dt|_{\Delta t_1=0} = ab$ . This leads to the nucleation rate  $J = ab/V$ , where  $J$  is the nucleation rate in  $\#/m^3s$ ,  $ab$  is the initial slope in  $\#/s$ , and  $V$  is the volume of the droplet in  $m^3$ .

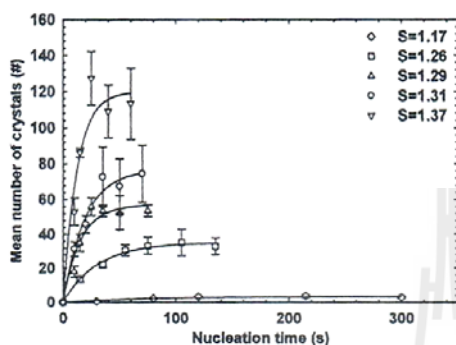


Fig. 4: Mean number of crystals as a function of nucleation time ( $\Delta t_1$ ) and supersaturation at 18 °C.

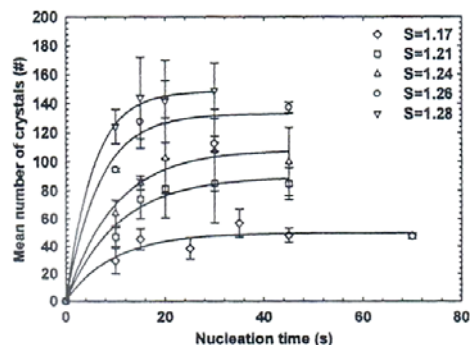


Fig. 5: Mean number of crystals as a function of nucleation time ( $\Delta t_1$ ) and supersaturation at 25 °C.

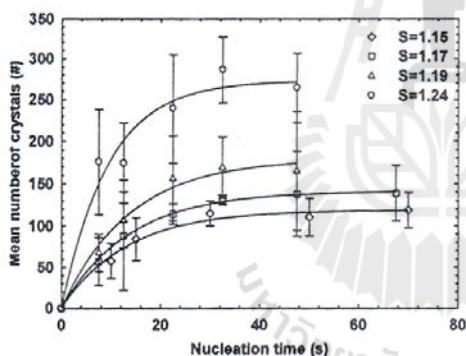


Fig. 6: Mean number of crystals as a function of nucleation time ( $\Delta t_1$ ) and supersaturation at 35 °C.

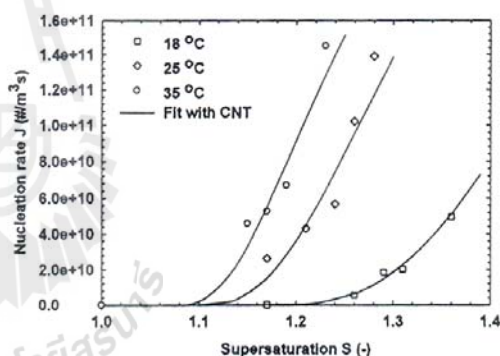


Fig. 7: Nucleation rate as a function of supersaturation.

The dependence of the nucleation rates on the supersaturation and temperature are shown in Fig. 7. It can be seen that at constant temperature the nucleation rates increase exponentially with increasing supersaturation. This is since the higher supersaturation ( $S = c/c^*$  = actual concentration/solubility) leads to a higher driving force ( $\Delta c = c - c^*$ ) for nucleation. Also, at constant supersaturation the nucleation rates increase with increasing temperature. This is due to the change in the pre-exponential constant with temperature and is typical with kinetic processes.

The nucleation rate ( $J$ ) can be predicted as a function of supersaturation based on the classical nucleation theory (CNT) according to eq. 1 [9].

$$J = AS \exp\left(-\frac{B}{\ln^2 S}\right) \quad (1)$$

where  $A$  is a pre-exponential kinetic parameter and  $B$  is a thermodynamic parameter. Assuming spherical nuclei the following relationship is predicted

$$B = \frac{16\pi v_0^2 \gamma^3}{3(kT)^3} \quad (2)$$

where  $v_0$  is molecular volume and is equal to  $18.50 \times 10^{-29} \text{ m}^3$  for DL-met,  $\gamma$  is interfacial energy in  $\text{J/m}^2$ ,  $k$  is the Boltzmann constant and is equal to  $1.38 \times 10^{-23} \text{ J/K}$ , and  $T$  is temperature in K. The experimental data were fitted eq. 1, with the results shown in Fig. 7. The model fits the data well. The results show that the measured nucleation kinetics follow the trends expected from the CNT. The best-fit values of  $A$  and  $B$  are shown Tab. 1. Approximate interfacial energy values for all temperatures can be predicted from the parameter  $B$ , and these are also tabulated in Tab. 1. It is important to note that these may only be approximations to true surface energies. The  $\gamma$  values obtained are comparable to those reported for other poorly water soluble organic molecules, for example L-histidine [5] ( $5.1 \text{ mJ/m}^2$ ) and paracetamol [10] ( $1.4\text{--}2.8 \text{ mJ/m}^2$ ). The values obtained for  $A$  are relatively low but are comparable to values for lysozyme [11] ( $10^7 - 10^9 \text{ m}^{-3}\text{s}^{-1}$ ) and L-asparagine [12] ( $10^{11} \text{ m}^{-3}\text{s}^{-1}$ ).

**Table 1:** The predicted interfacial energy and pre-exponential factor.

Temperature (°C)	Pre-exp. Factor, $A$ ( $\text{m}^{-3} \text{s}^{-1}$ )	Parameter $B$ [-]	Interfacial Energy, $\gamma$ ( $\text{mJ/m}^2$ )
18	$5.10 \times 10^{11}$	0.247	3.03
25	$3.47 \times 10^{11}$	0.0813	2.14
35	$3.08 \times 10^{11}$	0.0464	1.84

#### 4. Conclusions

In this work, direct determinations of the rate of nucleation of  $\gamma$ -DL-met in aqueous solution were performed. This method is based on direct particle (crystal) counts as a function of time. The nucleation rate was determined from the limiting slope of the plot between the total number of crystals and the nucleation time as the nucleation time approached zero, divided by the volume of the solution droplet. The results show that the number of nucleated crystals increases with increasing nucleation time and supersaturation, and approaches a constant value at higher nucleation time, because at higher nucleation times there is sufficient growth to deplete the solution. The determined nucleation rates follow the trends expected from the classical nucleation theory (CNT). The nucleation rates increase with increasing temperature and exponentially increase with increasing supersaturation. Based on the CNT, the kinetic parameter  $A$  and thermodynamic parameter  $B$  were estimated by fitting the determined nucleation rates with CNT. The interfacial energy was estimated from the parameter  $B$  and the values are in the range  $1.8\text{--}3.1 \text{ mJ/m}^2$ . The interfacial energy value tends to decrease with increasing solubility.

#### References:

- [1] L. Wantha, A. E. Flood: *Crystal Growth Rates and Secondary Nucleation Threshold for  $\gamma$ -DL-Methionine in Aqueous Solution*, J. Cryst. Growth, 318(1) (2011), 117–121.
- [2] O. Galkin, P.G. Vekilov: *Direct Determination of the Nucleation Rate of Protein Crystals*, J. Phys. Chem. B, 103(49) (1999), 10965–10971.
- [3] C. Lindenberg, M. Mazzotti: *Continuous Precipitation of L-Asparagine Monohydrate in a Micromixer: Estimation of Nucleation and Growth Kinetics*, AIChE J., 57(4) (2011) 942–950.
- [4] J. Garside, A. Mersmann, J. Nyvlt: *Measurement of Crystal Growth and Nucleation Rates*, 2<sup>nd</sup> ed., Institute of Chemical Engineering, UK (2002).
- [5] S. Jiang, J.H. ter Horst: *Crystal Nucleation Rates from Probability Distributions of Induction Times*, Cryst. Growth Des., 11(1) (2011), 256–261.

- [6] S. Teychené, B. Biscans: *Nucleation Kinetics of Polymorphs: Induction Period and Interfacial Energy Measurements*, Cryst. Growth Des., 8(4) (2008), 1133-1139.
- [7] N.A. Mitchell, P.J. Frawley: *Nucleation Kinetics of Paracetamol–Ethanol Solutions from Metastable Zone Widths*, J. Cryst. Growth, 312(19) (2010), 2740-2746.
- [8] M. Matsuoka, M. Yamanobe, N. Tezuka, H. Takiyama, H. Ishii: *Polymorphism, Morphologies and Bulk Densities of DL-Methionine Agglomerate Crystals*, J. Cryst. Growth, 198-199 (1999), 1299-1306.
- [9] D. Kashchiev, G.M. van Rosmalen: *Review: Nucleation in Solutions Revisited*, Cryst. Res. Technol., 38(7-8) (2003), 555-574.
- [10] R.A. Granberg, C. Ducreux, S. Gracin, Å.C. Rasmuson: *Primary Nucleation of Paracetamol in Acetone-Water Mixtures*, Chem. Eng. Sci., 56(7) (2001) 2305-2313.
- [11] O. Galkin, P.G. Vekilov: *Nucleation of Protein Crystals: Critical Nuclei, Phase Behavior, and Control Pathways*, J. Cryst. Growth, 232(1-4) (2001) 63–76.
- [12] A.J. Mahajan, D.J. Kirwan: *Nucleation and Growth Kinetics of Biochemicals Measured at High Supersaturations*, J. Cryst. Growth, 144(3-4) (1994) 281-290.

#### Acknowledgements:

The authors acknowledge the support of the Commission on Higher Education, Thailand through the program of Strategic Scholarships for Frontier Research Network for the Ph.D. Program Thai Doctoral degree for the support of LW and for the research funding. Research funding from the SUT Research Fund, grant SUT7-706-51-36-31 is also acknowledged.



## **BIOGRAPHY**

Mr. Lek Wantha was born on October 7, 1980 in Surin Province. He graduated with a Bachelor degree in chemical engineering in 2004 and a Master's degree in chemical engineering in 2006, from Suranaree University of Technology (SUT). He received a scholarship for students with outstanding academic performance from SUT to study for the Master's degree in chemical engineering at SUT from 2004 to 2006. He received a scholarship through the program of Strategic Scholarships for Frontier Research Network for the Ph.D. Program, Thai Doctoral degree from the Commission on Higher Education, which sponsored his Ph.D. study and supported his research for the period 2006-2010.

